

UNIVERSITÉ DE LILLE

UNITÉ DE MÉCANIQUE DE LILLE

LABORATOIRE DE GÉNIE CIVIL ET GÉO-ENVIRONNEMENT

ÉCOLE DOCTORALE SCIENCES POUR L'INGÉNIEUR (SPI)

Thèse pour l'obtention du grade de docteur

de l'Université de Lille

**Discipline : Mécanique des solides, des matériaux, des structures
et des surfaces**

Présentée et soutenue par

Karim KANDIL

Le 26 Novembre 2020

Intitulée

**Modélisation multi-physique et multi-échelle des tissus mous stratifiés :
Application à la réponse multi-axiale du disque intervertébral humain**

**Multi-physics and multi-scale modeling of laminated soft tissues:
Application to the multi-axial response of human intervertebral disc**

Jury

| | | | |
|---------------------------------|-----------------|--------------------------|-----------------------|
| Thomas PARDOEN | Professeur | UCLouvain | Président |
| Jean-François GANGHOFFER | Professeur | Université de Lorraine | Rapporteur |
| Jean-Claude GRANDIDIER | Professeur | ENSMA | Rapporteur |
| Nadia BAHLOULI | Professeur | Université de Strasbourg | Examineur |
| Tanguy MESSEGER | MCF-HDR | Université de Lille | Directeur de thèse |
| Fahmi ZAIRI | Professeur | Université de Lille | Co-directeur de thèse |
| Fahed ZAIRI | Neurochirurgien | Ramsay Générale de Santé | Invité |

Acknowledgements

I wish to thank Prof. Jean-François GANGHOFFER, Prof. Jean-Claude GRANDIDIER, Prof. Nadia BAHLOULI, and Prof. Thomas PARDOEN for accepting to take part in my dissertation committee and to share this honorable event with me. I would like to thank them also for the interesting questions and the valuable discussions during the defense.

I would like to express my sincere gratitude to my director Tanguy MESSAGER for his prodigious support and valuable advice that were present since the beginning of my PhD. His priceless instructions were substantial for improving my teaching and research skills. He always showed a lot of care and managed to provide all tools needed to carry out my research under the best conditions.

My deep appreciation goes to my co-director Fahmi ZAIRI for his continuous motivation, since our first meeting during my bachelor studies, for his time, support, patience, and immense knowledge. His guidance helped me in all the time of research and writing of this thesis. He was the first person to encourage me to pursue my post-graduate career in the research field and thanks to him I have decided to do the current PhD.

Fahed ZAIRI, my sincere thanks for the fundamental advice, the priceless medical information, and the valuable discussions that helped to improve my research.

I want also to thank my friends and my colleagues in UML and LGCgE laboratories and all my friends who partook in this long journey and accompanied me during serious work and light-hearted break times.

Finally, I would like to thank my family for their love and continuous support. They were always here every time I needed them for the good and hard moments and without them, I wouldn't have realized any of my dreams.

Table of contents

- General introduction 1**
 - Objective and thesis plan 2
- Chapter I: Intervertebral disc composition and overview of existing intervertebral disc models 5**
 - I.1. Vertebral column 5
 - I.1.1. Intervertebral disc 6
 - I.1.2 Osmolarity and swelling effect..... 8
 - I.2. Key points for realistic disc modeling..... 9
 - I.2.1. Disc mechanics 9
 - I.2.2. Multi-axiality 10
 - I.2.3. Interlamellar-induced volumetric behavior 11
 - I.2.4. Intervertebral disc health state and aging..... 12
 - I.3. Constitutive modeling of the disc behavior 13
 - I.3.1. Microstructure features 13
 - I.3.2. Number of phases 14
 - I.3.3. Disc heterogeneity and regional dependency 15
 - I.3.4. Disc geometry 15
 - I.3.5. Animal models 16
 - I.3.6. Summary of disc models of the last two decades 17
- Chapter II: Interlamellar-induced time-dependent response of intervertebral disc annulus: a microstructure-based chemo-viscoelastic model..... 23**
 - Abstract..... 23
 - II.1. Partial introduction 24
 - II.2. A microstructure-based model 27
 - II.2.1. At the ECM scale 29
 - II.2.1.1. Constitutive relations 29
 - II.2.1.2. Numerical implementation 33
 - II.2.2. At the stratified scale..... 36
 - II.2.2.1. Numerical model 36
 - II.2.2.2. ILM-lamellar interaction 36
 - II.2.2.3. Microstructure-based considerations..... 39

| | |
|--|-----------|
| II.2.3. Model application | 40 |
| II.2.3.1. Structural features | 40 |
| II.2.3.2. Database | 41 |
| II.3. Results and discussion | 44 |
| II.3.1. Material kinetics..... | 44 |
| II.3.1.1. Stress-free swelling response | 44 |
| II.3.1.2. Quasi-static loading-unloading response | 45 |
| II.3.1.3. Relaxation response..... | 49 |
| II.3.2. Model-experiment comparisons..... | 51 |
| II.3.3. Local strain fields..... | 55 |
| II.4. Partial conclusion..... | 59 |
| Chapter III: Interlamellar matrix governs human annulus fibrosus multi-axial behavior | 65 |
| Abstract..... | 65 |
| III.1. Partial introduction..... | 66 |
| III.2. Methods | 68 |
| III.2.1. Computational models | 68 |
| III.2.2. Uniaxial stretching conditions and designed material kinetics | 70 |
| III.2.3. Biaxial stretching conditions | 72 |
| III.2.4. Shearing conditions..... | 72 |
| III.2.5. Microstructure-based constitutive model..... | 72 |
| III.2.5.1. Kinematics..... | 72 |
| III.2.5.2. Constitutive equations..... | 74 |
| III.2.5.3. Parameters identification..... | 77 |
| III.3. Results..... | 78 |
| III.3.1. Uniaxial stretching path along with regional effects..... | 78 |
| III.3.2. Biaxial stretching paths | 80 |
| III.3.3. Shearing paths..... | 82 |
| III.4. Discussion | 85 |
| III.5. Partial conclusion | 90 |
| Chapter IV: A microstructure-based modeling approach to assess aging-sensitive mechanics of human intervertebral disc | 95 |
| Abstract..... | 95 |

| | |
|--|------------|
| IV.1. Partial introduction..... | 96 |
| IV.2. Microstructure-based model..... | 100 |
| IV.2.1. Single-lamellar annulus model..... | 101 |
| IV.2.1.1. Free energy of ECM..... | 102 |
| IV.2.1.2. Free energy of oriented type I collagen fibers..... | 104 |
| IV.2.1.3. Free energy of chemical-induced volumetric part..... | 104 |
| IV.2.2. Multi-lamellar annulus model..... | 105 |
| IV.2.3. Age-related microstructure changes..... | 106 |
| IV.3. Results and discussion..... | 109 |
| IV.3.1. Age-related stress response changes..... | 109 |
| IV.3.2. Age-related transversal response changes..... | 110 |
| IV.3.3. Local stress-strain fields..... | 111 |
| IV.3.4. Correlation between intrinsic mechanics of disc and its functionality..... | 113 |
| IV.4. Partial conclusion..... | 116 |
| Chapter V: A microstructure-based human spine unit model integrating tissue volumetric strain and lamellar-interlamellar-nucleus interaction..... | 123 |
| Abstract..... | 123 |
| V.1. Partial introduction..... | 124 |
| V.2. Numerical model of the human spine unit..... | 127 |
| V.2.1. Model construction and boundary conditions..... | 127 |
| V.2.2. Constitutive model..... | 130 |
| V.2.2.1. Finite strain kinematics..... | 131 |
| V.2.2.2. Stress decomposition..... | 134 |
| V.2.2.3. Constitutive equations..... | 136 |
| V.2.2.3.1. Extracellular matrix..... | 136 |
| V.2.2.3.2. Oriented type I collagen fibers..... | 137 |
| V.2.2.3.3. Swelling..... | 138 |
| V.2.3. Algorithm and numerical implementation..... | 138 |
| V.2.4. Microstructure and model parameters..... | 143 |
| V.3. Results..... | 145 |
| V.3.1. Displacement fields..... | 145 |
| V.3.2. Strain fields..... | 145 |
| V.4. Discussion..... | 149 |

| | |
|--|------------|
| V.4.1. Nucleus-annulus interaction | 149 |
| V.4.2. Mechanical damage | 150 |
| V.5. Partial conclusion | 152 |
| General conclusion and perspectives | 158 |

General introduction

Back pain is a common health problem affecting about 50 to 80% of humans at least one time during their life. The pain is sometimes related to muscles and ligaments, but when it is intense and chronic it is often linked to the intervertebral disc injuries and dysfunctions. This soft tissue located in the vertebral column gives to the body the mobility needed to achieve the different movements while resisting in parallel to the loads coming from the body weight and the daily activities. Any small issue in the intervertebral discs may cause many troubles in the human back varying from a simple back pain to disc hernia and sometimes could lead to paralysis. For this reason, the importance of studying the intervertebral disc conduct and predicting its response under the different physiological movements is mandatory in order to understand the chemo-mechano-biological mechanisms taking place inside the disc soft tissues which could help avoiding damage and producing better treatment procedures if damage is already present. Great progresses in this field were achieved over the recent years. Although important differences could be witnessed between the discs of different individuals, many experimental contributions succeeded to identify the mechanical response of the disc at different scales: complete spine scale, functional spine unit scale and material volume element scale. However, accessing the core of the disc in-vivo while maintaining unchanged its natural response is very hard to achieve which represents an obstructing point in the intervertebral disc research. That is why multi-physics simulations relating the microstructure of the chemo-biological tissue to its multi-axial response become mandatory for understanding the disc behavior under normal activity. However, the multi-subject problematic translated by the complex interactions between the different microstructural elements of the disc makes the task very complex. Also, due to the high heterogeneity of the biological tissues intervening in the intervertebral disc and the varying response between different individuals, a huge amount

of experimental works of hardly available human cadavers should be established in order to construct and validate a reliable numerical model of the disc.

Objective and thesis plan

The main objective of this thesis is to construct a robust modeling approach that is able to reproduce through finite element simulations a correct multi-axial volumetric response of the human intervertebral disc while taking into account the regional differences of the highly heterogeneous tissues and the chemo-mechanical interactions with the surrounding biomechanical environment. The model should allow us to observe the internal disc response without affecting its global behavior. As well, it should permit the prediction of the age-related microstructure-response alteration. In order to realize our objective, the actual thesis was planned following several well-constructed steps that will be described in details through the following chapters:

After a description of intervertebral disc role and composition, the **chapter I** provides a brief overview of existing intervertebral disc models and important aspects that should be considered for intervertebral disc modeling in order to situate the present contributions over the state-of-art.

In **chapter II**, a microstructure-based chemo-viscoelastic model is developed to highlight the interlamellar-induced time-dependent response of the disc annulus fibrosus by means of a two-scale strategy linking the disc microstructure scale to the lamellar-interlamellar scale. The model kinetics was designed based on experiments established on specimen extracted from bovine disc. It considers the time-dependent transversal response affecting the volumetric behavior of the annulus tissue. The capability of the model to reproduce the annulus fibrosus time-dependent conduct along with regional dependency for different strain rates and salinities of the surrounding environment was tested and verified numerically.

Due to the strong difficulties of making experiments on human cadavers, a novel hybrid approach is introduced in **chapter III** permitting the adaptation and the application of the animal constructed model to human model by adjusting some physical parameters of the model and introducing human microstructure features. The constructed microstructural constitutive model is generalized to predict the behavior of all annulus fibrosus regions (four regions) based on the behavior of only two identified disc regions by means of their corresponding microstructures. Incorporating the volumetric behavior of the annulus allows for the first time simulating the multi-axial behavior of the disc tissues in terms of biaxial and shear tests using the same parameters found for the uniaxial behavior.

In **chapter IV**, we present an innovative method which is able to estimate the long-term aging effect on the intervertebral disc chemo-mechanical response by means of a novel microstructural approach that is based on the most recent discoveries about the disc introduced in the previous chapters. The model allows giving many explanations about the relation between the mechanical response of the disc and the age-related microstructural changes which is very hard to achieve experimentally.

In **chapter V**, the L4-L5 functional spine unit was constructed based on computerized tomography scans of a mature healthy individual. A realistic lamellar-interlamellar representation of the intervertebral disc annulus fibrosus is modeled while taking into account the circumferential and radial regional microstructural variations and their interaction with the gelatinous nucleus. For different simple and complex physiological movements, displacement vector fields and shear strain fields were plotted and compared. The access to the core of the healthy disc is established and the critical zones with the highest shear strain values were determined and related to the local kinetics and microstructure.

Chapter I

Intervertebral disc composition and overview of existing intervertebral disc models

I.1. Vertebral column

The vertebral column is the pillar that supports the human body. It is constituted of a number of vertebrae that are separated by the intervertebral discs. The vertebral column is divided to three main parts (as shown in Figure I.1):

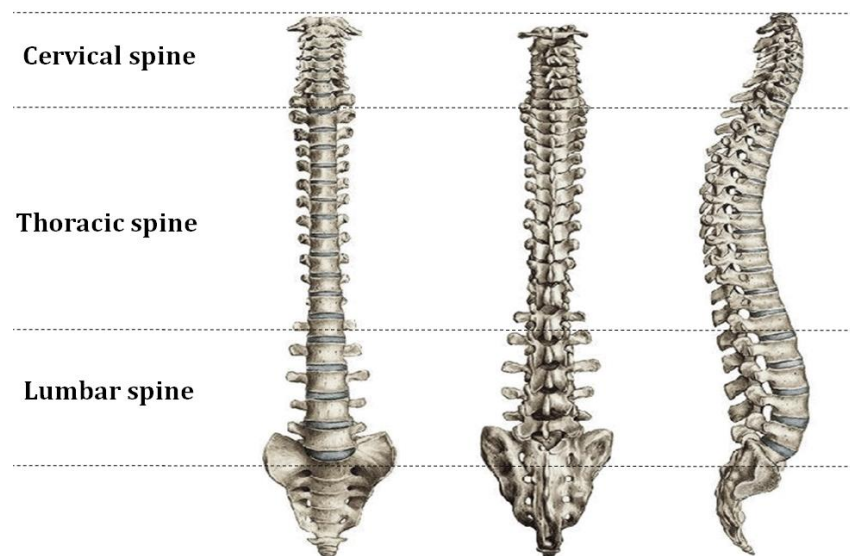


Figure I.1. The vertebral column structure.

The first one is the cervical spine which is situated in the neck region. It is composed of 6 intervertebral discs that separate the 7 cervical vertebrae. There is no disc between the first and second vertebrae that are directly connected to each other. The second one is the thoracic spine. It contains 12 discs separating 12 thoracic vertebrae. The third part is the lumbar spine.

It is located in the lower back region of the body and contains 5 discs separating 5 lumbar vertebrae. The microstructural constitutions of all the discs are almost the same but their contents and proportions differ from a human to another, from a disc to another and from a region to another inside the same disc. The lumbar discs are bigger than the cervical discs which help the discs of the back down part to support more loads.

I.1.1. Intervertebral disc

The intervertebral disc is constituted of 3 main parts as shown in Figure I.2:

- 1- The annulus fibrosus (AF): It is a fibrous cartilage composed of a number of layers reinforced by stiff oriented type I collagen fibers. These fibers are embedded in a viscous extracellular matrix (ECM) that is composed mainly of proteoglycan macromolecules, water and non-oriented type II collagen fibers, see Figure I.3.

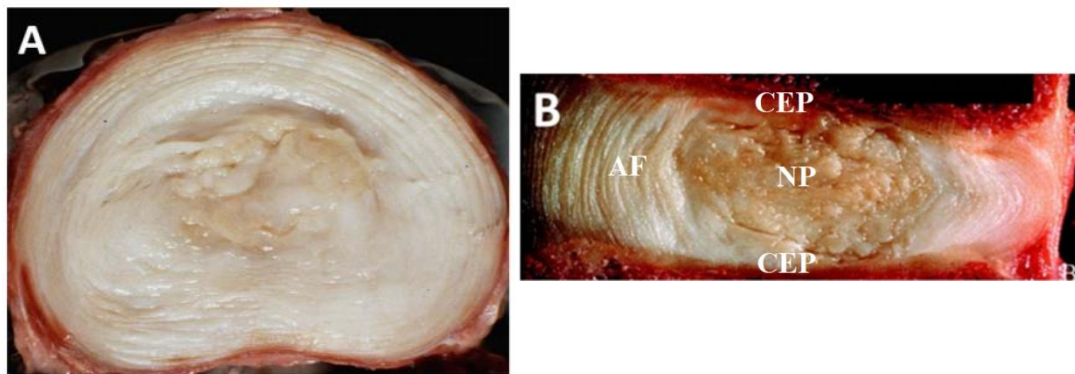


Figure I.2. (A) Transverse cut and (B) mid-sagittal cut of healthy human intervertebral disc (Adams et al., 2014).

The fiber bundles are almost arranged in a fixed direction in each layer that alters from a layer to the following one. Their concentration is the highest in the outer region of the annulus and decreases while getting closer to the nucleus. Unlike collagen, the concentration of proteoglycans is very low in the outer layers of the AF and increases gradually while getting closer to the nucleus. The lamellae are separated by a non-

fibrillar interlamellar matrix (ILM) which is very rich of negatively charged proteoglycans and that contains elastic fibers and fibrils as shown in Figure I.4. The later constituents work as bridging elements connecting the successive lamellae which ensure the structural integrity of the annulus (Tavakoli et al., 2016).

- 2- The nucleus pulposus: It is a gelatinous core constituting the heart of the disc and containing negatively charged proteoglycans reaching about 50% of the dry weight of the nucleus. The negative charges attract the water inside the disc. It also contains type II collagen fibers that are randomly distributed in the matrix and unlike the AF layers do not have a favorite distribution direction. Nucleus and surrounding AF layers interact together under applied strains in order to attain a better resistance to different external loads.

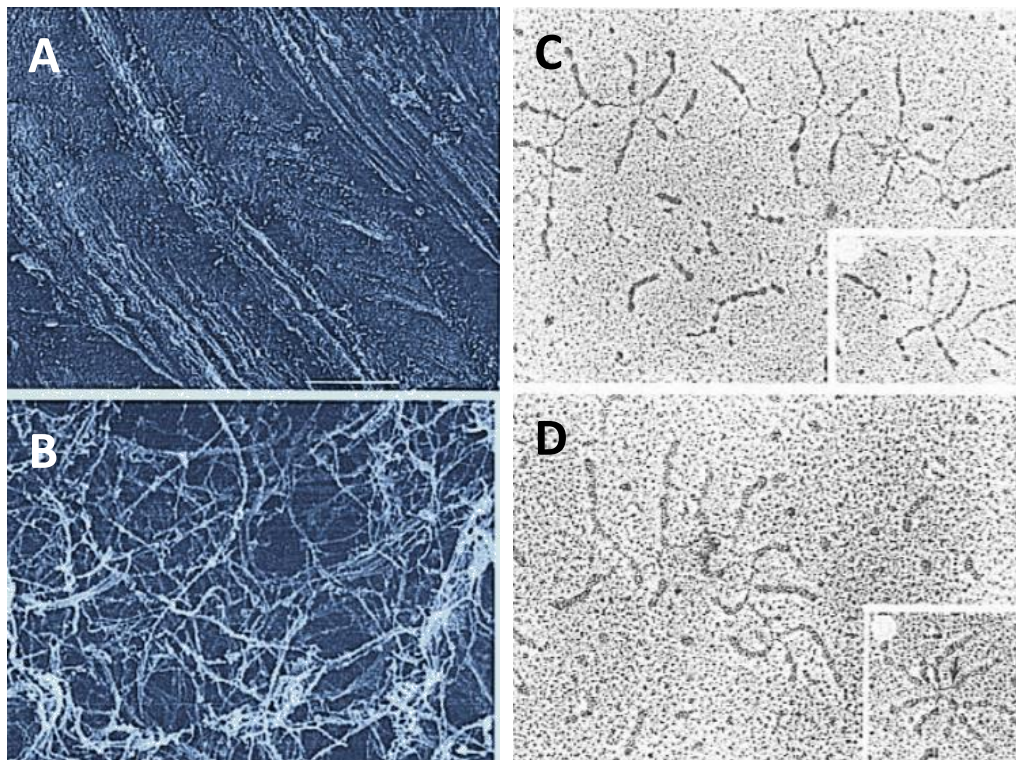


Figure I.3. Disc microstructure elements: (A) aligned collagen fibers in human annulus fibrosus, (B) dispersed collagen fibers in nucleus pulposus, (C) proteoglycans matrix in annulus fibrosus and (D) proteoglycans in nucleus pulposus (Buckwalter et al., 1985, 1995).

- 3- The cartilage endplates: They are thin cartilages connecting the nucleus pulposus to the adjacent vertebrae. Their permeability plays a very important role in the transportation of the different nutrients to the disc and the viability of the disc cells.

The intervertebral disc has a very low concentration of cells, which is about 1% of the total disc volume. The disc cells consume nutrients like oxygen and glucose and produce lactic acid which is very important for their viability. The balance of these chemical entities and their amount is very important (Wills et al., 2016). The lack of oxygen may affect the proteoglycans production which could have a big influence on the swelling of the disc tissue and its volumetric response. Also, the excess production of lactic acid might lead to some drops in the PH of the ECM affecting the disc biology.

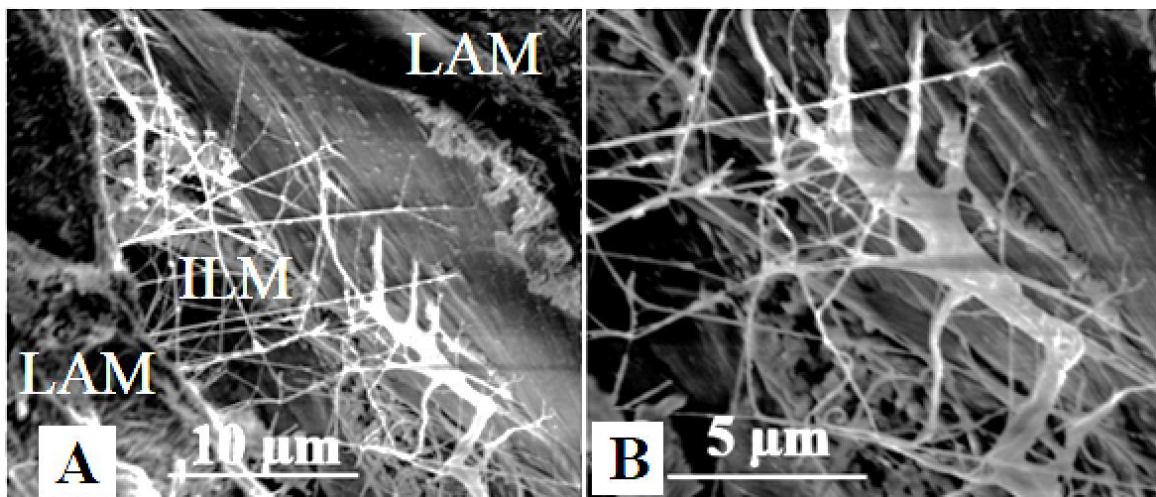


Figure I.4. Organization of elastic fibers and fibrils in ILM (Tavakoli et al., 2017).

I.1.2 Osmolarity and swelling effect

The proteoglycans contained in the ECM of the disc are rich with negatively charged ions. These ions attract the external salted water inside the disc trying to achieve the electric neutrality state (Urban and McMullin, 1985). The concentration of the negative proteoglycan ions is greater than the ions concentration of the external water environment (concentration of

NaCl). This difference creates a pressure called osmotic pressure that is responsible of the fluid transfer and tissue swelling (Maroudas, 1970). Since proteoglycans negative ions are the main responsible of water retained inside the disc, water content follows the same trend observed for proteoglycans with highest content in the nucleus and lowest content in the outer annulus fibrosus.

I.2. Key points for realistic disc modeling

I.2.1. Disc mechanics

Many experimental investigations tried to study the regional stress-strain response of the disc at the scale of the single lamellar (Holzapfel et al., 2005) and multi-lamellar specimens (Ebara et al., 1996). As shown in Figure I.5, the conduct is seen to be non-linear with higher rigidity in the outer regions of the disc compared to the inner regions and in the anterior ventral regions compared to the posterior dorsal regions. The strain-rate dependency and the hysteretic cyclic response of the annulus specimen, observed in Derrouiche et al. (2020), indicate the time-dependency of the tissue induced by the intrinsic viscosity of the disc and the fluid exchange with the surrounding environment. Therefore, accurate modeling of the intervertebral disc behavior should not only take into account the non-linear hyperelastic response but also consider the regional and the time-dependency of the annulus tissue. Such considerations are mandatory to achieve physically realistic comparisons of any constructed model with experimental data from the literature that are often made under different testing conditions, different strain rates and established on specimens extracted from different regions of the disc.

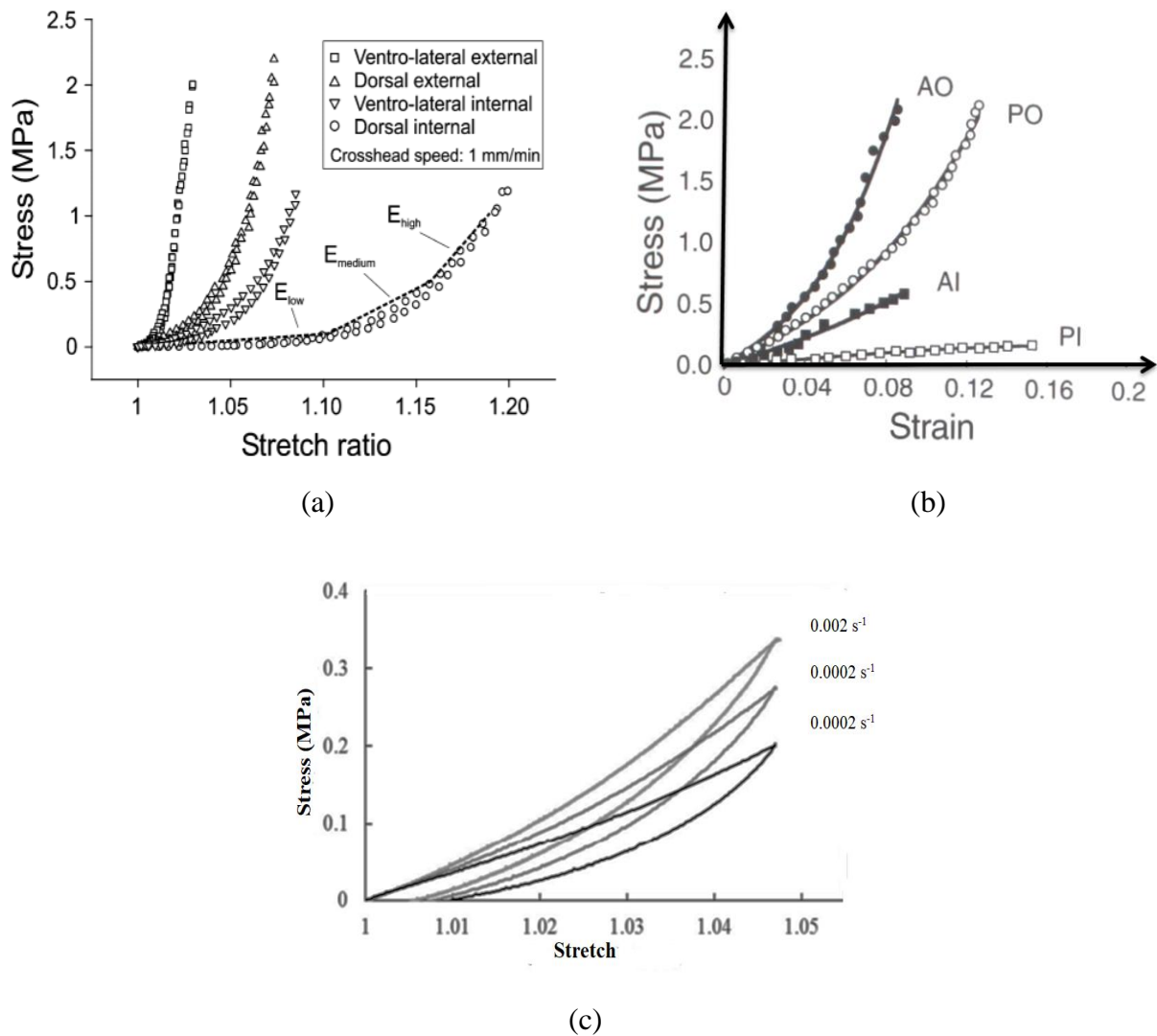


Figure I.5. Uniaxial stress-stretch response of annulus specimens extracted from different radial and circumferential regions of the intervertebral disc (Anterior ventral outer (AO), Anterior ventral inner (AI), Posterior dorsal outer (PO), Posterior dorsal inner (PI)) at the scale of (a) single lamellar specimen (Holzapfel et al., 2005), (b) multi-lamellar specimen (Ebara et al., 1996), (c) strain rate effect (Derrouiche et al., 2020).

I.2.2. Multi-axiality

The intervertebral disc is subjected to multi-axial loads under the different body movements. Under compression, the annulus fibrosus is loaded axially by the adjacent vertebrae and radially by the nucleus. It is subjected to shearing strains under flexion, extension and torsion

(Jacobs et al., 2011; O’Connell et al., 2012). Producing the local axial and multi-axial response of each part of the disc by means of the same constitutive equations and the same model parameters was estimated to be not possible by many papers in the literature (Bass et al., 2004; O’Connell et al., 2012). This remark raises an open question about the missing link between the uniaxial and multi-axial response of the disc that would allow a complete general representation of the intervertebral disc behavior that will be discussed in details throughout the present thesis.

I.2.3. Interlamellar-induced volumetric behavior

The intervertebral disc has a very unique volumetric response. Under uniaxial circumferential tension tests established experimentally on specimens extracted from different regions of the annulus, the later was found to swell in the radial direction showing positive Poisson’s ratio values and to highly retract in the axial direction showing large Poisson’s ratios that exceed 1 (Baldit et al., 2014; Derrouiche et al., 2020). Actually most of advanced disc models consider the effect of the osmotic pressure on the internal disc stresses but not on its volumetric strain which could largely affect the multi-axial study of the disc response. The role of the annulus fibrosus interlamellar zones in the disc mechanics in general and in the time-dependent transversal response particularly has been only revealed recently (Tavakoli et al., 2016, 2017, 2018; Derrouiche et al., 2019a). Before, they were only viewed as sliding zones between the lamellae with either cohesive or non-cohesive features (Labus et al., 2014; Adam et al., 2015; Mengoni et al., 2015). There consideration as active physical zones by a model integrating the interlamellar swelling effects to the lamellar structure of the intervertebral disc would allow a correct representation of the volumetric strain and the three-dimensional time-dependent behavior of the disc.

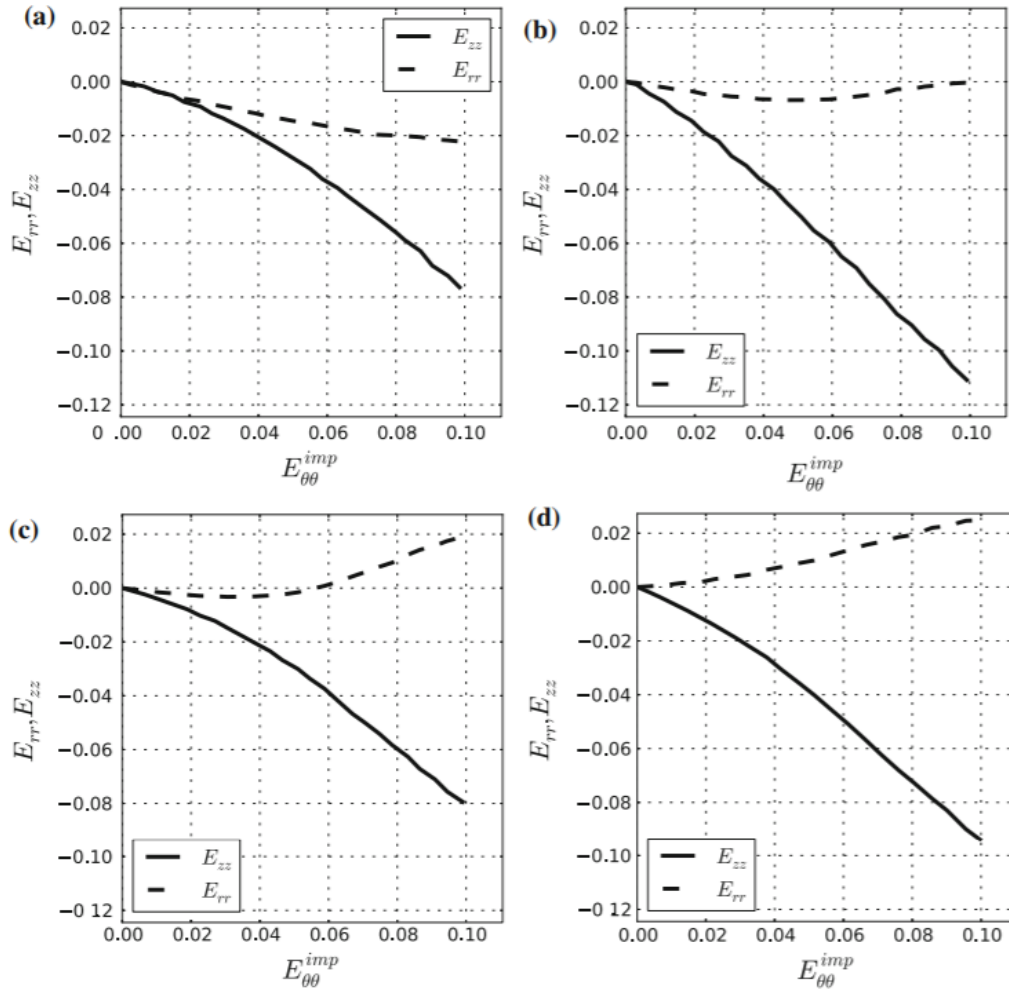


Figure I.6. Four different typical axial E_{zz} and radial E_{rr} transversal strain curves function of the circumferential strain $E_{\theta\theta}$ (Baldit et al., 2014).

I.2.4. Intervertebral disc health state and aging

The intervertebral disc behavior depends on its health state that could vary under biological effects, mechanical effects, or both. With age, the different microstructural components degrade and their contents alter (Brickley-Parsons and Glimcher, 1984; Koeller et al., 1984) inducing progressive changes in the disc biomechanics and morphology which could weaken certain regions of the disc and create micro-cracks (Vo et al., 2016), see Figure I.7. In parallel, excessive efforts and high supported loads affect these weak regions increasing local damages, causing back pain and sometimes lead to disc herniation. Hence, for the

construction of a new intervertebral disc model, the health state and the age of the studied disc should be taken into while choosing material parameters, microstructural components contents and disc geometry in order to achieve a correct prediction of the real disc response.

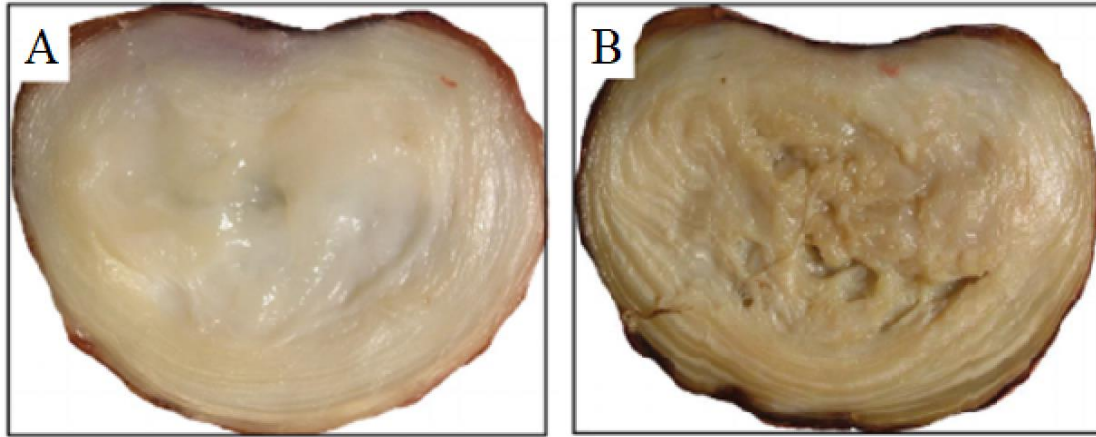


Figure I.7. Comparison between (A) healthy young disc and (B) degenerated old disc (Vo et al., 2016).

I.3. Constitutive modeling of the disc behavior

Many models were proposed in the literature trying to reproduce the mechanical response of the intervertebral disc under uniaxial and multi-axial loadings. Most of these models are different in their vision of the soft tissue, there adopted approach and the degree of simplifications of the disc geometry and structure. A description of the different existing models classified according to their specificities as well as their strong and weak points are discussed in details in the following sub-sections.

I.3.1. Microstructure features

The disc tissue is constituted of a multi-network superposition of the collagen fibers networks constituted principally of oriented type I collagen fibers, randomly oriented type II collagen fibers, negatively charged proteoglycans network and water. Each component of the disc

microstructure contributes to the disc mechanics. The first models considered the different components to have a perfect elastic or hyperelastic response neglecting the time-dependent conduct of the tissue observed under cyclic loadings or relaxation tests. However, the experimental stress-strain curves of stretched annulus specimens and functional spine units show a hysteric cyclic response (Derrouiche et al., 2019b) and significant strain-rate dependency (Holzapfel et al., 2005) proving the time-dependency of the intervertebral disc tissue response. The latter is associated to the fluid transfer inside the disc (Cheung et al., 2003; Jacobs et al., 2014) as well as the intrinsic viscosity of the disc tissue. The origin of this intrinsic viscosity is still unknown. It was sometimes related to the collagen fibers (Wilson et al., 2004; Schroeder et al., 2006) but recently many experimental contributions supported its relation to the non-fibrillar extracellular matrix. In (Tavakoli and Costi, 2018) it was found that the non-fibrillar interlamellar zones are strain dependent and have high ability of energy absorption which confirms the relation between the tissue viscoelasticity and the extracellular matrix.

I.3.2. Number of phases

The intervertebral disc is a multi-phasic tissue that is composed of a reinforced negatively charged solid phase and a fluid phase (Klisch and Lotz 2000; Ayotte et al., 2000). The consideration of the two phases is essential for reproducing a correct volumetric response of the disc. Many models ignored the effect of the fluid phase (Elliott and Setton, 2000; Holzapfel and Gasser, 2001; Markert et al., 2005; Balzani et al., 2006) which will affect the multi-axial response of the disc. Such simplification would not allow giving physical explanations of the computed behavior. The role of proteoglycans negative charges and osmotic effect in the tissue swelling was then considered by extended biphasic models giving a more accurate vision of the disc response under mechanical deformation and the interaction

with the surrounding environment (Wilson et al., 2005; Ehlers et al., 2009). Some triphasic and quadriphasic models were also proposed in the literature (Frijns et al., 1997; Huyghe and Janssen, 1997; Van Loon et al., 2003). However, these models present only a different description of the existing extended biphasic models by representing the fluid positives ions and the proteoglycans negatives ions as separated phases of the material.

I.3.3. Disc heterogeneity and regional dependency

The intervertebral disc is mainly divided to a nucleus pulposus surrounded by the annulus fibrosus which is essential due to their completely different response. The local annulus behavior as well should be taken into account by dividing the disc to different circumferential and radial zones with different mechanical properties for each zone (del Palomar et al., 2008; Eberlein et al., 2004; Jaramillo et al., 2015) or by considering the radial and circumferential variation of the disc microstructural components such as water and collagen fibers.

I.3.4. Disc geometry

The intervertebral disc geometry is very complex due to its non-symmetrical periphery and thickness that is higher in the anterior side compared to the posterior side of the disc. For simplicity and in order to reduce calculation time and avoid contact problems with the adjacent vertebrae during numerical computations, many contributions modeled the disc as a perfect cylinder or supposed regular thickness for the different disc regions (Massey et al., 2012) and others modeled only the half or the quarter of the disc using many non-realistic symmetry assumptions (Laible et al., 1993; Lee et al., 2000; Schroeder et al., 2006, 2010; Jackson et al., 2011) which would affect the local fields predictions established at the scale of complete disc or complete spinal structure.

I.3.5. Animal models

The availability of human cadavers needed to establish the different biomechanical experiments is very limited and highly restricted. As a consequence, a lot of researchers performed their experiments on animal spines such as bovine and sheep spines and construct numerical models based on them (Schmidt et al., 2013; Adam et al., 2015; Calvo-Echenique et al., 2018; Dusfour et al., 2020). Although differences exist between disc geometry, size and microstructural contents (see Figure I.8), a high number of these animal models were found sufficient to give the same trends of the human disc and afford important explanations about the disc mechanical response. However, these animal models remain not very accurate and cannot give quantitative predictions of the human disc mechanics.

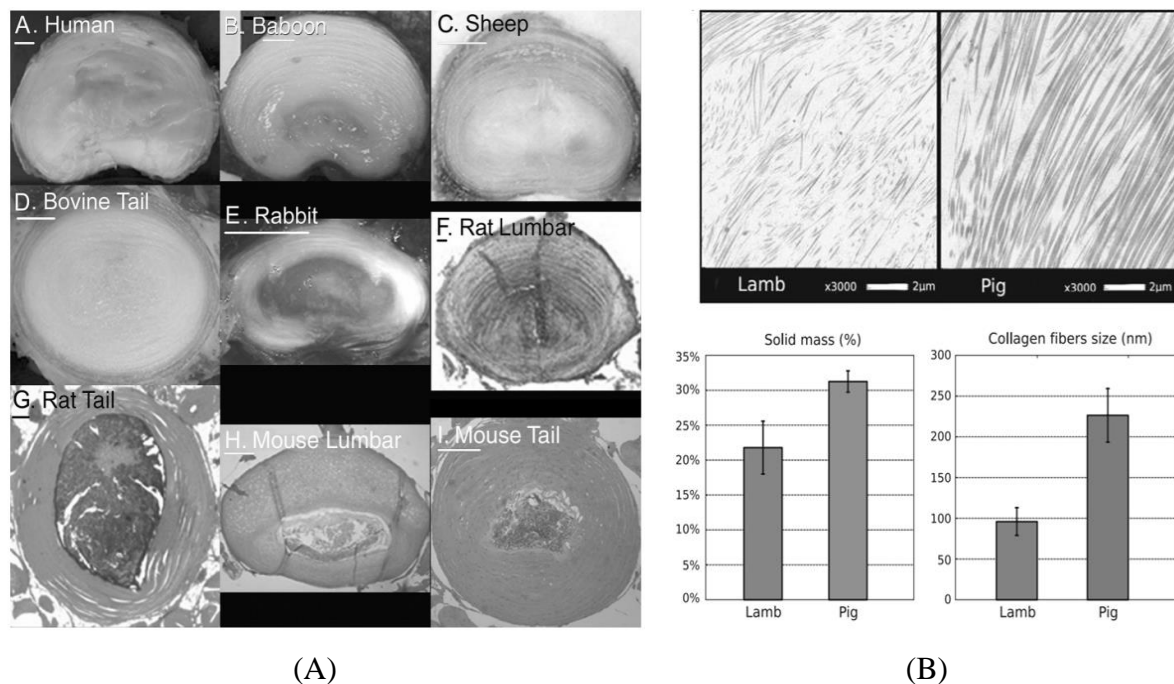


Figure I.8. Comparison between animal discs: (A) disc geometry (O'Connell et al., 2007) and (B) microstructure (Ambard and Cherblanc, 2009).

I.3.6. Summary of disc models of the last two decades

Table I.1. Intervertebral disc models developed between 2001 and 2020 (Formulation: the article focuses on the model analytical formulation, 1D or 2D simplified finite element calculations; Specimen: the geometry based on experiments established on specimen extracted from the disc volume).

| Model | Single phase model (No fluid effect) | Biphasic, triphasic or quadriphasic, models & osmotic effect | Intrinsic viscosity | Accurate complete disc geometry | Accurate radial & circ. regional dependency of the disc | Human model | Animal model | ILM zones (As sliding zones) | ILM zones & volumetric response |
|-------------------------------------|--------------------------------------|--|---------------------|---------------------------------|---|-------------|--------------|------------------------------|---------------------------------|
| Holzappel and Gasser (2001) | X Formulation | | X | | | | | | |
| Cheung et al. (2003) | | X | | X | | X | | | |
| Van Loon et al. (2003) | | X Formulation | | | | | | | |
| Eberlein et al. (2004) | X | | | X | X | X | | | |
| Noailly et al. (2005) | X | | | X | | X | | | |
| Guo et al. (2006) | X Shear formulation | | | | | | | | |
| Schroeder et al. (2006, 2010) | | X | X | | | X | | | |
| Guerin and Elliott (2007) | X | | | Specimen | | X | | | |
| Renner et al. (2007) | X | | | X | | X | | | |
| Yao and Guo (2007) | | X | | | | X | | | |
| del Palomar et al. (2008) | X | | | X | X | X | | | |
| Ehlers et al. (2009) | | X | X | | X | X | | | |
| Massey et al. (2012) | | X | | | | X | | | |
| O'connell et al. (2012) | X Biaxial & shear formulation | | | | | X | | | |
| Schmidt et al. (2013) | | X | | | | X | X | | |
| Malandrino et al. (2013) | | X | | X | X | X | | | |
| Cegonino et al. (2014) | | X | | | | X | | | |
| Jacobs et al. (2014) | | X | | X | | X | | | |
| Labus et al. (2014) | X | | | Specimen | | | | X | |
| Jaramillo et al. (2015) | X | | | X | X | X | | | |
| Mengoni et al. (2015, 2016) | X | | | Specimen | | | X | | |
| Adam et al. (2015) | X | | | | | | X | X | |
| Calvo-Echenique et al. (2018) | X | | X | | | | X | | |
| Derrouiche et al. (2019a) | | X | X | Specimen | | | X | X | X |
| Chetoui et al. (2019) | | X | | | | | X | | |
| Dusfour et al. (2020) | X | | | Specimen | | | X | | |
| The current thesis objective | | X | X | X | X | X | X | X | X |

References

- Adam, C., Rouch, P., Skalli, W., 2015. Inter-lamellar shear resistance confers compressive stiffness in the intervertebral disc: an image-based modelling study on the bovine caudal disc. *Journal of Biomechanics* 48, 4303-4308
- Adams, M.A., Lama, P., Zehra, U., Dolan, P., 2014. Why do some intervertebral discs degenerate, when others (in the same spine) do not? *Clinical Anatomy* 28, 195-204.
- Ambard, D., Cherblanc, F., 2009. Mechanical behavior of annulus fibrosus: a microstructural model of fibers reorientation. *Annals of Biomedical Engineering* 37, 2256-2265.
- Ayotte, D.C., Ito, K., Perren, S.M., Tepic, S., 2000. Direction-dependent constriction flow in a poroelastic solid: the intervertebral disc valve. *Journal of Biomechanical Engineering* 122, 587-593.
- Baldit, A., Ambard, D., Cherblanc, F., Royer, P., 2014. Experimental analysis of the transverse mechanical behaviour of annulus fibrosus tissue. *Biomechanics and Modeling in Mechanobiology* 13, 643-652.
- Balzani, D., Neff, P., Schroder, J., Holzapfel, G.A., 2006. A polyconvex framework for soft biological tissues. Adjustment to experimental data. *International Journal of Solids and Structures* 43, 6052-6070.
- Bass, E.C., Ashford, F.A., Segal, M.R., Lotz, J.C., 2004. Biaxial testing of human annulus fibrosus and its implications for a constitutive formulation. *Annals of Biomedical Engineering* 32, 1231-1242.
- Brickley-Parsons, D., Glimcher, M.J., 1984. Is the chemistry of collagen in intervertebral discs an expression of Wolff's Law? A study of the human lumbar spine. *Spine* 9, 148-163.
- Buckwalter, J.A., Pedrini-Mille, A., Pedrini V., Tudisco, C., 1985. Proteoglycans of human infant intervertebral disc. Electron microscopic and biochemical studies. *The Journal of Bone and Joint Surgery* 67, 284-294.
- Buckwalter, J.A., 1995. Aging and degeneration of the human intervertebral disc. *Spine* 20, 1307-1314.
- Calvo-Echenique, A., Cegonino, J., Correa-Martin, L., Bances, L., Palomar, A.P., 2018. Intervertebral disc degeneration: an experimental and numerical study using a rabbit model. *Medical & Biological Engineering & Computing* 56, 865-877.
- Cegonino, J., Moramarco, V., Pappalettere, C., Palomar, A.P., 2014. A constitutive model for the annulus of human intervertebral disc: Implications for developing a degeneration model and its influence on lumbar spine functioning. *Journal of Applied Mathematics*, 658719.
- Chetoui, M.A., Boiron, O., Ghiss, M., Dogui, A., Deplano, V., 2019. Assessment of intervertebral disc degeneration-related properties using finite element models based on ρ_H -weighted MRI data. *Biomechanics and Modeling in Mechanobiology* 18, 17-28.
- Cheung, J.T., Zhang, M., Chow, D.H., 2003. Biomechanical responses of the intervertebral joints to static and vibrational loading: a finite element study. *Clinical Biomechanics* 18, 790-799.
- del Palomar, A.P., Calvo, B., Doblare, M., 2008. An accurate finite element model of the cervical spine under quasi-static loading. *Journal of Biomechanics* 41, 523-531.

- Derrouiche, A., Zaïri, F., Zaïri, F., 2019a. A chemo-mechanical model for osmo-inelastic effects in the annulus fibrosus. *Biomechanics and Modeling in Mechanobiology* 18, 1773-1790.
- Derrouiche, A., Zaouali, A., Zaïri, F., Ismail, J., Chaabane, M., Qu, Z., Zaïri, F., 2019b. Osmoinelastic response of the intervertebral disc. *Proceedings of the Institution of Mechanical Engineers. Part H: Journal of Engineering in Medicine* 233, 332-341.
- Derrouiche, A., Karoui, A., Zaïri, F., Ismail, J., Qu, Z., Chaabane, M., Zaïri, F., 2020. The two Poisson's ratios in annulus fibrosus: relation with the osmo-inelastic features. *Mechanics of Soft Materials* 2, 1.
- Dusfour, G., LeFloc'h, S., Canadas, P., Ambard, D., 2020. Heterogeneous mechanical hyperelastic behavior in the porcine annulus fibrosus explained by fiber orientation: an experimental and numerical approach. *Journal of the Mechanical Behavior of Biomedical Materials* 104, 103672.
- Ebara, S., Iatridis, J.C., Setton, L.A., Foster, R.J., Mow, V.C., Weidenbaum, M., 1996. Tensile properties of nondegenerate human lumbar annulus fibrosus. *Spine* 21, 452-461.
- Eberlein, R., Holzapfel, G., Fröhlich, M., 2004. Multi-segment FEA of the human lumbar spine including the heterogeneity of the annulus fibrosus. *Computational Mechanics* 34, 147-163.
- Ehlers, W., Karajan, N., Markert, B., 2009. An extended biphasic model for charged hydrated tissues with application to the intervertebral disc. *Biomechanics and Modeling in Mechanobiology* 8, 233-251.
- Elliott, D.M., Setton, L.A., 2001. Anisotropic and inhomogeneous tensile behavior of the human annulus fibrosus: experimental measurement and material model predictions. *Journal of Biomechanical Engineering* 123, 256-263.
- Frijns, A.J.H., Huyghe, J.M., Janssen, J.D., 1997. A validation of the quadriphasic mixture theory for intervertebral disc tissue. *International Journal of Engineering Science* 35, 1419-1429.
- Guerin, H.A.L., Elliott, D.M., 2007. Quantifying the contributions of structure to annulus fibrosus mechanical function using a nonlinear, anisotropic, hyperelastic model. *Journal of Orthopaedic Research* 25, 508-516.
- Guo, Z.Y., Peng, X.Q., Moran, B. 2006. A composites-based hyperelastic constitutive model for soft tissue with application to the human annulus fibrosus. *Journal of the Mechanics and Physics of Solids* 54, 1952-1971.
- Holzapfel, G.A., Gasser, T.C., 2001. A viscoelastic model for fiber-reinforced composites at finite strains: continuum basis, computational aspects and applications. *Computer Methods in Applied Mechanics and Engineering* 190, 4379-4403.
- Holzapfel, G.A., Schulze-Bauer, C.A.J., Feigl, G., Regitnig, P., 2005. Single lamellar mechanics of the human lumbar annulus fibrosus. *Biomechanics and Modeling in Mechanobiology* 3, 125-140.
- Huyghe, J.M., Janssen, J.D., 1997. Quadriphasic mechanics of swelling incompressible porous media. *International Journal of Engineering Science* 35, 793-802.
- Jackson, A.R., Huang, C.Y., Gu, W.Y., 2011. Effect of endplate calcification and mechanical deformation on the distribution of glucose in intervertebral disc: a 3D finite element study, *Computer Methods in Biomechanics and Biomedical Engineering* 14, 195-204.

- Jacobs, N.T., Smith, L.J., Han, W.M., Morelli, J., Yoder, J.H., Elliott, D.M., 2011. Effect of orientation and targeted extracellular matrix degradation on the shear mechanical properties of the annulus fibrosus. *Journal of the Mechanical Behavior of Biomedical Materials* 4, 1611-1619.
- Jacobs, N.T., Cortes, D.H., Peloquin, J.M., Vresilovic, E.J., Elliott, D.M., 2014. Validation and application of an intervertebral disc finite element model utilizing independently constructed tissue-level constitutive formulations that are nonlinear, anisotropic, and time-dependent. *Journal of Biomechanics* 47, 2540-2546.
- Jaramillo, H.E., Gomez, L., Garcia, J.J., 2015. A finite element model of the L4-L5-S1 human spine segment including the heterogeneity and anisotropy of the discs. *Acta of Bioengineering and Biomechanics* 17, 15-24.
- Klisch, S.M., Lotz, J.C., 2000. A special theory of biphasic mixtures and experimental results for human annulus fibrosus tested in confined compression. *Journal of Biomechanical Engineering* 122, 180-188.
- Koeller, W., Funke, F., Hartmann, F., 1984. Biomechanical behaviour of human intervertebral discs subjected to long lasting axial loading. *Biorheology* 21, 675-86.
- Labus, K.M., Han, S.K., Hsieh, A.H., Puttlitz, C.M., 2014. A computational model to describe the regional interlamellar shear of the annulus fibrosus. *Journal of Biomechanical Engineering* 136, 051009.
- Laible, J.P., Pflaster, D.S., Krag, M.H., Simon, B.R., Haugh, L.D., 1993. A poroelastic-swelling finite element model with application to the intervertebral disc. *Spine* 18, 659-670.
- Lee, C.K., Kim, Y.E., Lee, C.S., Hong, Y.M., Juang, J.M., Goel V.K., 2000. Impact response of the intervertebral disc in a finite-element model. *Spine* 25, 2431-2439.
- Malandrino, A., Noailly, J., Lacroix, D., 2013. Regional annulus fibre orientations used as a tool for the calibration of lumbar intervertebral disc finite element models. *Computer Methods in Biomechanics and Biomedical Engineering* 16, 923-928.
- Markert, B., Ehlers, W., Karajan, N., 2005. A general polyconvex strain energy function for fiber-reinforced materials. *Proceedings in Applied Mathematics and Mechanics* 5, 245-246.
- Massey, C.J., van Donkelaar, C.C., Vresilovic, E., Zavaliangos, A., Marcolongo, M., 2012. Effects of aging and degeneration on the human intervertebral disc during the diurnal cycle: a finite element study. *Journal of Orthopaedic Research* 30, 122-128.
- Maroudas, A., 1970. Distribution and diffusion of solutes in articular cartilage. *Biophysical Journal* 10, 365-379.
- Mengoni, M., Luxmoore, B.J., Wijayathunga, V.N., Jones, A.C. Broom, N.D., Wilcox, R.K., 2015. Derivation of inter-lamellar behaviour of the intervertebral disc annulus. *Journal of the Mechanical Behavior of Biomedical Materials* 48, 164-172.
- Noailly, J., Lacroix, D., Planell, J.A. 2005. Finite element study of a novel intervertebral disc substitute, *Spine* 30, 2257-2264.
- O'Connell, G.D., Vresilovic, E.J., Elliott, D.M., 2007. Comparison of animals used in disc research to human lumbar disc geometry. *Spine* 32, 328-333.
- O'Connell, G.D., Sen, S., Elliott, D.M., 2012. Human annulus fibrosus material properties from biaxial testing and constitutive modeling are altered with degeneration. *Biomechanics and Modeling in Mechanobiology* 11, 493-503.

- Riches, P.E., Dhillon, N., Lotz, J., Woods, A.W., McNally, D.S., 2002. The internal mechanics of the intervertebral disc under cyclic loading. *Journal of Biomechanics* 35, 1263-1271.
- Rubin, D.I., 2017. Epidemiology and risk factors for spine pain. *Neurologic Clinics* 25, 353-371.
- Schmidt, H., Reitmaier, S., 2013. Is the ovine intervertebral disc a small human one?: A finite element model study. *Journal of the Mechanical Behavior of Biomedical Materials* 17, 229-241.
- Schroeder, Y., Wilson W., Huyghe, J.M., Baaijens, F.P.T., 2006. Osmoviscoelastic finite element model of the intervertebral disc. *European Spine Journal* 15, 361-371.
- Schroeder, Y., Huyghe, J.M., van Donkelaar, C.C., Ito, K., 2010. A biochemical/biophysical 3D FE intervertebral disc model. *Biomechanics and Modeling in Mechanobiology* 9, 641-650.
- Tavakoli, J., Elliott, D.M., Costi, J.J., 2016. Structure and mechanical function of the inter-lamellar matrix of the annulus fibrosus in the disc. *Journal of Orthopaedic Research* 34, 1307-1315.
- Tavakoli, J., Elliott, D.M., Costi, J.J., 2017. The ultra-structural organization of the elastic network in the intra- and inter-lamellar matrix of the intervertebral disc. *Acta Biomaterialia* 58, 269-277.
- Tavakoli, J., Costi, J.J., 2018. New findings confirm the viscoelastic behaviour of the inter-lamellar matrix of the disc annulus fibrosus in radial and circumferential directions of loading. *Acta Biomaterialia* 71, 411-419.
- Urban, J.P., McMullin, J.F., 1985. Swelling pressure of the intervertebral disc: influence of proteoglycan and collagen contents. *Biorheology* 22, 145-157.
- Van Loon, R., Huyghe, J.M., Wijlaars, M.W., Baaijens, F.P.T., 2003. 3D FE implementation of an incompressible quadriphasic mixture model. *International Journal for Numerical Methods in Engineering* 57, 1243-1258.
- Vo, N.V., Hartman, R.A., Patil, P.R., Risbud, M.V., Kletsas, D., Iatridis, J.C., Hoyland, J.A., Le Maitre, C.L., Sowa, G.A., Kang, J.D., 2016. Molecular mechanisms of biological aging in intervertebral discs. *Journal of Orthopaedic Research* 34, 1289-1306.
- Wills, C.R., Malandrino, A., van Rijsbergen, M., Lacroix, D., Ito, K., Nouailly, G. 2016. Simulating the sensitivity of cell nutritive environment to composition changes within the intervertebral disc. *Journal of the Mechanics and Physics of Solids* 90, 108-123.
- Wilson, W., van Donkelaar, C.C., van Rietbergen, C., Ito, K., Huiskes, R., 2004. Stresses in the local collagen network of articular cartilage: a poroviscoelastic fibril-reinforced finite element study. *Journal of Biomechanics* 37, 357-366.
- Wilson, W., van Donkelaar, C.C., Huyghe, J.M., 2005. A comparison between mechano-electrochemical and biphasic swelling theories for soft hydrated tissues. *Journal of Biomechanical Engineering* 127, 158-165.
- Yao, H., Gu, W.Y., 2007. Three-dimensional inhomogeneous triphasic finite element analysis of physical signals and solute transport in human intervertebral disc under axial compression. *Journal of Biomechanics* 40, 2071-2077.

Chapter II

Interlamellar-induced time-dependent response of intervertebral disc annulus: a microstructure-based chemo-viscoelastic model¹

Abstract

The annulus fibrosus of the intervertebral disc exhibits an unusual transversal behavior for which a constitutive representation that considers as well regional effect, chemical sensitivity and time-dependency has not yet been developed, and it is hence the aim of the present contribution. A physically-based model is proposed by introducing a free energy function that takes into account the actual disc annulus structure in relation with the surrounding biochemical environment. The response is assumed to be dominated by the viscoelastic contribution of the extracellular matrix, the elastic contribution of the oriented collagen fibers and the osmo-induced volumetric contribution of the internal fluid content variation. The regional dependence of the disc annulus response due to variation in fibers content/orientation allows a micromechanical treatment of the soft tissue. A finite element model of the annulus specimen is designed while taking into consideration the ‘interlamellar’ ground substance zone between lamellae of the layered soft tissue. The kinetics is designed using full-field strain measurements performed under different osmotic conditions and two disc annulus regions. The time-dependency of the tissue response is reported on stress-free volumetric changes, on hysteretic stress and transversal strains during quasi-static stretching at different strain-rates and on their temporal changes during an interrupted stretching. Considering the effective contributions of the internal fluid transfer and the extracellular matrix viscosity, the microstructure-based chemo-mechanical model is found able to successfully reproduce the significant features of the macro-response and the unusual transversal behavior including the strong regional dependency from inner to outer parts of the disc: Poisson’s ratio lesser than 0 (auxetic) in lamellae plane, higher than 0.5 in fibers plane, and their temporal changes towards usual values (between 0 and 0.5) at chemo-mechanical equilibrium. The underlying time-dependent mechanisms occurring in the tissue are analyzed via the local numerical fields and important insights about the effective role of the interlamellar zone are revealed for the different disc localizations.

Keywords: Annulus fibrosus; Microstructure; Extracellular matrix viscosity; Osmo-induced transversal response; Regional dependency; Finite element computation.

¹ *This chapter is based on the following article: Kandil, K., Zaïri, F., Derrouiche, A., Messenger, T., Zaïri, F., 2019. Interlamellar-induced time-dependent response of intervertebral disc annulus: a microstructure-based chemo-viscoelastic model. Acta Biomaterialia 100, 75-91.*

II.1. Partial introduction

As the main soft component of the spine, the intervertebral disc (IVD) is probably the most extraordinary tissue that the nature produces, mainly for its unusual time-dependent properties strongly influenced by the biochemical environment and the mechanical loading (Baldit et al., 2014; Derrouiche et al., 2018, 2019a). Basically, it is well-known that the nucleus, situated in the core of the IVD, is surrounded by concentric fiber-reinforced lamellae termed annulus fibrosus (AF). The latter opposes nucleus swelling which in turn exposes it to tensile stresses in the circumferential direction of the IVD. As a fiber-matrix composite, the AF extracellular matrix (ECM) is reinforced by stiff oriented type I collagen fibers (CFs) with a circumferential and radial variation in content and orientation (Inoue and Takeda, 1975; Eyre, 1979; Klein and Hukins, 1982; Cassidy et al., 1989) resulting in a regional dependency of the mechanical properties (Skaggs et al., 1994; Ebara et al., 1996; Holzapfel et al., 2005; Michalek et al., 2009; Newell et al., 2017). Non-oriented type II CFs, elastin fibers and negatively charged proteoglycans (PGs) are the main constituents of the ECM. The concentration of these constituents differs also locally from a disc region to another. As a vital physiological function of the IVD (Maroudas, 1970), the negatively charged PGs react with the mobile ions of the physiological fluid resulting in an internal osmotic pressure. The intrinsic viscosity is also a contributor of the IVD response in a certain extent but its origin is still largely misunderstood (Emanuel et al., 2018; Derrouiche et al., 2019b). Nonetheless, it may be attributed to the individual constituent, either oriented CFs (Wilson et al., 2004; Schroeder et al., 2006) or non-oriented CFs inside ECM (Ehlers et al., 2009), their rearrangement during the loading and their interactions. The time-dependent response is therefore due to the fluid transfer inside the soft tissue and the viscous effects (Iatridis et al., 1996).

The development of constitutive models is of prime importance to better understand the IVD biomechanics. The earliest contributions tried to account for the explicit presence of oriented CFs in a numerical model of the IVD (Shirazi et al., 1984; Natarajan and Andersson, 1994). Later, continuum-based constitutive models were developed in the aim of capturing the anisotropic behavior of biological soft tissues regarded as fiber-matrix composites (Klisch and Lotz., 1999; Elliott and Setton, 2001; Holzapfel and Gasser, 2001; Schroeder and Neff, 2003; Wagner and Lotz; 2004; Peng et al., 2005; Balzani et al., 2006; Guo et al., 2006; Guerin and Elliott, 2007). Other constitutive models considered a biphasic solid-fluid representation to account for the internal fluid flow (Holmes and Mow, 1990; Argoubi and Shirazi-Adl, 1996; Li et al., 1999; Ayotte et al., 2000; Klisch and Lotz 2000; Riches et al., 2002; Ehlers et al., 2009). Nonetheless, the structural complexity of the tissue has only been appreciated through recent experimental contributions (Tavakoli et al., 2016) and presents a challenging task for the development of constitutive models. Indeed, when the interaction between layers is considered, the AF becomes a stratified composite, each anisotropic lamellar phase being interspaced by an interlamellar (ILM) ground substance zone. The ILM zone is a non-collagenous ECM constituted by negatively charged PGs and elastin fibers that act as bridging elements connecting the adjacent lamellae (Pezowicz et al., 2006; Yu et al., 2007; Tavakoli et al., 2016, 2017, 2018). The connection between lamellae and ILM zones, as well as the interaction with the surrounding biochemical environment, construct a unique material with “unexpected” time-dependent properties (Baldit et al., 2014; Derrouiche et al., 2019a). The latter is surely due to a complex interaction between intrinsic properties and fluid transfer through the layered tissue. Although the exact role of the ILM zone is not fully understood at the stratified scale (Tavakoli et al., 2016), it is well accepted that it ensures the structural integrity and the shearing resistance of the disc (Marchand and Ahmed, 1990; Nerurker et al., 2011; Gregory et al., 2012; Labus et al., 2014; Adam et al., 2015; Mengoni et al., 2015).

The formulation of a model that integrates the ILM zone, with a detailed knowledge of the separate and synergistic effects of the intrinsic properties of individual constituents, would certainly allow a better understanding of the disc biomechanics.

As far as we know, only Labus et al. (2014), Adam et al. (2015), Mengoni et al. (2015) and Derrouiche et al. (2019a) introduced the ILM zone in a numerical model of the IVD. In the models of Labus et al. (2014), Adam et al. (2015) and Mengoni et al. (2015) the ILM function is limited to a sliding zone with either cohesive or non-cohesive features. More recently, Derrouiche et al. (2019a) developed a model considering the ILM phase as the actuator of the chemical sensibility of the inelastic response of the annulus. In the adopted approach, the ILM zone is defined as the key element in the fluid transfer through the layered tissue and thus at the origin of the unusual transversal behavior. Although the model integrates the relationship between structural features and chemo-mechanical response, it is unable to predict this relationship for the whole disc. Due to the strong regional dependency of the disc properties, the development of a model accounting for microstructure and chemical sensitivity is a challenging task. To date, no model considering as well regional effect, chemical sensitivity and time-dependency of the unusual transversal behavior has been developed.

In this work, we formulate, identify and verify a new chemo-viscoelastic model based upon a microstructure-based approach to predict the regional dependency of the annulus response that is essential to predict the biomechanics of the whole disc including the tissue chemo-viscoelastic features. A two-scale strategy is used. Firstly, at the ECM scale, a constitutive model is formulated to account for the contribution of the ECM inelastic effects, the CFs-induced anisotropy and the fluid transfer by osmosis. By this way, the constitutive model considers as well the contributions of the osmo-induced volumetric changes and the intrinsic viscosity in the time-dependent behavior. Secondly, at the stratified scale, a numerical model of stratified AF is designed. The constitutive model, fully three-dimensional and implemented

into a computer code, is used to represent the response of the different layers of AF including collagenous lamellae and non-collagenous ILM zones. The developed microstructure-based chemo-mechanical approach provides important insights about the origin of the time-dependent phenomena in disc annulus, essential for understanding disc functionality. The time-dependency of the chemo-mechanical response is reported on stress-free volumetric changes, on hysteretic stress and transversal strains during quasi-static stretching at different strain-rates and on temporal changes of stress and transversal strains during an interrupted quasi-static stretching. The investigations are performed on two annulus regions and different osmotic conditions in the aim to establish the relation of the time-dependent features with microstructure and surrounding biochemical environment.

The following notation is used throughout the text. Tensors and vectors are denoted by normal boldfaced letters and italicized boldfaced letters, respectively, while scalars and individual components of vectors and tensors are denoted by normal italicized letters. The superposed dot designates the time derivative. The term tr denotes the trace. The superscript T indicates the transpose quantity. The prime denotes the deviatoric part.

II.2. A microstructure-based model

Figure II.1 presents a schematic view of the annulus microstructure for lamellar and ILM zones. The lamellar and ILM phases are reinforced and non-reinforced soft parts, respectively. The lamellar zone is regarded as a multiple-network ECM on which is superimposed regularly-oriented type I CFs: (i) network of negatively charged PGs, (ii) network of randomly oriented type II CFs and elastin (Tavakoli et al., 2016; Roughley, 2004). The ILM zone that inter-connects two adjacent lamellae is a non-collagenous ECM constituted by (i) negatively charged PGs on which are superimposed (ii) a network of elastin, microfibrils and radial cross-bridges (Pezowicz et al., 2006; Yu et al., 2007; Tavakoli et al.,

2016). The chemical response is governed by the negatively charged PGs attracting mobile ions and physiological fluid by osmotic effect.

Our approach considers two scales to deal with the hierarchical organization and the local fluid exchange in the soft tissue. At the ECM scale, a decomposition of the microstructure and of the effects (inelastic and osmotic) allows to associate each constituent to a constitutive relation. At the scale of the layered reinforced soft tissue (stratified scale), the ILM zone is explicitly considered in a computational model. In view of the complex microstructure, the description of the tissue is focalized on the interactions between the different constituents at the two scales in relation with the surrounding biochemical environment.

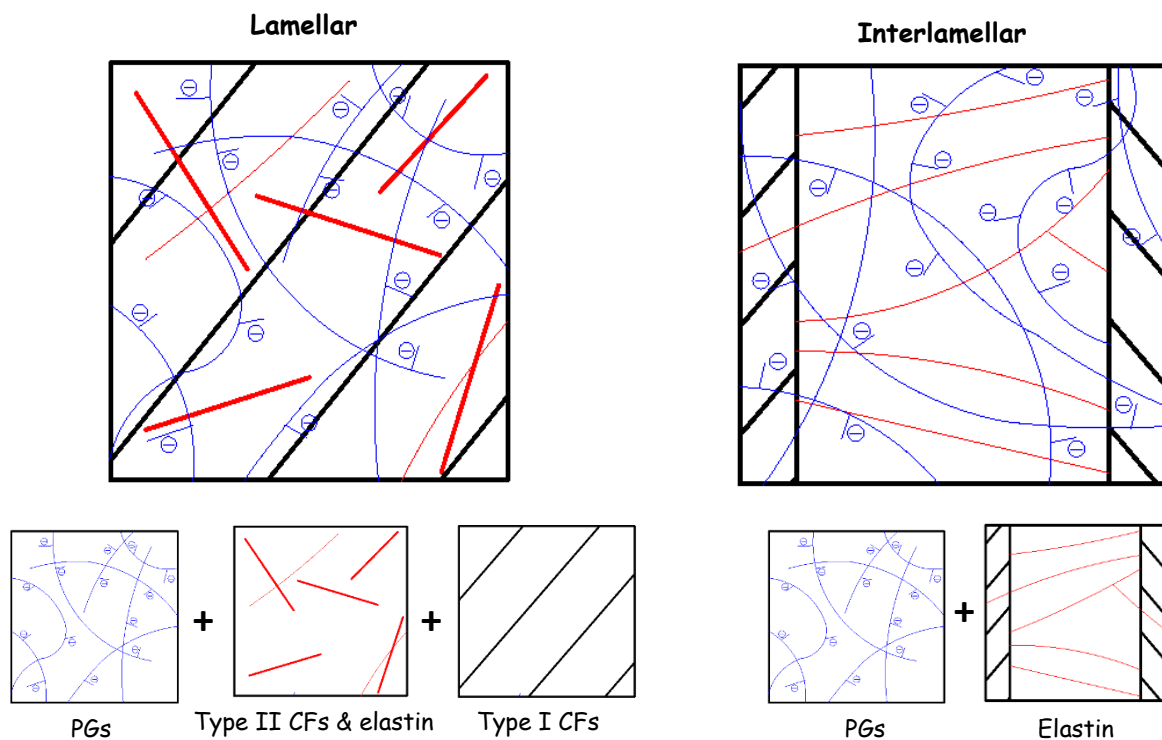


Figure II.1. Annulus microstructure: decomposition of lamellar and interlamellar zones.

II.2.1. At the ECM scale

II.2.1.1. Constitutive relations

This subsection describes the constitutive relations of the soft tissue response at the ECM scale, the interactions with the CFs as well as the biochemical coupling with the surrounding environment. The constitutive representation is based on the network decomposition of the two zones (see Figure II.1), and the equations are formulated within the framework of continuum mechanics. According to this framework, the transformation of a typical material point from an initial position \mathbf{X} in the initial configuration to a position \mathbf{x} in the current configuration is mapped by the deformation gradient $\mathbf{F} = \partial\mathbf{x}/\partial\mathbf{X}$. The Jacobian of the deformation gradient \mathbf{F} is $J = \det(\mathbf{F}) > 0$ and its time derivative is $\dot{\mathbf{F}} = \mathbf{L}\mathbf{F}$ in which $\mathbf{L} = \partial\mathbf{v}/\partial\mathbf{x}$ is the spatial velocity gradient with $\mathbf{v} = \partial\mathbf{x}/\partial t$. A basic statement of the finite-strain kinematics framework is the multiplicative decomposition of the deformation gradient in the aim to achieve any type of coupling. The chemo-viscoelastic modeling is based on a conceptual sequence of configurations as illustrated in Figure II.2. The deformation is split into chemical-induced volumetric and mechanical parts by introducing an intermediate virtual stress-free chemical configuration. The mechanical part is in turn split into elastic and viscous parts by considering an intermediate relaxed configuration during a spontaneous virtual elastic unloading.

The chemo-mechanical constitutive model is based on the free energy decomposition into the viscoelastic contribution ψ_{ECM} of the ECM, the elastic contribution ψ_{CF} of the oriented CFs and the chemical-induced volumetric contribution ψ_{chem} due to the internal fluid content variation:

$$\psi = \psi_{ECM} + \psi_{CF} + \psi_{chem} \quad (\text{II.1})$$

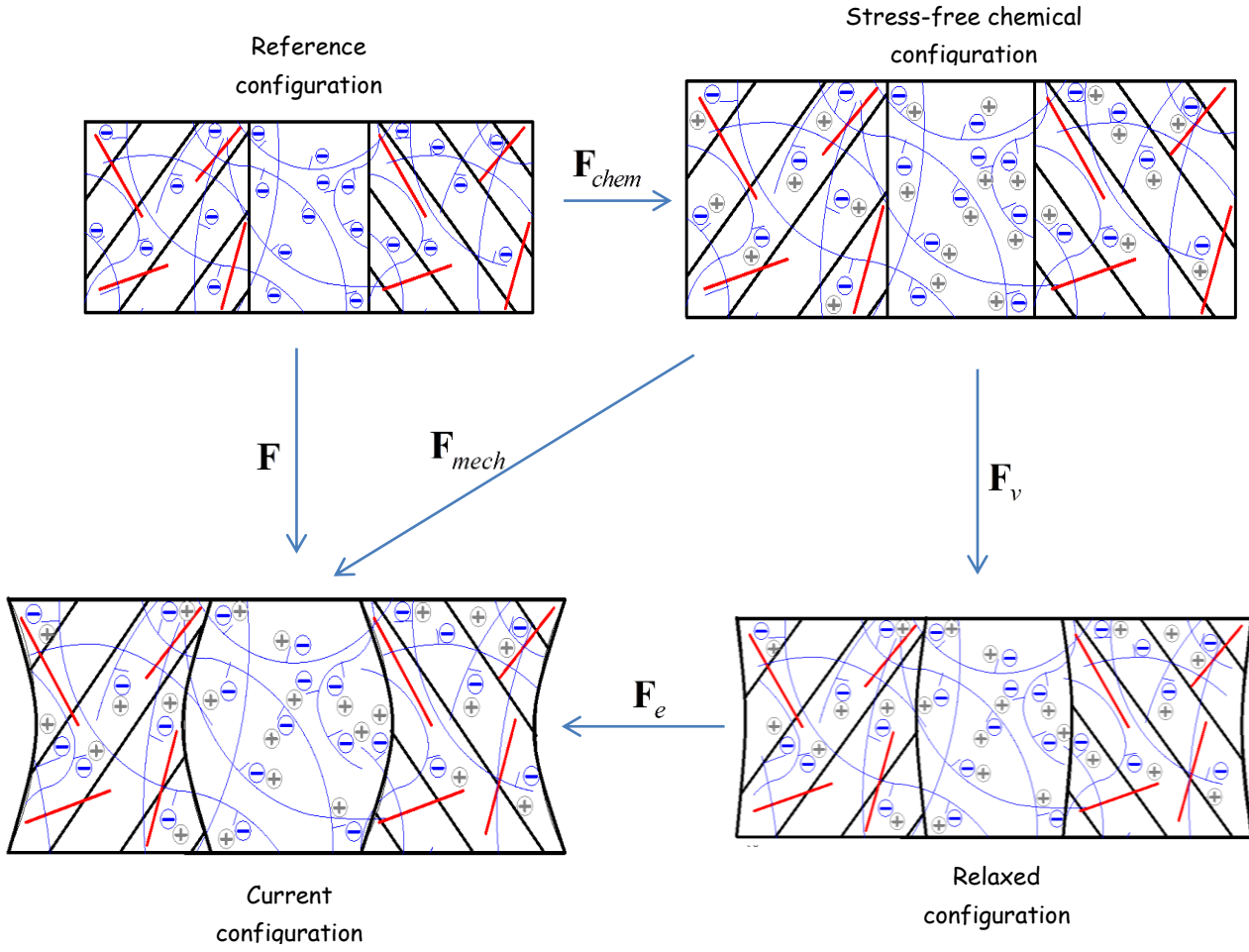


Figure II.2. Multiplicative decomposition of the deformation gradient.

The free energy function ψ_{ECM} of the ECM is the sum of a purely elastic part and an inelastic part both expressed using a Gent formulation (Gent, 1996):

$$\psi_{ECM} = -\frac{E}{6} I_1^{\max} \ln \left(1 - \frac{I_1 - 3}{I_1^{\max}} \right) - \frac{E_v}{6} I_{1v}^{\max} \ln \left(1 - \frac{I_{1e} - 3}{I_{1v}^{\max}} \right) \quad (\text{II.2})$$

in which E is the small-strain tensile modulus, I_1^{\max} is the limiting extensibility parameter, E_v and I_{1v}^{\max} are viscous parameters, the terms $I_1 = \text{tr} \mathbf{B}_{mech}$ and $I_{1e} = \text{tr} \mathbf{B}_e$ are the first invariants of the mechanical and elastic left Cauchy-Green strain tensors $\mathbf{B}_{mech} = \mathbf{F}_{mech} \mathbf{F}_{mech}^T$ and $\mathbf{B}_e = \mathbf{F}_e \mathbf{F}_e^T$, respectively, in which \mathbf{F}_{mech} is the mechanical deformation gradient tensor

multiplicatively split into an elastic part \mathbf{F}_e and a viscous part \mathbf{F}_v as: $\mathbf{F}_{mech} = \mathbf{F}_e \mathbf{F}_v$. The different parts can be further decomposed into a stretching part (right \mathbf{U} or left \mathbf{V}) and a rotation part \mathbf{R} : $\mathbf{F}_e = \mathbf{R}_e \mathbf{U}_e = \mathbf{V}_e \mathbf{R}_e$ and $\mathbf{F}_v = \mathbf{R}_v \mathbf{U}_v = \mathbf{V}_v \mathbf{R}_v$.

The type I CFs construct arranged bundles with a privileged orientation direction that alternate between successive lamellae (Inoue and Takeda, 1975; Eyre, 1979; Klein and Hukins, 1982; Cassidy et al., 1979). They may be described using the following free energy function ψ_{CF} (Cantournet et al., 2007):

$$\psi_{CF} = A_1 (\lambda_{CF}^2 - 1) + A_2 (\lambda_{CF}^2 - 1)^2 - 2A_1 \ln(\lambda_I^{x^2} \lambda_{II}^{y^2} \lambda_{III}^{z^2}) \quad (\text{II.3})$$

where A_1 and A_2 are parameters, λ_I , λ_{II} and λ_{III} are the stretches along the CFs principal axes:

$$\lambda_I = \sqrt{\mathbf{e}_1 \mathbf{C}_{mech} \mathbf{e}_1}, \quad \lambda_{II} = \sqrt{\mathbf{e}_2 \mathbf{C}_{mech} \mathbf{e}_2} \quad \text{and} \quad \lambda_{III} = \sqrt{\mathbf{e}_3 \mathbf{C}_{mech} \mathbf{e}_3} \quad (\text{II.4})$$

in which $\mathbf{C}_{mech} = \mathbf{F}_{mech}^T \mathbf{F}_{mech}$ is the mechanical right Cauchy-Green strain tensor.

The term λ_{CF} represents the stretch of CFs according to the direction given by the unit vector \mathbf{a} , see Figure II.4:

$$\lambda_{CF} = \sqrt{\mathbf{a} \mathbf{C}_{mech} \mathbf{a}}, \quad \mathbf{a} = x\mathbf{e}_1 + y\mathbf{e}_2 + z\mathbf{e}_3 \quad (\text{II.5})$$

The free energy function ψ_{chem} of the stress-free swelling due to internal fluid content variation may be expressed as (Miehe, 1995):

$$\psi_{chem} = \frac{1}{4} k (J^2 - 1 - 2 \ln J) \quad (\text{II.6})$$

in which k is the bulk modulus.

As illustrated in Figure II.2, the chemo-viscoelastic (volumetric-mechanical) coupling is realized by the multiplicative decomposition of the total deformation gradient \mathbf{F} into a mechanical (viscoelastic) part \mathbf{F}_{mech} and a chemical (volumetric) part \mathbf{F}_{chem} as: $\mathbf{F} = \mathbf{F}_{mech} \mathbf{F}_{chem}$.

The Jacobian of the mechanical deformation gradient tensor $\det(\mathbf{F}_{mech})$ is equal to unity due to mechanical incompressibility and the volumetric deformation gradient tensor is expressed as: $\mathbf{F}_{chem} = J^{1/3}\mathbf{I}$, \mathbf{I} being the unit tensor. The chemo-mechanical coupling is inserted into our constitutive theory by considering a chemical dependence of the Jacobian J . The chemical-induced effects are reproduced by conferring to it a dependence on the surrounding biochemical environment and the internal fluid content:

$$J = \hat{J}(c_{ext}, n_f) \quad (\text{II.7})$$

where c_{ext} and n_f are the external ionic and internal fluid concentrations.

The spatial velocity gradient tensor \mathbf{L} is described by:

$$\mathbf{L} = \underbrace{\dot{\mathbf{F}}_{mech} \mathbf{F}_{mech}^{-1}}_{\mathbf{L}_{mech}} + \underbrace{\mathbf{F}_{mech} \dot{\mathbf{F}}_{chem} \mathbf{F}_{chem}^{-1} \mathbf{F}_{mech}^{-1}}_{\mathbf{L}_{chem}} \quad (\text{II.8})$$

in which \mathbf{L}_{mech} is the stress-induced mechanical part and \mathbf{L}_{chem} is the stress-free chemical part expressed as:

$$\mathbf{L}_{mech} = \underbrace{\dot{\mathbf{F}}_e \mathbf{F}_e^{-1}}_{\mathbf{L}_e} + \underbrace{\mathbf{F}_e \dot{\mathbf{F}}_v \mathbf{F}_v^{-1} \mathbf{F}_e^{-1}}_{\mathbf{L}_v} \quad (\text{II.9})$$

$$\mathbf{L}_{chem} = \frac{j}{3J} \mathbf{I} \quad (\text{II.10})$$

The viscous part $\mathbf{L}_v = \mathbf{D}_v + \mathbf{W}_v$ of \mathbf{L}_{mech} is the sum of a viscous stretching rate tensor (symmetric part) $\mathbf{D}_v = (\mathbf{L}_v + \mathbf{L}_v^T)/2$ and a spin tensor (skew-symmetric part) $\mathbf{W}_v = (\mathbf{L}_v - \mathbf{L}_v^T)/2$.

The viscous part $\mathbf{L}_v = \mathbf{F}_e \dot{\mathbf{F}}_v \mathbf{F}_v^{-1} \mathbf{F}_e^{-1}$ is equivalent to the symmetric part \mathbf{D}_v while the common assumption of inelastic irrotationality $\mathbf{W}_v = \mathbf{0}$ is respected (Gurtin and Anand, 2005). The flow rule for \mathbf{D}_v is given by:

$$\mathbf{D}_v = \dot{\gamma}_v \frac{\boldsymbol{\sigma}'_v}{\sqrt{2} \|\boldsymbol{\sigma}_v\|}, \quad \|\boldsymbol{\sigma}_v\| = \sqrt{\frac{1}{2} \text{tr}(\boldsymbol{\sigma}'_v \boldsymbol{\sigma}'_v)} \quad (\text{II.11})$$

where $\|\boldsymbol{\sigma}_v\|$ is the effective value of the viscous Cauchy stress $\boldsymbol{\sigma}_v$ and $\dot{\gamma}_v$ is the accumulated viscous strain rate (Bergstrom and Boyce, 1998):

$$\dot{\gamma}_v = d \left| \sqrt{I_{1v}/3} - 1 \right|^{-m} \|\boldsymbol{\sigma}_v\|^n \quad (\text{II.12})$$

where d , m and n are viscous parameters related to the reorganization of the ECM network, and $I_{1v} = \text{tr} \mathbf{B}_v$ is the viscous first invariant, $\mathbf{B}_v = \mathbf{F}_v \mathbf{F}_v^T$ being the viscous left Cauchy-Green strain tensor.

The Cauchy stress tensor $\boldsymbol{\sigma}$ in the tissue is deduced from the differentiation of the free energy functions (II.2), (II.3) and (II.6) with respect to the corresponding deformations:

$$\boldsymbol{\sigma} = \underbrace{\frac{2}{J} \mathbf{F}_{mech} \frac{\partial \psi_{ECM}}{\partial \mathbf{C}_{mech}} \mathbf{F}_{mech}^T}_{\boldsymbol{\sigma}_e} + \underbrace{\frac{2}{J} \mathbf{F}_e \frac{\partial \psi_{ECM}}{\partial \mathbf{C}_e} \mathbf{F}_e^T}_{\boldsymbol{\sigma}_v} + \underbrace{\frac{2}{J} \mathbf{F}_{mech} \frac{\partial \psi_{CF}}{\partial \mathbf{C}_{mech}} \mathbf{F}_{mech}^T}_{\boldsymbol{\sigma}_{CF}} + \underbrace{\frac{\partial \psi_{chem}}{\partial J} \mathbf{I}}_{\boldsymbol{\sigma}_{chem}} \quad (\text{II.13})$$

in which $\mathbf{C}_e = \mathbf{F}_e^T \mathbf{F}_e$ is the elastic right Cauchy-Green strain tensor.

In line with the free energy decomposition (II.1), the Cauchy stress $\boldsymbol{\sigma}$ is split into three main contributors: the Cauchy stress in the ECM $\boldsymbol{\sigma}_{ECM} = \boldsymbol{\sigma}_e + \boldsymbol{\sigma}_v$, the Cauchy stress in the oriented CFs $\boldsymbol{\sigma}_{CF}$ (their addition representing the mechanical-based component) and the chemical-based Cauchy stress $\boldsymbol{\sigma}_{chem}$. Due to mechanical incompressibility, the mechanical-based part $\boldsymbol{\sigma}_{mech} = \boldsymbol{\sigma}_{ECM} + \boldsymbol{\sigma}_{CF}$ is a traceless tensor, i.e. $\text{tr}(\boldsymbol{\sigma}_{mech}) = 0$, and $\boldsymbol{\sigma}_{chem} = p \mathbf{I}$ with the hydrostatic pressure $p = \text{tr}(\boldsymbol{\sigma})/3$.

II.2.1.2. Numerical implementation

The chemo-viscoelastic constitutive model has been implemented into the non-linear finite element software MSC.Marc by means of a set of subroutines (MSC.Marc, 2015). A hyperelastic subroutine dedicated to compressible large strain elasticity was defined in conjunction with a viscous subroutine for the definition of the inelastic dissipation. The

hyperelastic subroutine allows the writing of an algorithm using invariant-based energy functions. Due to the absence of a subroutine allowing the generation of the chemical-induced swelling effects, a thermal subroutine was adapted to assimilate and integrate the swelling equations working in parallel with the viscohyperelastic algorithm. The main steps of the implementation procedure are described by the flowchart shown in Figure II.3. At the beginning of each increment, the deformation gradient tensor is introduced by the numerical expression (de Souza et al., 2008):

$$\mathbf{F}_i = \exp(\ln(\mathbf{F}_i)) = \sum_{j=0}^{\infty} \frac{1}{j!} (\ln(\mathbf{F}_i))^j \quad (\text{II.14})$$

where $\ln(\mathbf{F}_i)$ represents the deformation tensor given by the numerical code.

The viscous deformation $\mathbf{F}_{v_{i-1}}$, user-stored from the previous increment, is called by the viscous subroutine in order to deduce the current elastic deformation \mathbf{F}_{e_i} :

$$\mathbf{F}_{e_i} = \mathbf{F}_i (\mathbf{F}_{v_{i-1}})^{-1} \quad (\text{II.15})$$

The resulted elastic deformation is then injected in the expression of the viscous velocity gradient $\mathbf{L}_{v_i} = \mathbf{D}_{v_i}$ and:

$$\dot{\mathbf{F}}_{v_i} = (\mathbf{F}_{e_i})^{-1} \mathbf{D}_{v_i} \mathbf{F}_i \quad (\text{II.16})$$

where \mathbf{D}_{v_i} is the viscous stretching rate tensor at the end of the current increment, and the current viscous deformation \mathbf{F}_{v_i} is obtained by integration over a time increment Δt :

$$\mathbf{F}_{v_i} = \dot{\mathbf{F}}_v \Delta t + \mathbf{F}_{v_{i-1}} \quad (\text{II.17})$$

The singularity of the viscous stretching rate at the beginning of the mechanical loading is avoided by adding a perturbation coefficient $\kappa=0.01$ to $\sqrt{I_{1v}/3}$ in Eq. (II.12). The value of

\mathbf{F}_{v_i} is stored by the user in the form of a 3-D matrix $[m, nn, p]$ composed of m number of elements, nn number of nodes and p number of tensor directions.

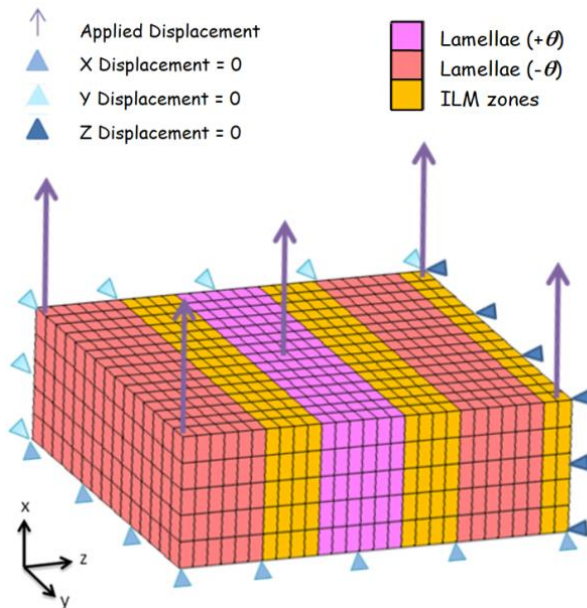
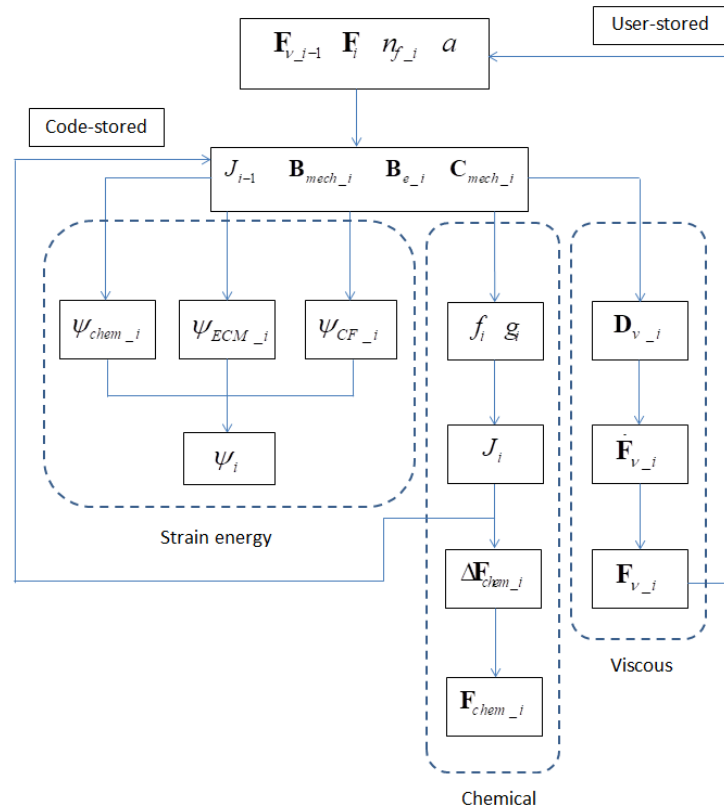


Figure II.3. Flowchart of the chemo-viscoelastic algorithm and annulus specimen mesh.

As well, the chemo-mechanical subroutine calculates the incremental volumetric variation $\Delta \mathbf{F}_{chem_i}$ and the total volumetric deformation $\mathbf{F}_{chem_i} = \mathbf{F}_{chem_i-1} + \Delta \mathbf{F}_{chem_i}$ by means of the kinetics of the volume change variation ΔJ_i . The value of the resulted chemical deformation is code-stored and then called in the following increment by the hyperelastic subroutine permitting the evaluation of the current volumetric strain energy $\psi_{chem_i}(J_{i-1})$.

II.2.2. At the stratified scale

II.2.2.1. Numerical model

At the stratified scale, the annulus structure is studied in-silico using the finite element method by considering explicitly successive lamellar and ILM layers. An example of the three-dimensional numerical model of an annulus specimen is shown in Figure II.3. The selected dimensions of layers are not measured and are used for illustrative purpose. Perfect ILM-lamellar interfaces were considered. Three-dimensional 8-node meshing elements, isoparametric and arbitrarily hexahedrics were used for the finite element mesh, the element size being chosen for mesh-independency. The same boundary conditions regarding the in-vitro experiments, detailed below, were simulated. Due to the symmetry considerations, only one-fourth of the specimen cross-section and one-eighth of the specimen height were simulated.

II.2.2.2. ILM-lamellar interaction

Experimentally-based kinetics will be coupled to the constitutive model in the aim of representing the response of the different layers of the stratified soft tissue. During a homogeneous stress-free swelling, the Jacobian J depends on the external ionic concentration c_{ext} and the internal fluid concentration n_{f_s} :

$$J = \hat{J}(c_{ext}, n_{f_s}) \quad (18)$$

The osmo-induced volumetric change variation is $\Delta J = \Delta n_{f_s} f(c_{ext})$ where $f(c_{ext})$ is a free swelling function detemined experimentally and Δn_{f_s} represents the internal fluid content variation sucked by the tissue from the dehydrated state ($n_{f_s} = 0$) to the chemical equilibrium state:

$$\dot{n}_{f_s} = \beta_s \left(1 - \frac{n_{f_s}}{n_{f_{ref}}} \right) \quad (19)$$

in which β_s is a rate factor and $n_{f_{ref}}$ is the reference fluid content in the saturated tissue.

The osmosis of the tissue with the surrounding biochemical environment generates a hydrostatic pressure p inside the disc that is equal to the sum of the osmotic pressure gradient $\Delta\pi = \pi_{int} - \pi_{ext}$ and the chemical potential of the fluid μ_f (Schroeder et al., 2006): $p = \Delta\pi + \mu_f$. When the ionic equilibrium is achieved, the chemical potential μ_f is equal to zero, and in this equilibrated state, the swelling pressure $\Delta\pi$ may be calculated from the ECM fixed charge density c_F and the external ionic concentration c_{ext} as follows (Huyghe and Janssen, 1997):

$$\Delta\pi = \delta_{int} RT \left(\sqrt{c_F^2 + 4 \frac{(\gamma_{ext})^2}{(\gamma_{int})^2} c_{ext}^2} \right) - 2\delta_{ext} RT c_{ext} \quad (II.20)$$

where R is the universal gas constant, T is the absolute temperature, δ_{int} and δ_{ext} are osmotic coefficients, γ_{int} and γ_{ext} are activity coefficients and the ECM fixed charge density c_F is given by (Lanir, 1987):

$$c_F = \frac{n_{f_{ref}} c_{F,0}}{n_{f_{ref}} - 1 + J} \quad (II.21)$$

in which $c_{F,0}$ is the initial fixed charge density.

Using Eqs. (II.13) and (II.20), the bulk modulus k appears as an explicit function of the external ionic concentration c_{ext} as a result of chemo-mechanical coupling:

$$\Delta\pi = \frac{k}{2J}(J^2 - 1) \quad (\text{II.22})$$

A chemical disequilibrium in the tissue is provoked by the mechanical loading which induces an internal fluid content variation. The latter has an influence on the tissue volume deformation and the Jacobian J of the hydrated tissue is:

$$J = \hat{J}(c_{ext}, n_{f_m}) \quad (\text{II.23})$$

The osmo-induced volumetric change variation is $\Delta J = \Delta n_{f_m} f(c_{ext}) g(c_{ext})$ where $f(c_{ext})$ is again the free swelling function, $g(c_{ext})$ is a dimensionless transportation coefficient determined experimentally and Δn_{f_m} is the internal fluid content variation in the tissue during the mechanical loading:

$$\dot{n}_{f_m} = \beta_m \left(1 - \frac{n_{f_m}}{n_{f_{lim}}} \right) \quad (\text{II.24})$$

in which β_m is a rate factor and $n_{f_{lim}}$ is the limiting fluid content taken equal to 0.99 (during mechanical loading) and 0.01 (during mechanical unloading).

Whereas a nearly isotropic swelling occurs under stress-free conditions, it is believed that lamellae and ILM zones behave differently when a mechanical loading is applied. The ILM zone is very rich of negatively charged PGs (Ortolani et al., 1988) and contains almost no CF (Tavakoli and Costi, 2018) which permits to the fluid to penetrate easily inside it with a high rate. Moreover, the lamellae contain less PGs and high CFs density that retards the fluid flow. These different microstructures differentiate significantly the swelling behavior of the two zones. As well, the chemical disequilibrium caused by the mechanical loading could lead to a

fluid transfer from the lamellae to the ILM zones in order to restore the ionic equilibrium of the two zones. The rate factor β_m in the fluid flow kinetics (24) may be thus different in the two zones: $\beta_m^{lam} \neq \beta_m^{ILM}$.

II.2.2.3. Microstructure-based considerations

The microstructure-based model describes the chemo-mechanical response in relation to the regional variation of the concentration of the different components through the annulus. The amount of CFs decreases whereas the amount of PGs and water increases radially towards the nucleus (Eyre and Muir, 1976,1977; Urban and McMullin, 1985; Culav et al., 1999; Skaggs et al., 1994; Holzapfel et al., 2005). The regional dependence of the annulus response due to the microstructure variation in terms of orientation and content of CFs allows a micromechanical treatment of the soft tissue. The volume fraction of the oriented CFs is explicitly introduced in the free energy as a direct input data. Eq. (II.1) may be re-written with the volume fraction concept as follows:

$$\psi = (1 - \phi_{CF})\psi_{ECM} + \phi_{CF}\psi_{CF} + (1 - \phi_{CF})\psi_{chem} \quad (II.25)$$

where ϕ_{CF} is the volume fraction of the oriented CFs and all other constitutive relations provided above remain identical. For the lamellar zone, Eq. (II.25) still prevails:

$$\psi_{lam} = \psi \quad (II.26)$$

but for the non-collageneous ILM zone, $\phi_{CF} = 0$ and:

$$\psi_{ILM} = \psi_{ECM} + \psi_{chem} \quad (II.27)$$

II.2.3. Model application

II.2.3.1. Structural features

Two sub-regions in the disc annulus are of interest: anterior inner (AI) and anterior outer (AO) as illustrated in Figure II.4. Because the structural features of the human disc are much better documented in the literature than for animals, we introduced some of them into our model. The water and fibers content, in addition to the fibers orientation, constitute the solely data taken from the human model². The orientation and content of CFs are well-documented in several papers (Skaggs et al., 1994; Holzapfel et al., 2005; Eyre and Muir, 1976, 1977). The orientation θ of oriented type I CFs in the AO and AI regions are approximately 23° and 31° , respectively (Holzapfel et al., 2005). The total amount $\phi_{CF(I+II)}$ of CFs (type I + type II) constitutes about 53% to 70% of the dry tissue (Skaggs et al., 1994): 55%-70% for AO and 53%-65% for AI. The fraction $\phi_{CF(I)}$ of the oriented type I CFs represents 36% to 53% of the total amount $\phi_{CF(I+II)}$ of CFs (Eyre and Muir, 1976, 1977). Considering the reference fluid amount $n_{f_{ref}}$, the fraction ϕ_{CF} of the oriented type I CFs in the wet tissue is:

$$\phi_{CF} = (1 - n_{f_{ref}}) \phi_{CF(I+II)} \phi_{CF(I)} \quad (\text{II.28})$$

The value of the reference fluid content is taken according to published results (Beckstein et al., 2008; Showalter et al., 2012): $n_{f_{ref}} = 0.65$ in outer part and $n_{f_{ref}} = 0.78$ in inner part. The resulting volume fraction ϕ_{CF} , used as a direct input data into the model, is equal to about 10% for AO and 5% for AI.

² Although it is obvious that the morphologies of the spine of a biped and a quadruped are different and the spine biomechanical behavior between species is different, some similarities in the structural features are shown in comparative studies. For example, the water content in Beckstein et al. (2008) and the fibers content in Showalter et al. (2012) of the inner and outer parts of the human lumbar disc are very close to those of the bovine tail.

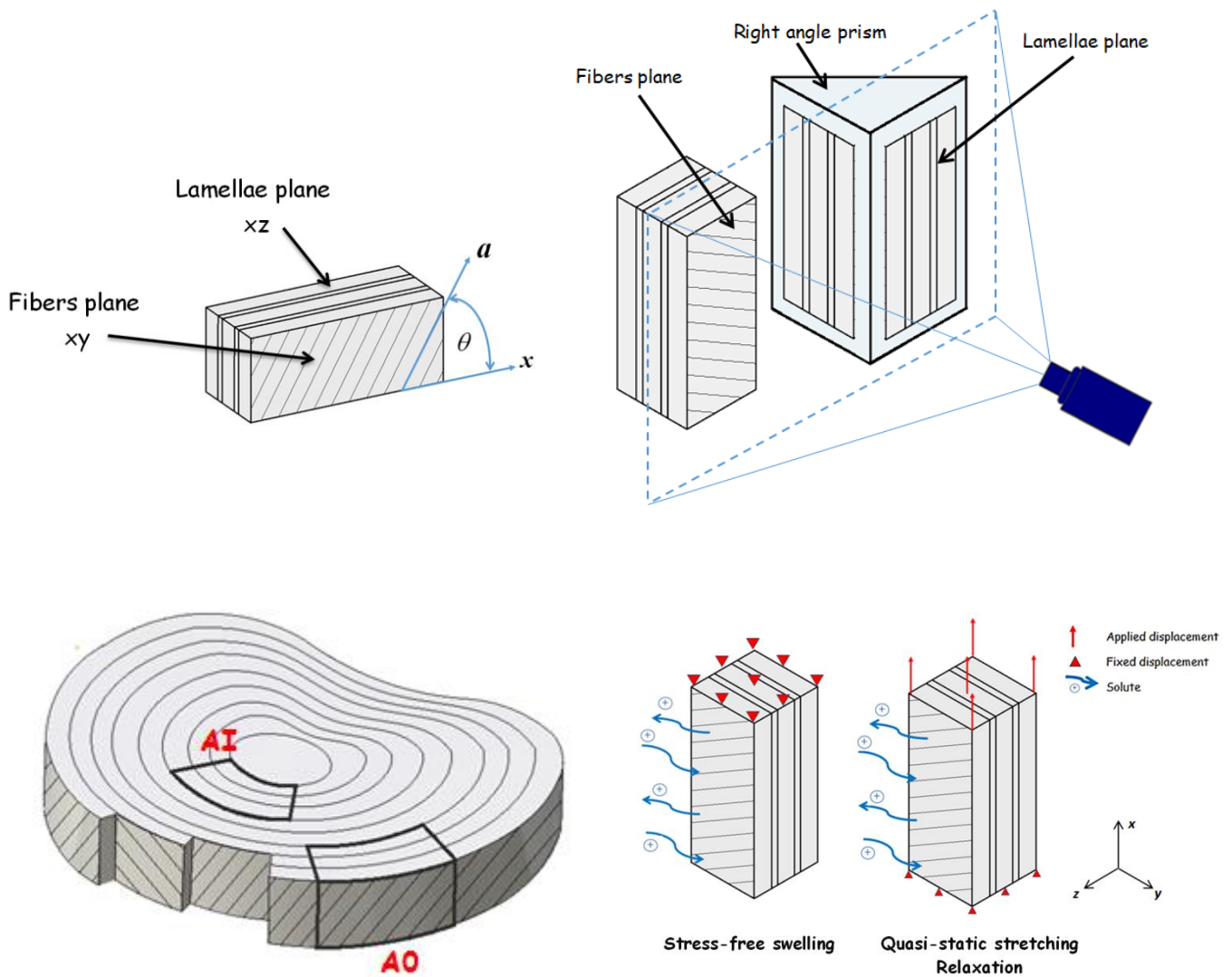


Figure II.4. AI and AO specimens extracted along the circumferential x -axis and tested under three conditions (stress-free swelling, quasi-static stretching and relaxation) to assess the time-dependent chemo-mechanical response under controlled surrounding biochemical environment; the main a -axis of type I CFs forms an angle θ with the x -axis. The transversal strains in the two specimen planes are simultaneously measured thanks to a right angle prism.

II.2.3.2. Database

The experimental database concerns the time-dependent annulus response in the two sub-regions of interest, AI and AO, extracted along circumferential direction of mature bovine

cervical discs. The protocol of the experimental results is described elsewhere (Derrouiche et al., 2020), but the essential information is provided in this subsection. All the experiments have been performed on rectangular specimens ($25 \times 10 \times 10 \text{ mm}^3$) and tested under well-controlled surrounding chemical environment at ambient temperature, the specimen being constantly immersed in a water bath. The osmotic effects have been introduced in the analysis by variation of the saline concentration of the bath: $[\text{NaCl}] < 9 \text{ g/L}$ (hypo-osmotic), $[\text{NaCl}] = 9 \text{ g/L}$ (iso-osmotic), $[\text{NaCl}] > 9 \text{ g/L}$ (hyper-osmotic)³, the concentration of 9 g/L being the reference value of the physiological solution. Before each experiment, the specimen was preconditioned⁴ to reach chemical equilibrium by stimulating fluid transfers after concentration change.

As illustrated in Figure II.4, three distinct experiments are used for the application of our model and the assessment of the viscoelastic behavior in relation with the osmolarity:

- Stress-free swelling in the aim of obtaining the chemical-induced volumetric response until equilibrium: The specimen has been gripped at one side on the testing machine and free at the other one.
- Quasi-static stretching highlighting the time-dependent chemo-mechanical response in terms of stress-strain and transversal behaviors: The fully-hydrated specimen has been stretched at a constant strain-rate until an axial strain of 5% and then unloaded at the same absolute strain-rate, two strain-rates being considered: $2 \times 10^{-4} \text{ s}^{-1}$ and $2 \times 10^{-3} \text{ s}^{-1}$.
- Interrupted stretching (relaxation) revealing the stationary state of the transversal behavior: The fully-hydrated specimen has been stretched at a constant strain-rate of 10^{-3} s^{-1} until an axial strain of 4%, then maintained constant during a certain holding time.

³ A two-way analysis of variance ANOVA without replication indicated a statistical significance of the osmotic and strain-rates effects with a p-value < 0.05 .

⁴ For the preconditioning, the specimen was subjected to a mechanical rest during 30 min followed by a mechanical loading of 10 cycles under a low-strain amplitude of 1% at an axial strain-rate of 10^{-3} s^{-1} .

The level of the axial strain in the annulus during physiological motions is of 10% (Shirazi-Adl, 1989; Costi et al., 2007). In the mechanical tests, a maximum axial strain of 5% was chosen in the aim to exclude micro-alteration risks and to ensure the solely occurrence of recoverable mechanisms in the tissue. In addition, the strain-rates correspond to quasi-static conditions. In all the experiments, the two-dimensional full-field of in-plane displacements has been measured by means of an optical strain measuring technique based upon the digital image correlation. Images of the lamellae plane (plane xz in Figure II.4) and the fibers plane (plane xy) of the specimen have been simultaneously recorded during the experiments thanks to a right angle prism⁵ with a strategy similar to that proposed for other materials (Parsons et al., 2004; Roux et al., 2003). The local deformation gradient tensor \mathbf{F} has been calculated from the in-plane displacements allowing to deduce the Green-Lagrange tensor in the two planes: $\mathbf{E} = (\mathbf{F}\mathbf{F}^T - \mathbf{I})/2$. The axial stress σ_{xx} has been calculated by using the actual load recorded by the load-cell and the actual specimen cross-section deduced from the average of the full-field transversal strains in an inner central part of both planes: E_{zz} in lamellae plane and E_{yy} in fibers plane. The standard deviation was evaluated on the axial stress and the strains. The errors on the full-field strains due to the correlation process were estimated by applying, before the mechanical test, a rigid body movement on fifteen specimens, gripped at one side and free at the other one. The stress standard deviation integrates the load inter-specimen variability (analyzed by one-way analysis of variance ANOVA on fifteen specimens with a p-value < 0.05) and the error on the local transversal strains.

⁵ The lens axis of the camera is kept perpendicular to the fibers plane while a right angle prism placed besides the annulus specimen allows to track the lamellae plane. Images of the fibers and lamellae planes were simultaneously recorded at regular interval of 3 Hz and digitized in 1628×1236 pixels, with a resolution of 290 pixels/mm. The noise coming from the use of the prism was reduced by a filtering process.

II.3. Results and discussion

II.3.1. Material kinetics

In what follows, we present the experimentally-based material kinetics that we have designed via a three-step strategy using successively the stress-free swelling followed by the quasi-static loading-unloading and then the relaxation. By contrast to numerical optimization procedures which provide directly the set of model parameters without ensuring their unicity (Pyrz and Zaïri, 2007), this deterministic method allows to guide the parameters identification and to propose material kinetics in accordance with our physical interpretation.

II.3.1.1. Stress-free swelling response

The stress-free swelling behavior is depicted in Figure II.5 from which the rate factor β_s and the free swelling function $f(c_{ext})$ are obtained through the adjustment of the best response by means of trial and error:

$$\beta_s = 0.000495 \text{ s}^{-1} \text{ and } f(c_{ext}) = 0.2385 + 0.74 \exp(-6948.84c_{ext}) \quad (\text{II.29})$$

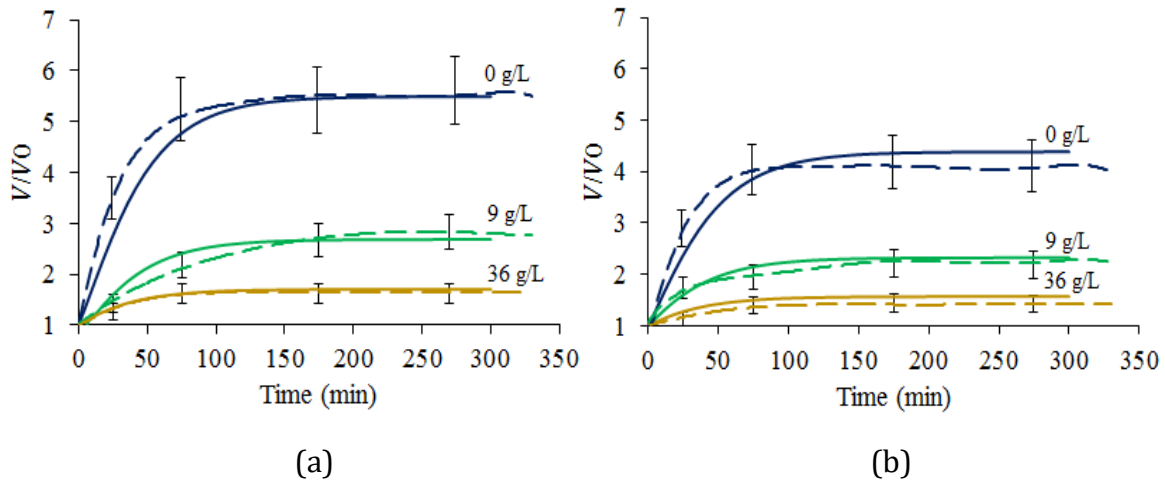


Figure II.5. Volume variation during stress-free swelling of (a) AI and (b) AO specimens under hypo, iso and hyper-osmotic conditions (dashed lines with standard deviation error bars: experiments, solid lines: simulations).

II.3.1.2. Quasi-static loading-unloading response

Keeping the designed free-swelling kinetics (29), the rate factor β_m in the fluid flow kinetics (24) and the dimensionless transportation coefficient $g(c_{ext})$ in the volume change variation were identified on the transversal strain history provided in Figures II.6 and II.7.

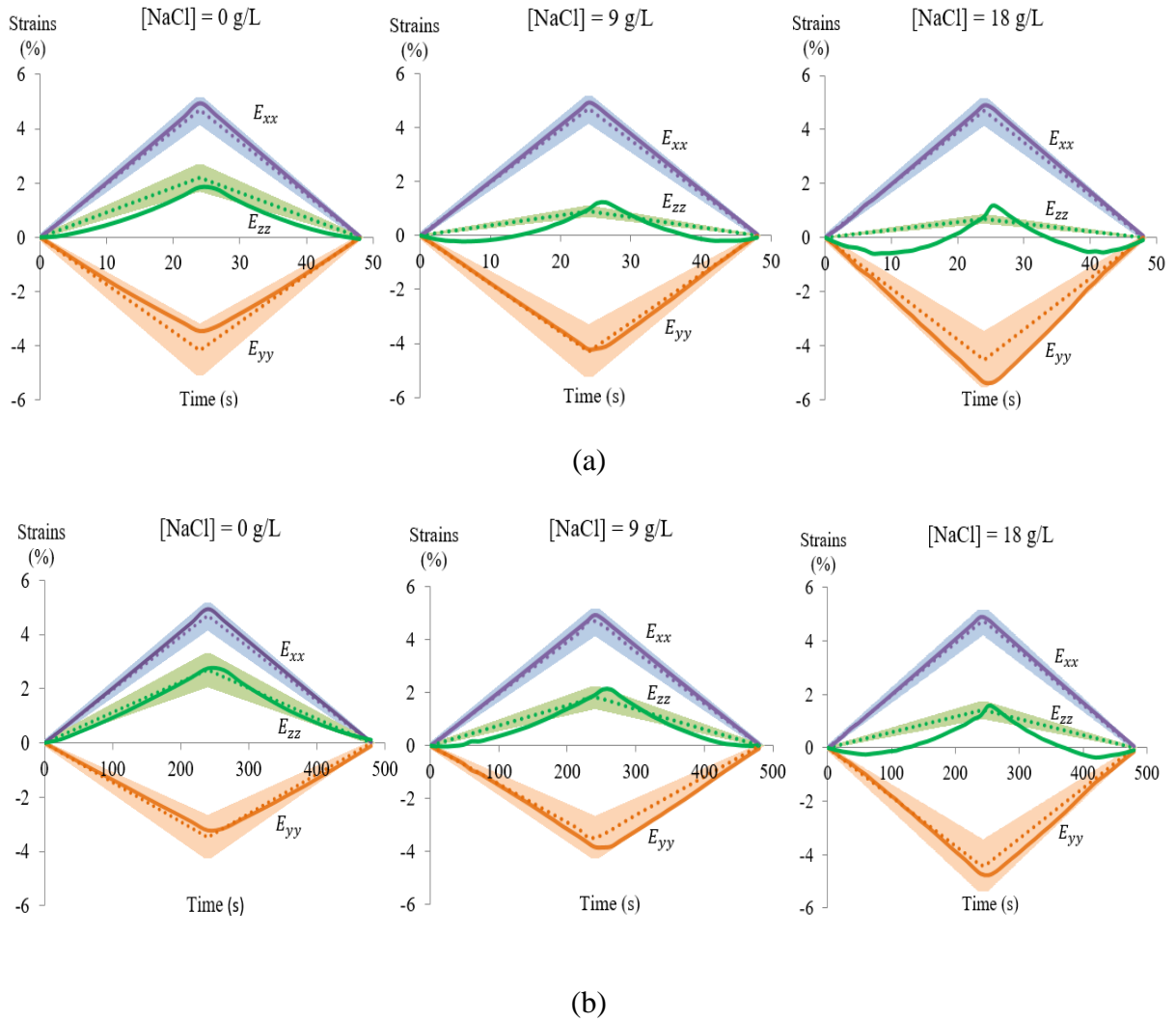


Figure II.6. Applied strain (E_{xx}) and transversal strains (E_{yy} and E_{zz}) for a loading-unloading cycle of the AI specimen under hypo, iso and hyper-osmotic conditions and different strain-rates: (a) $2 \times 10^{-3} \text{ s}^{-1}$ and (b) $2 \times 10^{-4} \text{ s}^{-1}$ (dashed lines with standard deviation error zones: experiments, solid lines: simulations).

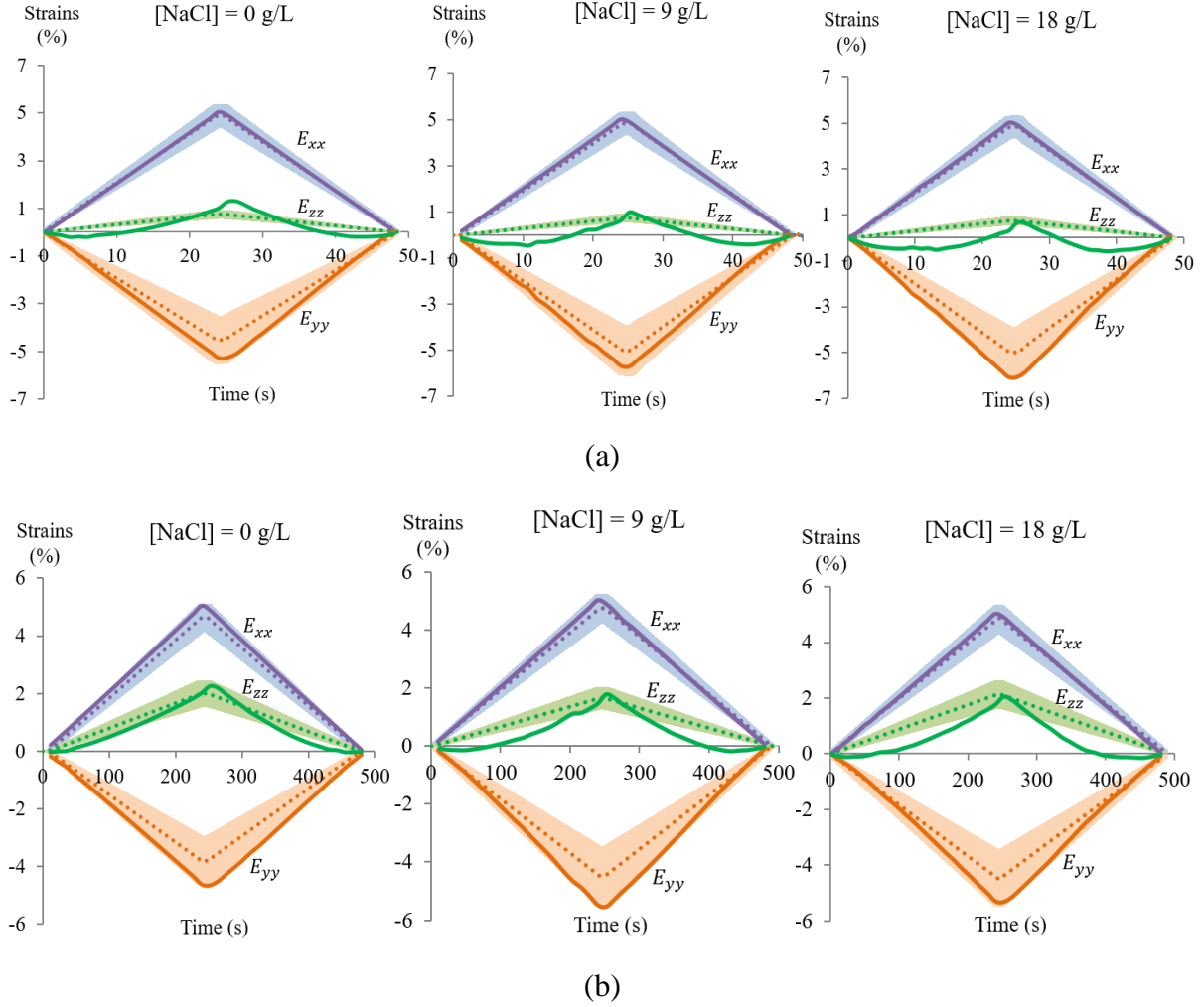


Figure II.7. Applied strain (E_{xx}) and transversal strains (E_{yy} and E_{zz}) for a loading-unloading cycle of the AO specimen under hypo, iso and hyper-osmotic conditions and different strain-rates: (a) $2 \times 10^{-3} \text{ s}^{-1}$ and (b) $2 \times 10^{-4} \text{ s}^{-1}$ (dashed lines with standard deviation error zones: experiments, solid lines: simulations).

The constant β_m takes the following values for lamellae and ILM zones⁶, respectively: $\beta_m^{lam} = -0.0004 \text{ s}^{-1}$ and $\beta_m^{ILM} = 0.00097 \text{ s}^{-1}$. Note that the value of β_m has a low magnitude in the lamellae compared to the ILM zone. The coefficient $g(c_{ext})$ describes the mechanical-induced chemical disequilibrium of the tissue swelling. It is a function of the external ionic concentration c_{ext} and the fluid flow rate:

⁶ The sign indicates the flow direction during the stretching: Positive rate factor refers to fluid transfer inside the tissue and negative rate factor refers to fluid transfer outside the tissue.

$$g(c_{ext})_{lam} = 7574\dot{\varepsilon} \exp(5650c_{ext}) \text{ and } g(c_{ext})_{ILM} = 8250\dot{\varepsilon} \exp(4050c_{ext}) \quad (\text{II.30})$$

in inner part and:

$$g(c_{ext})_{lam} = 6250\dot{\varepsilon} \exp(4285c_{ext}) \text{ and } g(c_{ext})_{ILM} = 4500\dot{\varepsilon} \exp(3500c_{ext}) \quad (\text{II.31})$$

in outer part.

The ECM and CFs elastic parameters, A_1 , A_2 , E and I_1^{\max} were extracted from the slope of the quasi-static response, see Figure II.8. In the spirit of a micromechanics-based modeling we assume that the respective properties of ECM and CFs in the reinforced tissue are the same whatever the concentrations. The regional dependence of the response is therefore due to the microstructural features of CFs in terms of content and angle. The oriented CFs being of the same type (type I) in the whole annulus, the same elastic properties may be considered in AO and AI zones: $A_1=1.5$ MPa and $A_2=290$ MPa. Also, the same elastic properties of the ECM were supposed in the two zones: $E = 4.8$ MPa and $I_1^{\max} = 3$. It is worth noticing that the ECM modulus is the same whatever the disc region, in line with the micromechanics-based approach, and that it does not vary with the biochemical environment contrary to (Derrouiche et al., 2019a). As a matter of fact, the bulk modulus k decreases with the equilibrium water content (Armstrong and Mow, 1982). Due to a higher amount of CFs in AO, higher CFs/ECM interactions are expected which may lead to lower compressibility at the same osmolarity. The bulk modulus k is considered regional dependent and as a function of the external ionic concentration c_{ext} :

$$k = 173 \exp(11309c_{ext}) - 143 \quad (\text{II.32})$$

in inner part and:

$$k = 1633 \exp(7634c_{ext}) - 1133 \quad (\text{II.33})$$

in outer part.

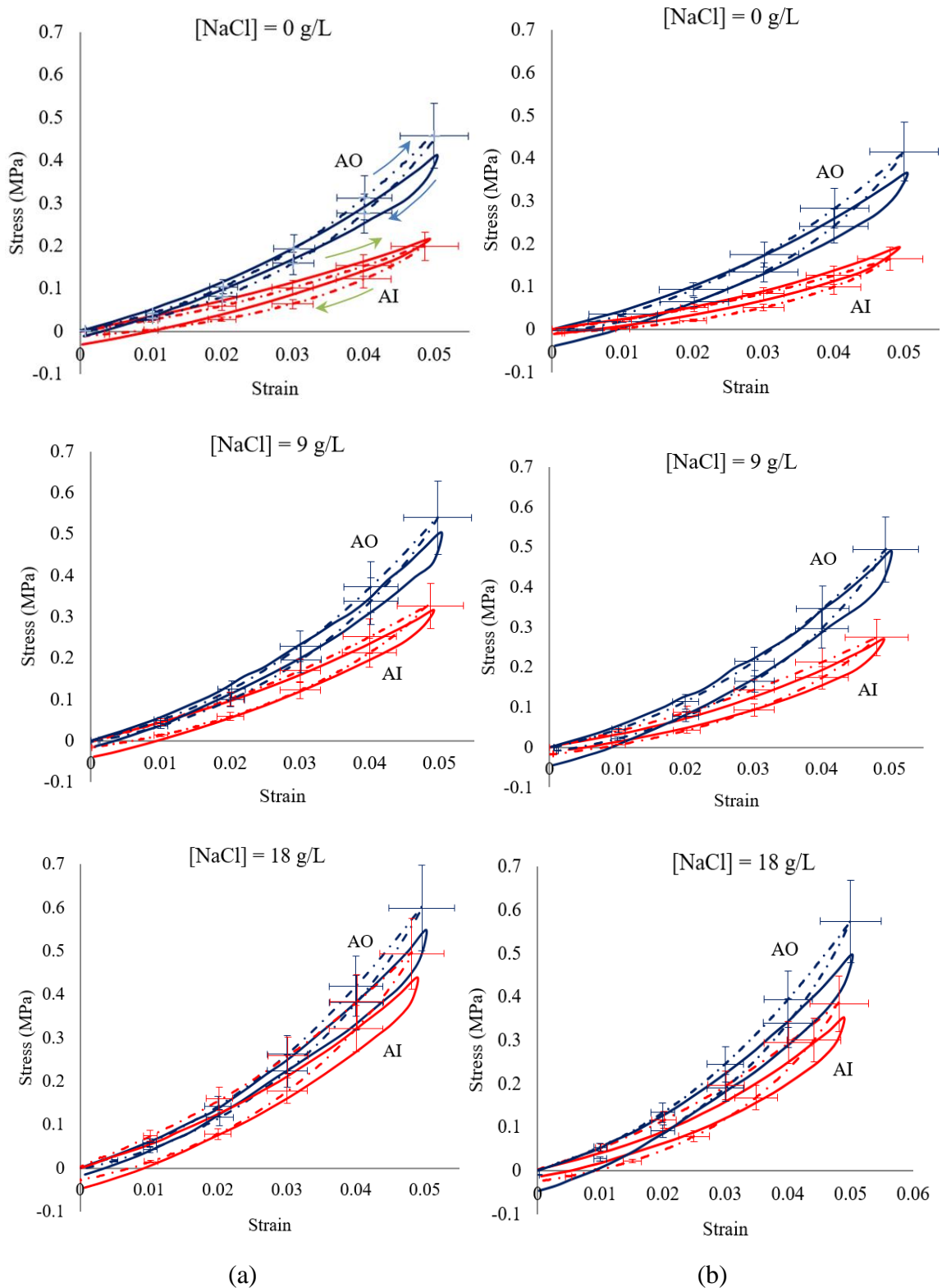


Figure II.8. Stress-strain response for a loading-unloading cycle of the AI and AO specimens under hypo, iso and hyper-osmotic conditions and different strain-rates: (a) $2 \times 10^{-3} \text{ s}^{-1}$ and (b) $2 \times 10^{-4} \text{ s}^{-1}$ (dashed lines with standard deviation error bars: experiments, solid lines: simulations).

The intrinsic viscosity in the tissue is assumed to be exclusively related to the ECM. Indeed, no loading rate dependency has been observed when an annulus specimen, constituted by a single lamella, is stretched in the CFs direction (Holzapfel et al., 2005). The viscous parameters of the ECM governing the hysteretic loop of the axial stress are: $E_v = 0.1666$ MPa, $I_{lv}^{\max} = 1.5$, $d = 0.02 \text{ MPa}^{-1} \text{ s}^{-1}$, $m = 0.001$ and $n = 1.0$ (AI) or $n = 1.8$ (AO).

II.3.1.3. Relaxation response

As a time-dependent feature, the relaxation leads to a decrease in load that is intrinsically related to the internal fluid transfer through the disc, see Figure II.9. We propose to reproduce this effect by the following expression of n_f as a function of the relaxation time t_{relax} :

$$n_f = \left(2n_{f_{\max}} - n_{f_{stab}}\right) - \left(\left(n_{f_{\max}} - n_{f_{stab}}\right) \exp(\beta_{relax} t_{relax})\right) \quad (\text{II.34})$$

where β_{relax} is the relaxation rate factor, $n_{f_{\max}}$ is the maximum value reached during the previous stretching and $n_{f_{stab}}$ is the stabilized value.

The identified values of Eq. (II.34) follow the kinetics:

$$n_{f_{stab}} = 0.06 - 0.05 \exp(-70c_{ext}) \quad (\text{II.35})$$

$$\beta_{relax}^{lam} / \beta_{relax(c_{ext}=0)}^{lam} = 5.41 - 4.41 \exp(-15739c_{ext}) \quad (\text{II.36})$$

$$\beta_{relax}^{ILM} / \beta_{relax(c_{ext}=0)}^{ILM} = 0.5 + 0.5 \exp(-37853c_{ext}) \quad (\text{II.37})$$

in which $\beta_{relax(c_{ext}=0)}^{ILM} = -1.76 \times 10^{-4} \text{ s}^{-1}$ and $\beta_{relax(c_{ext}=0)}^{lam} = 5.3 \times 10^{-7} \text{ s}^{-1}$ are the values of β_{relax} in the absence of salinity. Due to a higher absorbed amount of fluid during the previous stretching, the factor β_{relax} is found higher in the ILM zones than in the lamellae. Moreover, the negative value in the ILM zone reflects the fluid movement outside it towards the adjacent lamellae.

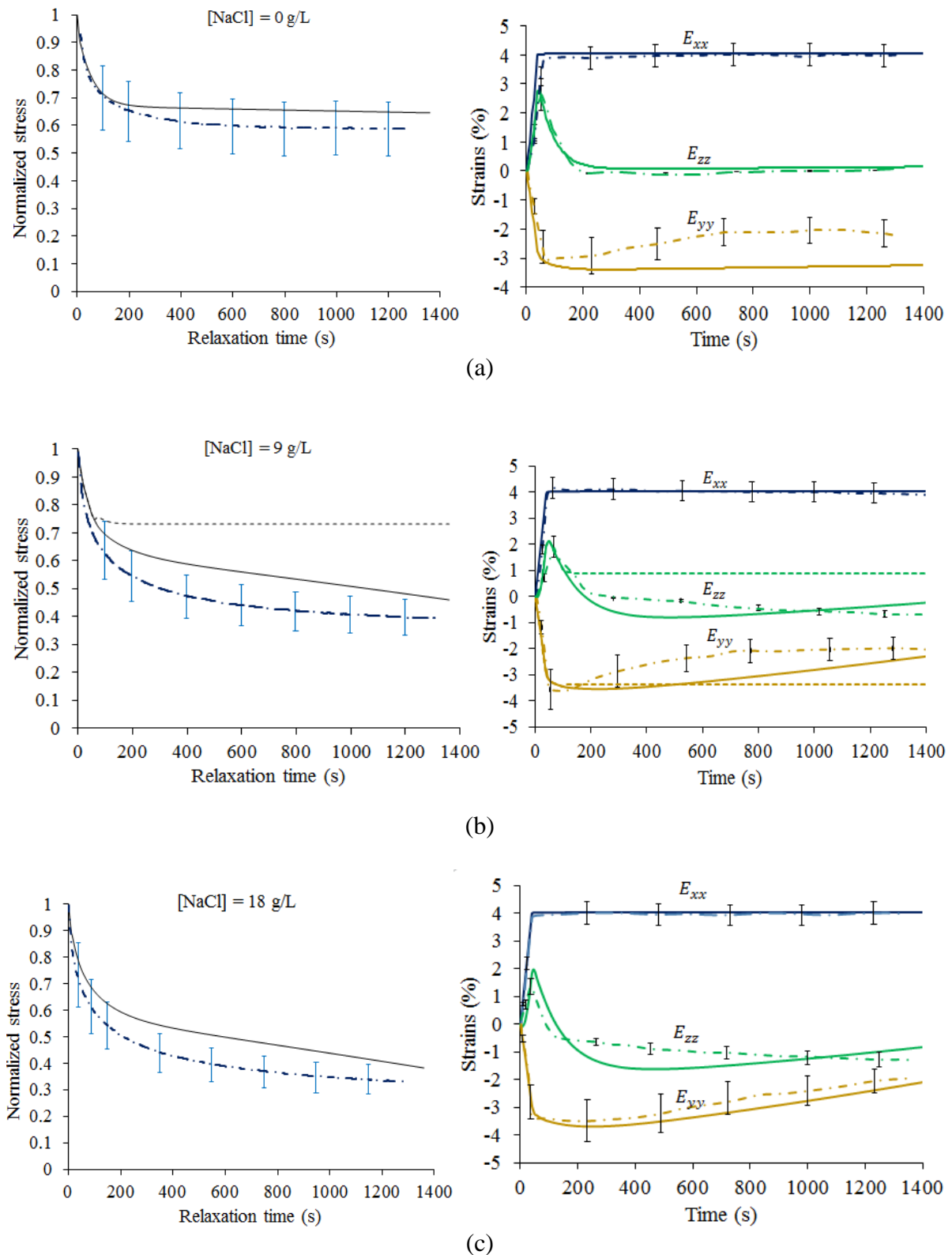


Figure II.9. Stress, applied strain (E_{xx}) and transversal strains (E_{yy} and E_{zz}) under relaxation of the AI specimen under (a) hypo, (b) iso and (b) hyper-osmotic conditions (dashed lines with standard deviation error bars: experiments, solid lines: simulations). The dotted lines in Figure II.9b represent the solely contribution of the ECM viscosity.

II.3.2. Model-experiment comparisons

As shown in Figure II.5, the model simulation is in very good agreement with the homogeneous chemical response of AI and AO regions. Note that the model captures this response with the same set of swelling constants, only the reference fluid content (Section II.3.1) is adapted for AI and AO. For a given saline concentration, the amount of absorbed fluid is higher in the AI zone than in the AO zone. This regional effect on the stress-free volumetric response may be explained by a difference in the amount of PGs (Urban and McMullin, 1985). Moreover, CFs may act as barriers retarding the fluid flow and reducing the osmotic effect (Maroudas et al., 1991; Schroeder et al., 2007). The two combined microstructural features, higher PGs density and lower CFs in AI than in AO, induce higher swelling capacities.

Figures II.6, II.7 and II.8 present the comparison between experiments and simulations. Figures II.6 and II.7 provide the transversal strain history for AI and AO, respectively, and Figure II.8 presents the stress-strain behavior under quasi-static stretching. A global view at these plots shows that the general trends of the model are satisfactory. It is worth noticing that our goal was not to match perfectly with the experimental observations, but to reproduce the main trends of the experimental observations in the aim to design the material kinetics. By this way, a predictive tool is obtained to provide the behavior of any specific region in the disc in relation with the tissue chemo-viscoelastic features.

As illustrated in Figure II.8, the model provides a good description of the main features of the hysteretic stress-strain response while taking into consideration the microstructure difference between AO and AI regions. Especially, the stiffer response in AO than in AI is well reproduced. When the sample is unloaded down to zero-stress, the instantaneous recovery of a large part of the inelastic strain is observed whereas a small amount of the inelastic strain is

retained when the stress is zero after unloading. It is worth noticing that this remanent strain is completely recovered after preconditioning of the sample between two successive tests. Although the model is able to capture this feature, it overestimates the tissue response when the stress becomes negative after unloading. The influence of the biochemical environment, translated by the saline concentration, and the loading rate are reproduced in a satisfactory manner by the model.

In most conditions, the shrinking in fibers plane and the swelling in lamellae plane are reproduced in a satisfactory manner by the model as illustrated in Figures II.6 and II.7. The two transversal strains are not equally reproduced by the model. Indeed, due to a strongest nonlinearity of the simulation result, the transversal strain in the z -direction is approached by the model in most cases only around the maximum. Nonetheless, the two transversal strains in the reversal path give much better results than those provided by the model in Derrouiche et al. (2019a). The transversal behavior presents a strain-rate dependency which in turn depends on the osmolarity translated by the changes in salt concentration. That illustrates perfectly the chemo-viscoelastic coupling during the stretching. Moreover, the opposite transversal behavior, $E_{yy} < 0$ and $E_{zz} > 0$, between the fibers plane and the lamellae plane reinforces this idea of coupling with a significant role of the fluid transfer. The transversal behavior shows a shrinking in fibers plane nearly equivalent to the applied axial strain, i.e. $|E_{yy}| \approx |E_{xx}|$. This was already reported in the literature (Elliott and Setton, 2001; O'Connell et al., 2012; Singha and Singha, 2012). The swelling in lamellae plane, i.e. $E_{zz} > 0$, is indicative of a negative Poisson's ratio. Although other biological soft tissues exhibit this auxetic feature (Lees et al., 1991; Timmins et al., 2010; Gatt et al., 2015), this was previously reported only by Baldit et al. (2014) and Derrouiche et al. (2019a) for annulus. The auxeticity exhibits a strong strain-rate/osmotic dependency and suggests an inter-layer fluid transport mechanism. The behavior

of transversal strains may be translated to a common mechanical quantity of materials, namely the Poisson's ratio. Due to chemo-mechanical coupling, the annulus Poisson's ratio is time-dependent and must be regarded as an “apparent” Poisson's ratio. This two-dimensional apparent material property is defined as the ratio between the average transversal strains, E_{zz} or E_{yy} , and the average axial strain E_{xx} :

$$\nu_{xz} = -\frac{E_{zz}}{E_{xx}} \quad (\text{II.38})$$

in the lamellae plane and:

$$\nu_{xy} = -\frac{E_{yy}}{E_{xx}} \quad (\text{II.39})$$

in the fibers plane.

The experimental values of the apparent Poisson's ratio and model estimates are provided in Figure II.10. The experiments are presented as symbols with their standard deviation bars while the simulations are presented as rectangular bars. The model estimates are found in excellent agreement with the experimental observations, falling in most of cases in the experimental standard deviation bars. The positive quadrant represents the Poisson's ratio in the fibers plane while the negative quadrant represents the Poisson's ratio in the lamellae plane. The apparent Poisson's ratio is clearly out of classical bounds. In the fibers plane, it is higher than 0.5, and even exceeds 1.0, while it is negative in the lamellae plane. The regional dependence is clearly seen in Figure II.10. The AO region exhibits a higher Poisson's ratio value than that of the AI region. By contrast, the AI region appears to be more auxetic (i.e. higher value of the negative Poisson's ratio) than the AO region in the lamellae plane. The increase in saline concentration increases the Poisson's ratio in the fibers plane and decreases the auxeticity of the lamellae plane. The strong influence of the loading rate in the lamellae plane is very well reproduced by the model.

The stress and transversal strains during relaxation are presented in Figure II.9. The model satisfactorily reproduces the significant features of the temporal changes of the chemo-mechanical response of the tissue. In reason of the model structure, the simulation reproduces the time-dependent response in connection to the internal fluid variation and the ECM viscosity as the two main underlying mechanisms. The response towards equilibrium provides a valuable judgment of the capability of the tissue to reach its internal chemical balance. Especially, opposite evolutions of the transversal strain history leads to more usual Poisson's ratio values ranged between 0 and 0.5 at chemo-mechanical equilibrium, i.e. $E_{zz} < 0$ in lamellae plane with loss of auxeticity and $|E_{yy}| \approx |E_{xx}|/2$ in fibers plane.

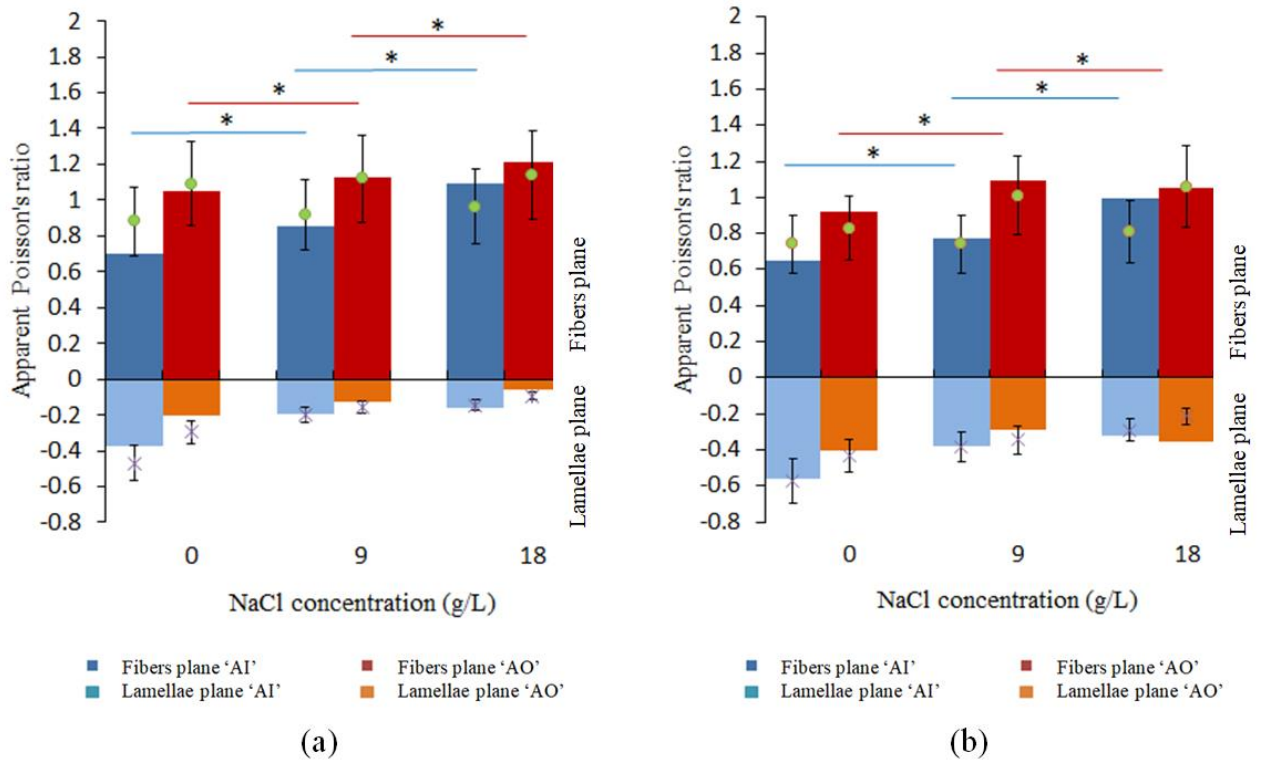


Figure 10. Apparent Poisson's ratio of the AI and AO specimens under hypo, iso and hyperosmotic conditions and different strain-rates: (a) $2 \times 10^{-3} \text{ s}^{-1}$ and (b) $2 \times 10^{-4} \text{ s}^{-1}$ (symbols with standard deviation error bars: experiments, rectangular bars: simulations). * denotes significant differences (p-value < 0.05) from values at 9 g/L saline solution (considered as the reference value of the physiological solution)

The effective contribution of the two main time-dependent mechanisms can be decoupled using our approach. As an example, Figure II.9b presents the solely contribution of the ECM viscosity, in the form of dashed lines, which can be compared to the macro-stress that includes as well the chemical stress contribution. The viscous stress appears to contribute to the macro-stress at the beginning of the relaxation while the chemical stress governs the degree to which the tissue is relaxed. A higher ionic concentration involves a higher fluid transfer and induces a higher effect of the chemical stress, and hence a longer hold time to equilibrium return.

II.3.3. Local strain fields

Figures II.11 and II.12 present the transversal strain field in the z - and y -directions, respectively, in the AI and AO specimens strained in the x -direction at a maximum strain of 5% and a strain-rate of $2 \times 10^{-3} \text{ s}^{-1}$. The results for the two extreme biochemical environments are shown for illustrative purpose. As also observed in Derrouiche et al. (2019a), it appears clearly in Figure II.11 negative and positive alternated bands due to, respectively, shrinking of the lamellar phase and swelling of the ILM phase during the stretching process. The ILM zone experiences significantly higher strains than the lamellae, with absolute values of about two to three times higher. Quite interesting, this numerical finding is corroborated with the experimental observations of Huyghe and Jongeneelen (2012), and later of Vergari et al. (2016), on bovine AF specimens. In spite of a higher content of CFs, the outer zone presents smaller strains than the inner zone. This is a consequence of a higher chemical sensitivity of the inner zone due to the presence of a higher content of negatively charged PGs that allows a higher fluid to be sucked by osmotic effect.

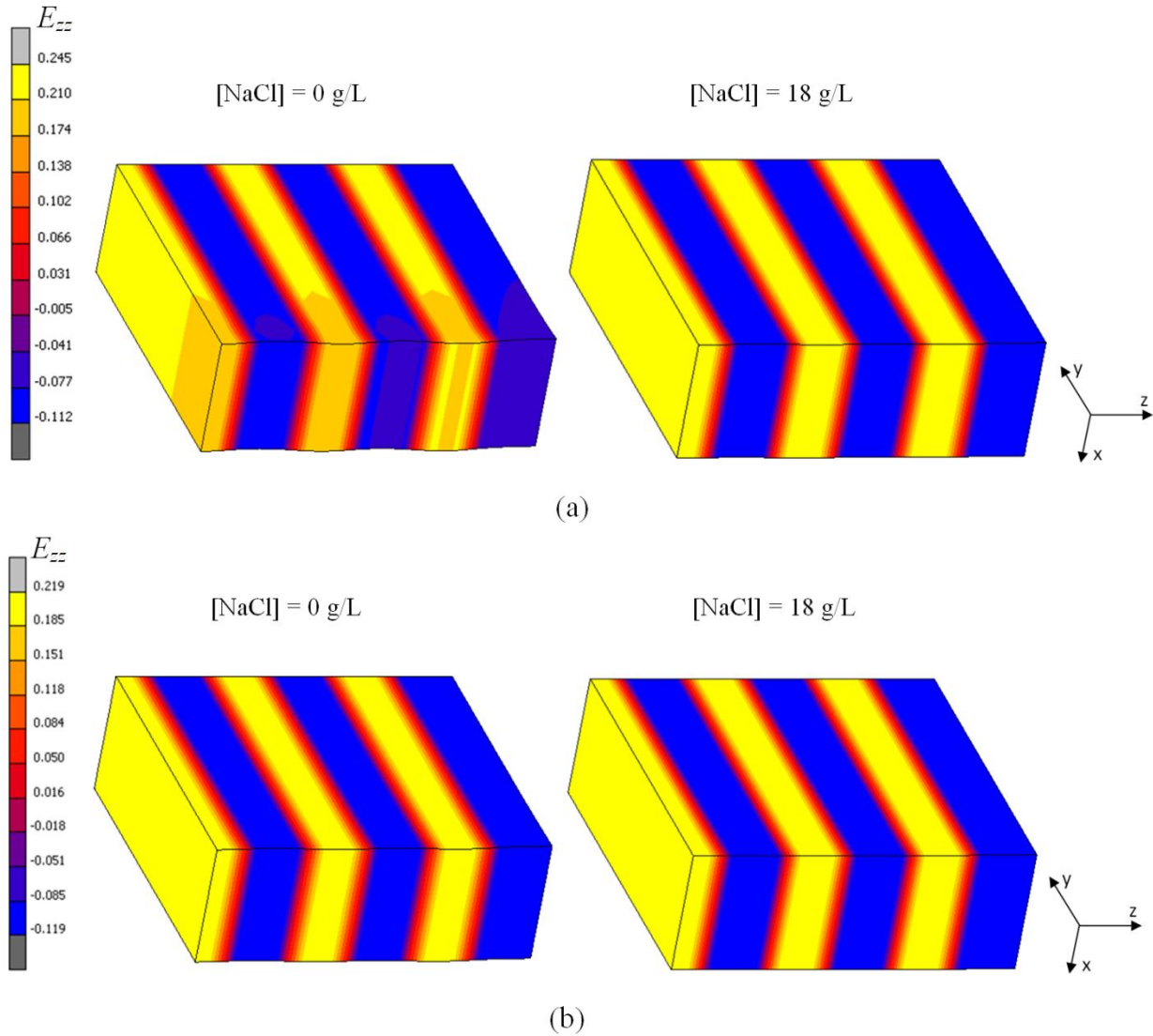


Figure II.11. Distribution of the transversal strain E_{zz} in the specimen strained in the x -direction at a maximum strain of 5% and a strain-rate of $2 \times 10^{-3} \text{ s}^{-1}$ under hypo and hyper-osmotic conditions: (a) AI and (b) AO.

Due to the swelling phenomenon in the ILM zone, the transversal strain intensity in the y -direction shown in Figure II.12 is decreased in this zone and the strain field in the annulus appears non-homogeneous. This effect is more significant under hypo-osmotic condition. Due to the importance of this strain component on the propensity to damage initiation, the shear strain field is plotted in Figure II.13. A nearly uniform shear strain is found across the specimen, i.e. ILM and lamellar shear strains are equivalent. The experimental observations of Michalek et al. (2009), and later of Vergari et al. (2016), on bovine AF specimens

corroborate this numerical finding. They found no significant difference between the lamellar shear strain and the ILM shear strain. According to their respective experimental results, they concluded no sliding mechanism in reason of a strong cohesion between the lamellae and the ILM zone. The designated mechanism by these authors is referred to as a skewing mechanism. The strong lamellae-ILM cohesion is inherent to our simulations since perfect interfaces are assumed between zones.

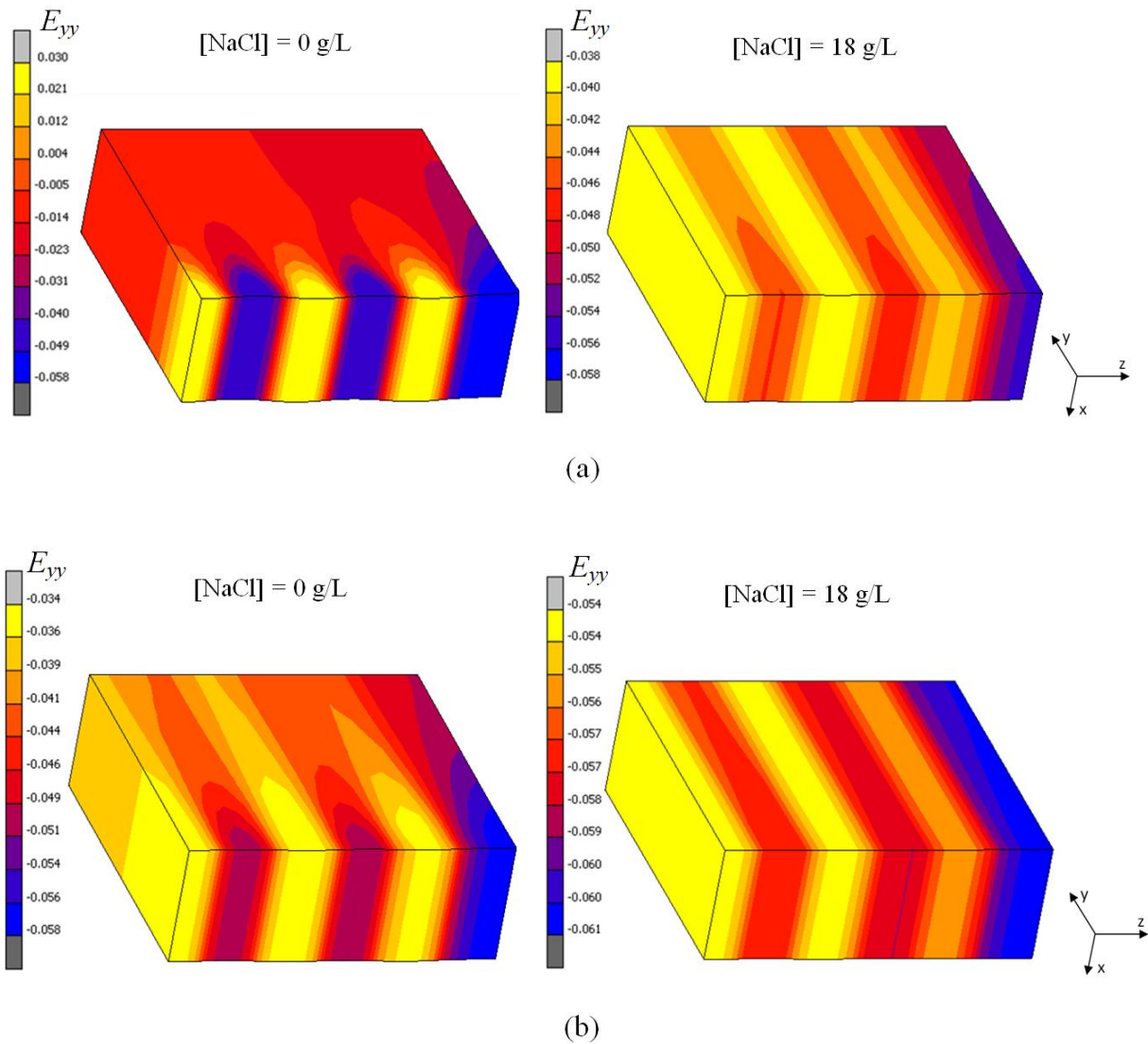


Figure II.12. Distribution of the transversal strain E_{yy} in the specimen strained in the x -direction at a maximum strain of 5% and a strain-rate of $2 \times 10^{-3} \text{ s}^{-1}$ under hypo and hyper-osmotic conditions: (a) AI and (b) AO.

Nonetheless, our simulations show also that near the specimen free edges the shear strain increases and differs in the transition regions between zones. Potentially, this region, near contact surfaces between the disc and the adjacent vertebrae, may be subjected to damage initiation.

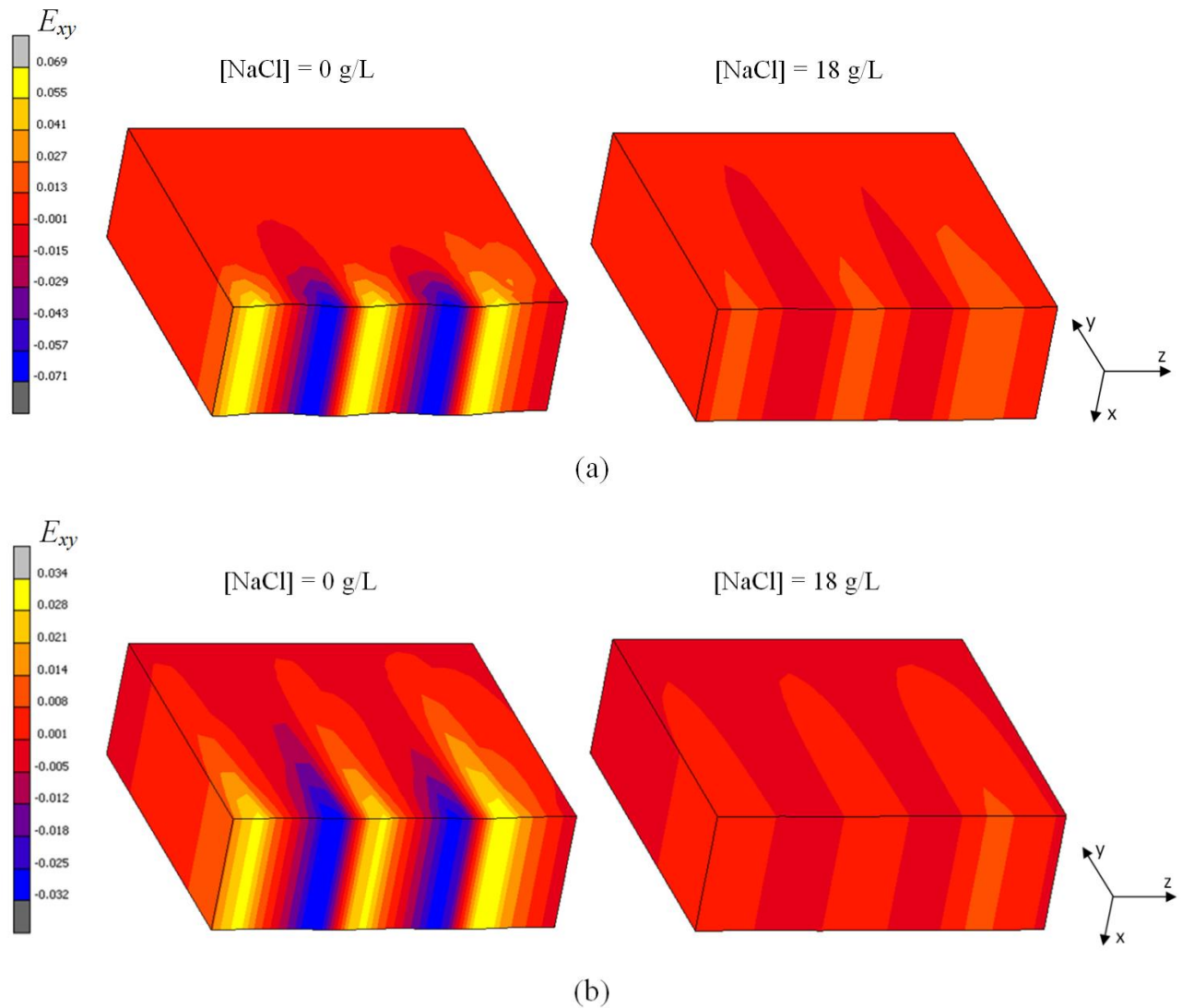


Figure II.13. Distribution of the shear strain E_{xy} in the specimen strained in the x -direction at a maximum strain of 5% and a strain-rate of $2 \times 10^{-3} \text{ s}^{-1}$ under hypo and hyper-osmotic conditions: (a) AI and (b) AO.

As shown in Figure II.12, the intensity of the transversal strain is affected by the ILM swelling and is significantly decreased when the osmolarity passes from hyper to hypo-osmotic conditions. As a consequence, the lamellae and the ILM zones present a large strain

contrast that increases largely and leads to the higher shear strain intensity shown in Figure II.13. An inverse ILM-induced effect on the local shearing was predicted in Derrouiche et al. (2019a). This is probably due to the difference in the underlying mechanisms suggested by different material kinetics in the present model and those in Derrouiche et al. (2019a). Whereas in Derrouiche et al. (2019a) the ECM shear modulus evolves with the surrounding biochemical conditions in order to reproduce the osmo-induced stiffening, it is constant in the present work and that whatever the disc region. Indeed, in the present model, the osmo-induced stiffening is solely governed by the volumetric contribution. The plots in Figure II.13 bring fruitful information regarding the intensity of the shear component. This one is found higher in the inner part than the outer part of the disc enhancing the risk of damage initiation close to the disc nucleus. This numerical finding is consistent with well-known disc damage mechanisms such as disc herniation that initiates in the inner region and propagates towards the outer region of the disc.

II.4. Partial conclusion

The chemo-viscoelastic model presented in this chapter allows a better comprehension of the intrinsic intervertebral disc behavior in relation to the microstructure (regional dependence due to variation in fibers content/orientation), the surrounding biochemical environment (ionic concentration in solution) and the mechanical loading conditions. The simulated results are in close agreement with experimental observations on two disc annulus regions for different osmotic conditions under stress-free volumetric changes, quasi-static stretching at different strain-rates and relaxation. The time-dependency of the tissue response is regarded as a combination of the intrinsic viscosity of the ECM and the internal fluid transfer. The model is based upon a microstructure representation of the tissue at two scales: (i) a microstructure decomposition at the ECM scale allows to attribute a constitutive relation to

each main material constituent along with the chemical-induced internal fluid variation, (ii) the non-collagenous interlamellar zone at the stratified scale is introduced as the key structural factor of the inter-layer fluid transfer mechanism responsible for the unusual time-dependent transversal behavior.

The most remarkable aspect at this stage of the tool development is its ability to provide useful predictions of the annulus response in any disc region. By this way, local stress/strain patterns in annulus can be analyzed in relation with loading conditions (osmolarity and strain-rate) and with the variations in concentration of the different constituents through the disc. A quantitative evaluation of the model predictions at different locations in the spinal column remains however an important issue for future works. Moreover, although the annulus stretching is representative of the compression mechanics of intervertebral disc, a complete verification of the model needs to consider other loading conditions.

References

- Adam, C., Rouch, P., Skalli W., 2015. Inter-lamellar shear resistance confers compressive stiffness in the intervertebral disc: an image-based modelling study on the bovine caudal disc. *Journal of Biomechanics* 48, 4303-4308.
- Argoubi, M., Shirazi-Adl, A., 1996. Poroelastic creep response analysis of a lumbar motion segment in compression. *Journal of Biomechanics* 29, 1331-1339.
- Armstrong, C.G., Mow, V.C., 1982. Variations in the intrinsic mechanical properties of human articular cartilage with age, degeneration, and water content. *The Journal of Bone and Joint Surgery* 64, 88-94.
- Ayotte, D.C., Ito, K., Perren, S.M., Tepic, S., 2000. Direction-dependent constriction flow in a poroelastic solid: the intervertebral disc valve. *Journal of Biomechanical Engineering* 122, 587-593.
- Baldit, A., Ambard, D., Cherblanc, F., Royer, P., 2014. Experimental analysis of the transverse mechanical behaviour of annulus fibrosus tissue. *Biomechanics and Modeling in Mechanobiology* 13,643-652.
- Balzani, D., Neff, P., Schroder, J., Holzapfel, G.A., 2006. A polyconvex framework for soft biological tissues. Adjustment to experimental data. *International Journal of Solids and Structures* 43, 6052-6070.
- Beckstein, J.C., Sen, S., Schaer, T.P., et al., 2008. Comparison of animal discs used in disc research to human lumbar disc: axial compression mechanics and glycosaminoglycan content. *Spine* 33, 166-173.

- Bergstrom, J.S., Boyce, M.C., 1998. Constitutive modeling of the large strain time-dependent behavior of elastomers. *Journal of the Mechanics and Physics of Solids* 46, 931-954.
- Cantournet, S., Boyce, M.C., Tsou, A.H., 2007. Micromechanics and macromechanics of carbon nanotube-enhanced elastomers. *Journal of the Mechanics and Physics of Solids* 55, 1321-1339.
- Cassidy, J.J., Hiltner, A., Baer, E., 1989. Hierarchical structure of the intervertebral disc. *Connective Tissue Research* 23, 75-88.
- Costi, J.J., Stokes, I.A., Gardner-Morse, M., Laible, J.P., Scoffone, H.M., Iatridis, J.C., 2007. Direct measurement of intervertebral disc maximum shear strain in six degrees of freedom: motions that place disc tissue at risk of injury. *Journal of Biomechanics* 40, 2457-2466.
- Culav, E.M., Clark, C.H., Merrilees, M.J., 1999. Connective tissues: matrix composition and its relevance to physical therapy. *Physical Therapy* 79, 308-319.
- de Souza Neto, E.A., Peric, D., Owen, D.R.J., 2008. *Computational Methods for Plasticity: Theory and Applications*. John Wiley and Sons Publication.
- Derrouiche, A., 2018. PhD thesis. University of Lille. Osmo-inelastic response of intervertebral disc: experiments and constitutive modeling.
- Derrouiche, A., Zaïri, F., Zaïri, F., 2019a. A chemo-mechanical model for osmo-inelastic effects in the annulus fibrosus. *Biomechanics and Modeling in Mechanobiology* 18, 1773-1790.
- Derrouiche, A., Zaouali, A., Zaïri, F., Ismail, J., Chaabane, M., Qu, Z., Zaïri, F., 2019b. Osmo-inelastic response of the intervertebral disc. *Proceedings of the Institution of Mechanical Engineers. Part H: Journal of Engineering in Medicine* 233, 332-341.
- Derrouiche, A., Karoui, A., Zaïri, F., Ismail, J., Qu, Z., Chaabane, M., Zaïri, F., 2020. The two Poisson's ratios in annulus fibrosus: relation with the osmo-inelastic features. *Mechanics of Soft Materials* 2, 1.
- Ebara, S., Iatridis, J.C., Setton, L.A., Foster, R.J., Mow, V.C., Weidenbaum, M., 1996. Tensile properties of nondegenerate human lumbar anulus fibrosus. *Spine* 21, 452-461.
- Ehlers, W., Karajan, N., Markert, B., 2009. An extended biphasic model for charged hydrated tissues with application to the intervertebral disc, *Biomechanics and Modeling in Mechanobiology*, 8, 233–251.
- Elliott, D.M, Setton, L.A., 2001. Anisotropic and inhomogeneous tensile behavior of the human anulus fibrosus: experimental measurement and material model predictions. *Journal of Biomechanical Engineering* 123, 256-263.
- Emanuel, K.S., van der Veen, A.J., Rustenburg, C.M.E., Smit, T.H., Kingma, I., 2018. Osmosis and viscoelasticity both contribute to time-dependent behaviour of the intervertebral disc under compressive load: a caprine in vitro study. *Journal of Biomechanics* 70, 10-15.
- Eyre, D.R., Muir, H. 1976. Types I and II collagens in intervertebral disc. Interchanging radial distributions in annulus fibrosus. *Biochemical Journal* 157, 267-270.
- Eyre, D.R., Muir, H., 1977. Quantitative analysis of types I and II collagens in the human intervertebral discs at various ages. *Biochimica Biophysica Acta*. 492, 29-42.
- Eyre, D.R., 1979. Biochemistry of the intervertebral disc. *International Review of Connective Tissue Research* 8, 227-291.
- Gatt, R., Wood, M.V., Gatt, A., Zarb, F., Formosa, C., Azzopardi, K.M., Casha, A., Agius, T.P., Schembri-Wismayer, P., Attard, L., Chockalingam, N., Grima, J.N., 2015. Negative Poisson's ratios in tendons: an unexpected mechanical response. *Acta Biomaterialia* 24, 201-208.
- Gent, A.N., 1996. A new constitutive relation for rubber. *Rubber Chemistry and Technology* 69, 59-61.

- Gregory, D.E., Bae, W.C., Sah, R.L., Masuda, K., 2012. Anular delamination strength of human lumbar intervertebral disc. *European Spine Journal* 21, 1716-1723.
- Guerin, H.A.L., Elliott, D.M., 2007. Quantifying the contributions of structure to annulus fibrosus mechanical function using a nonlinear, anisotropic, hyperelastic model. *Journal of Orthopaedic Research* 25, 508-516.
- Guo, Z.Y., Peng, X.Q., Moran, B. 2006. A composites-based hyperelastic constitutive model for soft tissue with application to the human annulus fibrosus. *Journal of the Mechanics and Physics of Solids* 54, 1952-1971.
- Gurtin, M.E., Anand, L., 2005. The decomposition $F=F^eF^p$, material symmetry, and plastic irrotationality for solids that are isotropic-viscoplastic or amorphous. *International Journal of Plasticity* 21, 1686-1719.
- Holmes, M.H., Mow, V.C., 1990. The nonlinear characteristics of soft gels and hydrated connective tissues in ultrafiltration. *Journal of Biomechanics* 23, 1145-1156.
- Holzappel, G.A., Gasser, T.C., 2001. A viscoelastic model for fiber-reinforced composites at finite strains: continuum basis, computational aspects and applications. *Computer Methods in Applied Mechanics and Engineering* 190, 4379-4403.
- Holzappel, G.A., Schulze-Bauer, C.A.J., Feigl, G., Regitnig, P., 2005. Single lamellar mechanics of the human lumbar anulus fibrosus. *Biomechanics and Modeling in Mechanobiology* 3, 125-140.
- Huyghe, J.M., Janssen, J.D., 1997. Quadriphasic mechanics of swelling incompressible porous media. *International Journal of Engineering Science* 35, 793-802.
- Huyghe, J.M., Jongeneelen, C.J.M., 2012. 3D non-affine finite strains measured in isolated bovine annulus fibrosus tissue samples. *Biomechanics and Modeling in Mechanobiology* 11,161–170
- Iatridis, J.C., Weidenbaum, M., Setton, L.A., Mow, V.C., 1996. Is the nucleus pulposus a solid or a fluid? mechanical behaviors of the human intervertebral disc. *Spine* 21, 1174-1184.
- Inoue, H., Takeda, T., 1975. Three-dimensional observation of collagen framework of lumbar intervertebral discs. *Acta Orthopaedica* 46, 949-956.
- Klein, J.A., Hukins, D.W.L., 1982. X-ray diffraction demonstrates reorientation of collagen fibres in the annulus fibrosus during compression of the intervertebral disc. *Biochimica et Biophysica Acta* 717, 61-64.
- Klisch, S.M., Lotz, J.C., 1999. Application of a fiber-reinforced continuum theory to multiple deformations of the annulus fibrosus. *Journal of Biomechanics* 32, 1027-1036.
- Klisch, S.M., Lotz, J.C., 2000. A special theory of biphasic mixtures and experimental results for human annulus fibrosus tested in confined compression. *Journal of Biomechanical Engineering* 122, 180-188.
- Labus, K.M., Han, S.K., Hsieh, A.H., Puttlitz, C.M., 2014. A computational model to describe the regional interlamellar shear of the annulus fibrosus. *Journal of Biomechanical Engineering* 136, 051009.
- Lanir, Y., 1987. Biorheology and fluid flux in swelling tissues. I. Bicomponent theory for small deformations, including concentration effects. *Biorheology* 24, 173-187.
- Lees, C., Vincent, J.F., Hillerton, J.E., 1991. Poisson's ratio in skin. *Bio-Medical Materials and Engineering* 1, 19-23.
- Li, LP, Soulhat, J., Buschmann, MD, Shirazi-Adl, A., 1999. Nonlinear analysis of cartilage in unconfined ramp compression using a fibril reinforced poroelastic model. *Clinical Biomechanics* 14, 673-682.
- Marchand, F., Ahmed, A.M., 1990. Investigation of the laminate structure of lumbar disc anulus fibrosus. *Spine* 15, 402-410.

- Maroudas, A., 1970. Distribution and diffusion of solutes in articular cartilage. *Biophysical Journal* 10, 365-379.
- Maroudas, A., Wachtel, E., Grushko, G., Katz, E.P., Weinberg, P., 1991. The effect of osmotic and mechanical pressures on water partitioning in articular cartilage. *Biochimica et Biophysica Acta* 1073, 285-294.
- Mengoni, M., Luxmoore, B.J., Wijayathunga, V.N., Jones, A.C. Broom, N.D., Wilcox, R.K., 2015. Derivation of inter-lamellar behaviour of the intervertebral disc annulus. *Journal of the Mechanical Behavior of Biomedical Materials* 48, 164-172.
- Michalek, A.J., Buckley, M.R., Bonassar, L.J., Cohen, I., Iatridis, J.C., 2009. Measurement of local strains in intervertebral disc anulus fibrosus tissue under dynamic shear: contributions of matrix fiber orientation and elastin content. *Journal of Biomechanics* 42, 2279-2285.
- Miehe, C., 1995. Entropic thermoelasticity at finite strains. Aspects of the formulation and numerical implementation. *Computer Methods in Applied Mechanics and Engineering* 120, 243-269.
- MSC.Marc, 2015. MSC.Marc Volume D: User Subroutines and Special Routines. MSC Software Corporation.
- Natarajan, R.N., Ke, J.H., Andersson, G.B., 1994. A model to study the disc degeneration process. *Spine* 19, 259-265.
- Nerurkar, N.L., Mauck, R.L., Elliott, D.M., 2011. Modeling interlamellar interactions in angle-ply biologic laminates for annulus fibrosus tissue engineering. *Biomechanics and Modeling in Mechanobiology* 10, 973-984.
- Newell, N., Little, J.P., Christou, A., Adams, M.A., Adam, C.J., Masouros, S.D., 2017. Biomechanics of the human intervertebral disc: a review of testing techniques and results. *Journal of the Mechanical Behavior of Biomedical Materials* 69, 420-434.
- O'Connell, G.D., Sen, S., Elliott, D.M., 2012. Human annulus fibrosus material properties from biaxial testing and constitutive modeling are altered with degeneration. *Biomechanics and Modeling in Mechanobiology* 11, 493-503.
- Ortolani, F., Raspanti, M., Franchi, M., Marchini, M., 1988. Localization of different alcian blue-proteoglycan particles in the intervertebral disc. *Basic and Applied Histochemistry* 32, 443-453.
- Parsons, E., Boyce, M.C., Parks, D.M., 2004. An experimental investigation of the large-strain tensile behavior of neat and rubber-toughened polycarbonate. *Polymer* 45, 2665-2684.
- Peng, X.Q., Guo, Z.Y., Moran, B., 2005. An anisotropic hyperelastic constitutive model with fiber-matrix shear interaction for the human annulus fibrosus. *Journal of Applied Mechanics* 73, 815-824.
- Pezowicz, C.A., Robertson, P.A., Broom, N.D., 2006. The structural basis of interlamellar cohesion in the intervertebral disc wall. *Journal of Anatomy* 208, 317-330.
- Pyrz, M., Zaïri, F., 2007. Identification of viscoplastic parameters of phenomenological constitutive equations for polymers by deterministic and evolutionary approach. *Modelling and Simulation in Materials Science and Engineering* 15, 85-103.
- Riches, P.E., Dhillon, N., Lotz, J., Woods, A.W., McNally, D.S., 2002. The internal mechanics of the intervertebral disc under cyclic loading. *Journal of Biomechanics* 35, 1263-1271
- Roughley, P.J., 2004. Biology of intervertebral disc aging and degeneration: involvement of the extracellular matrix. *Spine* 29, 2691-2999.
- Roux, D.C., Cooper-White, J.J., McKinley, G.H., Tirtaatmadja, V., 2003. Drop impact of newtonian and elastic fluids. *Physics of Fluids* 15, S12-S12.

- Schroeder, J., Neff, P., 2003. Invariant formulation of hyperelastic transverse isotropy based on polyconvex free energy functions. *International Journal of Solids and Structures* 40, 401-445.
- Schroeder, Y., Wilson W., Huyghe, J.M., Baaijens, F.P.T., 2006. Osmoviscoelastic finite element model of the intervertebral disc. *European Spine Journal* 15, 361-371.
- Schroeder, Y., Sivan, S., Wilson, W., Merkher, Y., Huyghe, J.M., Maroudas, A., Baaijens, F.P.T., 2007. Are disc pressure, stress, and osmolarity affected by intra- and extrafibrillar fluid exchange? *Journal of Orthopaedic Research* 25, 1317-1324.
- Shirazi-Adl, S.A., Shrivastava, S.C., Ahmed, A.M., 1984. Stress analysis of the lumbar disc-body unit in compression. A three dimensional nonlinear finite element study. *Spine* 9, 120-134.
- Shirazi-Adl, A., 1989. Strain in fibers of a lumbar disc: analysis of the role of lifting in producing disc prolapsed. *Spine* 14, 96-103.
- Showalter, B.L., Beckstein, J.C., Martin, J.T., Beattie, E.E., Orias, A.A.E., Schaer, T.P., Vresilovic, E.J., Elliott, D.M., 2012. Comparison of animal discs used in disc research to human lumbar disc: torsion mechanics and collagen content. *Spine* 37, 900-907.
- Singha, K., Singha, M., 2012. Biomechanism profile of intervertebral disc's (IVD): strategies to successful tissue engineering for spinal healing by reinforced composite structure. *Journal of Tissue Science & Engineering* 3, 1000118.
- Skaggs, D.L., Weidenbaum, M., Iatridis, J.C., Ratcliffe, A., Mow, V.C., 1994. Regional variation in tensile properties and biochemical composition of the human lumbar annulus fibrosus. *Spine* 19, 1310-1319.
- Tavakoli, J., Elliott, D.M., Costi, J.J., 2016. Structure and mechanical function of the interlamellar matrix of the annulus fibrosus in the disc. *Journal of Orthopaedic Research* 34, 1307-1315.
- Tavakoli, J., Elliott, D.M., Costi, J.J., 2017. The ultra-structural organization of the elastic network in the intra- and inter-lamellar matrix of the intervertebral disc. *Acta Biomaterialia* 58, 269-277.
- Tavakoli, J., Costi, J.J., 2018. New findings confirm the viscoelastic behaviour of the interlamellar matrix of the disc annulus fibrosus in radial and circumferential directions of loading. *Acta Biomaterialia* 71, 411-419.
- Timmins, L.H., Wu, Q., Yeh, A.T., Moore, J.E., Greenwald, S.E., 2010. Structural inhomogeneity and fiber orientation in the inner arterial media. *American Journal of Physiology - Heart and Circulatory Physiology* 298, 1537-1545.
- Urban, J.P., McMullin, J.F., 1985. Swelling pressure of the intervertebral disc: influence of proteoglycan and collagen contents. *Biorheology* 22, 145-157.
- Vergari, C., Mansfield, J., Meakin, J.R., Winlove, P.C., 2016. Lamellar and fibre bundle mechanics of the annulus fibrosus in bovine intervertebral disc. *Acta Biomaterialia* 37, 14-20.
- Wagner, D.R., Lotz, J.C., 2004. Theoretical model and experimental results for the nonlinear elastic behavior of human annulus fibrosus. *Journal of Orthopaedic Research* 22, 901-909.
- Wilson, W., van Donkelaar, C.C., van Rietbergen, C., Ito, K., Huiskes, R., 2004. Stresses in the local collagen network of articular cartilage: a poroviscoelastic fibril-reinforced finite element study. *Journal of Biomechanics* 37, 357-366.
- Yu, J., Tirlapur, U., Fairbank, J., Handford, P., Roberts, S., Winlove, C.P., Cui, Z., Urban, J., 2007. Microfibrils, elastin fibres and collagen fibres in the human intervertebral disc and bovine tail disc. *Journal of Anatomy* 210, 460-471.

Chapter III

Interlamellar matrix governs human annulus fibrosus multi-axial behavior⁷

Abstract

Establishing accurate structure-property relationships for intervertebral disc annulus fibrosus tissue is a fundamental task for a reliable computer simulation of the human spine but needs excessive theoretical-numerical-experimental works. The difficulty emanates from multi-axiality and anisotropy of the tissue response along with regional dependency of a complex hierarchic structure interacting with the surrounding environment. We present a new and simple hybrid microstructure-based experimental/modeling strategy allowing adaptation of animal disc model to human one. The trans-species strategy requires solely the basic knowledge of the uniaxial circumferential response of two different animal disc regions to predict the multi-axial response of any human disc region. This work demonstrates for the first time the determining role of the interlamellar matrix connecting the fibers-reinforced lamellae in the disc multi-axial response. Our approach shows encouraging multi-axial predictive capabilities making it a promising tool for human spine long-term prediction.

Keywords: Human annulus fibrosus; Multi-axiality; Regional dependency; Prediction.

⁷ *This chapter is based on the following article: Kandil, K., Zaïri, F., Messenger, T., Zaïri, F., 2020. Interlamellar matrix governs human annulus fibrosus multiaxial behavior. Scientific Reports 10, 19292.*

III.1. Partial introduction

The intervertebral disc is the most critical body part due to its essential and mandatory role during the daily activities such as work, sport, walking or even while only standing up without any movement. It is always subjected to multi-axial loadings increasing its internal local stresses which could lead to disc damage, hernia and severe pain (Vos et al., 2016). Because of the complex couplings existing between microstructure at different scales, intrinsic properties (viscosity and nonlinearity), internal fluid flow and external loading mode, the knowledge of stress distribution in disc needs to call computer simulations. Over the last four decades, it was an important subject of research but, to date, there is no disc computational model that introduces the entire set of features. The first contributions modeled the disc as an elastic tangled extracellular matrix (ECM) solid phase rigidified by elastic collagen fibers (CFs) (Shirazi-Adl et al., 1984; Klisch and Lotz, 1999; Wagner and Lotz, 2004; Guo et al., 2006; Guerin and Elliot, 2007). Then, biphasic models appeared adding the fluid phase to the disc structure and taking into account its diffusion inside the disc (Argoubi and Shirazi-Adl, 1996; Ayotte et al., 2000; Klisch and Lotz, 2000; Riches et al., 2002). Finally, biphasic models were extended in order to incorporate the ECM negative charges effect and their influence on the fluid movement and intradiscal osmotic pressure in the loaded and unloaded states (Huyghe and Janssen, 1997; Schroeder et al., 2006; Ehlers et al., 2009; Zhou et al., 2020). In the most recent publications, the time-dependency of the soft tissue response is neglected. This is obviously not consistent with the viscoelastic insights of the different disc components (Schroeder et al., 2006; Ehlers et al., 2009; Wilson et al., 2004) but also with the fluid transfer inside and outside the disc that affects largely the biochemical volumetric behavior of the tissue (Baldit el al., 2014; Derrouiche et al., 2019a; Kandil et al., 2019), see chapter II. As common weak points, most of recent models need plenty of experimental testing sets in order to calibrate, fit and design them. Moreover, as mentioned in

the literature, it is not possible to predict the multi-axial behavior of the disc by means of uniaxial data (Bass et al., 2004; O'Connell et al., 2012). As a consequence, for each local region of the disc a new experimental test should be established for the construction of each uniaxial and multi-axial model, and the identification of a new set of parameters corresponding to each test is required (Bass et al., 2004; O'Connell et al., 2012; Peng et al., 2005; del Palomar et al., 2008) or a fitting procedure including all uniaxial and multi-axial data that leads to non-accurate results for both data (Klisch and Lotz, 2000; Wagner et al., 2006; Hollingsworth and Wagner 2011). Also, the construction of an accurate heterogeneous model taking into account the different radial and circumferential microstructure features of the disc requires exploring and identifying the corresponding related parameters of each region. No model until now is able to predict the uniaxial behavior of some disc regions based only on their microstructure components and to extend this behavior in order to predict the multi-axial response of the tissue. The actual models are able to estimate stress levels inside the disc with a completely wrong tissue volumetric deformation. In this regard, in the most recent models (Derrouiche et al., 2019a; Kandil et al., 2019), the interlamellar (ILM) matrix connecting the fibers-reinforced lamellae was introduced as a key structural factor of the inter-layer fluid transfer mechanism responsible for the tissue transversal behavior in the axial and radial disc directions. Strictly speaking, the structural contribution of this zone cannot be overlooked (Pezowicz et al., 2005, 2006; Gregory et al., 2012; Labus et al., 2014; Adam et al., 2015; Mengoni et al., 2015; Tavakoli et al., 2017, 2018) but its exact role in the disc biomechanics remains still mysterious.

This work addresses the problem of the multi-axial mechanics prediction of human disc. The main objective is to provide a quantitative prediction of the multi-axial response of a complete human disc with a minimum of experiments by means of a hybrid trans-species experimental/modeling strategy requiring the basic knowledge of the uniaxial circumferential

response of only two different animal disc regions. Different model simulations are designed based upon well-known experimental tests issued from the literature in order to perfectly approve the model validity under identical conditions. As far as we know, a few experimental data are available in the literature for uniaxial stretching (Skaggs et al., 1994; Ebara et al., 1996; Holzapfel et al., 2005), biaxial stretching (Bass et al., 2004; O'Connell et al., 2012) and shearing (Fujita et al., 2000) tests often conducted under different testing conditions (Other publications could be found in the literature but they are limited to a single annulus region or present only one case of biaxial loading or shear response of a single shear mode). Our approach, fully three-dimensional, incorporates the different intrinsic and microstructure features that play a key role in the disc multi-axial response: ECM viscoelasticity, osmo-induced ECM swelling, CFs content/orientation and ILM matrix. Its principle advantage is its ability to be used almost under any experimental conditions reported in the open literature including variations in specimen shape and loading conditions in terms of strain rate and maximum strains in order to reproduce exactly the effectuated test. The model results are investigated and correlated to the different physiological movements and important conclusions are deduced.

III.2. Methods

III.2.1. Computational models

Uniaxial stretching, biaxial stretching and shearing are all considered in this work. The three sets of experiments are replicated in-silico using the finite element method according to the experimental recommendations available in the literature regarding specimen shapes, sizes and mechanical conditions in terms of strain rate and maximum strain. As observed in the works of Gregory and Callaghan (2010) and Derrouiche et al. (2020a) the strain rate has an effect on the stress-strain and transversal responses of the multi-lamellar annulus specimen.

As a consequence, for all the simulated tests, quasi-static conditions were ensured by using strain rates of 0.002 s^{-1} and 0.0002 s^{-1} depending on the strain rate level of the reproduced experimental test. The maximum strain used in all the simulations varies between 5% and 10% which corresponds to the maximum physiological strain level observed experimentally for annulus under compression (Costi et al., 2007; Shirazi-Adl, 1989). The latter values have been often used in many experimental studies (Baldit el al., 2014; Ebara et al., 1996). All the geometrical models were meshed using isoparametric and arbitrarily hexahedrics 8-node meshing elements. An adequate element size is chosen to ensure mesh-independency. All the ILM-lamellar interfaces of the stratified soft tissue are considered perfect. The structural features used as model inputs for the different human disc regions are reported in Table III.1 and are extracted from well-documented papers of the literature (Holzapfel et al., 2005; Showalter et al., 2012; Eyre and Muir, 1976, 1977; Iatridis et al., 2007).

| | AO | PO | AI | PI |
|--------------------|-------|-------|-----|-----|
| Fibers content | 12.5% | 12.5% | 5% | 5% |
| Fibers orientation | 21° | 45° | 35° | 45° |
| Water content | 74% | 74% | 80% | 80% |

Table III.1. Structure features of the human disc. The fibers content decreases radially while getting closer to the nucleus (Showalter et al., 2012; Eyre and Muir, 1976, 1977). The fibers orientation increases and tends towards the spinal axial direction while getting closer to the nucleus³⁵. The water content increases radially in the disc while getting closer to the nucleus. A non-significant water content difference exists between the posterior and anterior regions (Iatridis et al., 2007).

III.2.2. Uniaxial stretching conditions and designed material kinetics

A computational model was designed as described in chapter II for the uniaxial conditions. Due to the large specimen size and large calculation time, a representative elementary volume (REV) of the specimen was designed in order to reproduce the in-vitro experiments of Ebara et al. (1996) and Balnit et al. (2014). A REV of $2 \times 2 \times 1.6$ mm is modeled. The same REV was used to model the experiments of the two papers. Similar boundary conditions were applied but different symmetry conditions were considered in each case. For the Balnit et al. (2014) specimen, the corresponding modeled REV is one-fourth of the specimen cross-section and one-sixth of the specimen height and for the Ebara et al. (1996) specimen, it corresponds to one-half of the specimen cross-section and one-sixth of the specimen height.

Experimentally-based kinetics has been designed in chapter II using the bovine model. The human disc contains a lower CFs content and slightly higher water content compared to bovine disc (Beckstein et al., 2008; Showalter et al., 2012). As illustrated in Figure III.1, a hybrid experimental/modeling strategy for the trans-species transfer from bovine to human intervertebral disc model is adopted via a three-step methodology to reach the final result of model vs. experiments and the related predictions. In the first step, the fluid transfer equations first developed for bovine annulus in chapter II were adapted to the human annulus by adjusting the fluid kinetics on the human (AO and AI) experimental transversal curves of Balnit et al. (2014) shown in Figure III.1. In the second step, the fiber intrinsic mechanical parameters were identified using the human (AO and AI) experimental stress-strain curves of Ebara et al. (1996). In the third step, the predictions were made possible in the remaining posterior (PO and PI) regions by applying the related fibers content/orientation and water concentration.

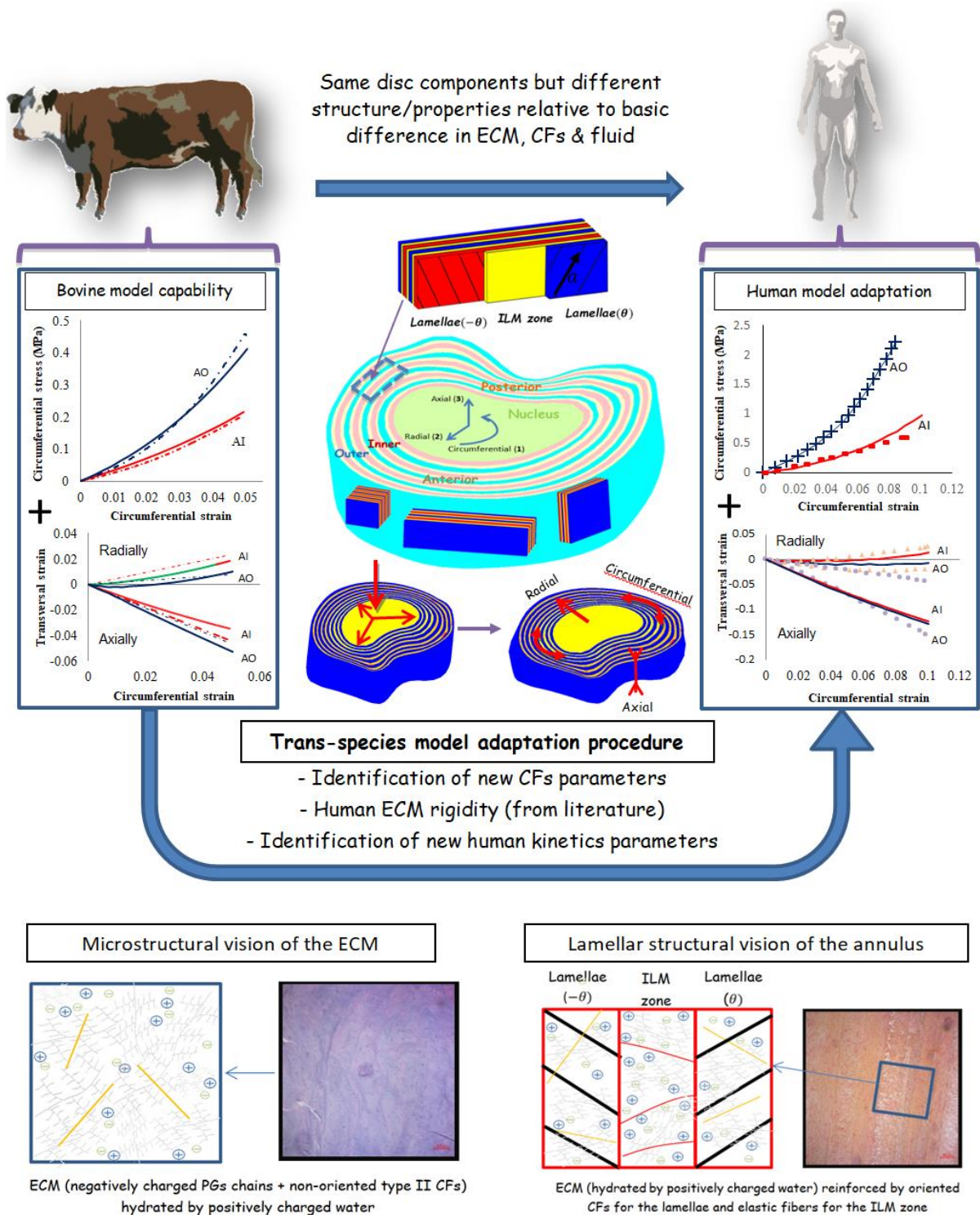


Figure III.1. Hybrid experimental/modeling strategy for the trans-species transfer from bovine to human intervertebral disc model (solid lines: simulations, dashed lines/symbols: experiments). The microstructure-based model, identified using a very few data (only two uniaxial stress-strain responses in the circumferential direction at two disc regions and its related transversal strain history in axial and radial directions), provides the multi-axial quantitative predictions of the entire human disc.

III.2.3. Biaxial stretching conditions

Different biaxial loading cases were simulated with the same specimen dimensions reported for the in-vitro experiments of O'Connell et al. (2012): $7 \times 7 \times 1.6$ mm. The computational models were subjected to different strain loading ratios (= circumferential strain : axial strain, {1:0, 0:1, 1:2, 2:1 and 1:1}) along with a maximum strain of 5% and a strain rate of 0.0002 s^{-1} . Two sets of tests were established. The first one consisted on circumferential stress calculation while the second one on axial stress calculation, both under the different loading ratios.

III.2.4. Shearing conditions

Three shear modes were simulated following the boundary conditions of Fujita et al. (2000): 12, 13 and 23 (see Figure III.4) using 3.33 mm cubes subjected to a maximum shear strain of 5% and a shear strain rate of 0.0002 s^{-1} . Because the in-vitro experiments of Fujita et al. (2000) were performed on anterior specimens but without mentioning their exact radial positions, both AO and AI computational models were considered. Due to a negligible fluid transfer upon shearing, the latter was not considered in the computational models.

III.2.5. Microstructure-based constitutive model

In what follows, the key points of the chemo-mechanical model are briefly summarized. The model is fully three-dimensional and considers the time-dependency of the annulus fibrosus tissue response in relation to the microstructure, the intrinsic features and the chemical-induced internal fluid variation.

III.2.5.1. Kinematics

Starting point for the derivation of any finite-strain constitutive model is the kinematics within the framework of nonlinear continuum mechanics. If \boldsymbol{x} is the current position of a

material point of the continuum body located at \mathbf{X} in the initial configuration, the deformation gradient tensor is: $\mathbf{F} = \partial \mathbf{x} / \partial \mathbf{X}$. The time derivative is defined as: $\dot{\mathbf{F}} = \mathbf{L}\mathbf{F}$ in which $\mathbf{L} = \partial \mathbf{v} / \partial \mathbf{x}$ is the spatial velocity gradient tensor with $\mathbf{v} = \partial \mathbf{x} / \partial t$. Let us consider an intermediate virtual configuration for the chemical coupling with the surrounding environment. This concept allows to further multiplicatively split the tensor \mathbf{F} into two contributions: $\mathbf{F} = \mathbf{F}_{mech} \mathbf{F}_{chem}$ in which \mathbf{F}_{mech} is the mechanical part and \mathbf{F}_{chem} is the chemical-induced volumetric part. Using a similar sequence of configurations with an intermediate virtual configuration during a spontaneous elastic unloading, the mechanical deformation gradient tensor \mathbf{F}_{mech} is in turn multiplicatively split into an elastic part \mathbf{F}_e and a viscous part \mathbf{F}_v such as: $\mathbf{F}_{mech} = \mathbf{F}_e \mathbf{F}_v$ in the aim representing the intrinsic viscosity of the ECM including all non-fibrillar “solid” components. In view of the mechanical incompressibility of all “solid” components (ECM and CFs), the determinants (Jacobian) of the viscous and elastic deformation gradients are: $J_v = \det(\mathbf{F}_v) = 1$ and $J_e = \det(\mathbf{F}_e) = 1$. The chemical-induced volumetric part is: $\mathbf{F}_{chem} = \mathbf{I} J^{1/3}$ in which \mathbf{I} is the unit tensor and $J = \det(\mathbf{F}) > 0$ is the determinant of the deformation gradient tensor, i.e. the tissue volumetric deformation. The spatial velocity gradient tensor \mathbf{L} is additively split into a mechanical part \mathbf{L}_{mech} and a chemical part \mathbf{L}_{chem} as: $\mathbf{L} = \mathbf{L}_{mech} + \mathbf{L}_{chem}$ with $\mathbf{L}_{chem} = \mathbf{F}_{mech} \dot{\mathbf{F}}_{chem} \mathbf{F}_{chem}^{-1} \mathbf{F}_{mech}^{-1} = \mathbf{I} \dot{J} / 3J$ and $\mathbf{L}_{mech} = \dot{\mathbf{F}}_{mech} \mathbf{F}_{mech}^{-1} = \mathbf{L}_e + \mathbf{L}_v$ in which $\mathbf{L}_e = \dot{\mathbf{F}}_e \mathbf{F}_e^{-1}$ is the elastic part and $\mathbf{L}_v = \mathbf{F}_e \dot{\mathbf{F}}_v \mathbf{F}_v^{-1} \mathbf{F}_e^{-1}$ is the viscous part that in turn may be written as: $\mathbf{L}_v = \mathbf{D}_v + \mathbf{W}_v$ in which $\mathbf{D}_v = (\mathbf{L}_v + \mathbf{L}_v^T) / 2$ is the (symmetric) viscous stretching rate tensor and $\mathbf{W}_v = (\mathbf{L}_v - \mathbf{L}_v^T) / 2$ is the (skew-symmetric) viscous spin rate tensor. The common assumption of viscous irrotationality is applied with no loss in generality (Gurtin and Anand, 2005), i.e. $\mathbf{W}_v = \mathbf{0}$ and $\mathbf{D}_v = \mathbf{L}_v$. The different

contributions of the right and left Cauchy-Green deformation tensors, $\mathbf{C} = \mathbf{F}^T \mathbf{F}$ and $\mathbf{B} = \mathbf{F} \mathbf{F}^T$, are: $\mathbf{C}_{mech} = \mathbf{F}_{mech}^T \mathbf{F}_{mech}$, $\mathbf{B}_{mech} = \mathbf{F}_{mech} \mathbf{F}_{mech}^T$, $\mathbf{C}_e = \mathbf{F}_e^T \mathbf{F}_e$, $\mathbf{B}_e = \mathbf{F}_e \mathbf{F}_e^T$, $\mathbf{C}_v = \mathbf{F}_v^T \mathbf{F}_v$, $\mathbf{B}_v = \mathbf{F}_v \mathbf{F}_v^T$, $\mathbf{C}_{chem} = J^{2/3} \mathbf{I}$ and $\mathbf{B}_{chem} = J^{2/3} \mathbf{I}$.

III.2.5.2. Constitutive equations

In the aim of attributing a constitutive relationship to each main component (ECM, CFs and fluid) of the annulus fibrosus tissue, the free energy function ψ is additively split via the volume fraction concept:

$$\psi = (1 - \phi_{CF}) \psi_{ECM} + \phi_{CF} \psi_{CF} + (1 - \phi_{CF}) \psi_{chem} \quad (\text{III.1})$$

where ϕ_{CF} is the CFs content, ψ_{ECM} is the ECM free energy function, ψ_{CF} is the CFs free energy function and ψ_{chem} is the chemical-induced volumetric free energy function, respectively, given by:

$$\psi_{ECM} = -\frac{E}{6} I_1^{\max} \ln \left(1 - \frac{I_1 - 3}{I_1^{\max}} \right) - \frac{E_v}{6} I_{1v}^{\max} \ln \left(1 - \frac{I_{1e} - 3}{I_{1v}^{\max}} \right) \quad (\text{III.2})$$

$$\psi_{CF} = A_1 (I_4 - 1) + A_2 (I_4 - 1)^2 - 2A_1 \ln \left(\lambda_I^{x^2} \lambda_{II}^{y^2} \lambda_{III}^{z^2} \right) \quad (\text{III.3})$$

$$\psi_{chem} = \frac{1}{4} k (J^2 - 1 - 2 \ln J) \quad (\text{III.4})$$

The free energy function (III.2) corresponds to a Gent formulation (Gent, 1996) in which an additive split into elastic and inelastic contributions is considered. The terms $I_1 = \text{tr} \mathbf{B}_{mech}$ and $I_{1e} = \text{tr} \mathbf{B}_e$ are the first invariants. The free energy function (III.3) introduces $I_4 = \mathbf{a} \mathbf{C}_{mech} \mathbf{a}$ as the fourth invariant where $\mathbf{a} = x \mathbf{e}_1 + y \mathbf{e}_2 + z \mathbf{e}_3$ is the unit vector in the initial configuration (Cantournet et al., 2007) (see Figure III.1). The terms $\lambda_I = \sqrt{\mathbf{e}_1 \mathbf{C}_{mech} \mathbf{e}_1}$, $\lambda_{II} = \sqrt{\mathbf{e}_2 \mathbf{C}_{mech} \mathbf{e}_2}$ and $\lambda_{III} = \sqrt{\mathbf{e}_3 \mathbf{C}_{mech} \mathbf{e}_3}$ are the stretches along the CFs principal axes. Remind that ILM is a non-

fibrillar zone, i.e. $\phi_{CF}=0$ in ILM. The material constants are the ECM tensile modulus E , the ECM limiting extensibility constant I_1^{\max} , the ECM viscous constants E_v and I_{1v}^{\max} , the CFs constants A_1 and A_2 , and the bulk modulus k .

The set of free energy functions (III.2), (III.3) and (III.4) forms the basis of a suitable theory to constitutively coordinate the dual stress and strain tensors:

$$\boldsymbol{\sigma} = (1 - \phi_{CF}) \boldsymbol{\sigma}_{ECM} + \phi_{CF} \boldsymbol{\sigma}_{CF} + (1 - \phi_{CF}) \boldsymbol{\sigma}_{chem} \quad (\text{III.5})$$

where the mechanical-based Cauchy stresses in the ECM and CFs, $\boldsymbol{\sigma}_{ECM}$ and $\boldsymbol{\sigma}_{CF}$, are deduced from the differentiation of the free energy functions (III.2) and (III.3) with respect to the corresponding deformations:

$$\boldsymbol{\sigma}_{ECM} = \frac{2}{J} \mathbf{F}_{mech} \frac{\partial \psi_{ECM}}{\partial \mathbf{C}_{mech}} \mathbf{F}_{mech}^T + \frac{2}{J} \mathbf{F}_e \frac{\partial \psi_{ECM}}{\partial \mathbf{C}_e} \mathbf{F}_e^T \quad \text{and} \quad \boldsymbol{\sigma}_{CF} = \frac{2}{J} \mathbf{F}_{mech} \frac{\partial \psi_{CF}}{\partial \mathbf{C}_{mech}} \mathbf{F}_{mech}^T \quad (\text{III.6})$$

in which the first term of the left formula corresponds to the elastic Cauchy stress $\boldsymbol{\sigma}_e$ and the second term corresponds to the viscous Cauchy stress $\boldsymbol{\sigma}_v$, such that $\boldsymbol{\sigma}_{ECM} = \boldsymbol{\sigma}_e + \boldsymbol{\sigma}_v$. Note that the mechanical incompressibility of all “solid” components (ECM and CFs) means that the mechanical-based Cauchy stresses in the ECM and CFs are traceless tensors, i.e. $\text{tr}(\boldsymbol{\sigma}_e) = 0$, $\text{tr}(\boldsymbol{\sigma}_v) = 0$ and $\text{tr}(\boldsymbol{\sigma}_{CF}) = 0$. The chemical-based Cauchy stress $\boldsymbol{\sigma}_{chem} = p \mathbf{I}$ ($p = \text{tr}(\boldsymbol{\sigma})/3$ being the hydrostatic pressure) is deduced from the differentiation of the free energy function (III.4) with respect to the tissue volumetric deformation:

$$\boldsymbol{\sigma}_{chem} = \frac{\partial \psi_{chem}}{\partial J} \mathbf{I} \quad (\text{III.7})$$

The driving force for the viscous Cauchy stress $\boldsymbol{\sigma}_v$ is the elastic deformation gradient tensor $\mathbf{F}_e = \mathbf{F}_{mech} \mathbf{F}_v^{-1}$, the viscous deformation gradient tensor \mathbf{F}_v being computed via $\dot{\mathbf{F}}_v = \mathbf{F}_e^{-1} \mathbf{D}_v \mathbf{F}_{mech}$.

The viscous stretching rate tensor \mathbf{D}_v is described by the following flow rule:

$\mathbf{D}_v = \dot{\gamma}_v \boldsymbol{\sigma}'_v / \sqrt{2} \|\boldsymbol{\sigma}_v\|$ where $\|\boldsymbol{\sigma}_v\| = \sqrt{\text{tr}(\boldsymbol{\sigma}'_v \boldsymbol{\sigma}'_v) / 2}$ is the effective value of the viscous Cauchy stress $\boldsymbol{\sigma}_v$, $\boldsymbol{\sigma}'_v$ is the deviatoric part of $\boldsymbol{\sigma}_v$ and $\dot{\gamma}_v$ is the accumulated viscous strain rate. Invoking a viscoplasticity with no threshold (Pyrz and Zairi, 2007), the following expression is retained (Bergstrom and Boyce, 1998):

$$\dot{\gamma}_v = d \left| \sqrt{I_{1v}/3} - 1 \right|^{-m} \|\boldsymbol{\sigma}_v\| \quad (\text{III.8})$$

where d is the ECM viscous multiplier constant and m is the ECM viscous stretch-dependency constant. The term $I_{1v} = \text{tr} \mathbf{B}_v$ is the first invariant of the left Cauchy-Green strain tensor $\mathbf{B}_v = \mathbf{F}_v \mathbf{F}_v^T$.

The fluid flow governs the transversal strains (radially and axially) and is responsible of the unusual Poisson's ratios of the tissue. For this reason accurate experimentally-based fluid kinetics is required, which is the missing point of all available papers in the literature. The adopted fluid flow kinetics is defined by the Jacobian J as follows:

$$J = n_{f_m} \xi \eta \quad (\text{III.9})$$

in which ΔJ represents the tissue swelling function controlling the fluid movement inside the disc under mechanical loading, n_{f_m} is the internal fluid content, ξ is a dimensionless transportation coefficient, η is a dimensionless free swelling coefficient (equal to 0.5 in the case of physiological salt condition) and n_{f_m} is the internal fluid content. The latter is controlled by:

$$\dot{n}_{f_m} = \beta_m \left(1 - \frac{n_{f_m}}{n_{f_{im}}} \right) \quad (\text{III.10})$$

where β_m is the fluid flow constant and $n_{f_{im}}$ is the maximum fluid content that could be reached inside the disc.

The constitutive model has been implemented into the finite element code MSC.Marc by means of a set of subroutines. The main calculation steps of the model implementation are provided in chapter I. The reader is also referred to complementary references (Ovalle-Rodas et al., 2016; Guo et al., 2018) for the general implementation procedure of coupled models.

III.2.5.3. Parameters identification

The model parameters and the material kinetics have been determined using experimental data in order to represent the human disc annulus response in connection to microstructure differences in the different disc regions (Table III.1). The experimentally-based fluid flow kinetics is guided by the applied mechanical loading and the osmotic effect. Also, due to the fibers presence retarding the fluid movement in lamellae and the difference of the fixed charges density in the two zones, ILM and lamellae behave differently. The values of β_m are, respectively, for the lamellae and ILM zones:

$$\beta_{m_{lam}} = -0.0004 \text{ s}^{-1} \text{ and } \beta_{m_{ILM}} = 0.00097 \text{ s}^{-1} \quad (\text{III.11})$$

The transportation coefficient ξ is a function of the strain rate $\dot{\epsilon}$ and is described by the following equations for the lamellae and ILM zones:

$$\xi_{AI_{lam}} = \xi_{PI_{lam}} = 20328 \dot{\epsilon} - 0.4056 \text{ and } \xi_{AO_{lam}} = \xi_{PO_{lam}} = 13283 \dot{\epsilon} - 0.1767 \quad (\text{III.12})$$

$$\xi_{AI_{ILM}} = \xi_{PI_{ILM}} = 7455.6 \dot{\epsilon} + 0.3789 \text{ and } \xi_{AO_{ILM}} = \xi_{PO_{ILM}} = 3719.4 \dot{\epsilon} + 0.2011 \quad (\text{III.13})$$

The difference in the inner and outer disc volumetric responses is translated by different bulk moduli:

$$k_{AI} = k_{PI} = 800 \text{ MPa and } k_{AO} = k_{PO} = 3500 \text{ MPa} \quad (\text{III.14})$$

Note that the fluid kinetics that were defined in chapter II is found able to reproduce the typical transversal strain history reported by Baldit et al. (2014). Similar trends are obtained with the newly identified human parameters due to the close water content between human

and bovine. Although the ECM stiffness could vary from a disc region to another, it was chosen to be the same throughout the disc due to its small contribution to the complete disc stiffness compared to the fibers and its value was taken from the literature (Yao et al., 2006; Tang et al., 2011). The intrinsic viscoelasticity of the ECM was also considered regional independent. The set of ECM material constants is:

$$\{E, E_v, I_1^{\max}, I_{1v}^{\max}, d, m\} = \{1 \text{ MPa}, 0.167 \text{ MPa}, 3 \text{ MPa}, 1.5 \text{ MPa}, 0.02 \text{ MPa}^{-1}\text{s}^{-1}, 0.001\} \quad (\text{III.15})$$

The effect of CFs is considered to be mainly governed by their content and orientation. The CFs intrinsic mechanical parameters would not change for the different disc regions:

$$\{A_1, A_2\} = \{27 \text{ MPa}, 100 \text{ MPa}\} \quad (\text{III.16})$$

III.3. Results

III.3.1. Uniaxial stretching path along with regional effects

Uniaxial stretching responses were reproduced in-silico for specimens extracted from four different circumferential and radial disc regions (AO, PO, AI and PI) as shown in Figure III.1. The circumferential stress-strain and transversal responses of the four regions are reported in Figure III.2. The AO and AI regions were used to identify the fluid kinetics and the CFs parameters inside human intervertebral disc using a hybrid experimental/modeling strategy as described in Figure III.1. The latter will be discussed in details in Methods Section. The response of the remaining disc regions, namely PO and PI, was then predicted by adapting well-known microstructure features in terms of CFs content/orientation and water content. The fitted and predicted numerical curves show an excellent agreement with the regional experimental results of Ebara et al. (1996) and Baldit et al. (2014). The behavior highlights a direct relation between the overall soft tissue mechanics, in terms of stiffness and Poisson's

ratio, and the microstructures along with the regional (circumferential and radial) variation in CFs content/orientation. The slopes of the predicted stress-strain curves of the posterior regions are lower than those obtained for the anterior regions. As well, the outer annulus is stiffer than the inner annulus. Quite interestingly, a very small radial deformation of the inner disc region compared to the outer disc region is obtained. The circumferential deformation is almost regional independent and its variation is negligible from a region to another. The very soft PI response reported for multi-lamellar or single lamellar specimens (Ebara et al., 1996; Holzapfel et al., 2005) are impossible to catch with the model along CFs content is used as input data whereas it could almost be obtained by considering a non-fibrous ECM. The fibers content effect on the PI stiffness was investigated trying to find good explanations about this finding. An effective CFs content is suggested inspired from the microscopic observations of Tsuji et al. (1993) and Smith and Fazzalari (2006) who noticed a non-well-arranged CFs in the PI region compared to others. The stress-strain behavior was reproduced under different amounts of effective CFs and the corresponding stiffness was calculated and compared to the experimental results in Figure III.2. The effective CFs content shows a high ability to describe the low PI rigidity. Lower effective CFs content induces a lower rigidity modulus and a lower slope of the stress-strain conduct.

It is worth noticing that the model parameters were fitted using the uniaxial stretching data and the identified set of model parameters was used to generate the multi-axial predictions without any change or adjustment.

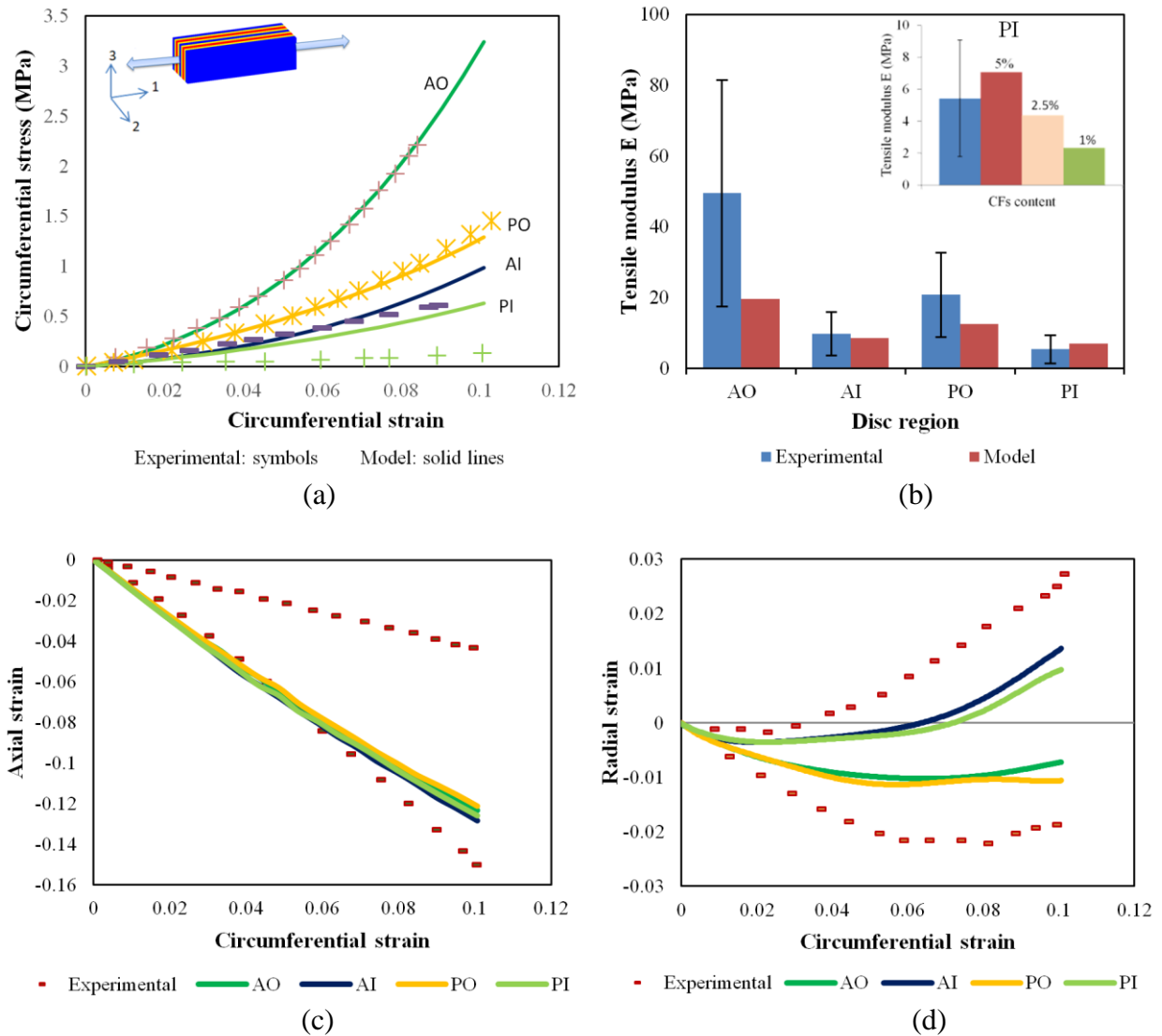
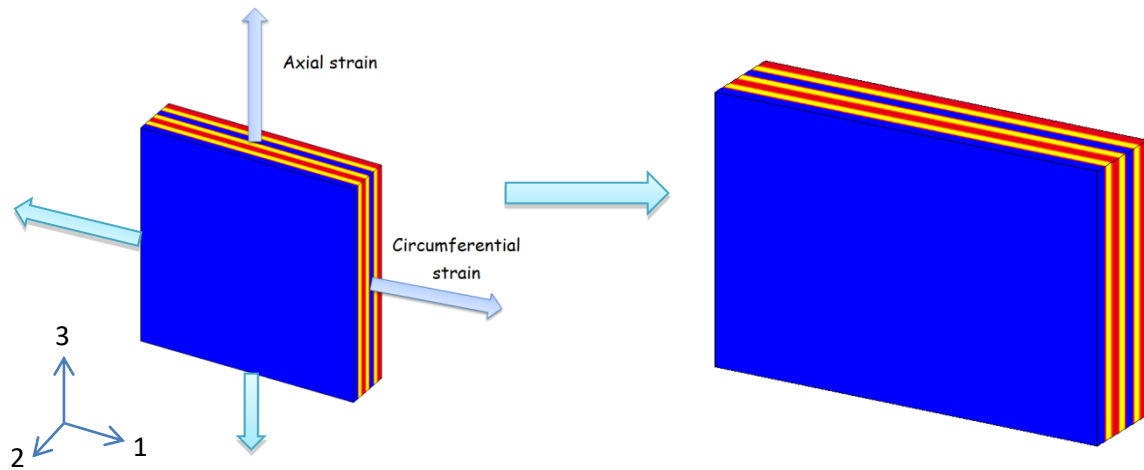


Figure III.2. Uniaxial stretching model results in terms of (a) stress-strain responses and (b) tensile moduli compared to experimental data of Ebara et al. (1996), the insert shows PI predictions for different amounts of effective CFs, (c) transversal strain history in axial direction and (d) transversal strain history in radial direction compared to experimental data of Baldit et al. (2004). The figure shows the model fitting results for AO and AI to experimental data and the model predictions for PO and PI.

III.3.2. Biaxial stretching paths

The predictions in terms of AO biaxial stretching responses are plotted for different biaxial strain ratios in Figure III.3. The in-silico results are compared to the typical in-vitro experimental results of O’Connell et al. (2012) reproducing the same experimental conditions.



Biaxial strain ratio = Circumferential strain : Axial strain

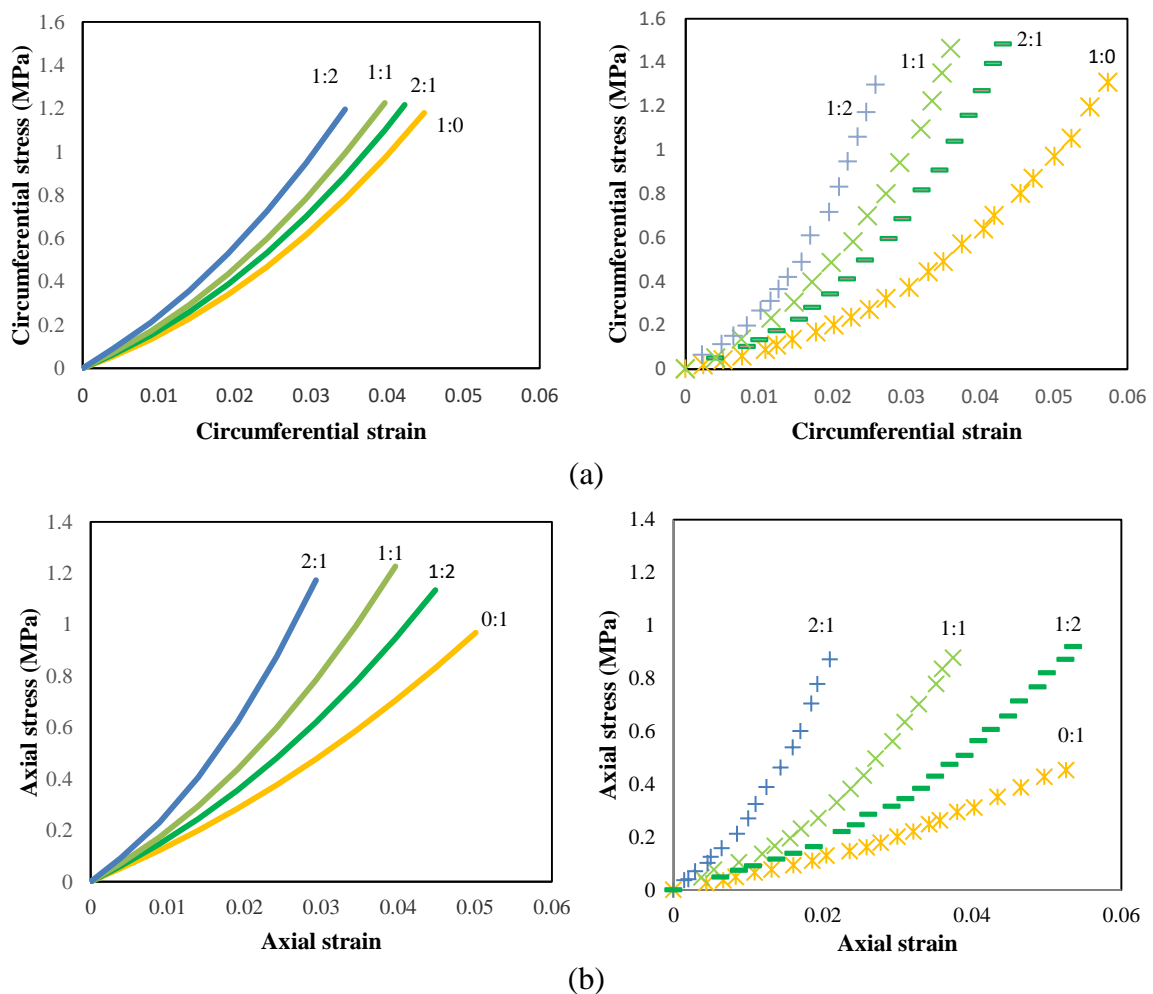


Figure III.3. Biaxial stretching model results for different biaxial strain ratios (1:0, 0:1, 1:2, 2:1 and 1:1 where the two numbers refer to the circumferential and axial directions, respectively) in terms of (a) circumferential and (b) axial stress-strain responses compared to experimental data of O’Connell et al. (2012) (solid lines: simulations, symbols: experiments for AO specimens).

A global view at these plots shows that the rigidity of the specimen is affected by the biaxial strain ratio. The stress levels obtained under different biaxial cases are higher than the uniaxial stress levels. The strain ratio has a larger effect on the axial stresses than the circumferential ones. The experimental results show the same effect. For the strain ratios 1:0 and 0:1, the circumferential stress is higher than the axial stress. This is also observed for the strain ratio 1:2. For the strain ratio 2:1, a higher axial stress is obtained as also experimentally remarked.

III.3.3. Shearing paths

The annulus shearing responses were predicted for specimens subjected to the three different shear modes illustrated in Figure III.4. These loading modes translate the different loading cases occurring under torsional and bending physiological movements. The shear mode 12 corresponds to the interlamellar shear generated especially under spinal torsion due to the relative movements between lamellae and between the inner and outer annulus regions. The shear mode 13 corresponds to the shearing generated by the adjacent vertebrae on the annulus under torsional movement due to the relative motion between the upper and lower disc surfaces. The shear mode 23 corresponds to the shearing generated by the relative displacement of the inner and outer disc regions under especially flexion movement. The predicted shear modulus was computed under the different shear modes and compared to the experimental results of Iatridis et al. (1999) and Fujita et al. (2000). The in-silico results are found slightly higher than the experimental observations but the same trends are observed for the three modes. The mode 12 gives the lowest shear modulus and the mode 13 gives the highest shear modulus while the 23 shear modulus is in between. As well, the outer region shows higher shear modulus than the inner disc region. In order to analyze these modes locally, the local shear stress fields of the three modes are plotted in Figure III.5.

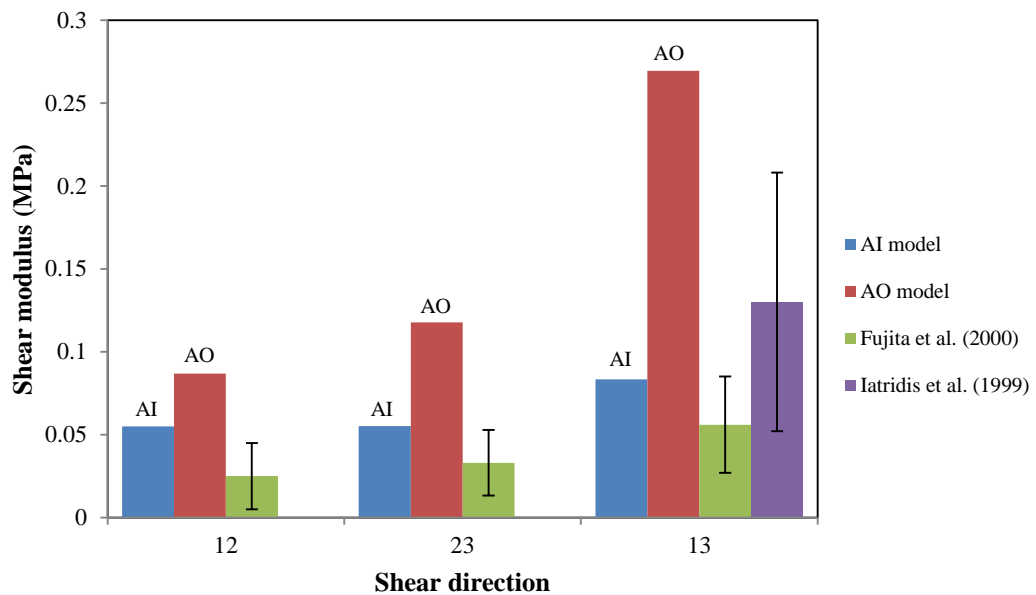
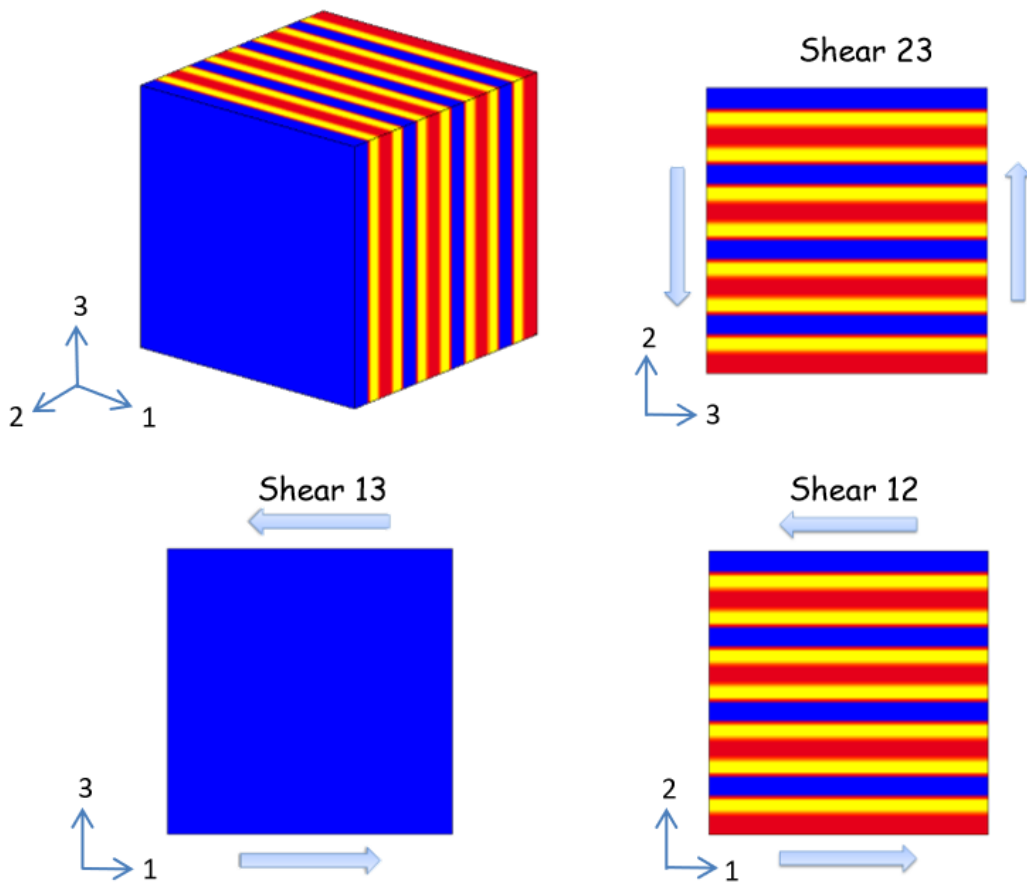
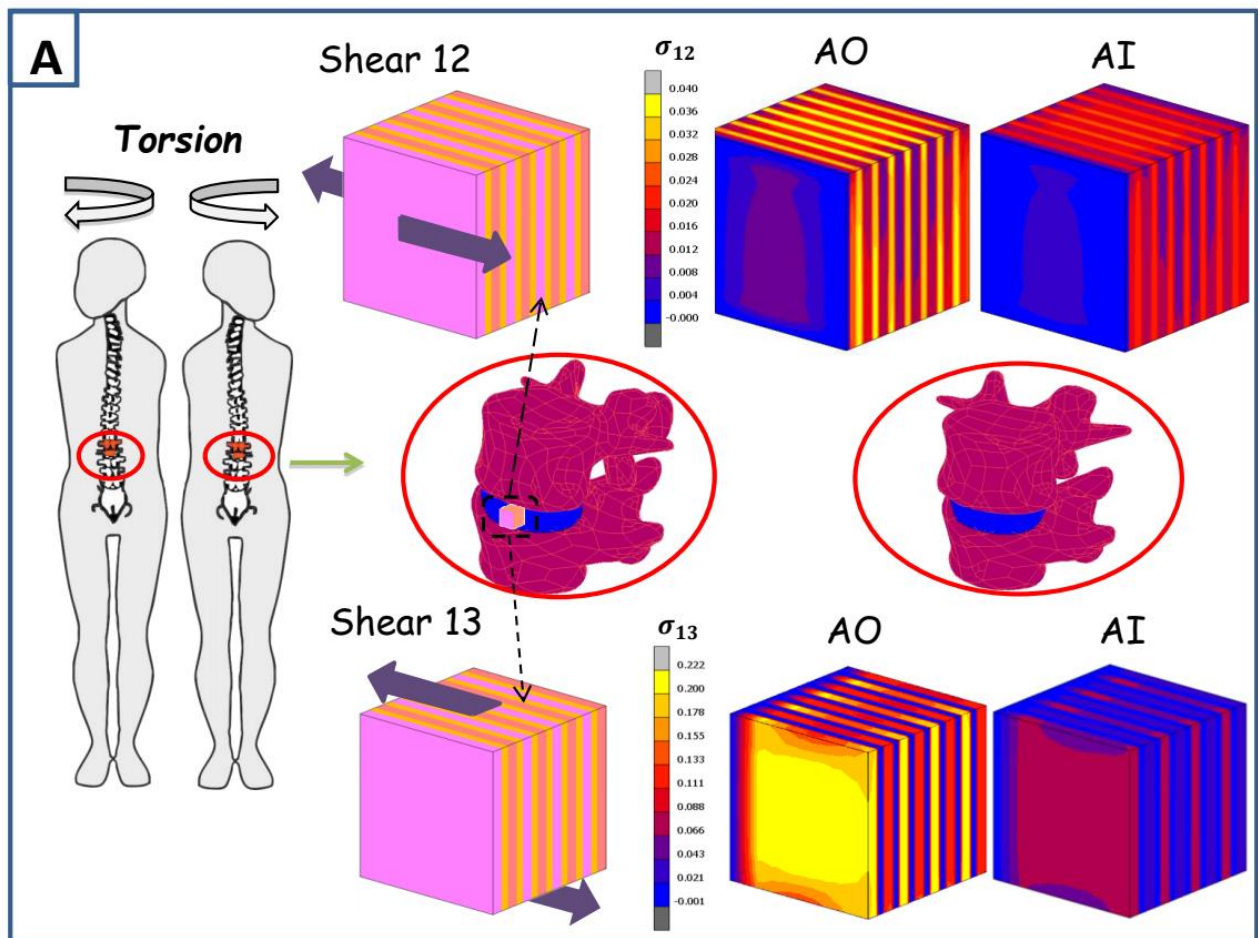


Figure III.4. Shearing model results for different shear modes (12, 23 and 13) in terms of shear modulus compared to experimental data of Iatridis et al. (1999) and Fujita et al. (2000).

Important insights are observed. For all the modes the local stress levels in the lamellae and ILM zones are higher in the outer disc region than the inner one. Under the 12 shear mode the highest stress levels are observed in the ILM zones unlike the 13 and 23 shear modes where the highest stresses are observed in the lamellae. While comparing the 23 and 13 modes we can notice that for the first one the highest stress concentrations are similar in all the lamellae but in the second one the highest concentrations are in the lamellae containing only fibers oriented towards the displacement direction. The contribution of the different local annulus zones to the shear disc mechanics under the daily physiological movements is investigated and the probability of damage initiation under these different modes is discussed.



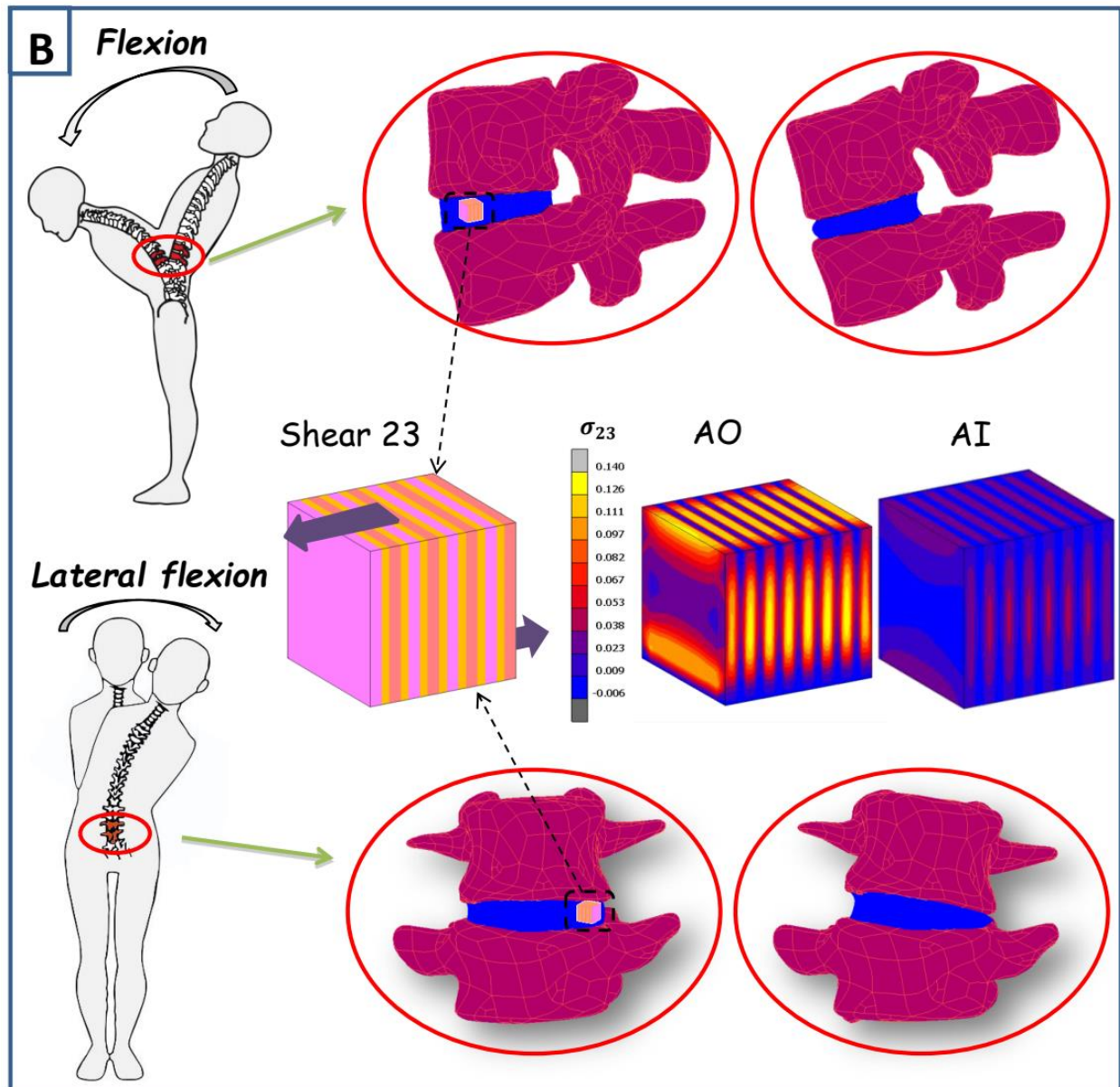


Figure III.5. Correlation of the physiological movements with local shear stress fields in three-dimensional space of disc parts: (A) Shear modes 12 and 13 related to the torsional movement and (B) shear mode 23 related to the flexion and lateral flexion movements.

III.4. Discussion

The tensile stress-strain response of the annulus fibrosus is highly dependent on the regional variation of the CFs content/orientation (Skaggs et al., 1994; Holzapfel et al., 2005). Due to a higher CFs content, the outer annulus is stiffer than the inner annulus while the CFs angle

difference leads to stiffer anterior regions than their posterior counterparts. This is a basic two-phase composite understanding in which the effective contributions of the ECM and the oriented CFs phases to the tensile stress-strain response are integrated. The regional variation of the negative charges content in the proteoglycans, decreasing from the nucleus to the outer disc region, leads to a variation in the ionic transfer by fluid exchange resulting in a variation of the transversal response translated by the Poisson's ratio. The Poisson's ratio related to the radial deformation is negative with higher values in the inner disc region compared to the outer disc region. Taking into account structural features and fluid exchange allows simulating the auxetic response of the tissue. In the meantime, the Poisson's ratio related to the axial deformation is not affected by the microstructure features and is almost the same for all the studied disc regions. The model shows that the Poisson's ratio is principally influenced by the water content and the swelling of the ILM zones. As well, the presence of the high CFs content in the outer disc region compared to the inner one retards more the fluid flow and decreases its content which affects in turn the tissue swelling and the radial strains. On the other side, the Poisson's ratio related to the axial deformation is higher than 1 for the four regions and it is less sensible to the microstructure variation compared to the Poisson's ratio related to the radial deformation, its value being relatively constant throughout the annulus. The PI region has experimentally the lowest rigidity that could correspond to to the non-fibrillar ECM modulus due to the non-well-arranged and high dispersion of CFs (Tsuji et al., 1993; Smith and Fazzalari, 2006). The calculation of an effective oriented fibers content relating not only the fibers volume fraction but also considering their arrangement helped to vary the rigidity and to reach the low rigidity levels.

Our hybrid experimental/modeling strategy leads to drastically reduce the amount of experimental work needed to characterize the complete human disc behavior thanks to an accurate and effective chemo-mechanical microstructure-based approach. Modeling the

annulus uniaxial stretching in the circumferential direction (representative of the disc compression mechanics) gives a lot of fruitful information and new explanations about the disc chemo-mechanical interactions as well as the different phenomena occurring in the disc. Nonetheless, predicting more realistic and complex spine movements requires the simulation of accurate annulus behavior under multi-axial (biaxial and shear) loadings.

Because it is constrained radially by the nucleus and axially by the adjacent vertebrae, the biaxial deformation of the annulus represents a more realistic loading case. The circumferential and axial stresses under different biaxial strain levels and strain ratios give similar results than those previously experimentally observed in the literature (O'Connell et al., 2012). The annulus rigidity under different biaxial cases are higher than the uniaxial rigidity and the stress levels under the same maximum strain are relatively higher which have been also noticed experimentally (Bass et al., 2004; Gregory and Callaghan, 2011). The strain ratio shows as well a high effect on the biaxial behavior of the annulus especially on the axial stress. Many recent numerical and analytical models tried to compute the shear stress inside the disc under uniaxial loadings (Goel et al., 1995; Adam et al., 2015) due to their simplicity. Only one recent contribution (Zhou et al., 2020) succeeded to reproduce the multi-axial behavior of the annulus based on the uniaxial behavior of the disc. Unfortunately, this contribution considered only the preloading free swelling effect and did not take into account the chemical coupling inside the disc with the surrounding environment and the related time-dependent behavior under mechanical loading that is always present during the physiological complex movements, which was described in details in chapter II. This coupling affects largely the transversal deformations which could lead to completely wrong results especially under biaxial tests. As well, it is considered that the Poisson's ratios of the annulus related to axial and radial directions are constant and their values are between 0 and 0.5 which is proven experimentally to be wrong (Baldit et al., 2014; Derrouiche et al., 2019a; Kandil et al., 2019).

The annulus behavior under shearing is very important and could be of a prime interest while studying the disc biomechanics under especially bending and torsion movements. The latter are common mechanical loadings during the different daily spinal motions (Michalek et al., 2009) and generate shearing inside the disc that could lead to many disc dysfunctions when combined with other axial loads. Numerically, the 12 shear modulus is lower than the 23 shear modulus which is also lower than the 13 shear modulus. All moduli of the outer specimens are found higher than the internal ones for the same shear mode. The latter difference is confirmed by the same experimental conduct observed in the literature (Fujita et al., 2000; Jacobs et al., 2011). The shear predictions reveal very interesting observations. The lowest shear stress levels are observed under the 12 shear mode but occurred throughout the disc with a higher concentration in the non-fibrillar ILM zones that are much weaker than the adjacent lamellae increasing the risk of annulus delamination. This has been also observed experimentally in many contributions in the literature suggesting the contribution of especially the ILM connections and the lamellar fiber matrix interactions to this shearing mode (Jacobs et al., 2011). The highest stresses for the 23 and 13 shear modes are observed in the lamellae. Nonetheless, only the lamellae with fibers oriented towards the loading direction are subjected to the maximum stress values in the mode 13. Under the 23 shear mode all the lamellae are subjected to those high stresses with lower maximum stress values compared to those observed in the 13 shear mode.

This could be explained by the relation between the shear modulus of these two modes and the oriented CFs that was observed in previous experimental contributions (Jacobs et al., 2011). While relating these shear modes to physiological movements we could notice that the 12 and 23 shear modes are more related to the torsional movements produced under twisting body actions as shown in Figure III.5 generating the highest stresses in the lamellae and the ILM zones as well. The 23 shear mode, related to bending and lateral bending body

movements, generates moderate stress levels in the lamellae and very low stresses in the ILM zones. These results highlight for the same shear strains the high damage risk under torsional body movements making it the most dangerous and risky multi-axial move of the body. This is not in accordance with the experimental observations of Costi et al. (2007) who investigated the maximum shear strain suggesting that the lateral bending and flexion are the most dangerous movements affecting the disc due to their high physiological values compared to axial torsion for the lumbar spine. These contradictory results reveal the importance of making more complex calculations combining the two studies and measuring the stress levels under the maximum physiological shear strains and taking as well into consideration the local maximum shear stress levels. Indeed, lower maximum shear stress levels could be observed globally in the specimen under a certain mode with high stresses affecting the weak ILM zones that exhibit a lower ultimate stress due to the absence of fibers.

We can conclude that our modeling approach succeeds to predict the multi-axial behavior of the annulus by means of uniaxial experimental data which was supposed to be not possible in the previous literature (Bass et al., 2004; O'Connell et al., 2012). The use of a layered model with distinct lamellar and interlamellar layers is mandatory to access the core of the annulus fibrosus and to define their respective role in the disc mechanics. By such a modeling approach, we can identify the critical zones where a likely higher risk of local damage is present under complex external mechanical loadings. All previous layered models considered these zones as common sliding zones separating the lamellae but the role of the ILM zones does not stop trivially there. Their essential role as chemical actuator of the transfer fluid through the annulus tissue and the corresponding unusual transversal behavior was only appreciated through very recent contributions (Kandil et al., 2019; Derrouiche et al., 2019a; 2020a). In the present chapter, we highlighted for the first time the determining role of the ILM zones on the multi-axial response of the annulus.

As a final point of discussion, let us come back to the mechanics of the whole disc. The compression of the whole disc (due in-vivo to muscular tension and body weight) provokes the uniaxial circumferential stretching of the annulus due to swelling of the nucleus (inner gel-like disc portion), combined to multi-axial mechanical paths during body movements. Although in-vitro experiments allowed to bring insights on the mechanics of the whole disc (Derrouiche et al., 2019b, 2020b; Feki et al., 2020), the annulus/nucleus interaction under complex external mechanical loadings is still an open issue. The construction of a whole disc model including our annulus model (with the regional effects) and the explicit presence of the nucleus would be useful for a thorough understanding of the functionality of the disc and its local behavior. The annulus structure-response relationship varies between individuals, between the different discs of the same spinal column and depends on the degeneration state of the disc. Therefore, it would be useful in the continuity of the model development to generate patient-specific models based on a hybrid methodology combining our modeling approach and direct MRI measurements on functional spine units.

III.5. Partial conclusion

The transversal response principally driven by the interlamellar zones was found essential for a correct multiaxial modeling of the disc annulus fibrosus. Its consideration by the microstructural-based model presented in the present and the previous chapters allowed reproducing the annulus uniaxial, biaxial and shear responses using the same set of parameters which is impossible to achieve if we omit it. Discovering the big role of the interlamellar zones and the transversal response of the disc in the mechanics catch the attention to their influence on the long-term mechanical behavior of the disc affected principally by the age induced microstructural changes which will be the objective of the next chapter of the thesis. As well, after the validation of the multi-axial behavior of the different

annulus regions the application of the microstructural model to complete intervertebral disc structure becomes important in order to investigate the interaction between the different disc parts under real physiological movements.

References

- Adam, C., Rouch, P., Skalli W., 2015. Inter-lamellar shear resistance confers compressive stiffness in the intervertebral disc: an image-based modelling study on the bovine caudal disc. *Journal of Biomechanics* 48, 4303-4308.
- Argoubi, M., Shirazi-Adl, A., 1996. Poroelastic creep response analysis of a lumbar motion segment in compression. *Journal of Biomechanics* 29, 1331-1339.
- Ayotte, D.C., Ito, K., Perren, S.M., Tepic, S., 2000. Direction-dependent constriction flow in a poroelastic solid: the intervertebral disc valve. *Journal of Biomechanical Engineering* 122, 587-593.
- Baldit, A., Ambard, D., Cherblanc, F., Royer, P., 2014. Experimental analysis of the transverse mechanical behaviour of annulus fibrosus tissue. *Biomechanics and Modeling in Mechanobiology* 13,643-652.
- Bass, E.C., Ashford, F.A., Segal, M.R., Lotz, J.C., 2004. Biaxial testing of human annulus fibrosus and its implications for a constitutive formulation. *Annals of Biomedical Engineering* 32, 1231-1242.
- Beckstein, J.C., Sen, S., Schaer, T.P., Vresilovic, E.J., Elliott, D.M., 2008. Comparison of animal discs used in disc research to human lumbar disc: axial compression mechanics and glycosaminoglycan content. *Spine* 33, 166-173.
- Bergstrom, J.S., Boyce, M.C., 1998. Constitutive modeling of the large strain time-dependent behavior of elastomers. *Journal of the Mechanics and Physics of Solids* 46, 931-954.
- Cantournet, S., Boyce, M.C., Tsou, A.H., 2007. Micromechanics and macromechanics of carbon nanotube-enhanced elastomers. *Journal of the Mechanics and Physics of Solids* 55, 1321-1339.
- Costi, J.J., Stokes, I.A., Gardner-Morse, M., Laible, J.P., Scoffone, H.M., Iatridis, J.C., 2007. Direct measurement of intervertebral disc maximum shear strain in six degrees of freedom: motions that place disc tissue at risk of injury. *Journal of Biomechanics* 40, 2457-2466.
- del Palomar, A.P., Calvo, B., Doblare, M., 2008. An accurate finite element model of the cervical spine under quasi-static loading. *Journal of Biomechanics* 41, 523-531.
- Derrouiche, A., Zaïri, F., Zaïri, F., 2019a. A chemo-mechanical model for osmo-inelastic effects in the annulus fibrosus. *Biomechanics and Modeling in Mechanobiology* 18, 1773-1790.
- Derrouiche, A., Zaouali, A., Zaïri, F., Ismail, J., Chaabane, M., Qu, Z., Zaïri, F., 2019b. Osmo-inelastic response of the intervertebral disc. *Proceedings of the Institution of Mechanical Engineers. Part H: Journal of Engineering in Medicine* 233, 332-341.
- Derrouiche, A., Karoui, A., Zaïri, F., Ismail, J., Qu, Z., Chaabane, M., Zaïri, F., 2020a. The two Poisson's ratios in annulus fibrosus: relation with the osmo-inelastic features. *Mechanics of Soft Materials* 2, 1.

- Derrouiche, A., Feki, F., Zaïri, F., Taktak, R., Moulart, M., Qu, Z., Ismail, J., Charfi, S., Haddar, N., Zaïri, F., 2020b. How pre-strain affects the chemo-torsional response of the intervertebral disc. *Clinical Biomechanics* 76, 105020.
- Ebara, S., Iatridis, J.C., Setton, L.A., Foster, R.J., Mow, V.C., Weidenbaum, M., 1996. Tensile properties of nondegenerate human lumbar annulus fibrosus. *Spine* 21, 452-461.
- Ehlers, W., Karajan, N., Markert, B., 2009. An extended biphasic model for charged hydrated tissues with application to the intervertebral disc. *Biomechanics and Modeling in Mechanobiology* 8, 233-251.
- Eyre, D.R., Muir, H. 1976. Types I and II collagens in intervertebral disc. Interchanging radial distributions in annulus fibrosus. *Biochemical Journal* 157, 267-270.
- Eyre, D.R., Muir, H., 1977. Quantitative analysis of types I and II collagens in the human intervertebral discs at various ages. *Biochimica Biophysica Acta*. 492, 29-42.
- Feki, F., Taktak, R., Kandil, K., Derrouiche, A., Moulart, M., Haddar, N., Zaïri, F., Zaïri, F., 2020. How osmo-viscoelastic coupling affects recovery of cyclically compressed intervertebral disc. *Spine* 45, 160553.
- Fujita, Y., Wagner, D. R., Biviji, A. A., Duncan, N. A., Lotz, J. C., 2000. Anisotropic shear behavior of the annulus fibrosus: effect of harvest site and tissue prestrain. *Medical Engineering & Physics* 22, 349-357.
- Gent, A.N., 1996. A new constitutive relation for rubber. *Rubber Chemistry and Technology* 69, 59-61.
- Goel, V.K., Monroe, B.T., Gilbertson, L.G., Brinckmann, P., 1995. Interlaminar shear stresses and laminae separation in a disc. Finite element analysis of the L3-L4 motion segment subjected to axial compressive loads. *Spine* 20, 689-698.
- Gregory, D.E., Callaghan, J.P., 2010. An examination of the influence of strain rate on subfailure mechanical properties of the annulus fibrosus. *Journal of Biomechanical Engineering* 132, 091010.
- Gregory, D.E., Callaghan, J.P., 2011. A comparison of uniaxial and biaxial mechanical properties of the annulus fibrosus: a porcine model. *Journal of Biomechanical Engineering* 133, 024503.
- Gregory, D.E., Bae, W.C., Sah, R.L., Masuda, K., 2012. Annular delamination strength of human lumbar intervertebral disc. *European Spine Journal* 21, 1716-1723.
- Guerin, H.A.L., Elliott, D.M., 2007. Quantifying the contributions of structure to annulus fibrosus mechanical function using a nonlinear, anisotropic, hyperelastic model. *Journal of Orthopaedic Research* 25, 508-516.
- Guo, Z.Y., Peng, X.Q., Moran, B. 2006. A composites-based hyperelastic constitutive model for soft tissue with application to the human annulus fibrosus. *Journal of the Mechanics and Physics of Solids* 54, 1952-1971.
- Guo, Q., Zaïri, F., Guo, X., 2018. A thermo-viscoelastic-damage constitutive model for cyclically loaded rubbers. Part I: model formulation and numerical examples. *International Journal of Plasticity* 101, 106-124.
- Gurtin, M.E., Anand, L., 2005. The decomposition $F=F^e F^p$, material symmetry, and plastic irrotationality for solids that are isotropic-viscoplastic or amorphous. *International Journal of Plasticity* 21, 1686-1719.
- Hollingsworth, N.T., Wagner, D.R., 2011. Modeling shear behavior of the annulus fibrosus. *Journal of the Mechanical Behavior of Biomedical Materials* 4, 1103-1114.
- Holzappel, G.A., Schulze-Bauer, C.A.J., Feigl, G., Regitnig, P., 2005. Single lamellar mechanics of the human lumbar annulus fibrosus. *Biomechanics and Modeling in Mechanobiology* 3, 125-140.

- Huyghe, J.M., Janssen, J.D., 1997. Quadriphasic mechanics of swelling incompressible porous media. *International Journal of Engineering Science* 35, 793-802.
- Iatridis, J.C., Kumar, S., Foster, R.J., Weidenbaum, M., Mow, V.C., 1999. Shear mechanical properties of human lumbar annulus fibrosus. *Journal of Orthopaedic Research* 17, 732-737.
- Iatridis, J.C., MacLean, J.J., O'Brien, M., Stokes, I.A., 2007. Measurements of proteoglycan and water content distribution in human lumbar intervertebral discs. *Spine* 32, 1493-1497.
- Jacobs, N.T., Smith, L.J., Han, W.M., Morelli, J., Yoder, J.H., Elliott, D.M., 2011. Effect of orientation and targeted extracellular matrix degradation on the shear mechanical properties of the annulus fibrosus. *Journal of the Mechanical Behavior of Biomedical Materials* 4, 1611-1619.
- Kandil, K., Zaïri, F., Derrouiche, A., Messenger, T., Zaïri, F., 2019. Interlamellar-induced time-dependent response of intervertebral disc annulus: a microstructure-based chemo-viscoelastic model. *Acta Biomaterialia* 100, 75-91.
- Klisch, S.M., Lotz, J.C., 1999. Application of a fiber-reinforced continuum theory to multiple deformations of the annulus fibrosus. *Journal of Biomechanics* 32, 1027-1036.
- Klisch, S.M., Lotz, J.C., 2000. A special theory of biphasic mixtures and experimental results for human annulus fibrosus tested in confined compression. *Journal of Biomechanical Engineering* 122, 180-188.
- Labus, K.M., Han, S.K., Hsieh, A.H., Puttlitz, C.M., 2014. A computational model to describe the regional interlamellar shear of the annulus fibrosus. *Journal of Biomechanical Engineering* 136, 051009.
- Mengoni, M., Luxmoore, B.J., Wijayathunga, V.N., Jones, A.C. Broom, N.D., Wilcox, R.K., 2015. Derivation of inter-lamellar behaviour of the intervertebral disc annulus. *Journal of the Mechanical Behavior of Biomedical Materials* 48, 164-172.
- Michalek, A.J., Buckley, M.R., Bonassar, L.J., Cohen, I., Iatridis, J.C., 2009. Measurement of local strains in intervertebral disc anulus fibrosus tissue under dynamic shear: contributions of matrix fiber orientation and elastin content. *Journal of Biomechanics* 42, 2279-2285.
- O'Connell, G.D., Sen, S., Elliott, D.M., 2012. Human annulus fibrosus material properties from biaxial testing and constitutive modeling are altered with degeneration. *Biomechanics and Modeling in Mechanobiology* 11, 493-503.
- Ovalle-Rodas, C., Zaïri, F., Naït-Abdelaziz, M., Charrier, P., 2016. A thermo-visco-hyperelastic model for the heat build-up during low-cycle fatigue of filled rubbers: formulation, implementation and experimental verification. *International Journal of Plasticity* 79, 217-236.
- Peng, X.Q., Guo, Z.Y., Moran, B., 2005. An anisotropic hyperelastic constitutive model with fiber-matrix shear interaction for the human annulus fibrosus. *Journal of Applied Mechanics* 73, 815-824.
- Pezowicz, C.A., Robertson, P.A., Broom, N.D., 2005. Intralamellar relationships within the collagenous architecture of the annulus fibrosus imaged in its fully hydrated state. *Journal of anatomy* 207, 299-312.
- Pezowicz, C.A., Robertson, P.A., Broom, N.D., 2006. The structural basis of interlamellar cohesion in the intervertebral disc wall. *Journal of Anatomy* 208, 317-330.
- Pyrz, M., Zaïri, F., 2007. Identification of viscoplastic parameters of phenomenological constitutive equations for polymers by deterministic and evolutionary approach. *Modelling and Simulation in Materials Science and Engineering* 15, 85-103.
- Riches, P.E., Dhillon, N., Lotz, J., Woods, A.W., McNally, D.S., 2002. The internal mechanics of the intervertebral disc under cyclic loading. *Journal of Biomechanics* 35, 1263-1271

- Schroeder, Y., Wilson W., Huyghe, J.M., Baaijens, F.P.T., 2006. Osmoviscoelastic finite element model of the intervertebral disc. *European Spine Journal* 15, 361-371.
- Shirazi-Adl, S.A., Shrivastava, S.C., Ahmed, A.M., 1984. Stress analysis of the lumbar disc-body unit in compression. A three dimensional nonlinear finite element study. *Spine* 9, 120-134.
- Shirazi-Adl, A., 1989. Strain in fibers of a lumbar disc: analysis of the role of lifting in producing disc prolapsed. *Spine* 14, 96-103.
- Showalter, B.L., Beckstein, J.C., Martin, J.T., Beattie, E.E., Orias, A.A.E., Schaer, T.P., Vresilovic, E.J., Elliott, D.M., 2012. Comparison of animal discs used in disc research to human lumbar disc: torsion mechanics and collagen content. *Spine* 37, 900-907.
- Skaggs, D.L., Weidenbaum, M., Iatridis, J.C., Ratcliffe, A., Mow, V.C., 1994. Regional variation in tensile properties and biochemical composition of the human lumbar anulus fibrosus. *Spine* 19, 1310-1319.
- Smith, L.J., Fazzalari, N.L., 2006. Regional variations in the density and arrangement of elastic fibres in the anulus fibrosus of the human lumbar disc. *Journal of Anatomy* 209, 359-367.
- Tang, S., Rebholz, B.J., 2011. Does anterior lumbar interbody fusion promote adjacent degeneration in degenerative disc disease? A finite element study. *Journal of Orthopaedic Science*. 16, 221-228.
- Tavakoli, J., Elliott, D.M., Costi, J.J., 2017. The ultra-structural organization of the elastic network in the intra- and inter-lamellar matrix of the intervertebral disc. *Acta Biomaterialia* 58, 269-277.
- Tavakoli, J., Costi, J.J., 2018. New findings confirm the viscoelastic behaviour of the inter-lamellar matrix of the disc annulus fibrosus in radial and circumferential directions of loading. *Acta Biomaterialia* 71411-71419.
- Tsuji, H., Hirano, N., Ohshima, H., Ishihara, H., Terahata, N., Motoe, T., 1993. Structural variation of the anterior and posterior anulus fibrosus in the development of human lumbar intervertebral disc. *Spine* 18, 204-210.
- Vos, T. et al., 2016. Global, regional, and national incidence, prevalence, and years lived with disability for 310 diseases and injuries, 1990-2015: a systematic analysis for the Global Burden of Disease Study 2015. *Lancet* 388, 1545-1602.
- Wagner, D.R., Lotz, J.C., 2004. Theoretical model and experimental results for the nonlinear elastic behavior of human annulus fibrosus. *Journal of Orthopaedic Research* 22, 901-909.
- Wagner, D.R., Reiser, K.M., Lotz, J.C., 2006. Glycation increases human annulus fibrosus stiffness in both experimental measurements and theoretical predictions. *Journal of Biomechanics* 39, 1021-1029.
- Wilson, W., van Donkelaar, C.C., van Rietbergen, C., Ito, K., Huiskes, R., 2004. Stresses in the local collagen network of articular cartilage: a poroviscoelastic fibril-reinforced finite element study. *Journal of Biomechanics* 37, 357-366.
- Yao, J., Turteltaub, S.R., Ducheyne, P., 2006. A three-dimensional nonlinear finite element analysis of the mechanical behavior of tissue engineered intervertebral discs under complex loads. *Biomaterials* 27, 377-87.
- Zhou, M., Bezci, S.E., O'Connell, G.D., 2020. Multiscale composite model of fiber-reinforced tissues with direct representation of sub-tissue properties. *Biomechanics and Modeling in Mechanobiology* 19, 745-759.

Chapter IV

A microstructure-based modeling approach to assess aging-sensitive mechanics of human intervertebral disc⁸

Abstract

The human body soft tissues are hierarchic structures interacting in a complex manner with the surrounding biochemical environment. The loss of soft tissues functionality with age leads to more vulnerability regarding to the external mechanical loadings and increases the risk of injuries. As a main example of the human body soft tissues, the intervertebral disc mechanical response evolution with age is explored. Although the age-dependence of the intervertebral disc microstructure is a well-known feature, no noticeable age effect on the disc stiffness is evidenced in the in-vitro experimental studies of the literature. So, if the disc intrinsic mechanics remains constant, how to explain the correlation of disc degeneration and disc functionality loss with age. A microstructure-based modeling approach was developed to assess in-silico the aging-sensitive mechanics of human intervertebral disc. The model considers the relationship between stress/volumetric macro-response and microstructure along with effective age effects acting at the lamellar and multi-lamellar scales. The stress-stretch and transversal responses of the different disc regions were computed for various age groups (13-18, 36, 58, 69 and 82 years old) and their evolution with age was studied. While matching with in-vitro experimental data, the predicted stiffness was found to increase while passing from adolescent young discs to mature older discs then to remain almost constant for the rest of life. Important age-related changes in the disc transversal behavior were also predicted affecting the flexibility of the disc, changing its volumetric behavior, and modifying its dimensions. The developed approach was found able to bring new conclusions about age-dependent mechanical properties including regional dependency. The disc mechanics in terms of rigidity, radial and axial transversal responses were found to alter going from adolescent to middle age where the disc reaches a certain maturity. After reaching maturity, the mechanical properties undergo very slight changes until becoming almost constant with age.

Keywords: Human annulus fibrosus; Aging; Mechanics; Regional dependency; Microstructure.

⁸ *This chapter is based on the following article: Kandil, K., Zaïri, F., Messenger, T., Zaïri, F., 2020. A microstructure-based modeling approach to assess aging-sensitive mechanics of human intervertebral disc. Computer Methods and Programs in Biomedicine, 105890.*

IV.1. Partial introduction

Intervertebral disc dysfunctions are the main factors of chronic/severe back pain affecting humans at any stage of life but staying highly correlated to age with excessive higher vulnerability for elders (Parkkola and Kormano, 1992; Videman et al., 1995). The damage of this living soft tissue could occur mechanically under excessive repetitive efforts, wrong movements and high loads supported by the spinal body (Adams and Hutton, 1982). Through recent years, big efforts were done in medicine to create patient-specific models of the different human body organs (Szilagyi et al., 2011; Lauzeral et al., 2019; Razaghi et al., 2019). Nonetheless, if we need to have a realistic and accurate model of each patient, these models should refer to the actualized material properties of the organ and their evolution under the different degradation mechanisms principally caused by aging. Obviously, the mechanically-induced damage is influenced by intervertebral disc age-related changes. Natural aging induces, by essence, biological degeneration events (Roughley, 2004) interacting with the intervertebral disc mechanics and creating complex degeneration processes inside the intervertebral disc lamellar fibrillar cartilage (annulus fibrosus) along with complex changes of the interactions with the gelatinous central nucleus pulposus leading to disc morphological changes and sagittal balance disorders (Pfirrmann et al., 2006). Micro-cracks and tears are common damage mechanisms observed in the annulus fibrosus (Adams and Hutton, 1985; Osti et al., 1992; Vernon-Roberts et al., 2007). Any alteration in the annulus fibrosus structure potentially leads to several forms of degeneration such as disc bulging, herniated disc and disc thinning. The comprehension of annulus microstructure and its relation to the natural aging is the key point in order to better understand the origin of these degeneration mechanisms, to reduce their effects and in some cases to avoid their occurrence. Distortions of the nutrient distribution and metabolism alteration appear inside the disc with

age affecting directly the cellular density and indirectly the proteoglycan content, the volumetric pressure and the water content (Buckwalter, 1995; Horner and Urban, 2001; Bibby and Urban, 2004; Adams and Roughley, 2006; Mwale et al., 2011; Malandrino et al., 2018). As well, age affects the total collagen fibers concentration and changes the proportions of the different types of collagen (Brickley-Parsons and Glimcher, 1984) which would logically alter the mechanical behavior of the annulus in terms of rigidity and resistance. Many experimental studies tried to find a relation between the degeneration mechanisms and the microstructure changes of the disc components by natural aging (Urban and McMullin, 1988) and their consequences on the disc mechanics (Jenkins et al., 1985; Koeller et al., 1984; Hickey et al., 1986). Surprisingly, no effect of age was found on stiffness of single and multi-lamellar specimens of the annulus soft tissue (Galante, 1967; Ebara et al., 1996; Holzapfel et al., 2005). In the latter references, it was deduced that the mechanics of a healthy disc remains constant at any stage of its life. These observations raise several questions about the structure-mechanics relationship in disc tissues, such as how the amount of the disc microstructure compositions may change without impacting the mechanical behavior and why elders are more likely to be touched by disc diseases compared to young individuals. Answering these questions is very difficult from the experimental viewpoint due to the huge number of specimens needed from cadavers of various ages and the extensive mechanical and biological studies that should be established on each specimen without damaging it. Computer modeling remains the best way for this kind of complex investigations. Many constitutive models tried to describe the mechanical behavior of the intervertebral disc going from the firstly developed models describing the annulus tissue as a single solid phase reinforced by stiff oriented fibers (Schroeder and Neff, 2003; Peng et al., 2005; Balzani et al., 2006; Guo et al., 2006), arriving to biphasic and extended biphasic models where the fluid phase, its diffusion inward/outward the disc and in addition the negative charges density responsible of the water absorption

inside the disc and the tissue swelling due to osmotic effect were considered (Klisch and Lotz, 2000; Riches et al., 2002; Ehlers et al., 2009; Barthelemy et al., 2016; Chetoui et al., 2017). All the recent models were able to reproduce the instantaneous disc response under external mechanical loads without a real connection with the disc microstructure and biology making them unable to estimate long-term temporal changes inside the disc. The strong bio-mechanical coupling is not considered in these models. The effect of temporal biological changes on the disc mechanics and the inverse effect of the disc mechanics on the biological behavior and the disc metabolism were not considered. Hence, metabolic bio-mechanical models appeared focusing on the cellular viability mechanisms, the nutrient diffusion (oxygen, glucose and lactate) and the effect of applied mechanical loads on their distribution all over the disc (Soukane et al., 2007; Huang and Gu, 2008; Louman-Gardiner et al., 2011; Malandrino et al., 2011; Zhu et al., 2012; Galbusera et al., 2013; Chetoui et al., 2019). Recently, these models evolved largely by incorporating the influence of the nutrient distribution and the disc metabolism on the cells synthesis, the microstructure remodeling of the proteoglycan network and the water content (Zhu et al., 2014, 2020; Wills et al., 2016) and their incidence on the stress distribution inside the disc. Despite the important advance accomplished by these models and their promising results, they cannot yet investigate sufficiently the global long-term effects on the mechanical behavior of the disc tissues. None of these models highlight the inverse temporal effect of the microstructure changes on the mechanical properties of the soft tissue which could alter completely its response to the different mechanical loads and highly change the estimated results. For this reason, a recently developed microstructure-based computational model (Derrouiche et al., 2019a; Kandil et al., 2019; Kandil et al., 2020), see chapters II and III, that succeeded to reproduce the axial and multi-axial mechanical behavior of the disc annulus is used to assess the natural aging effects on the disc mechanics. Since the annulus Poisson's ratios (that is the negative of the ratio

between the transversal strains and the applied circumferential strain) were found experimentally to be time-dependent (Baldit et al., 2014; Derrouiche et al., 2020a), the model takes into account the transversal behavior of the annulus and its volumetric response that are mandatory to give a correct three-dimensional description of the disc behavior (Derrouiche et al., 2019a; Kandil et al., 2019). In order to focus on the direct relation between the microstructure and the mechanical response, the metabolic origins of the microstructure changes (Bibby et al., 2005; Zhu et al., 2014) were not considered in this research but the resulting altered microstructure contents of these components were taken directly from well-documented papers of the literature depending on the studied age and were adapted in order to be used by the model. The impact of age on the mechanical response in terms of stress-strain and transversal strains is investigated by varying for each disc region the oriented collagen fibers and the water contents along with the fibers orientations. The adopted approach allows us to study the age effect in a simple manner and reach almost the same final experimental conducts. The study was established on different annular and radial disc regions. The response of each region was investigated for disc models of several ages varying from young adolescents to elderly (13-18, 36, 58, 69 and 82 years old). Detailed analysis of the computational curves and the local stress-strain fields is performed. Important microstructure explanations about previously found experimental results are evoked and new conclusions about age-dependent mechanical properties are revealed.

This chapter is organized as follows. Section IV.2 gives the details of the microstructure-based model presented at the scale of a single-lamellar annulus and at the scale of a multi-lamellar annulus. Section IV.3 presents and discusses our findings on the consequences of natural aging on the disc mechanics. Finally, some concluding remarks are given in Section IV.4.

IV.2. Microstructure-based model

Figure IV.1 presents a multi-scale view of the disc tissues. Due to the heterogeneity of the disc microstructure (Inoue et al., 1975; Eyre et al., 1979; Cassidy et al., 1989), the disc annulus was divided circumferentially and radially into four regions: Posterior-Outer (PO), Posterior-Inner (PI), Anterior-Outer (AO) and Anterior-Inner (AI) that will be considered in the different calculations.

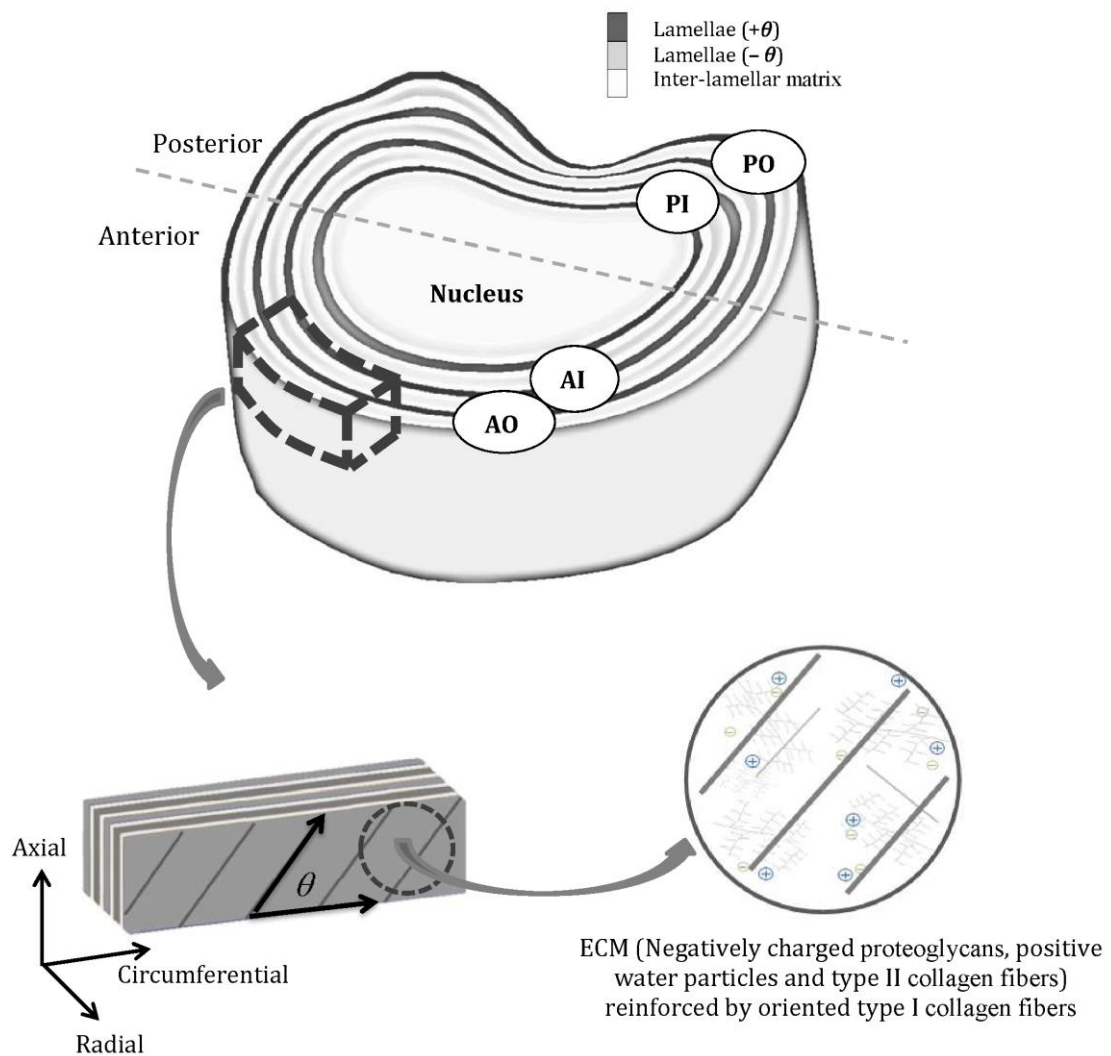


Figure IV.1. Multi-scale view of the disc tissues.

The lamellae of annulus fibrosus are composed of an extracellular matrix (ECM) rich of negatively charged proteoglycans that are responsible of the disc hydration and containing non-oriented type II collagen fibers that are dispersed randomly all over the matrix. The lamellae are reinforced by oriented type I collagen fibers giving the soft tissue the required strength and helping the disc to resist the different applied external mechanical loads. Each two adjacent lamellae are connected by a non-fibrillar ECM (inter-lamellar matrix) containing fibrils, elastin, crosslinks, and other bridging elements ensuring the structure integrity (Yu et al., 2007).

IV.2.1. Single-lamellar annulus model

The annulus behavior was reproduced using the recently developed microstructure-based chemo-viscoelastic model in chapters II and III. The annulus fibrosus mechanical behavior is composed of the viscoelastic contribution of the ECM, the elastic contribution of oriented type I collagen fibers and the volumetric contribution of the ECM induced by the high density negative charges present in its proteoglycans network and responsible of the osmotic water transfer inside and outside the disc. Figure IV.2 gives a rheological representation of the constitutive model along with the finite-strain kinematics. The free energy function ψ of the annulus fibrosus tissue is given by:

$$\psi = (1 - \phi_{CF})\psi_{ECM} + \phi_{CF}\psi_{CF} + (1 - \phi_{CF})\psi_{vol} \quad (IV.1)$$

where ϕ_{CF} is the volume fraction of oriented type I collagen fibers, ψ_{ECM} , ψ_{CF} and ψ_{vol} are the free energy functions from which the stress-strain relationship along with the transversal behavior are obtained.

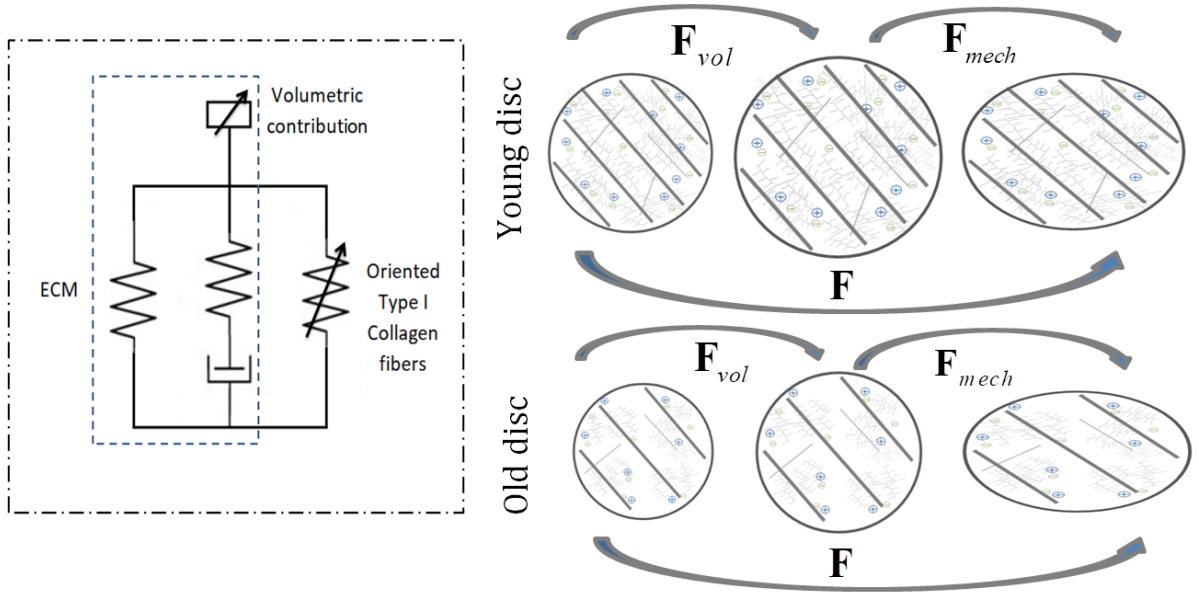


Figure IV.2. One-dimensional visualization of the model for single-lamellar annulus; the ECM deformation \mathbf{F} is split into a volumetric part \mathbf{F}_{vol} related to the chemical-induced pansion and a mechanical part \mathbf{F}_{mech} related to the intrinsic ECM response consisting in a nonlinear elastic spring in parallel with a Maxwell branch (a nonlinear elastic spring in series with a viscous damper). The elastic contribution of oriented type I collagen fibers acts as a nonlinear elastic spring in parallel.

IV.2.1.1. Free energy of ECM

The ECM free energy function ψ_{ECM} is split into an elastic part ψ_{ECM}^e and a viscous part ψ_{ECM}^v as:

$$\psi_{ECM} = \psi_{ECM}^e + \psi_{ECM}^v \quad (IV.2)$$

The elastic free energy function ψ_{ECM}^e uses a Gent expression (Gent, 1996):

$$\psi_{ECM}^e = -\frac{E}{6} I_1^{\max} \ln \left(1 - \frac{I_1 - 3}{I_1^{\max}} \right) \quad (IV.3)$$

where E is the ECM tensile modulus, I_1^{\max} is the ECM limiting extensibility and $I_1 = \text{tr}(\mathbf{B}_{mech})$ is the first strain invariant with $\mathbf{B}_{mech} = \mathbf{F}_{mech} \mathbf{F}_{mech}^T$ the mechanical left Cauchy-Green strain tensor.

The viscous free energy function ψ_{ECM}^v uses also a Gent expression (Gent, 1996):

$$\psi_{ECM}^v = -\frac{E_v}{6} I_{1v}^{\max} \ln \left(1 - \frac{I_{1e} - 3}{I_{1v}^{\max}} \right) \quad (\text{IV.4})$$

where E_v and I_{1v}^{\max} are ECM viscous constants and $I_{1e} = \text{tr}(\mathbf{B}_e)$ is the first strain invariant with $\mathbf{B}_e = \mathbf{F}_e \mathbf{F}_e^T$ the mechanical elastic left Cauchy-Green strain tensor and $\mathbf{F}_e = \mathbf{F}_{mech} \mathbf{F}_v^{-1}$. By introducing the convenient hypothesis of viscous irrotationality (Gurtin and Anand, 2005), the mechanical viscous deformation gradient tensor \mathbf{F}_v is driven by the viscous stretching rate tensor \mathbf{D}_v :

$$\dot{\mathbf{F}}_v = \mathbf{F}_e^{-1} \mathbf{D}_v \mathbf{F}_{mech} \quad (\text{IV.5})$$

with the following general flow rule:

$$\mathbf{D}_v = \dot{\gamma}_v \frac{\boldsymbol{\sigma}'_v}{\sqrt{2} \|\boldsymbol{\sigma}_v\|}, \quad \|\boldsymbol{\sigma}_v\| = \sqrt{\frac{1}{2} \text{tr}(\boldsymbol{\sigma}'_v \boldsymbol{\sigma}'_v)}, \quad \boldsymbol{\sigma}'_v = \boldsymbol{\sigma}_v - \frac{1}{3} \text{tr}(\boldsymbol{\sigma}_v) \mathbf{I} \quad (\text{IV.6})$$

in which $\dot{\gamma}_v$ is the accumulated viscous strain rate, $\|\boldsymbol{\sigma}_v\|$ is the effective value of the viscous Cauchy stress $\boldsymbol{\sigma}_v$, $\boldsymbol{\sigma}'_v$ is the deviatoric part of $\boldsymbol{\sigma}_v$ and \mathbf{I} is the identity tensor.

The mathematical formulation of Bergstrom and Boyce (Bergstrom and Boyce, 1998) is retained for $\dot{\gamma}_v$:

$$\dot{\gamma}_v = d \left| \sqrt{I_{1v}/3} - 1 \right|^{-m} \|\boldsymbol{\sigma}_v\| \quad (\text{IV.7})$$

where d and m are two supplementary ECM viscous constants and $I_{1v} = \text{tr}(\mathbf{B}_v)$ is the first strain invariant with $\mathbf{B}_v = \mathbf{F}_v \mathbf{F}_v^T$ the mechanical viscous left Cauchy-Green strain tensor.

IV.2.1.2. Free energy of oriented type I collagen fibers

The free energy function ψ_{CF} of oriented type I collagen fibers is given by (Cantournet et al., 2007):

$$\psi_{CF} = A_1 (I_4 - 1) + A_2 (I_4 - 1)^2 - 2A_1 \ln(\lambda_I^{x^2} \lambda_{II}^{y^2} \lambda_{III}^{z^2}) \quad (IV.8)$$

where A_1 and A_2 are material constants, λ_I , λ_{II} and λ_{III} are the stretches along the principal axes of oriented type I collagen fibers:

$$\lambda_I = \sqrt{\mathbf{e}_1 \mathbf{C}_{mech} \mathbf{e}_1}, \lambda_{II} = \sqrt{\mathbf{e}_2 \mathbf{C}_{mech} \mathbf{e}_2}, \lambda_{III} = \sqrt{\mathbf{e}_3 \mathbf{C}_{mech} \mathbf{e}_3} \quad (IV.9)$$

with $\mathbf{C}_{mech} = \mathbf{F}_{mech}^T \mathbf{F}_{mech}$ the mechanical right Cauchy-Green strain tensor. The term $I_4 = \mathbf{a} \mathbf{C}_{mech} \mathbf{a}$ is the fourth strain invariant with $\mathbf{a} = x\mathbf{e}_1 + y\mathbf{e}_2 + z\mathbf{e}_3$ the unit vector in the initial configuration as illustrated in Figure IV.1.

IV.2.1.3. Free energy of chemical-induced volumetric part

The chemical-induced volumetric free energy function ψ_{vol} is expressed as:

$$\psi_{vol} = \frac{1}{4} k (J^2 - 1 - 2 \ln J) \quad (IV.10)$$

where k is the bulk modulus and $J = \det \mathbf{F}$ is the Jacobian given by:

$$J = J_{mech} J_{vol} = \Delta n_{f_m} \xi \eta, J_{mech} = \det \mathbf{F}_{mech} = 1, J_{vol} = \det \mathbf{F}_{vol} \quad (IV.11)$$

in which J_{mech} and J_{vol} represent the intrinsic mechanical and chemical-induced volume changes, the chemical deformation gradient of the isotropic swelled continuum medium is $\mathbf{F}_{vol} = J^{1/3} \mathbf{I}$, ξ is a dimensionless transportation coefficient, η is a dimensionless free swelling coefficient (equal to 0.5 in the case of physiological salt condition) and n_{f_m} is the internal fluid content governed by the kinetics:

$$\dot{n}_{f_m} = \beta_m \left(1 - \frac{n_{f_m}}{n_{f_{lim}}} \right) \quad (\text{IV.12})$$

The osmotic water transfer inside and outside the annulus tissue is controlled by Δn_{f_m} where β_m is a fluid flow constant, $n_{f_{lim}}$ is the maximum fluid content in the tissue and n_{f_0} is the fluid content at $t = 0$ in the unloaded chemically equilibrated state.

IV.2.2. Multi-lamellar annulus model

A representative volume of the annulus fibrosus specimen that takes into account the lamellar structure of the annulus and the presence of the inter-lamellar matrix, that was found recently to play a key role in the disc mechanics (Derrouiche et al., 2019a; Adam et al., 2015; Mengoni et al., 2015; Tavakoli et al., 2016), was designed following the same recommendations of chapters II and III. A uniaxial circumferential tension strain of 10% was applied to all specimens under a strain rate of 0.002 /s. The model succeeded to reproduce the stress/volumetric behavior of the bovine annulus fibrosus in chapter II and then was extended later in chapter III to simulate the behavior of the different human disc regions by adjusting the fluid kinetics and the microstructure contents using human experimental data. The model constants are listed in Table IV.1.

The human model was implemented into the non-linear finite element software MSC.Marc using a set of subroutines. A flowchart of the model implementation procedure is represented in Figure IV.3. The reader is also referred to complementary references (Ovalle-Rodas et al., 2016; Guo et al., 2018) for the general implementation procedure of coupled models.

| Parameter | Unit | Significance | Value |
|-----------------|--------------------------------|---|---------|
| E | MPa | ECM stiffness | 1.0 |
| I_1^{\max} | MPa | ECM limiting extensibility constant | 3.0 |
| E_v | MPa | ECM viscosity | 0.167 |
| I_{1v}^{\max} | MPa | ECM viscosity | 1.5 |
| d | $\text{MPa}^{-1}\text{s}^{-1}$ | ECM viscosity | 0.02 |
| m | | ECM viscosity | 0.001 |
| A_1 | MPa | Collagen stiffness | 27.0 |
| A_2 | MPa | Collagen stiffness | 100.0 |
| β_m | s^{-1} | Fluid flow constant in lamella | -0.0004 |
| β_m | s^{-1} | Fluid flow constant in inter-lamellar matrix | 0.00097 |
| k | MPa | Inner Bulk modulus | 800 |
| k | MPa | Outer Bulk modulus | 3500 |
| ξ | | Inner transportation coefficient in lamella | 40.25 |
| ξ | | Outer transportation coefficient in lamella | 26.4 |
| ξ | | Inner transportation coefficient in inter-lamellar matrix | 15.29 |
| ξ | | Outer transportation coefficient in inter-lamellar matrix | 7.65 |

Table IV.1. Model constants.

IV.2.3. Age-related microstructure changes

We tried to investigate the effect of the microstructure changes induced by natural aging on the mechanical behavior of the annulus tissue. For each disc region, the average water content and type I collagen fibers and orientation was assigned depending on the studied disc age.

Five different disc ages (13-18, 36, 58, 69 and 82 years old) going from adolescents to elderly were considered.

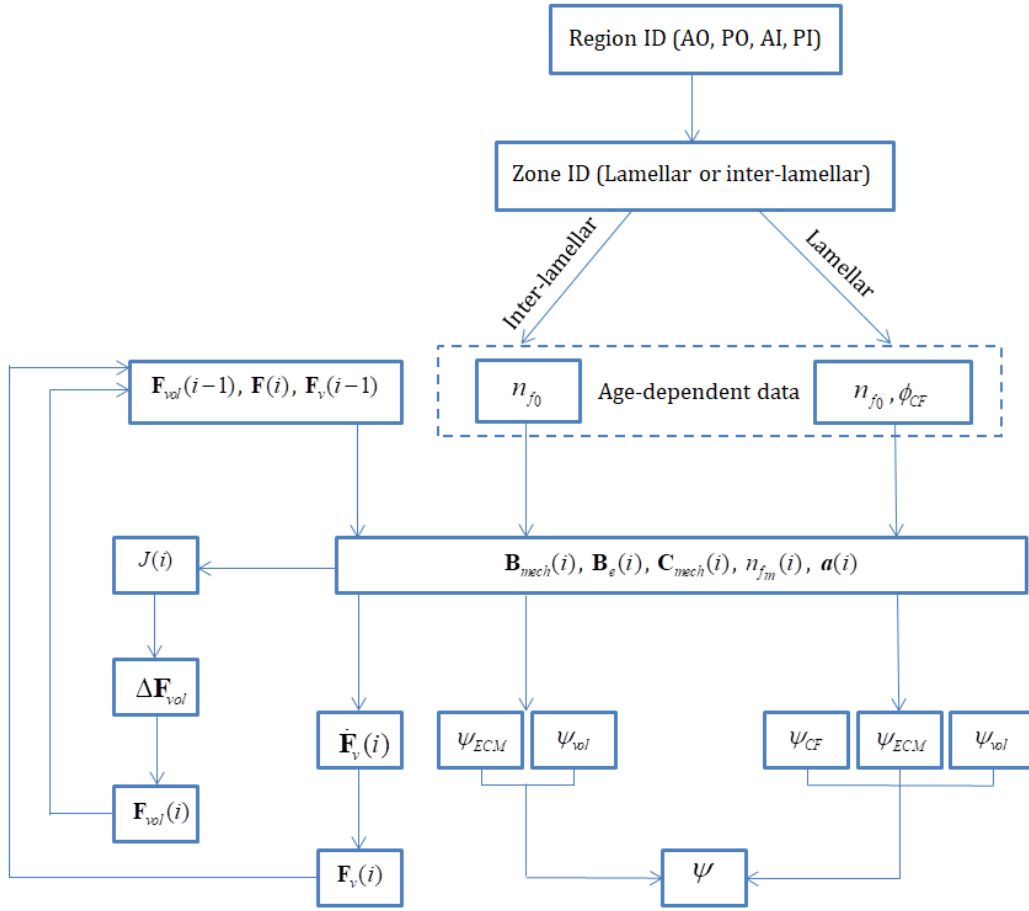


Figure IV.3. Flow chart of the model implementation. It considers the structural features of the studied region and the studied zone by mentioning their corresponding identification (ID) which then affects their corresponding microstructure quantities and free energy functions.

In order to calculate the wet density of type I collagen fibers ϕ_{CF} the following equation was used:

$$\phi_{CF} = (1 - n_{unloaded}) \phi_{CF(I+II)} \phi_{CF(I/(I+II))} \quad (IV.13)$$

where $\phi_{CF(I+II)}$ is the average total collagen fibers and $\phi_{CF(I/(I+II))}$ is the type I collagen fibers over the total collagen fibers. All fibers data were taken for L3-L4 disc. The values are provided in Table IV.2 for each region. Fibers angle values were chosen to be 23° for AO, 30° for AI and 48° for PO and PI (Holzapfel et al., 2005). Since no available data was found

about the initial water content in each disc region for the same ages, the average water content evolution was computed by a logarithmic regression of Koeller et al. (1984) data providing the average water content change in lumbar disc with age. The calculated curve was adapted for each disc region based on the regional water content $n_{initial}$ defined in Iatridis et al. (2008) for specimens aged of 58 years old. The finally computed initial water contents of the different disc regions and for the different ages are presented in Table IV.3.

| Age | AO | AI | PO | PI |
|--------------|---------------|-------------|---------------|---------------|
| Less than 18 | 66.5 (68.9) | 54 (36.2) | 66.5 (68.9) | 53.33 (36.25) |
| 36 | 65.4 (70) | 52 (43) | 68.65 (79.1) | 54.55 (35.95) |
| 58 | 64.25 (69.45) | 50 (49.2) | 70.75 (85.7) | 56.15 (35.15) |
| 69 | 62.45 (63.65) | 48.9 (49.7) | 72.15 (83.85) | 57.8 (33.65) |
| 82 | 60.5 (58.95) | 48.1 (48) | 76.65 (78.1) | 60.45 (35.1) |

Table IV.2. Total collagen and type I collagen contents in each disc region for different ages. Between brackets (type I collagen content over all collagen content). All values are extracted from Brickley-Parsons and Glimcher (1984) where the annulus width was divided into four parts. The collagen concentrations of the two outer parts were averaged for AO and PO and the concentrations of the two inner parts were averaged for AI and PI.

| Age | AO | AI | PO | PI |
|--------------|-----------|-----------|-----------|-----------|
| Less than 18 | 75.85 | 79.55 | 78.25 | 82.65 |
| 36 | 72.15 | 75.85 | 74.55 | 78.95 |
| 58 | 70.6 | 74.3 | 73 | 77.4 |
| 69 | 69.45 | 73.75 | 72.45 | 76.85 |
| 82 | 68.95 | 73.25 | 71.95 | 76.35 |

Table IV.3. Initial water content in each disc region for different ages. Values were obtained by logarithmic fitting of Koeller et al. (1984) experimental results where average water content of the disc were computed for different human specimen ages. The averaged curve was adapted for each region using water content at 58 disc regions defined in Iatridis et al. (2007).

IV.3. Results and discussion

IV.3.1. Age-related stress response changes

In Figure IV.4, the computed stress-strain responses of the four regions were plotted for different ages. AO region reveals the highest stress-strain slope and PI region the lowest stress-strain slope. For adolescents (13-18 years) the rigidity is relatively low for the different disc regions. It increases with age until middle age (36 years) and then it becomes almost constant for higher ages with a slight increase from 36 to 58 years old. All computed curves are in accordance with previously found experimental rigidity intervals of Ebara et al. (1996).

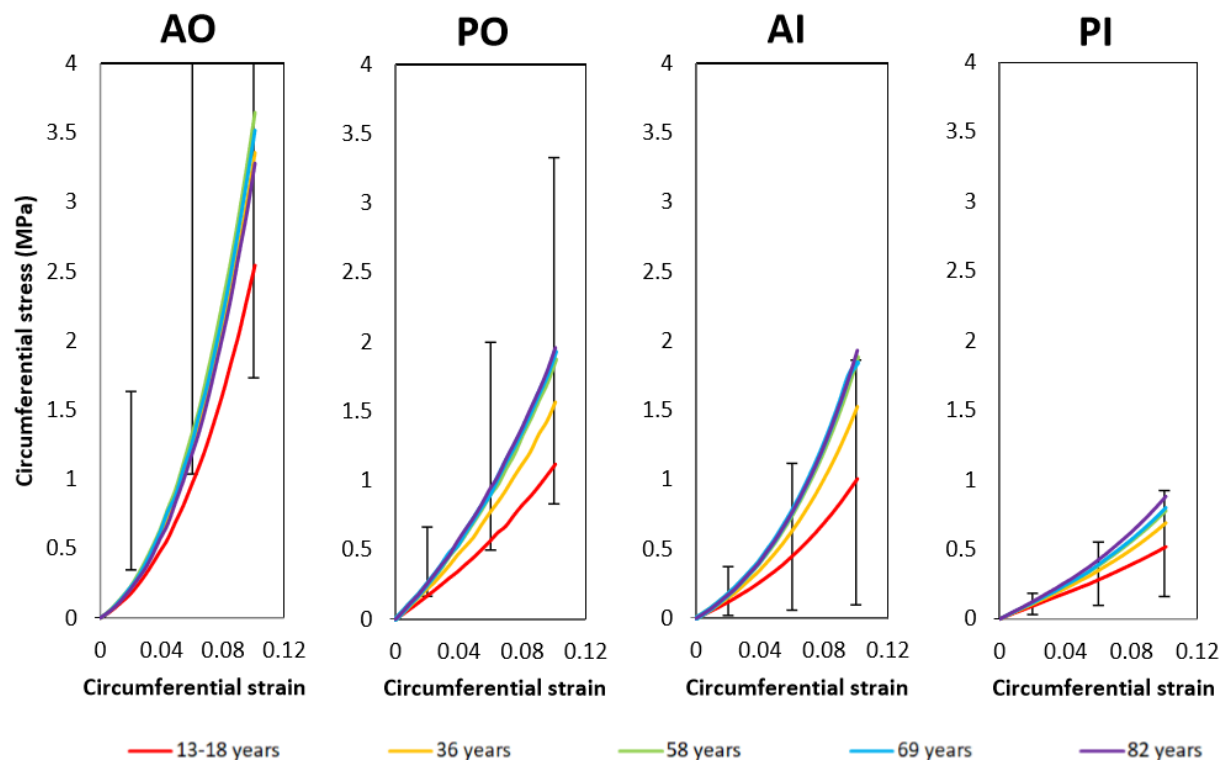
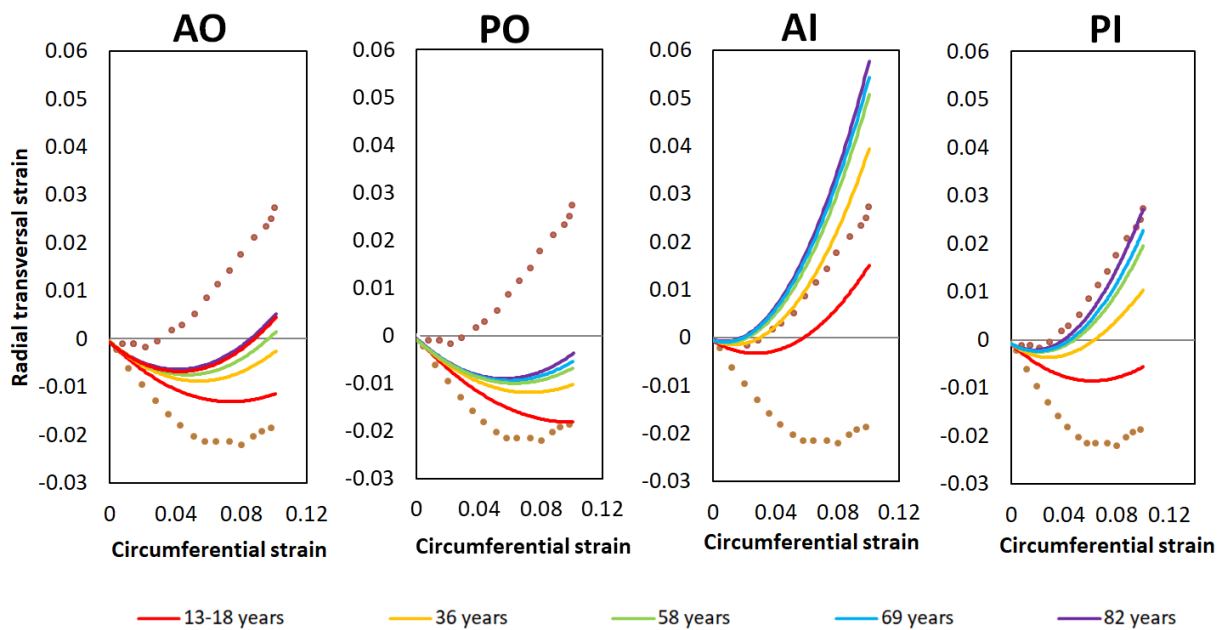


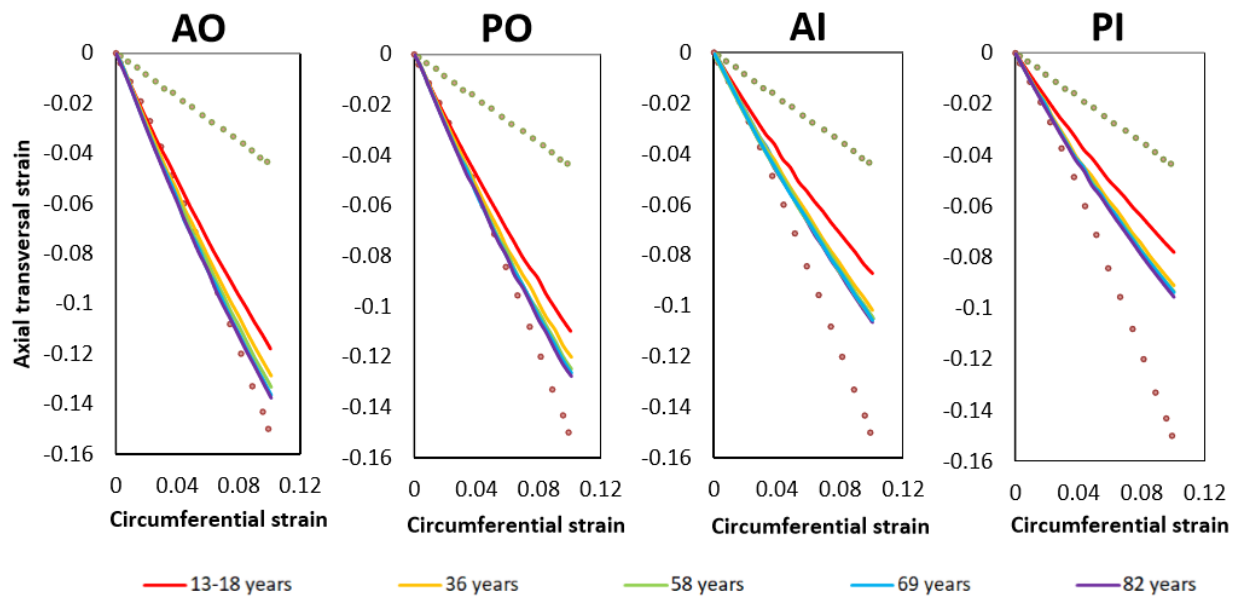
Figure IV.4. Uniaxial stretching model results for different ages and disc regions compared to the experimental data (including error bars) extracted from Ebara et al. (1996).

IV.3.2. Age-related transversal response changes

Figure IV.5 presents the computed transversal responses of the four regions as a function of the circumferential strain. Radial strains in the outer regions are negative for 13-18 age groups but they decrease with age presenting very small values (i.e., Poisson's ratio values close to zero). On the other side, the inner regions exhibit an auxetic response with a positive radial strain (i.e., negative Poisson's ratio) at 13-18 years old. Their auxeticity increases while getting older until reaching 36 years old then the effect of age decreases gradually and the values of strains become almost constant. The axial strains of all disc regions demonstrated unusual Poisson's ratio values exceeding 1.0. Their values increase a little bit with age inducing a very small decrease in disc height. Transversal strain results are compared to the typical experimental curves extracted from Baldit et al. (2014). Maximum and minimum values are selected. All predicted responses fall in the experimental limits curves, except AI regions that show higher (auxetic) positive radial strain values.



(A)



(B)

Figure IV.5. Transversal strain history in radial direction (A) and in axial direction (B) for different ages and disc regions compared to the upper and lower limits (in symbols) of experimental data extracted from Baldit el al. (2014).

IV.3.3. Local stress-strain fields

Local stress-strain fields are plotted and compared for 13-18 and 82 years old specimens of the four annulus regions in Figure IV.6. The circumferential stress in the lamellae increases with age for all disc regions except for PI. No change is noticed in the inter-lamellar matrix. The shear strain increases with age in all disc regions with a greater effect in the inner regions where the local values increase by two or three times compared to those of a young disc. The circumferential strain fields were also calculated but not plotted since no effect of age on the local results were observed whatever the regions.

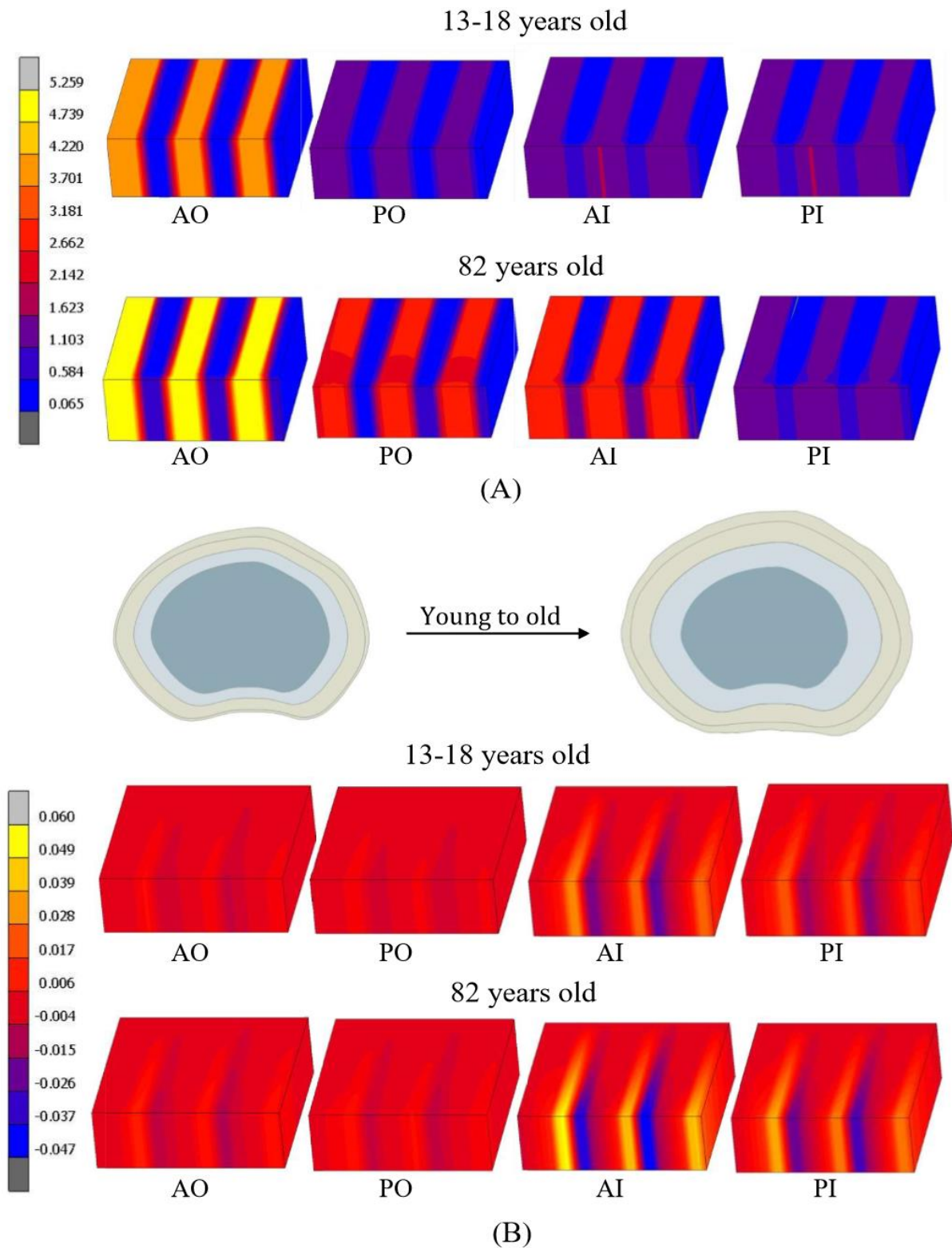


Figure IV.6. Distribution of the circumferential stress (in MPa) (A) and the shear strain (B) fields for young and old disc tissues along with regional dependency; The sketch shows the interpreted consequences on the disc volumetric change.

IV.3.4. Correlation between intrinsic mechanics of disc and its functionality

As any other soft tissue, the microstructure components that vary with age inside the intervertebral disc annulus should normally influence its mechanical response. An unexpected result was noticed by many experimental contributions which did not evidence a significant effect of age on the rigidity of the annulus and globally on its mechanical behavior under stretching. For this reason, a microstructure-based modeling approach previously validated for reproducing the multi-axial behavior of the intervertebral disc annulus is used to investigate this issue and to try to figure out the effect of aging on the mechanical behavior of the soft tissue. By varying the oriented fibers amount and the equilibrated water content as a function of the age, the effect of age on the stress-strain and transversal strains was studied and analyzed by means of the model. From the obtained in-silico results, we can notice that the rigidity of the disc is relatively low for young individuals (below 20 years old); then it increases while individuals are getting older until reaching maturity and then it remains almost constant for the rest of their life. It is important to mention that most of the in-vitro experimental tests of the literature are made on specimens of old cadavers because of their availability compared to specimens of young individuals. As an illustrative example, the in-vitro tests of Ebara et al. (1996) and Holzappel et al. (2005) were established on specimens extracted from spines of an age varying between 26 and 53 years old, and between 27 and 82 years old, respectively. Weak effect of age was found on the annulus rigidity since most of the experiments are done on cadavers of mature or quasi-mature discs that have an almost stable stress-strain conduct. This observation was reported by Yamine (2019) who mentioned that experimental results available in the literature that were established on human cadaveric are biased toward elderly. Also, we can see from the stress-strain curves in Figure IV.4 that the

rigidity of the posterior disc regions (PO and PI) are lower than that of the anterior disc regions (AO and PO) for the different life stages. The PI region remains the weakest part of the disc with the lowest slope of the stress-strain response and hence the lowest rigidity. This result is in accordance with the medical observations stating that many disc degeneration problems such as hernia often start from the PI region of the annulus for the different life stages. The transversal strains conducts highlight a very important mechanical parameter that varies with age, that is, the 'Poisson's ratio'. Since the disc is always under quasi-permanent load caused by the body weight, the Poisson's ratio will usually be active and will be a factor affecting the height and diameter of the disc (as illustrated in Figure IV.6). Any effect of age on this parameter will directly affect the disc morphology. Despite the major importance of this mechanical property, no previous contribution investigated the aging effect on it. Under controlled circumferential strain, the absolute value of the radial strain describing the change of the annulus width and as a consequence the disc diameter increases largely with age. At the same time, the absolute value of the axial strain affecting disc height slightly increases. Generally, these changes will not influence the global disc height, but it could be apparent in the thinner parts of the disc as the PO region. This would be seen especially for discs of the lowest part of the spinal column where big differences of the anterior and posterior thickness in the unloaded state are often witnessed. This is in line with many experimental observations in the literature where we could see that the diameter highly increases with age (Koeller et al., 1984; Twomey and Taylor, 1988) causing in some cases disc bulging problems that were found to be correlated with age (Videman et al., 1995). As well, although the disc is known to lose a part of its hydration, the healthy annulus height affected by only microstructure changes is found not to change a lot with age (Koeller et al., 1984; Twomey and Taylor, 1988; Amonoo-Kuofi, 1991). The positive strain in the radial direction (equivalent to a negative Poisson's ratio) indicates the tissue swelling in this direction and shows an auxetic effect. The

axial transversal strain values are very close from the applied circumferential strain (equivalent to a Poisson's ratio between 0.7 and 1.4). These Poisson's ratios are unusual since the normal range of this material property is between 0 and 0.5 which points out an extraordinary response of this soft tissue allowing it to accomplish its damping function under the different applied external mechanical loads. With age, we notice that the values get farther from the normal values which could affect the disc functionality and decreases its resistance. Seeking for more explanations about the effect of age on the different zones of annulus lamellar structure, local numerical stress and strain fields of the different disc regions are plotted and analyzed in Figure IV.6. With age the circumferential stresses increase in the lamellae while remaining constant in the inter-lamellar matrix. The strain fields in the same direction were constant for the different ages highlighting the stiffening of the lamellae induced by the microstructure changes. All the disc lamellar zones undergo noticeable stiffening except for PI which makes it the weakest part of the disc and increases the risk of injury initiation inside it under high mechanical loads. The observation of local strain fields shows that the shear strains are higher in the inner parts of the disc. Their amounts increase with age especially in the lamellar/inter-lamellar transition zones alerting for a high risk of delamination initiation. Great resemblances are identified between the aging effect and hyper-osmotic effect reported by recent experimental contributions (Derrouiche et al., 2019b, 2020b; Feki et al., 2020). Both effects decrease the water content, increase the rigidity and affect the annulus Poisson's ratios in a close manner. These common points open the discussion to the use of the hyper-osmotic conditions as an alternative accelerating aging method.

It is worth noticing that our in-silico results were obtained with some restrictions. The fibers and water contents for each age could vary between individuals, disc levels and could be even affected by the testing conditions that change from an experiment to another. The goal of this contribution is to qualitatively identify the effect of aging on the annulus mechanics and to try

finding explanations about previously captured in-vitro observations. For this reason and due to the complexity of such study, including age effect on the regional dependency, the average of the fibers and water contents was used for the calculations. The input data were designed using the same source disc level in order to avoid any effect of testing or specimen preparation conditions. As well, it is important to mention that each region of the disc does not have an exact value of fibers and water contents inside the disc. They vary gradually in both the circumferential and radial directions. Experimentally, these gradients are very difficult to identify. For this reason, the use of average values from each disc region is often considered in this type of studies. Finally, the ECM rigidity is known to alter with age (Cortes et al., 2013; Stewart et al., 2017). But there is no reliable data available in the literature about the amount of change of this parameter with age from adolescent to elderly. However, we believe that the contribution of the ECM is very small compared to the oriented fibers contribution in the disc stress-strain behavior. For this reason, the same rigidity modulus was used for all ages. This should have a negligible impact on all the results, except the PI stress-strain curves that demonstrate very small rigidity values.

IV.4. Partial conclusion

The effect of natural aging mechanisms on the human annulus fibrosus mechanics are very complex to identify experimentally. By means of a microstructure-based mechanistic modeling approach, the disc mechanics in terms of rigidity, radial and axial transversal responses was found to alter going from adolescent to middle age where the disc reaches a certain maturity. After reaching maturity the mechanical properties undergo very slight changes until becoming almost constant with age. For future works, the application of the developed approach on a complete spinal unit structure seems important in order to

investigate the age effect on more complex mechanical loads and combined spinal movements.

References

- Adam, C., Rouch, P., Skalli, W., 2015. Inter-lamellar shear resistance confers compressive stiffness in the intervertebral disc: an image-based modelling study on the bovine caudal disc. *Journal of Biomechanics* 48, 4303-4308.
- Adams, M.A., Hutton, W.C., 1982. Prolapsed intervertebral disc. A hyperflexion injury 1981 Volvo Award in Basic Science. *Spine* 7, 184-191.
- Adams, M.A., Hutton, W.C., 1985. Gradual disc prolapse. *Spine* 10, 524-531.
- Adams, M.A., Roughley, P.J., 2006. What is intervertebral disc degeneration, and what causes it? *Spine* 31, 2151-2161.
- Amonoo-Kuofi, H.S., 1991. Morphometric changes in the heights and anteroposterior diameters of the lumbar intervertebral discs with age. *Journal of Anatomy* 175, 159-168.
- Baldit, D., Ambard, D., Cherblanc, F., Royer, P., 2014. Experimental analysis of the transverse mechanical behaviour of annulus fibrosus tissue. *Biomechanics and Modeling in Mechanobiology* 13, 643-652.
- Balzani, D. Neff, P. Schroder, J. Holzapfel, G.A., 2006. A polyconvex framework for soft biological tissues: adjustment to experimental data. *International Journal of Solids and Structures* 43, 6052-6070.
- Barthelemy, V.M.P., van Rijsbergen, M.M., Wilson, W., Huyghe, J.M., van Rietbergen, B., Ito, K., 2016. A computational spinal motion segment model incorporating a matrix composition-based model of the intervertebral disc. *Journal of the Mechanical Behavior of Biomedical Materials* 54, 194-204.
- Bergstrom, J.S., Boyce, M.C., 1998. Constitutive modeling of the large strain time-dependent behavior of elastomers. *Journal of the Mechanics and Physics of Solids* 46, 931-954.
- Bibby, S.R., Urban, J.P., 2004. Effect of nutrient deprivation on the viability of intervertebral disc cells. *European Spine Journal* 13, 695-701.
- Bibby, S.R.S., Jones, D.A., Ripley, R.M., Urban, J.P., 2005. Metabolism of the intervertebral disc: effects of low levels of oxygen, glucose, and pH on rates of energy metabolism of bovine nucleus pulposus cells. *Spine* 30, 487-496.
- Brickley-Parsons, D., Glimcher, M.J., 1984. Is the chemistry of collagen in intervertebral discs an expression of Wolff's Law? A study of the human lumbar spine. *Spine* 9, 148-163.
- Buckwalter, J.A., 1995. Aging and degeneration of the human intervertebral disc. *Spine* 20, 1307-1314.
- Cantournet, S., Boyce, M.C., Tsou, A.H., 2007. Micromechanics and macromechanics of carbon nanotube-enhanced elastomers. *Journal of the Mechanics and Physics of Solids* 55, 1321-1339.
- Cassidy, J.J., Hiltner, A., Baer, E., 1989. Hierarchical structure of the intervertebral disc. *Connective Tissue Research* 23, 75-88.

- Chetoui, M.A., Boiron, O., Dogui, A., Deplano, V., 2017. Prediction of intervertebral disc mechanical response to axial load using isotropic and fiber reinforced FE models. *Computer Methods in Biomechanics and Biomedical Engineering* 20, 39-40.
- Chetoui, M.A., Boiron, O., Ghiss, M., Dogui, A., Deplano, V., 2019. Assessment of intervertebral disc degeneration-related properties using finite element models based on ρ_H -weighted MRI data. *Biomechanics and Modeling in Mechanobiology* 18, 17-28.
- Cortes, D.H., Han, W.M., Smith, L.J., Elliott, D.M., 2013. Mechanical properties of the extra-fibrillar matrix of human annulus fibrosus are location and age dependent. *Journal of Orthopaedic Research* 31, 1725-1732.
- Derrouiche, A., Karoui, A., Zaïri, F., Ismail, J., Qu, Z., Chaabane, M., Zaïri, F., 2020a. The two Poisson's ratios in annulus fibrosus: relation with the osmo-inelastic features. *Mechanics of Soft Materials* 2, 1.
- Derrouiche, A., Feki, F., Zaïri, F., Taktak, R., Moulart, M., Qu, Z., Ismail, J., Charfi, S., Haddar, N., Zaïri, F., 2020b. How pre-strain affects the chemo-torsional response of the intervertebral disc. *Clinical Biomechanics* 76, 105020.
- Derrouiche, A., Zaïri, F., Zaïri, F., 2019a. A chemo-mechanical model for osmo-inelastic effects in the annulus fibrosus. *Biomechanics and Modeling in Mechanobiology* 18, 1773-1790.
- Derrouiche, A., Zaouali, A., Zaïri, F., Ismail, J., Chaabane, M., Qu, Z., Zaïri, F., 2019b. Osmo-inelastic response of the intervertebral disc. *Proceedings of the Institution of Mechanical Engineers. Part H: Journal of Engineering in Medicine* 233, 332-341.
- Ebara, S., Iatridis, J.C., Setton, L.A., Foster, R.J., Mow, V.C., Weidenbaum, M., 1996. Tensile properties of nondegenerate human lumbar annulus fibrosus. *Spine* 21, 452-461.
- Ehlers, W., Karajan, N., Markert, B., 2009. An extended biphasic model for charged hydrated tissues with application to the intervertebral disc. *Biomechanics and Modeling in Mechanobiology* 8, 233-251.
- Eyre, D.R., 1979. Biochemistry of the intervertebral disc. *International Review of Connective Tissue Research* 8, 227-291.
- Feki, F., Taktak, R., Kandil, K., Derrouiche, A., Moulart, M., Haddar, N., Zaïri, F., Zaïri, F., 2020. How osmo-viscoelastic coupling affects recovery of cyclically compressed intervertebral disc. *Spine* 45, 160553.
- Galante, J.O., 1967. Tensile properties of the human lumbar annulus fibrosus. *Acta Orthopaedica Scandinavica* 100, 1-91.
- Galbusera, F., Mietsch, A., Schmidt, H., Wilke, H.J., Neidlinger-Wilke, C., 2013. Effect of intervertebral disc degeneration on disc cell viability: a numerical investigation. *Computer Methods in Biomechanics and Biomedical Engineering* 16, 328-337.
- Gent, A.N., 1996. A new constitutive relation for rubber. *Rubber Chemistry and Technology* 69, 59-61.
- Guo, Z.Y., Peng, X.Q., Moran, B., 2006. A composites-based hyperelastic constitutive model for soft tissue with application to the human annulus fibrosus. *Journal of the Mechanics and Physics of Solids* 54, 1952-1971.
- Guo, Q., Zaïri, F., Guo, X., 2018. A thermo-viscoelastic-damage constitutive model for cyclically loaded rubbers. Part I: model formulation and numerical examples. *International Journal of Plasticity* 101, 106-124.

- Gurtin, M.E., Anand, L., 2005. The decomposition $F = FeFp$, material symmetry, and plastic irrotationality for solids that are isotropic-viscoplastic or amorphous. *International Journal of Plasticity* 21, 1686-1719.
- Hickey, D.S., Aspden, R.M., Hukins, D.W., Jenkins, J.P., Isherwood, I., 1986. Analysis of magnetic resonance images from normal and degenerate lumbar intervertebral discs. *Spine* 11, 702-708.
- Holzappel, G.A., Schulze-Bauer, C.A.J., Feigl, G., Regitnig, P., 2005. Single lamellar mechanics of the human lumbar annulus fibrosus. *Biomechanics and Modeling in Mechanobiology* 3, 125-140.
- Horner, H.A., Urban, J.P.G., 2001. Effect of nutrient supply on the viability of cells from the nucleus pulposus of the intervertebral disc. *Spine* 26, 2543-2549.
- Huang, C.Y., Gu, W.Y., 2008. Effects of mechanical compression on metabolism and distribution of oxygen and lactate in intervertebral disc. *Journal of Biomechanics* 41, 1184-1196.
- Iatridis, J.C., MacLean, J.J., O'Brien, M., Stokes, I.A., 2007. Measurements of proteoglycan and water content distribution in human lumbar intervertebral discs. *Spine* 32, 1493-1497.
- Inoue, H., Takeda, T., 1975. Three-dimensional observation of collagen framework of lumbar intervertebral discs. *Acta Orthopaedica* 46, 949-956.
- Jenkins, J.P., Hickey, D.S., Zhu, X.P., Machin, M., Isherwood, I., 1985. MR imaging of the intervertebral disc: a quantitative study. *The British Journal of Radiology* 58, 705-709.
- Kandil, K., Zaïri, F., Derrouiche, A., Messenger, T., Zaïri, F., 2019. Interlamellar-induced time-dependent response of intervertebral disc annulus: a microstructure-based chemo-viscoelastic model. *Acta Biomaterialia* 100, 75-91.
- Kandil, K., Zaïri, F., Messenger, T., Zaïri, F., 2020. Interlamellar matrix governs human annulus fibrosus multiaxial behavior. *Scientific Reports* 10, 19292.
- Klisch, S.M., Lotz, J.C., 2000. A special theory of biphasic mixtures and experimental results for human annulus fibrosus tested in confined compression. *Journal of Biomechanical Engineering* 122, 180-188.
- Koeller, W., Funke, F., Hartmann, F., 1984. Biomechanical behaviour of human intervertebral discs subjected to long lasting axial loading. *Biorheology* 21, 675-86.
- Lauzeral, N., Borzacchiello, D., Kugler, M., George, D., Rémond, Y., Hostettler, A., Chinesta, F., 2019. A model order reduction approach to create patient-specific mechanical models of human liver in computational medicine applications. *Computer Methods and Programs in Biomedicine* 170, 95-106.
- Louman-Gardiner, K.M., Coombe, D., Hunter, C. J., 2011. Computation models simulating notochordal cell extinction during early ageing of an intervertebral disc. *Computer Methods in Biomechanics and Biomedical Engineering* 14, 1071-1077.
- Malandrino, A., Noailly, J., Lacroix, D., 2011. The effect of sustained compression on oxygen metabolic transport in the intervertebral disc decreases with degenerative changes. *PLOS Computational Biology* 7, e1002112.
- Malandrino, A., Mak, M., Kamm, R.D., Moeendarbary, E., 2018. Complex mechanics of the heterogeneous extracellular matrix in cancer. *Extreme Mechanics Letter* 21, 25-34.

- Mengoni, M., Luxmoore, B.J., Wijayathunga, V.N., Jones, A.C., Broom, N.D., Wilcox, R.K., 2015. Derivation of inter-lamellar behaviour of the intervertebral disc annulus. *Journal of the Mechanical Behavior of Biomedical Materials* 48, 164-172.
- Mwale, F., Ciobanu, I., Giannitsios, D., Roughley, P., Steffen, T., Antoniou, J., 2011. Effect of oxygen levels on proteoglycan synthesis by intervertebral disc cells. *Spine* 36, 131-138.
- Osti, O.L., Vernon-Roberts, B., Moore, R., Fraser, R.D., 1992. Annular tears and disc degeneration in the lumbar spine: a post-mortem study of 135 discs. *The Journal of Bone and Joint Surgery* 74, 678-682.
- Ovalle-Rodas, C., Zaïri, F., Naït-Abdelaziz, M., Charrier, P., 2016. A thermo-visco-hyperelastic model for the heat build-up during low-cycle fatigue of filled rubbers: formulation, implementation and experimental verification. *International Journal of Plasticity* 79, 217-236.
- Parkkola, R., Kormano, M., 1992. Lumbar disc and back muscle degeneration on MRI: correlation to age and body mass. *Journal of Spinal Disorders* 5, 86-92.
- Peng, X.Q., Guo, Z.Y., Moran, B., 2005. An anisotropic hyperelastic constitutive model with fiber-matrix shear interaction for the human annulus fibrosus. *Journal of Applied Mechanics* 73, 815-824.
- Pfaffmann, C.W., Metzdorf, A., Elfering, A., Hodler, J., Boos, N., 2006. Effect of aging and degeneration on disc volume and shape: a quantitative study in asymptomatic volunteers. *Journal of Orthopaedic Research* 24, 1086-1094.
- Razaghi, R., Biglari, H., Karimi, A., 2019. Risk of rupture of the cerebral aneurysm in relation to traumatic brain injury using a patient-specific fluid-structure interaction model. *Computer Methods and Programs in Biomedicine* 176, 9-16.
- Riches, P.E., Dhillon, N., Lotz, J., Woods, A.W., McNally, D.S., 2002. The internal mechanics of the intervertebral disc under cyclic loading. *Journal of Biomechanics* 35, 1263-1271.
- Roughley, P.J., 2004. Biology of intervertebral disc aging and degeneration: involvement of the extracellular matrix. *Spine* 29, 2691-2699.
- Schroeder, J., Neff, P., 2003. Invariant formulation of hyperelastic transverse isotropy based on polyconvex free energy functions. *International Journal of Solids and Structures* 40, 401-445.
- Soukane, D.M., Shirazi-Adl, A., Urban, J.P.G., 2007. Computation of coupled diffusion of oxygen, glucose and lactic acid in an intervertebral disc. *Journal of Biomechanics* 40, 2645-2654.
- Stewart, D.M., Monaco, L.A., Gregory, D.E., 2017. The aging disc: using an ovine model to examine age-related differences in the biomechanical properties of the intralamellar matrix of single lamellae. *European Spine Journal* 26, 259-266.
- Szilagy, S.M., Szilagy, L., Benyo, Z., 2011. A patient specific electro-mechanical model of the heart. *Computer Methods and Programs in Biomedicine* 101, 183-200.
- Tavakoli, J., Elliott, D.M., Costi, J.J., 2016. Structure and mechanical function of the inter-lamellar matrix of the annulus fibrosus in the disc. *Journal of Orthopaedic Research* 34, 1307-1315.
- Twomey, L., Taylor, J., 1988. Age changes in the lumbar spinal and intervertebral canals. *Paraplegia* 26, 238-49.

- Urban, J.P., McMullin, J.F., 1988. Swelling pressure of the lumbar intervertebral discs: influence of age, spinal level, composition, and degeneration. *Spine* 13, 179-187.
- Vernon-Roberts, B., Moore, R.J., Fraser, R.D., 2007. The natural history of age-related disc degeneration: the pathology and sequelae of tears. *Spine* 32, 2797-2804.
- Videman, T., Sarna, S., Battie, M.C., Koskinen, S., Gill, K., Paananen, H., Gibbons, L., 1995. The long-term effect of physical loading and exercise lifestyles on back-related symptoms, disability, and spinal pathology among men. *Spine* 20, 699-709.
- Wills, C.R., Malandrino, A., van Rijsbergen, M.M., Lacroix, D., Ito, K., Noailly, J., 2016. Simulating the sensitivity of cell nutritive environment to composition changes within the intervertebral disc. *Journal of the Mechanics and Physics of Solids* 90, 108-123.
- Yamine, K., 2019. Published human cadaveric measurements are strongly biased toward the elderly population. *Clinical Anatomy* 33, 804-808.
- Yu, J., Tirlapur, U., Fairbank, J., Handford, P., Roberts, S., Winlove, C.P., Cui, Z., Urban, J., 2007. Microfibrils, elastin fibres and collagen fibres in the human intervertebral disc and bovine tail disc. *Journal of Anatomy* 210, 460-471.
- Zhu, Q., Jackson, A.R., Gu, W.Y., 2012. Cell viability in intervertebral disc under various nutritional and dynamic loading conditions: 3D finite element analysis. *Journal of Biomechanics* 45, 2769-2777.
- Zhu, Q., Gao, X., Gu, W., 2014. Temporal changes of mechanical signals and extracellular composition in human intervertebral disc during degenerative progression. *Journal of Biomechanics* 47, 3734-3743.
- Zhu, Q., Gao, X., Chen, C., Gu, W., Brown, M.D., 2020. Effect of intervertebral disc degeneration on mechanical and electric signals at the interface between disc and vertebra. *Journal of Biomechanics* 104, 109756.

Chapter V

A microstructure-based human spine unit model integrating tissue volumetric strain and lamellar-interlamellar-nucleus interaction⁹

Abstract

This chapter presents the construction of a novel model of the human spine unit considering micromechanics and macromechanics of the intervertebral disc in correlation with its swelling response. The model constitutively considers the tissue swelling response that was recently shown as determinant in the correct multi-axial computation of the disc response. The truthful annulus lamellar-interlamellar organization is modeled while taking into account the anterior-posterior and inner-outer regional variations and their interaction with the gelatinous nucleus. Due to the complex heterogeneous disc configuration, each element of the finite element model was associated to its corresponding position inside an accurate L4-L5 disc geometry constructed based on computerized tomography data. By means of a fully tridimensional chemo-viscoelastic constitutive model, that we have implemented into a finite element code, the local mechanical properties are identified based on the microstructural features of each part of the disc (extracellular matrix, collagen and fluid). The chemical-induced volumetric response, introduced using experimentally-based fluid kinetics, is made anisotropic in the different disc planes due to interlamellar effect. Our numerical results are critically discussed upon different simple and complex physiological movements. The access to the disc core allows the observation of the displacement and shear strain fields that are compared to direct MRI experiments of the literature. Important conclusions about the annulus-nucleus interaction are provided thanks to the developed model. To illustrate further the model capacities, the observed critical zones are analyzed and related to the local kinetics and microstructure.

Keywords: Human spine unit; Volumetric strain; Microstructure; Complex mechanical loading; Local fields.

⁹ *This chapter is based on the following article: Kandil, K., Zaïri, F., Messenger, T., Zaïri, F., 2020. A microstructure-based human spine unit model integrating tissue volumetric strain and lamellar-interlamellar-nucleus interaction, submitted.*

V.1. Partial introduction

The intervertebral disc is probably the most sensitive human body part susceptible to damage. It is indeed highly strained throughout the day by the different accomplished activities and the constantly applied load of the body weight. Each movement of the body is the result of a series of simple and complex actions accomplished by the different functional spine units (an intervertebral disc and two adjacent vertebrae) of the vertebral column. The range of motions and the amount of loads applied to each intervertebral disc depend on its spinal position (Pearcy et al., 1984; Panjabi et al., 1994). The most common back injuries are thus known to occur in the lowest lumbar spine units, especially L4-L5 and L5-S1 (Panjabi et al., 1994; Ruberté et al., 2009) due to a much higher load bearing. Experimental researches on the intervertebral disc mechanics have led to considerable qualitative understanding of its response to simple loads (compression, torsion, flexion, extension and lateral bending) (Brown et al., 1957; Markolf, 1972; Markolf and Morris, 1974; Derrouiche et al., 2019a) or to complex loads (combination of two or more simple loads) (Spenciner et al., 2006; Heuer et al., 2008; Veres et al., 2010; Derrouiche et al., 2020a; Feki et al., 2020) aiming to better understand it and potentially prevent dangerous degenerative cases from happening. In line with these experiments, a lot of finite element models simulating the disc motions were developed trying to predict the response of the disc tissue and observe its conduct under different scenarios that are difficult to establish experimentally (Schmidt et al., 2007a, 2007b; Chevalier et al., 2008). The construction of an accurate disc model is a very difficult task for several reasons: (i) complexity of the disc geometry with a shape and size changing with the spinal level and age (Amonoo-Kuofi, 1991; Kim et al., 2013), (ii) complexity of the disc lamellar structure (Cassidy et al., 1989), (iii) complexity of the disc structure-properties relationship depending on the spinal level and the regional localization inside the same disc

(Ebara et al., 1996; Holzapfel et al., 2005), (iv) complexity of the interaction of the disc tissues with the surrounding environment (Urban and Maroudas, 1981; Derrouiche et al., 2019a) and (v) variability in health state of the disc.

The most advanced researches in the biomedical fields are seeking to build patient-specific models of human body organs (Szilagyí et al., 2011; Asner et al., 2017; Weis et al., 2017; Rama and Skatulla, 2018; Lauzeral et al., 2019; Razaghi et al., 2019; Grytz et al., 2020). To achieve this objective, the model should account for real local disc microstructure of each patient and volumetric change of its geometry under mechanical loading which could be only realized using a microstructural constitutive model. Many models were proposed trying to reproduce the correct response of the disc under different motions by using simplified approaches neglecting the annulus heterogeneity (Schroeder et al., 2006; Ehlers et al., 2009; Moramarco et al., 2010; Subramani et al., 2020) or the interaction with the surrounding environment (Shirazi-Adl et al., 1984; Natarajan and Andersson, 1999; Wang et al., 2013). These models allowed the prediction of the global disc motion without a real relation with the microstructural components or real local response inside the same disc. More accurate representation of the disc geometry was then presented by dividing the annulus into sub-regions or into concentric lamellae (del Palomar et al., 2008; Adam et al., 2015, Mengoni et al., 2015). The interlamellar matrix connecting the different lamellae is regarded as a potential damage zone due to its weak non-fibrillar microstructure compared to the adjacent lamellae. The reproduction of a correct volumetric response remains the main common weak point of all previous models. Indeed, a constant Poisson's ratio (the material property characterizing the transversal strain behavior) in all planes of the disc was assumed with a standard value between 0 and 0.5 for an isotropic medium. In recent contributions, apparent Poisson's ratios varying from negative values to values higher than 0.5 were disclosed in disc annulus (Baldit et al., 2014; Derrouiche et al., 2019b, 2020b; Kandil et al., 2019, 2020a). The transversal

strain behavior in disc annulus, attributed to the chemical-induced volumetric effects, was found different in the different disc planes due to interlamellar effect (Derrouiche et al., 2019b; Kandil et al., 2019). This peculiar behavior should be taken into consideration in any model to reflect the real mechanics of the disc as shown in chapter III.

The objective of the present study is to propose an accurate human spine unit model that is able to predict kinematic fields in the heart of the disc while accounting for the most recent discoveries about the structure-properties relationships of the annulus. As a consequence of the reasons cited above, an accurate L4-L5 disc geometry is constructed from computerized tomography (CT) scans. The disc annulus is divided into anterior-posterior and inner-outer regions that are themselves subdivided into lamellar-interlamellar zones. The local mechanical-structure properties are described using a recently developed microstructure-based chemo-viscoelastic constitutive model implemented into a computer code by means of a set of subroutines. The model introduces experimentally-based fluid transfer kinetics of the tissue allowing a correct time-dependent transversal behavior of the disc tissue. The model considers also the intrinsic viscosity of the disc extracellular matrix in the lamellar and interlamellar zones that contributes to the disc mechanics (Emanuel et al., 2018; Tavakoli and Costi, 2018) but still largely unappreciated and neglected in most of the current models. For different simple and complex physiological movements, the access to the disc core is established. Displacement and shear strain fields are observed and compared to direct MRI experiments of the literature.

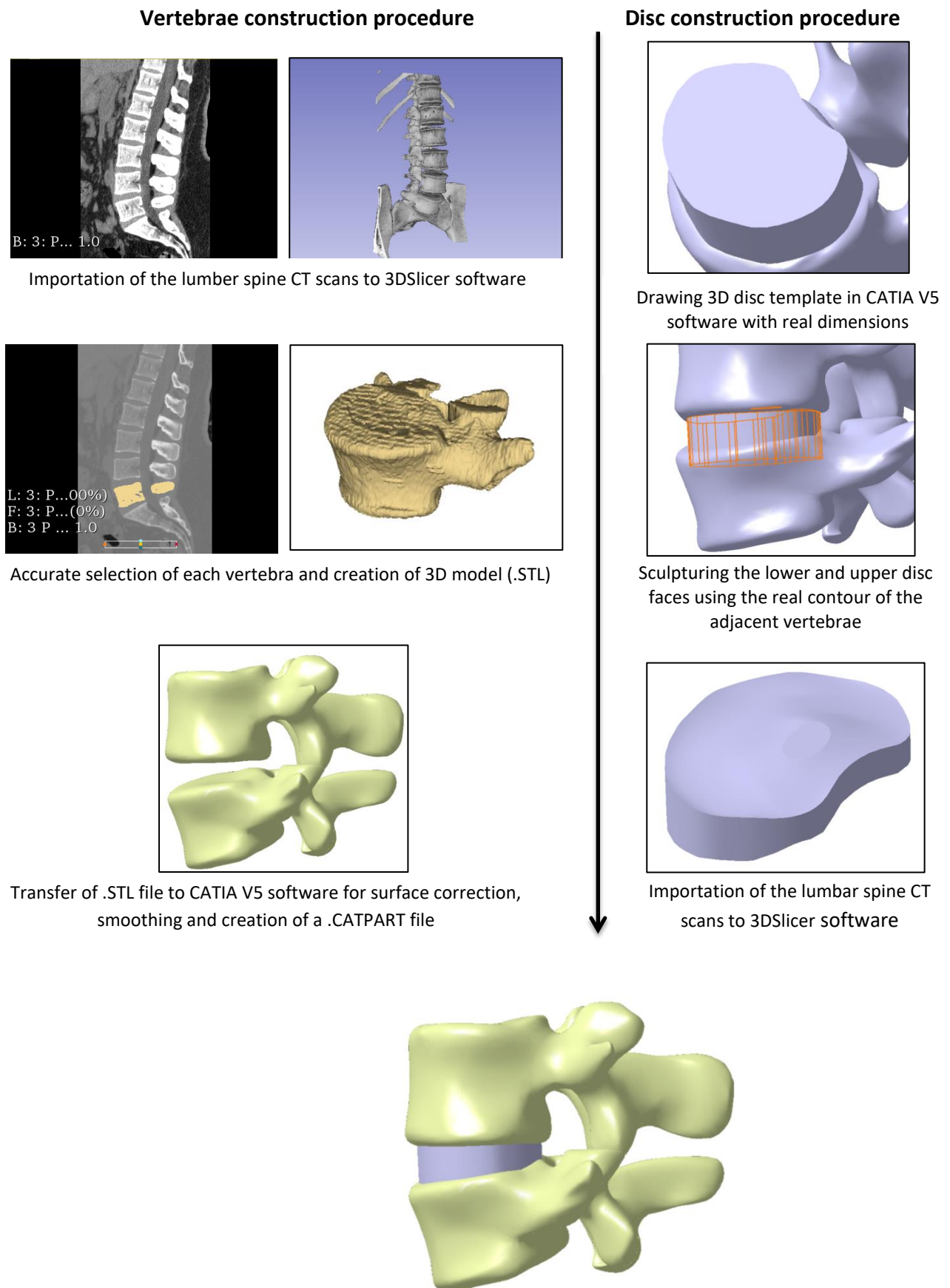
The chapter is organized as follows. Section V.2 details the development of the finite element model, the formulation of the constitutive model and its finite element implementation. The model capacities are presented in Section V.3 and discussed in Section V.4. Section V.5 closes the chapter with the concluding remarks.

V.2. Numerical model of the human spine unit

V.2.1. Model construction and boundary conditions

In order to simulate the accurate volumetric behavior of the intervertebral disc, L4-L5 functional spine unit was modeled using CT data of a 34 years old woman. The reconstruction procedure is summarized in Figure V.1. The L4 and L5 vertebrae were constructed by 3DSlicer image processing and three-dimensional visualization software. Then, they were transferred into Catia V5 software for surface treatment by applying different smoothing and correction operations. After obtaining perfect vertebrae geometry, the intervertebral disc was designed by following the contour of the adjacent vertebrae and its size was determined based on qualitative anatomical descriptions from the literature. Because the disc microstructure and properties differ from a zone to another with a radial and circumferential variation, the disc was divided into five main regions as shown in Figure V.2: Anterior Outer (AO), Anterior Inner (AI), Posterior Outer (PO), Posterior Inner (PI) and Nucleus Pulposus (NP). The disc was divided into annulus and nucleus parts by assuming nucleus size to be about 50% of the disc volume (Violas et al., 2007). The annulus was subdivided into seven lamellae separated by six interlamellar zones which correspond to the number of layers observed in (Rannou et al., 2000). Finally, the divided disc was imported in MSC.Marc finite element software and meshed by tetrahedral elements (Figure V.2). The vertebrae and the disc were assembled into MSC.Marc in order to obtain the model shown in Figure V.3. A perfectly glued connection was ensured for the contact between the vertebrae and the disc.

element model by following the maximum ranges of motions observed experimentally (Renner et al., 2007; Jaramillo et al., 2016). As shown in Figure V.3, five physiological movements are studied, namely, compression, torsion, flexion, extension, and lateral bending. All movements of the spine are combinations of these basic ones.



The different physiological movements were reproduced by the finite The lower vertebra was fixed and the upper vertebra was controlled in displacement using the following values: for compression 1 mm, for torsion 2.2°, for flexion 6.7°, for extension 3.9° and for lateral bending 5.9°. Loading rates of 0.02 mm/s for compression and 0.2°/s for torsion were chosen in order to maintain quasi-static loading conditions. The relative position of the disc and the adjacent vertebrae was kept the same as the originally captured CT scans in order to guarantee a physiological movement of the spinal unit. The disc was supposed to be immersed in a physiological saline solution of a 9 g/L concentration in order to guarantee a realistic osmotic swelling response of the disc.

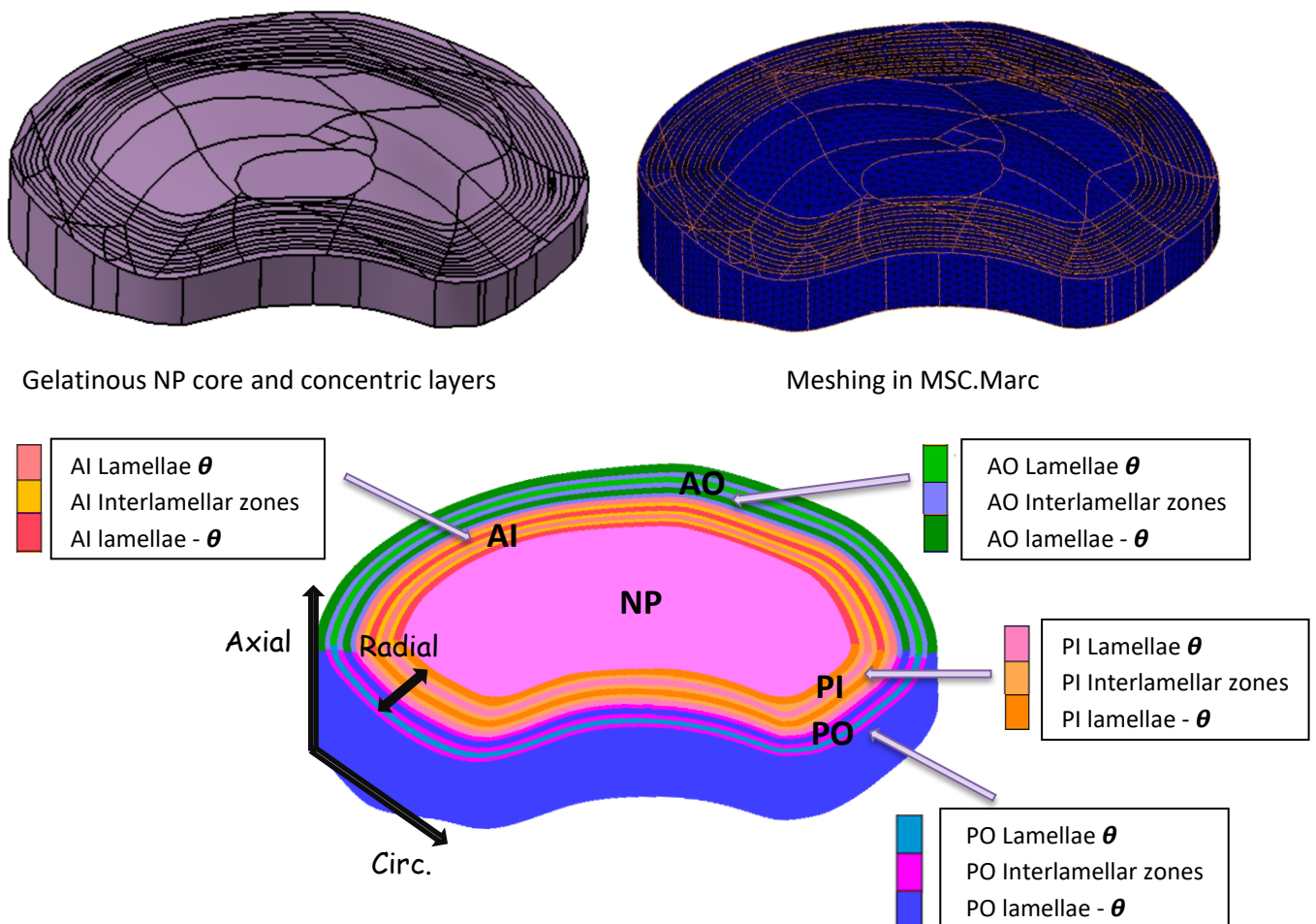


Figure V.2. Disc considering lamellar-interlamellar zones and different regions. AO: Anterior Outer, AI: Anterior Inner, PO: Posterior Outer, PI: Posterior Inner, NP: Nucleus Pulposus.

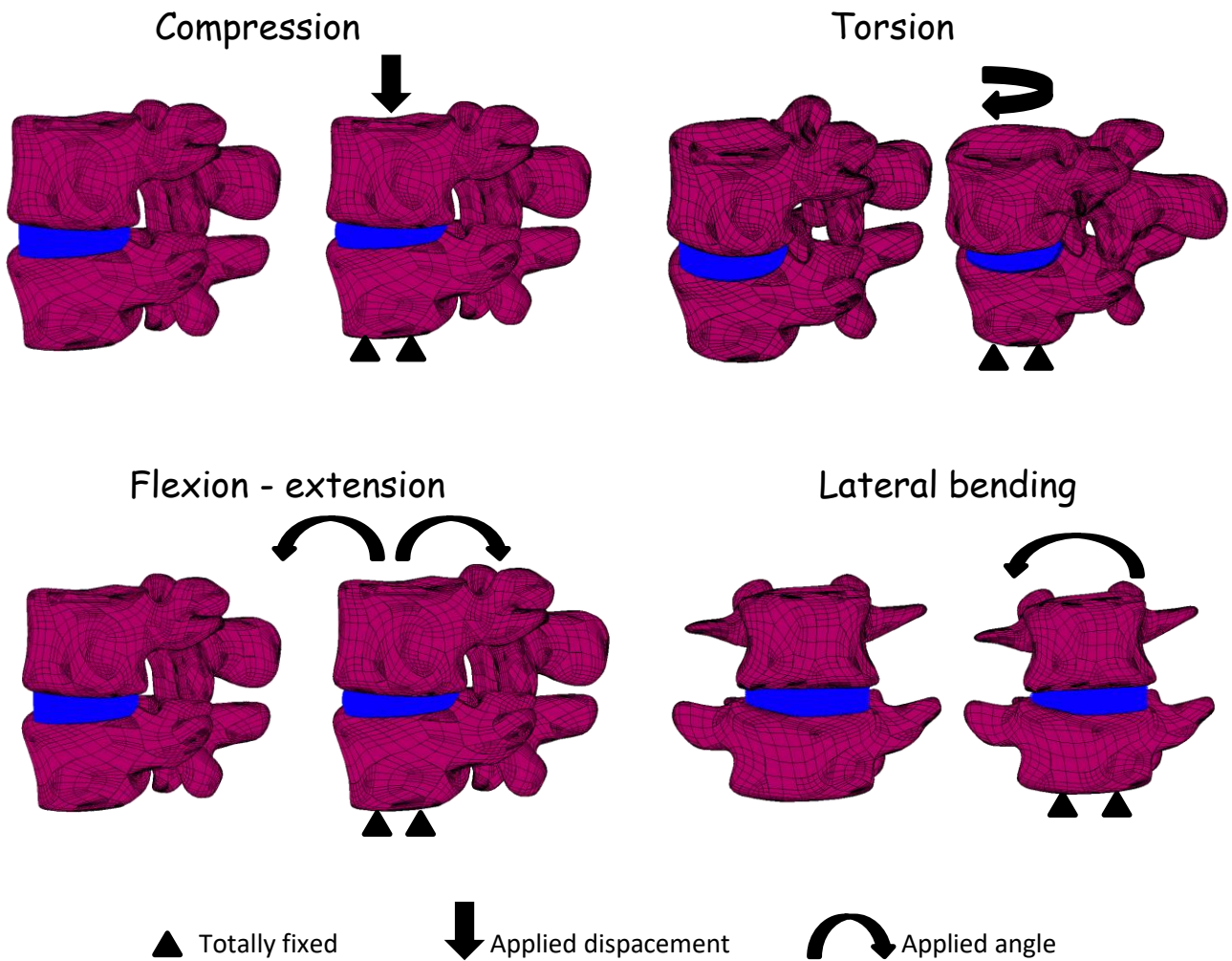


Figure V.3. Boundary conditions for different movements.

V.2.2. Constitutive model

The disc soft tissues are represented using the microstructure-based chemo-viscoelastic model recently developed in the second and third chapters of the thesis. The model integrates the elasticity of the rigid oriented type I collagen fibers, the viscoelasticity of the extracellular matrix and the fluid diffusion throughout the disc soft tissues. It allows a micromechanical treatment of the disc annulus, while taking into account the interlamellar matrix contribution to the volumetric behavior. The model efficiently reproduces 3D mechanical paths of the

local human lumbar disc annulus response were shown in chapter III. The gelatinous nucleus is constitutively modeled as an extracellular matrix with no organized collagen fibers. In what follows, the constitutive equations are presented after a brief description of the finite strain kinematics.

The following notation is used throughout the text. Tensors and vectors are denoted by normal boldfaced letters and italicized boldfaced letters, respectively, while scalars and individual components of vectors and tensors are denoted by normal italicized letters.

V.2.2.1. Finite strain kinematics

Let us first consider a reference configuration Ω_0 and a current configuration Ω . The transformation of a material point from an initial position vector \mathbf{X} in the configuration Ω_0 to a current position vector $\mathbf{x} = \boldsymbol{\varphi}(\mathbf{X}, t)$ in the configuration Ω is given by the deformation gradient tensor \mathbf{F} :

$$\mathbf{F} = \nabla_{\mathbf{x}} \boldsymbol{\varphi} \quad (\text{V.1})$$

The time derivative of the deformation gradient tensor \mathbf{F} is given by:

$$\dot{\mathbf{F}} = \mathbf{L}\mathbf{F} \quad (\text{V.2})$$

where \mathbf{L} is the gradient tensor of the spatial velocity $\mathbf{v} = \partial \boldsymbol{\varphi} / \partial t$:

$$\mathbf{L} = \nabla_{\mathbf{x}} \mathbf{v} \quad (\text{V.3})$$

The mechanical-volumetric coupling is realized by the introduction of an intermediate configuration allowing the multiplicative decomposition of the total deformation gradient tensor \mathbf{F} into a mechanical part \mathbf{F}_{mech} and a volumetric part \mathbf{F}_{vol} :

$$\mathbf{F} = \mathbf{F}_{mech} \mathbf{F}_{vol} \quad (\text{V.4})$$

In the isotropic case, the volumetric part \mathbf{F}_{vol} is given by:

$$\mathbf{F}_{vol} = J^{1/3} \mathbf{I} \quad (\text{V.5})$$

where \mathbf{I} is the unit tensor and $J = \det(\mathbf{F}) > 0$ is the Jacobian of the deformation gradient tensor \mathbf{F} .

The mechanical part \mathbf{F}_{mech} is given by:

$$\mathbf{F}_{mech} = J^{-1/3} \mathbf{F} \quad (\text{V.6})$$

The mechanical deformation gradient tensor \mathbf{F}_{mech} can be decomposed into a stretching part (right \mathbf{U}_{mech} or left \mathbf{V}_{mech}) and a rotation part \mathbf{R}_{mech} :

$$\mathbf{F}_{mech} = \mathbf{R}_{mech} \mathbf{U}_{mech} = \mathbf{V}_{mech} \mathbf{R}_{mech} \quad (\text{V.7})$$

The spatial velocity gradient tensor \mathbf{L} can be additively decomposed into a mechanical part \mathbf{L}_{mech} and a volumetric part \mathbf{L}_{vol} :

$$\mathbf{L} = \mathbf{L}_{mech} + \mathbf{L}_{vol} \quad (\text{V.8})$$

in which \mathbf{L}_{mech} is the mechanical part of the spatial velocity gradient tensor \mathbf{L} :

$$\mathbf{L}_{mech} = \dot{\mathbf{F}}_{mech} \mathbf{F}_{mech}^{-1} \quad (\text{V.9})$$

and \mathbf{L}_{vol} is the volumetric part of the spatial velocity gradient tensor \mathbf{L} :

$$\mathbf{L}_{vol} = \mathbf{F}_{mech} \dot{\mathbf{F}}_{vol} \mathbf{F}_{vol}^{-1} \mathbf{F}_{mech}^{-1} = \frac{\dot{J}}{3J} \mathbf{I} \quad (\text{V.10})$$

The mechanical deformation gradient tensor \mathbf{F}_{mech} can be written using a multiplicative form and decomposed into an elastic part \mathbf{F}_e and a viscous part \mathbf{F}_v :

$$\mathbf{F}_{mech} = \mathbf{F}_e \mathbf{F}_v \quad (\text{V.11})$$

The two tensors can be in turn decomposed into stretching and rotation components:

$$\mathbf{F}_e = \mathbf{R}_e \mathbf{U}_e = \mathbf{V}_e \mathbf{R}_e \quad (\text{V.12})$$

$$\mathbf{F}_v = \mathbf{R}_v \mathbf{U}_v = \mathbf{V}_v \mathbf{R}_v \quad (\text{V.13})$$

Introducing the elastic part \mathbf{L}_e and the viscous part \mathbf{L}_v of the mechanical spatial velocity gradient tensor \mathbf{L}_{mech} leads to:

$$\mathbf{L}_{mech} = \mathbf{L}_e + \mathbf{L}_v \quad (\text{V.14})$$

in which \mathbf{L}_e is the elastic part of the mechanical spatial velocity gradient tensor \mathbf{L}_{mech} :

$$\mathbf{L}_e = \dot{\mathbf{F}}_e \mathbf{F}_e^{-1} \quad (\text{V.15})$$

and \mathbf{L}_v is the viscous part of the mechanical spatial velocity gradient tensor \mathbf{L}_{mech} :

$$\mathbf{L}_v = \mathbf{F}_e \dot{\mathbf{F}}_v \mathbf{F}_v^{-1} \mathbf{F}_e^{-1} \quad (\text{V.16})$$

The viscous velocity gradient tensor \mathbf{L}_v can be further decomposed into a viscous stretching rate tensor \mathbf{D}_v (symmetric part) and a viscous spin rate tensor \mathbf{W}_v (skew-symmetric part):

$$\mathbf{L}_v = \mathbf{D}_v + \mathbf{W}_v \quad (\text{V.17})$$

where

$$\mathbf{D}_v = \frac{1}{2}(\mathbf{L}_v + \mathbf{L}_v^T) \quad (\text{V.18})$$

$$\mathbf{W}_v = \frac{1}{2}(\mathbf{L}_v - \mathbf{L}_v^T) \quad (\text{V.19})$$

Irrotationality of the viscous flow is assumed with no loss in generality (Gurtin and Anand, 2005):

$$\mathbf{W}_v = \mathbf{0} \quad (\text{V.20})$$

and consequently Eq. (V.17) becomes:

$$\mathbf{L}_v = \mathbf{D}_v \quad (\text{V.21})$$

In addition, the different contributions of the right and left Cauchy-Green deformation tensors, $\mathbf{C} = \mathbf{F}^T \mathbf{F}$ and $\mathbf{B} = \mathbf{F} \mathbf{F}^T$, can be introduced:

$$\mathbf{C}_{mech} = \mathbf{F}_{mech}^T \mathbf{F}_{mech}, \quad \mathbf{B}_{mech} = \mathbf{F}_{mech} \mathbf{F}_{mech}^T \quad (\text{V.22})$$

$$\mathbf{C}_{vol} = J^{2/3} \mathbf{I}, \mathbf{B}_{vol} = J^{2/3} \mathbf{I} \quad (\text{V.23})$$

$$\mathbf{C}_e = \mathbf{F}_e^T \mathbf{F}_e, \mathbf{B}_e = \mathbf{F}_e \mathbf{F}_e^T \quad (\text{V.24})$$

$$\mathbf{C}_v = \mathbf{F}_v^T \mathbf{F}_v, \mathbf{B}_v = \mathbf{F}_v \mathbf{F}_v^T \quad (\text{V.25})$$

The total Green-Lagrange strain tensor \mathbf{E} and the mechanical Green-Lagrange strain tensor \mathbf{E}_{mech} are expressed as:

$$\mathbf{E} = \frac{1}{2}(\mathbf{C} - \mathbf{I}), \mathbf{E}_{mech} = \frac{1}{2}(\mathbf{C}_{mech} - \mathbf{I}) \quad (\text{V.26})$$

The volumetric strain ε_{vol} is expressed as:

$$\varepsilon_{vol} = J - 1 \quad (\text{V.27})$$

V.2.2.2. Stress decomposition

The different contributions of the second Piola-Kirchhoff stress tensor $\mathbf{S} = \mathbf{F}^{-1} \boldsymbol{\tau} \mathbf{F}^{-T}$ and the Kirchhoff stress tensor $\boldsymbol{\tau} = J \boldsymbol{\sigma}$ can be introduced:

$$\mathbf{S}_{mech} = \mathbf{F}_{mech}^{-1} \boldsymbol{\tau}_{mech} \mathbf{F}_{mech}^{-T}, \boldsymbol{\tau}_{mech} = J \boldsymbol{\sigma}_{mech} \quad (\text{V.28})$$

$$\mathbf{S}_{vol} = J^{-2/3} \boldsymbol{\tau}_{vol} \mathbf{C}_{mech}^{-1}, \boldsymbol{\tau}_{vol} = J \boldsymbol{\sigma}_{vol} \quad (\text{V.29})$$

$$\mathbf{S}_e = \mathbf{F}_{mech}^{-1} \boldsymbol{\tau}_e \mathbf{F}_{mech}^{-T}, \boldsymbol{\tau}_e = J \boldsymbol{\sigma}_e \quad (\text{V.30})$$

$$\mathbf{S}_v = \mathbf{F}_e^{-1} \boldsymbol{\tau}_v \mathbf{F}_e^{-T}, \boldsymbol{\tau}_v = J \boldsymbol{\sigma}_v \quad (\text{V.31})$$

where $\boldsymbol{\sigma}$ is the Cauchy stress tensor additively split into a mechanical part $\boldsymbol{\sigma}_{mech}$ and a volumetric part $\boldsymbol{\sigma}_{vol}$ as:

$$\boldsymbol{\sigma} = \boldsymbol{\sigma}_{mech} + \boldsymbol{\sigma}_{vol} \quad (\text{V.32})$$

The volumetric Cauchy stress tensor $\boldsymbol{\sigma}_{vol}$ is given by:

$$\boldsymbol{\sigma}_{vol} = p \mathbf{I} \quad (\text{V.33})$$

in which p is the hydrostatic pressure:

$$p = \frac{1}{3} \text{trace}(\boldsymbol{\sigma}) \quad (\text{V.34})$$

The mechanical Cauchy stress tensor $\boldsymbol{\sigma}_{mech}$ is additively split into an elastic part $\boldsymbol{\sigma}_e$ and a viscous part $\boldsymbol{\sigma}_v$:

$$\boldsymbol{\sigma}_{mech} = \boldsymbol{\sigma}_e + \boldsymbol{\sigma}_v \quad (\text{V.35})$$

Due to mechanical incompressibility, the tensor $\boldsymbol{\sigma}_{mech}$ is a traceless tensor. The volumetric, elastic and viscous Cauchy parts, $\boldsymbol{\sigma}_{vol}$, $\boldsymbol{\sigma}_e$ and $\boldsymbol{\sigma}_v$, are obtained from the differentiation of the respective free energy functions with respect to the corresponding deformations:

$$\boldsymbol{\sigma}_{vol} = \frac{\partial \psi_{vol}}{\partial J} \mathbf{I} \quad (\text{V.36})$$

$$\boldsymbol{\sigma}_e = \frac{2}{J} \mathbf{F}_{mech} \frac{\partial \psi_e}{\partial \mathbf{C}_{mech}} \mathbf{F}_{mech}^T \quad (\text{V.37})$$

$$\boldsymbol{\sigma}_v = \frac{2}{J} \mathbf{F}_e \frac{\partial \psi_v}{\partial \mathbf{C}_e} \mathbf{F}_e^T \quad (\text{V.38})$$

where ψ_{vol} , ψ_e and ψ_v are the volumetric, elastic and viscous free energy functions.

The Cauchy stress in the lamellae and in the interlamellar matrix are, respectively, given by:

$$\boldsymbol{\sigma} = (1 - \phi_{CF}) (\boldsymbol{\sigma}_{e_ECM} + \boldsymbol{\sigma}_{v_ECM} + \boldsymbol{\sigma}_{vol}) + \phi_{CF} \boldsymbol{\sigma}_{e_CF} \quad (\text{V.39})$$

$$\boldsymbol{\sigma} = \boldsymbol{\sigma}_{e_ECM} + \boldsymbol{\sigma}_{v_ECM} + \boldsymbol{\sigma}_{vol} \quad (\text{V.40})$$

where ϕ_{CF} is the amount of oriented type I collagen fibers, $\boldsymbol{\sigma}_{e_ECM}$ and $\boldsymbol{\sigma}_{v_ECM}$ are the elastic and viscous Cauchy stress tensors of the extracellular matrix, $\boldsymbol{\sigma}_{vol}$ is the chemical-induced volumetric Cauchy stress and $\boldsymbol{\sigma}_{e_CF}$ is the elastic Cauchy stress tensor of the oriented type I collagen fibers.

V.2.2.3. Constitutive equations

In what follows, we present a summarize of the constitutive equations of the disc soft tissues. The detailed formulation of the fully three-dimensional constitutive model can be found elsewhere, see chapters II and III.

V.2.2.3.1. Extracellular matrix

The extracellular matrix is the common solid phase of the different disc tissues including the lamellae of the annulus, the non-fibrillar interlamellar matrix of the annulus and the nucleus pulposus. The constitutive response of the extracellular matrix is described by the elastic and viscous free energy functions ψ_{e_ECM} and ψ_{v_ECM} given by a Gent expression (Gent, 1996):

$$\psi_{e_ECM} = -\frac{E}{6} I_1^{\max} \ln \left(1 - \frac{I_1 - 3}{I_1^{\max}} \right) \quad (\text{V.39})$$

$$\psi_{v_ECM} = -\frac{E_v}{6} I_{1v}^{\max} \ln \left(1 - \frac{I_{1e} - 3}{I_{1v}^{\max}} \right) \quad (\text{V.40})$$

in which I_1 and I_{1e} are the first strain invariants:

$$I_1 = \text{trace}(\mathbf{B}_{mech}), \quad I_{1e} = \text{trace}(\mathbf{B}_e) \quad (\text{V.41})$$

Four parameters are involved in the free energy functions: the small-strain tensile modulus E and the limiting extensibility parameter I_1^{\max} of the extracellular matrix and, the two extracellular matrix viscous parameters E_v and I_{1v}^{\max} .

The viscous stretching rate \mathbf{D}_v is defined by the following general flow rule:

$$\mathbf{D}_v = \dot{\gamma}_v \mathbf{N}_v \quad (\text{V.42})$$

in which $\dot{\gamma}_v$ is the accumulated viscous strain rate and \mathbf{N}_v is the direction tensor of viscous flow aligned with the viscous Kirchhoff stress tensor $\boldsymbol{\tau}_v$:

$$\mathbf{N}_v = \frac{\boldsymbol{\tau}_v}{\|\boldsymbol{\tau}_v\|}, \quad \|\boldsymbol{\tau}_v\| = \sqrt{\text{trace}(\boldsymbol{\tau}_v \boldsymbol{\tau}_v^T)} \quad (\text{V.43})$$

where $\|\boldsymbol{\tau}_v\|$ is the effective viscous Kirchhoff stress by the Frobenius norm.

The accumulated viscous strain rate $\dot{\gamma}_v$ takes the form of the Bergstrom-Boyce power law (Bergstrom and Boyce, 1998):

$$\dot{\gamma}_v = d \left| \sqrt{I_{1v}/3} - 1 \right|^{-m} \|\boldsymbol{\tau}_v\| \quad (\text{V.44})$$

where I_{1v} is the first strain invariant:

$$I_{1v} = \text{trace}(\mathbf{B}_v) \quad (\text{V.45})$$

Two additional parameters are involved: the extracellular matrix viscous multiplier constant d and the extracellular matrix viscous stretch-dependency constant m .

V.2.2.3.2. Oriented type I collagen fibers

The oriented type I collagen fibers are superimposed to the extracellular matrix of the lamellae with alternate orientation between successive lamellae. The elasticity of the collagen fibers is described by an elastic free energy function (Cantournet et al., 2007):

$$\psi_{e_CF} = A_1 (I_4 - 1) + A_2 (I_4 - 1)^2 - 2A_1 \ln(\lambda_I^x \lambda_{II}^y \lambda_{III}^z) \quad (\text{V.46})$$

in which I_4 is the fourth strain invariant and, λ_I , λ_{II} and λ_{III} are the stretches along the principal axes of the fibers:

$$I_4 = \mathbf{a} \mathbf{C}_{mech} \mathbf{a}, \quad \lambda_I = \sqrt{\mathbf{e}_1 \mathbf{C}_{mech} \mathbf{e}_1}, \quad \lambda_{II} = \sqrt{\mathbf{e}_2 \mathbf{C}_{mech} \mathbf{e}_2}, \quad \lambda_{III} = \sqrt{\mathbf{e}_3 \mathbf{C}_{mech} \mathbf{e}_3} \quad (\text{V.47})$$

where $\mathbf{a} = x\mathbf{e}_1 + y\mathbf{e}_2 + z\mathbf{e}_3$ is the unit vector in the initial configuration, function of the fibers orientation.

Two parameters are involved in the free energy function: the collagen fibers parameters A_1 and A_2 .

V.2.2.3.3. Swelling

The chemical-induced volumetric free energy function ψ_{vol} due to internal fluid content variation is given by:

$$\psi_{vol} = \frac{1}{4}k \left[\varepsilon_{vol}^2 + 2\varepsilon_{vol} - 2\ln(\varepsilon_{vol} - 1) \right] \quad (V.48)$$

in which k is the bulk modulus.

The Jacobian J is given as a function of the internal fluid content n_{f_m} under mechanical loading:

$$J = n_{f_m} \xi \eta \quad (V.49)$$

where ξ is a dimensionless transportation coefficient and η is a dimensionless free swelling coefficient (equal to 0.5 in the case of physiological salt condition).

The kinetics of the internal fluid content n_{f_m} is given by:

$$\dot{n}_{f_m} = \beta_m \left(1 - \frac{n_{f_m}}{n_{f_{im}}} \right) \quad (V.50)$$

where β_m is the fluid flow constant, $n_{f_{im}}$ is the maximum fluid content that could be reached inside the disc and $n_{f_m}(0) = n_{f_{initial}}$.

V.2.3. Algorithm and numerical implementation

The chemo-viscoelastic constitutive model was implemented by means of a series of subroutines. A hyperelastic subroutine was coupled to a viscous subroutine in order to reproduce the viscoelastic material response and to a volumetric subroutine to account for the

volumetric strain ε_{vol} induced by free-swelling and mechanical deformation. A total Lagrange formulation was adopted for the present calculations. When the total Lagrange is selected, MSC.Marc software deals with the second Piola-Kirchhoff stress \mathbf{S} and the Green-Lagrange strain \mathbf{E} . An updated Lagrange formulation could be also used and in that case the software would deal with the Cauchy stress $\boldsymbol{\sigma}$ and the logarithmic strain $\ln(\mathbf{F})$.

A- The hyperelastic subroutine

The deformation gradient $\mathbf{F}(i)$ is computed at the beginning of each increment by (de Souza Neto et al., 2008):

$$\mathbf{F}(i) = \exp(\ln(\mathbf{F}(i))) = \sum_{j=0}^{\infty} \frac{1}{j!} (\ln(\mathbf{F}(i)))^{(j)} \quad (\text{V.51})$$

where $\ln(\mathbf{F}(i))$ is given by the numerical code.

The mechanical right Cauchy-Green deformation $\mathbf{C}_{mech}(i)$ is calculated using the mechanical deformation $\mathbf{F}_{mech}(i)$:

$$\mathbf{C}_{mech}(i) = \mathbf{F}_{mech}(i) \mathbf{F}_{mech}^T(i) \quad (\text{V.52})$$

The identification of the elastic deviatoric strain energy and its derivatives with respect to the deviatoric parts of the first invariant \tilde{I}_1 and second invariant \tilde{I}_2 as well as the chemical volumetric energy and its derivatives with respect to J are required by the hyperelastic subroutine as follows:

$$\left\{ \frac{\partial \psi_{dev}(i)}{\partial \tilde{I}_1}, \frac{\partial \psi_{dev}(i)}{\partial \tilde{I}_2}, \frac{\partial^2 \psi_{dev}(i)}{\partial \tilde{I}_1^2}, \frac{\partial^2 \psi_{dev}(i)}{\partial \tilde{I}_2^2}, \frac{\partial u(i)}{\partial J}, \frac{\partial^2 u(i)}{\partial J^2} \right\} \quad (\text{V.53})$$

where $\psi(i) = \psi_{dev}(i) + u(i)$ defined for the lamellae as:

$$\psi_{dev}(i) = (1 - \phi_{CF}) \psi_{ECM}(i) + \phi_{CF} \psi_{CF}(i) \quad \text{and} \quad u(i) = (1 - \phi_{CF}) \psi_{vol}(i) \quad (\text{V.54})$$

and for the interlamellar matrix as:

$$\psi_{dev}(i) = \psi_{ECM}(i) \text{ and } u(i) = \psi_{vol}(i) \quad (\text{V.55})$$

After the definition of the strain energy function and the derivatives, the software defines the elastic second Piola-Kirchhoff stress and the volumetric stress for the lamellae as:

$$\mathbf{S}_e(i) = 2 \frac{\partial \psi_{e_ECM}(i) + \partial \psi_{e_CF}(i)}{\partial \mathbf{C}_{mech}(i)} \text{ and } \mathbf{S}_{vol}(i) = J^{1/3} \frac{\partial u(i)}{\partial J} \quad (\text{V.56})$$

and for the interlamellar matrix as:

$$\mathbf{S}_e(i) = 2 \frac{\partial \psi_{e_ECM}(i)}{\partial \mathbf{C}_{mech}(i)} \text{ and } \mathbf{S}_{vol}(i) = J^{1/3} \frac{\partial u(i)}{\partial J} \quad (\text{V.57})$$

B- The viscous subroutine

To compute the current elastic deformation gradient $\mathbf{F}_e(i)$, the viscous deformation gradient $\mathbf{F}_v(i-1)$ user-stored from the previous increment is called:

$$\mathbf{F}_e(i) = \mathbf{F}_{mech}(i) \mathbf{F}_v(i-1)^{-1} \quad (\text{V.58})$$

The calculated elastic deformation gradient $\mathbf{F}_e(i)$ is then used to calculate the viscous velocity gradient $\mathbf{L}_v(i) = \mathbf{D}_v(i)$ with $\mathbf{D}_v(i)$ the viscous stretching rate at the end of the current increment. The rate of the viscous deformation gradient writes:

$$\dot{\mathbf{F}}_v(i) = \mathbf{F}_e(i)^{-1} \mathbf{D}_v(i) \mathbf{F}_{mech}(i) \quad (\text{V.59})$$

The current viscous deformation gradient $\mathbf{F}_v(i)$ is iteratively calculated using:

$$\mathbf{F}_v(i) = \dot{\mathbf{F}}_v(i) \Delta t + \mathbf{F}_v(i-1) \quad (\text{V.60})$$

where Δt is the time increment.

At the beginning of the mechanical loading, the singularity of the viscous stretching rate is avoided by adding a perturbation coefficient $\kappa=0.01$ to $\sqrt{I_{1v}/3}$. The value of $\mathbf{F}_v(i)$ is user-stored in the form of a 3-D matrix $[m, nn, p]$ constituted of m number of elements, nn number of nodes and p number of tensor directions.

The right viscous Cauchy-Green deformation is calculated as follows:

$$\mathbf{C}_v(i) = \mathbf{F}_v(i)\mathbf{F}_v^T(i) \quad (\text{V.61})$$

The strain invariants are calculated from the Cauchy-Green deformation components in order to be used next in the stress calculation. The viscous stress is calculated in the subroutine by the following expression:

$$\mathbf{S}_v(i) = 2 \frac{\partial \psi_{v-ECM}(i)}{\partial \mathbf{C}_e} \quad (\text{V.62})$$

Finally, the elastic and volumetric stresses are called from the hyperelastic subroutine and the total second Piola-Kirchhoff stress is calculated by the summation of the different stress components:

$$\mathbf{S}(i) = \mathbf{S}_e(i) + \mathbf{S}_v(i) + \mathbf{S}_{vol}(i) \quad (\text{V.63})$$

C- The swelling subroutine

A thermal subroutine was manipulated and adapted in order to reproduce the swelling effects.

The swelling volumetric volume change is calculated using:

$$J(i) = J(i-1) + \Delta n_{f_m}(i) \xi \eta \quad (\text{V.64})$$

The incremental change of fluid amount $\Delta n_{f_m}(i)$ is given by:

$$\Delta n_{f_m}(i) = \beta_m \left(1 - \frac{n_{f_m}(i)}{n_{f_{im}}} \right) \Delta t \quad (\text{V.65})$$

The swelling volumetric change is code stored and called in the following increment by the hyperelastic subroutine. A flowchart showing the connection between the different subroutines is presented in Figure V.4.

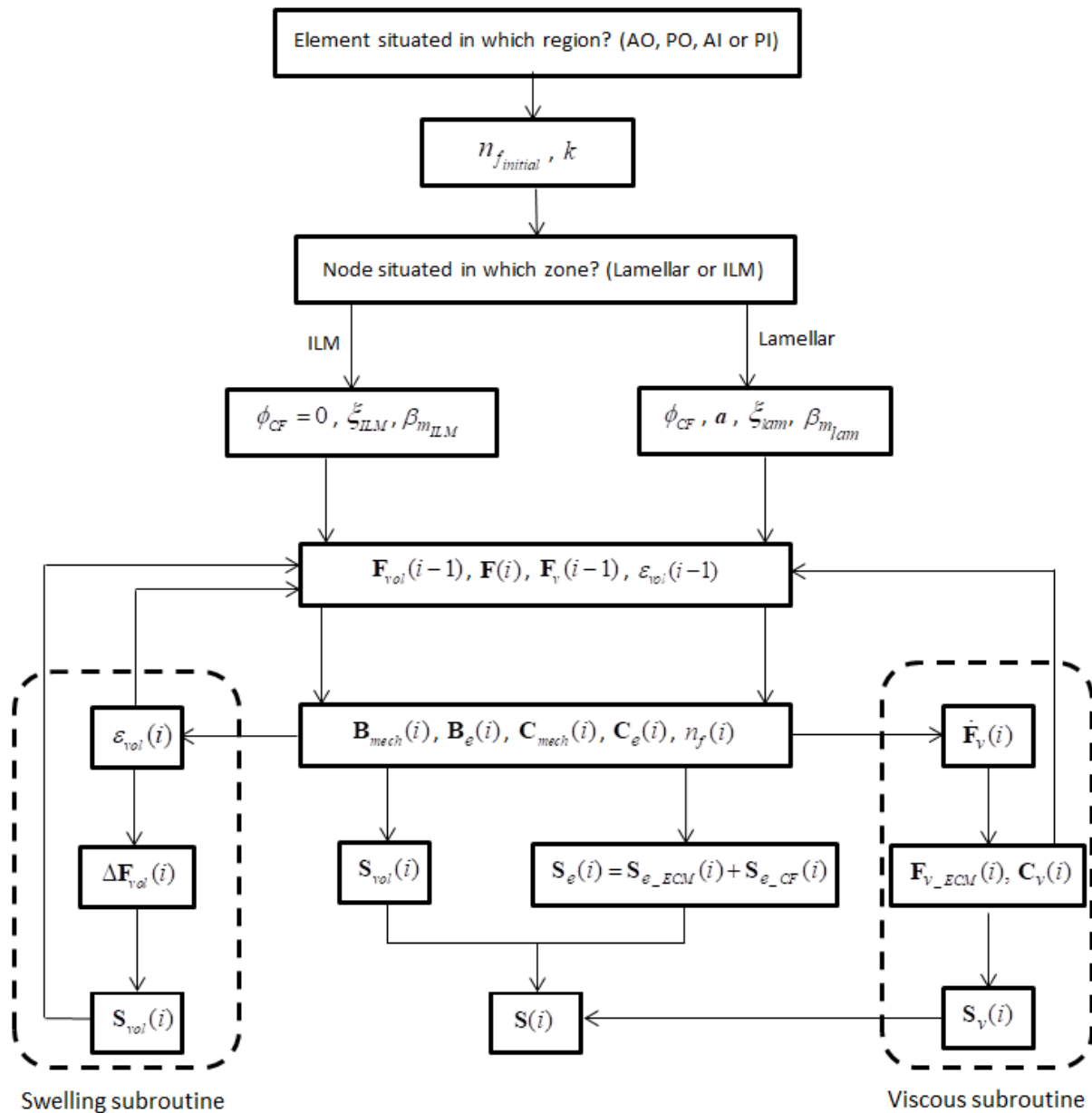


Figure V.4. Algorithm for the numerical implementation of the constitutive model.

V.2.4. Microstructure and model parameters

Each region is associated to its microstructure components in terms of initial water content, oriented collagen fibers content and orientation (see Table V.1). The values were extracted from previous documented experimental findings (Brickley-Parsons and Glimcher, 1984; Koeller et al., 1984; Iatridis et al., 2007) for an age of 36 years old in order to be the most closely to the constructed geometry age.

| | AO | AI | PO | PI | NP |
|------------------------|------------|-----------|---------------|----------------|-----------|
| Fibers content (%) | 65.4 (70)* | 52 (43)* | 68.65 (79.1)* | 54.55 (35.95)* | 0 |
| Fibers orientation (°) | 23 | 30 | 48 | 48 | - |
| Water content (%) | 72.15 | 75.85 | 74.55 | 78.95 | 81 |

Table V.1. Total collagen fibers content $\phi_{CF(I+II)}$ (* between brackets is type I collagen content over the total collagen content $\phi_{CF(I/(I+II))}$), fibers angle θ and initial chemically equilibrated water content $n_{f\ initial}$. The oriented collagen fibers content ϕ_{CF} is then calculated by the following expression $\phi_{CF} = (1 - n_{f\ initial}) \phi_{CF(I+II)} \phi_{CF(I/(I+II))}$.

The set of volumetric-mechanical parameters have been calibrated in chapter III at the scale of human annulus volume element using the circumferential uniaxial stress-strain data of Ebara et al. (1996) along with the transversal data of Balwit et al. (2014). A quantitative evaluation of the predictive capabilities of the model showed a good agreement with the biaxial data of O'Connell et al. (2012) and the shear data of Iatridis et al. (1999). The values of the model parameters (for extracellular matrix, collagen and fluid) are listed in Tables V.2 and V.3. They are used as direct input data in the whole disc model for the different disc annulus regions as illustrated in Figure V.5. The nucleus swelling is assumed to have the same behavior as the inner interlamellar zones since they have the same non-fibrillar negatively charged microstructure and follow the same osmotic trends under mechanical loading (Ortolani et al., 1988, Tavakoli and Costi, 2018).

| | Parameter | Unit | Value |
|----------------------|-----------------|-----------------------------------|-------|
| Extracellular matrix | E | MPa | 1.0 |
| | I_1^{\max} | MPa | 3.0 |
| | E_v | MPa | 0.167 |
| | I_{lv}^{\max} | MPa | 1.5 |
| | d | MPa ⁻¹ s ⁻¹ | 0.02 |
| | m | | 0.001 |
| Collagen | A_1 | MPa | 27.0 |
| | A_2 | MPa | 100.0 |

Table V.2. Extracellular matrix and collagen constants.

| Parameter | Unit | Significance | Value |
|-----------|-----------------|--|---------|
| β_m | s ⁻¹ | Fluid flow constant in lamella | -0.0004 |
| β_m | s ⁻¹ | Fluid flow constant in interlamellar matrix and in NP | 0.00097 |
| k | MPa | Bulk modulus in inner annulus and in NP | 800 |
| k | MPa | Bulk modulus in outer annulus | 3500 |
| ξ | | Transportation coefficient in inner lamella | 40.25 |
| ξ | | Transportation coefficient in outer lamella | 26.4 |
| ξ | | Transportation coefficient in inner interlamellar matrix and in NP | 15.29 |
| ξ | | Transportation coefficient in outer interlamellar matrix | 7.65 |

Table V.3. Chemical-induced volumetric constants.

V.3. Results

V.3.1. Displacement fields

The displacement fields are plotted in Figure V.6 for the different physiological movements. An overall view of the displacement vectors allows getting a basic insight about the nucleus migration and the annulus-nucleus interaction.

The nucleus tends to move closer towards the anterior disc under compression or extension but with a distinct annulus response for these two movements. The highest annulus displacement values are observed in the anterior disc upon compression and in the posterior disc upon extension. Under flexion, the nucleus moves closer towards the posterior disc and the annulus maximum displacement is observed in both anterior and posterior regions. Under lateral bending, the nucleus moves towards the lateral disc. Under torsion, the nucleus turns around in a similar manner in the different disc circumferential regions leading to a homogenous distribution of the displacement vectors fields in the nucleus. The lateral outer annulus regions are the most extended due to their position which is the furthest from the rotation center of the disc. Comparing the different movements, we can notice that the highest displacement values are observed for compression and lateral bending and the lowest displacement values for torsion.

V.3.2. Strain fields

In Figures V.7 and V.8, the shear strain fields are plotted in the sagittal plane of the disc respectively without and with compression. These plots allow to analyze in the core of the disc the effect of the different movements on the lamellar-interlamellar interaction. Globally, without compression, the average shear strain inside the disc is between 0.1 and 0.2 with higher values in the interlamellar matrix (between 0.3 and 0.4).

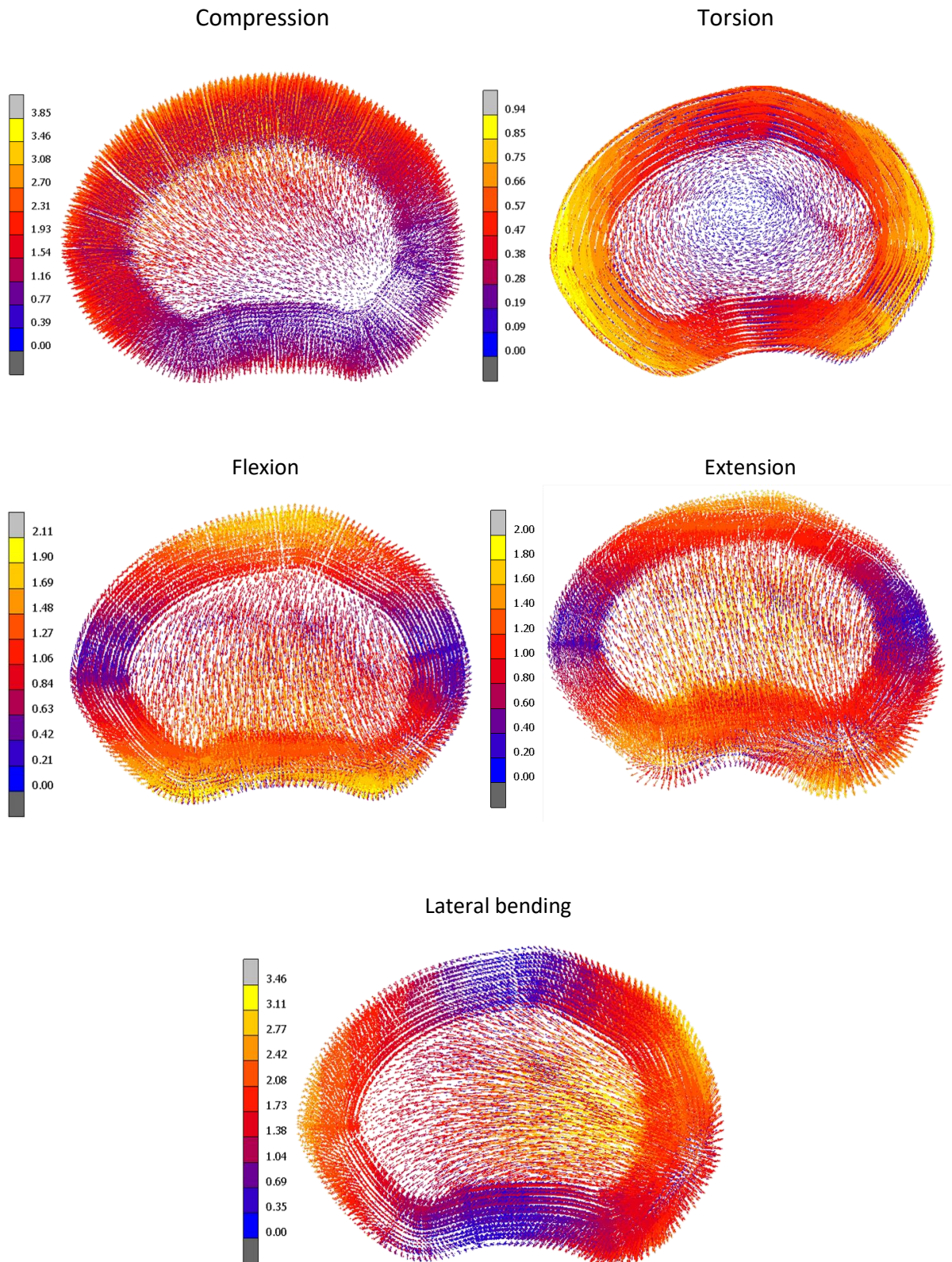


Figure V.6. Displacement fields within the superior plane of the disc.

In Figure V.7, the highest local shear strains are observed under compression, flexion and lateral bending. These high values (between 0.3 and 0.4) are mainly observed in the posterior interlamellar matrix of the inner and middle part of the annulus under compression and lateral bending. Also, under flexion, high shear strain values are seen in both the lamellae and interlamellar zones of the middle annulus region (between 0.2 and 0.4).

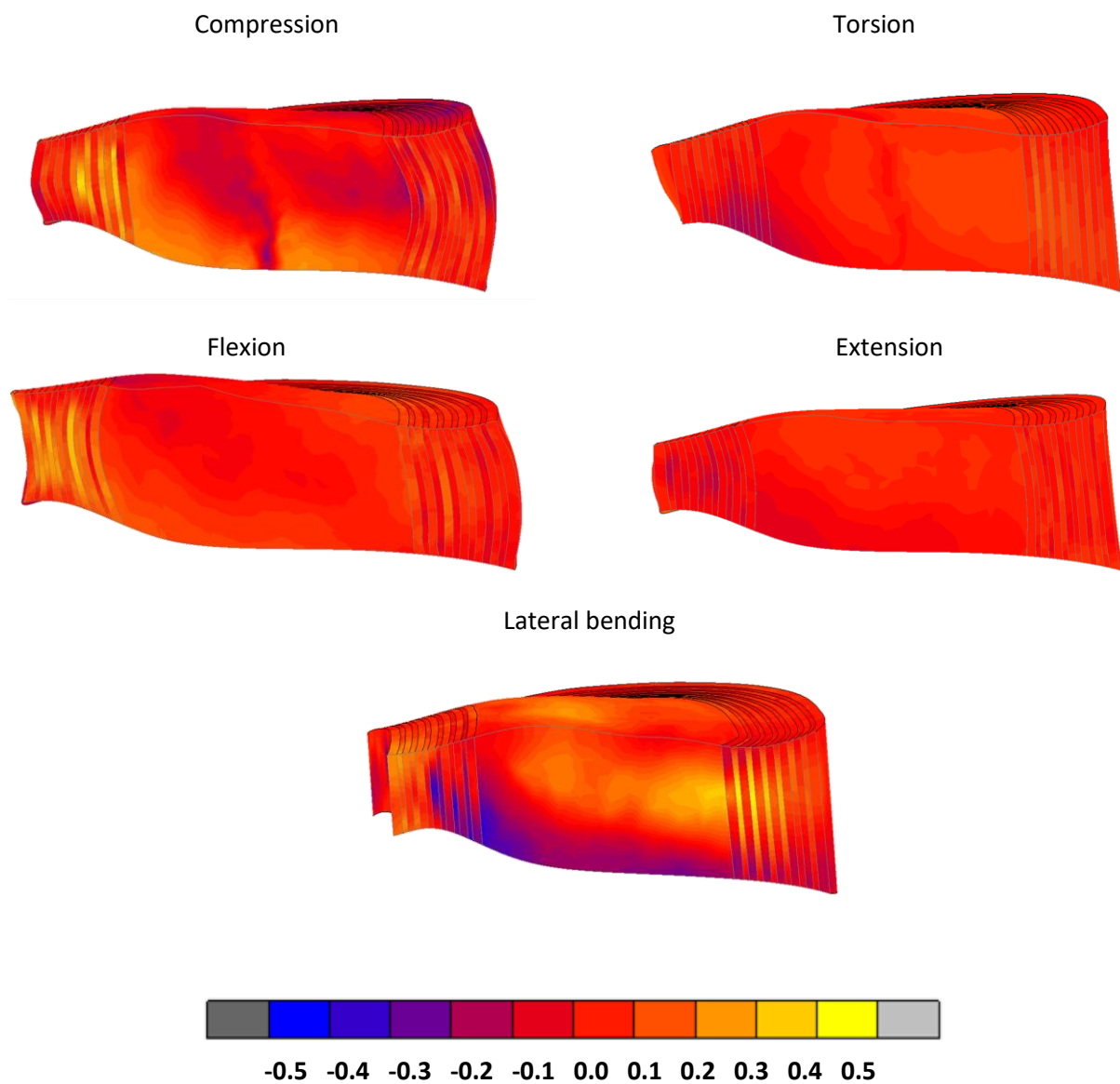


Figure V.7. Shear strain fields within the sagittal plane of the disc.

High negative shear strains are also observed in the inner anterior region but only for lateral bending (between -0.2 and -0.4). While accompanied with compression (Figure V.8), the shear strain increases in the interlamellar zones of the inner posterior annulus for the different movements reaching values of 0.4-0.5. For extension and torsion, the middle lamellae are also subjected to high shear strains but remain relatively lower than those of the interlamellar matrix.

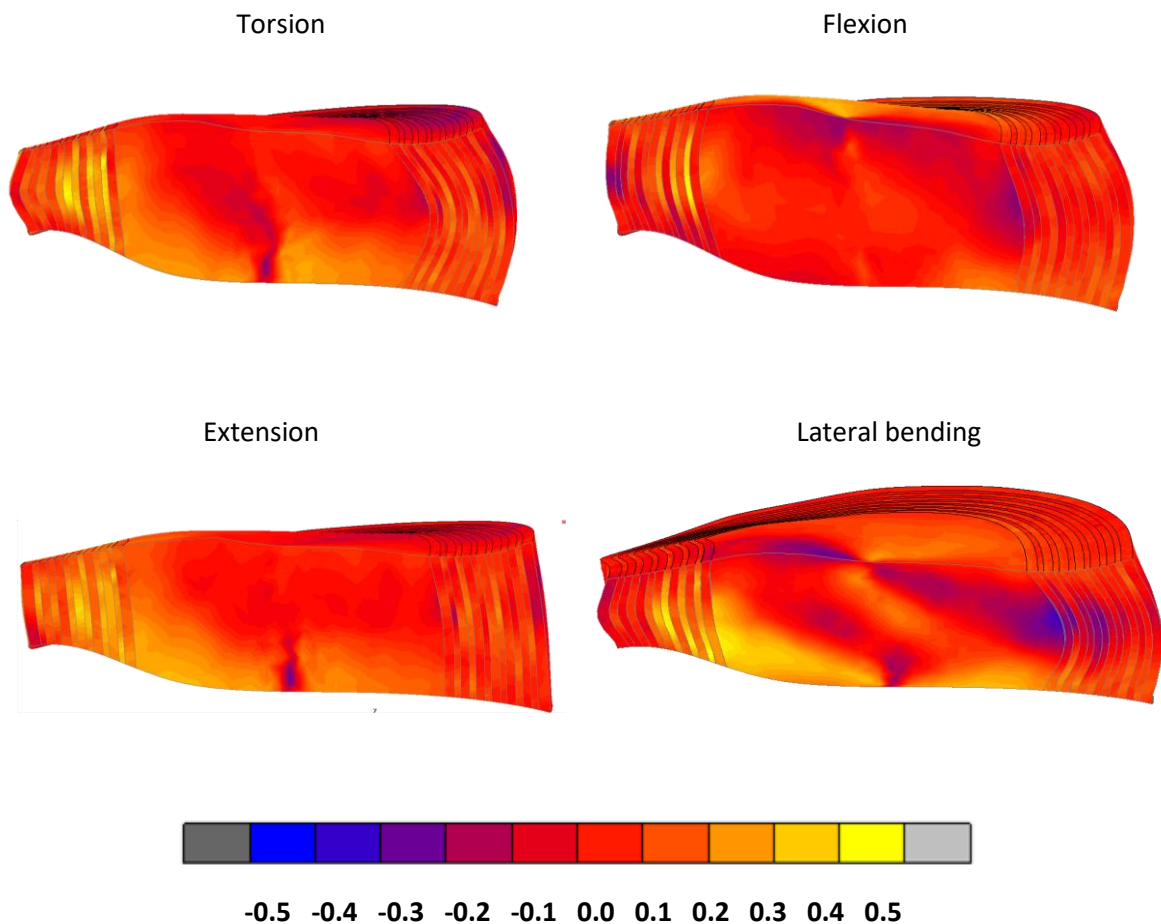


Figure V.8. Shear strain fields within the sagittal plane of the disc. The movements are coupled to an axial compression.

V.4. Discussion

V.4.1. Nucleus-annulus interaction

Experimentally, the nucleus-annulus interaction is very complex to examine because it requires the access to the core of the disc. The analysis of the numerical displacement fields under different movements allows us to better understand how the load is transmitted from the nucleus to the different regions of the annulus. Relating the local displacement to strain fields allows a better understanding of the disc functionality and the origin of the damage mechanisms affecting the disc. Under physiological disc displacements, we could see that the consideration of a correct geometry of the intervertebral disc is mandatory as it could highly affect the disc behavior.

Although the force is transmitted perpendicularly to the disc when compressed, the nucleus movement is not circumferentially symmetric. Indeed, nucleus tends to move closer towards the anterior regions of the disc. This can be mainly explained by the disc geometry, the anterior-posterior height difference, the anterior-posterior rigidity difference, the anterior-posterior swelling difference and the relative axial position between the lower and upper vertebrae. The annulus-nucleus non-symmetric interaction under compression was captured experimentally by many observations (Meakin et al., 2000, 2001). It reveals the importance of using a heterogeneous model coupled with a correct disc geometry. Otherwise, symmetric fields could be obtained affecting the validity and the reality of the disc local deformation. We can notice some important insights by comparing the displacement fields of the different movements. Under flexion and lateral bending, the strongest nucleus-annulus interaction is located in the neighborhood of the posterior and lateral posterior sides of the annulus. Knowing that inner part is the softest region (Ebara et al., 1996; Kandil et al., 2020a) and subjected to the highest internal strains, the posterior inner region could be highly exposed to

radial tears under these movements. Under extension, we can notice that, although the nucleus moves closer towards the anterior disc, the posterior annulus moves outward due to the small thickness of this region and due to the force applied by the adjacent vertebrae which are, in this part of the disc, relatively inclined and close to each other. The risk of damage could then highly increase when coupled with other movements that would drive the nucleus closer towards the posterior side of the disc. For the torsion movement, the nucleus-annulus interaction is almost similar all around the inner annulus but we can notice increasing relative displacement fields in the posterior outer lateral region due to its far position to the rotation center of the disc which result in high shear in the lamellae and interlamellar zones of this region. The computed fields are similar to those obtained experimentally by Costi et al. (2007) for compression and torsion. For flexion and lateral bending, the annulus shows similar motion but the experimentally obtained nucleus fields were not so clear, presenting no sufficient observable vectors.

V.4.2. Mechanical damage

Disc damage and tears were mainly related to high shear strains especially in the interlamellar zones of the annulus (Goel et al., 1995; Iatridis and ap Gwynn, 2004; Costi et al., 2007). For this reason, the shear strain fields were examined in details under the different physiological movements in order to identify the most deleterious movements for the disc. The exact local location of the zones with the highest strains is identified and related to existing disc damage mechanisms. The maximum shear strains detected for the different motions were similar to those observed by previous contributions (Costi et al., 2007; Masni and Tanaka, 2018). The highest shear strains are observed in the posterior region for compression, torsion, flexion and lateral bending which corresponds to the present numerical results. However, contrary to our model, the experimental results could not determine the exact position of the highest shear

inside each region which does not allow a sufficient interpretation and relation of these strains to possible damage mechanisms. By attentively examining the numerical fields we could notice the following facts. The average shear strain observed throughout the disc under the different movements was between 0.1 and 0.2 showing the same trends usually obtained by experimental observations with maximum local shear strain concentrations in some zones between 0.3 and 0.5 which agrees as well with the maximum shear strains observed experimentally (Costi et al., 2007; Wang et al., 2009). The highest shear strains were identified for most of the movements in the inner and middle interlamellar zones and the middle lamellae of the posterior region annulus suggesting increasing the possibility of damage initiation and tears creation in these zones. For uncompressed disc, the highest shear strains were observed under lateral bending then simple compression and flexion. The lowest shear strains appeared under torsion due to the small physiological rotation angle putting in mind that it could not be deleterious to the disc which was also captured experimentally (Costi et al., 2007) where the complete disc was observed at a larger scale without accessing lamellae and interlamellar zones. However, when torsion was coupled with compression which reflects the real loaded disc compressed by body load under torsion, shear strains were highly amplified to reach its maximum observed values. The compression coupled with the different physiological movements was seen to increase the shear strains in inner and middle posterior disc region especially under torsion, lateral bending and flexion in order. The latter results are in line with the observations of Wade et al. (2014, 2017) who found that damage initiates in the posterior mid annulus of the disc. Indeed, high shear strains are observed as well in our simulations for both the lamellae and interlamellar zones increasing then the risk of disc delamination and failure. Analyzing the previous results, we could conclude that the flexion and lateral bending that were usually known to generate the maximum shear strains in the disc showed, numerically as well, the highest shear strains in the lamellae and

interlamellar zones. But also, the torsion movement when combined with compression showed similar important shear strains that could represent a risk to the disc health and functionality.

V.5. Partial conclusion

An accurate finite element model of the human lumbar spine was developed considering micromechanics and macromechanics of the intervertebral disc in correlation with its swelling response. The model provides a useful tool to access to the core of the healthy disc for the estimation of the local fields under different physiological movements. The capabilities of the model to describe the annulus-nucleus interaction were favorably verified to existing MRI studies. The model is able to predict critical zones, in which damage can more likely occurred; in accordance with clinical assessments, they are observed in the mid-posterior region of the disc. These capacities of the proposed model must not be hidden from the fact that it is necessary to complete the verification of the model by subjecting it to more complex loadings. Because elderly is the mostly exposed to intervertebral disc problem, the incorporation of the long-term age effect on the micromechanics and macromechanics of the intervertebral disc remains an important issue for future developments of the model.

References

- Adam, C., Rouch, P., Skalli W., 2015. Inter-lamellar shear resistance confers compressive stiffness in the intervertebral disc: an image-based modelling study on the bovine caudal disc. *Journal of Biomechanics* 48, 4303-4308.
- Amonoo-Kuofi, H.S., 1991. Morphometric changes in the heights and anteroposterior diameters of the lumbar intervertebral discs with age. *Journal of Anatomy* 175, 159-168.
- Asner, L., Hadjicharalambous, M., Chabiniok, R., Peressutti, D., Sammut, E., Wong, J., Carr-White, G., Razavi, R., King, A., Smith, N., Lee, J., Nordsletten, D., 2017. Patient-specific modeling for left ventricular mechanics using data-driven boundary energies. *Computer Methods in Applied Mechanics and Engineering* 314, 269-295.

- Baldit, A., Ambard, D., Cherblanc, F., Royer, P., 2014. Experimental analysis of the transverse mechanical behaviour of annulus fibrosus tissue. *Biomechanics and Modeling in Mechanobiology* 13, 643-652.
- Bergstrom, J.S., Boyce, M.C., 1998. Constitutive modeling of the large strain time-dependent behavior of elastomers. *Journal of the Mechanics and Physics of Solids* 46, 931-954.
- Brickley-Parsons, D., Glimcher, M.J., 1984. Is the chemistry of collagen in intervertebral discs an expression of Wolff's Law? A study of the human lumbar spine. *Spine* 9, 148-163.
- Brown, T., Hansen, R.J., Yorra, A.J., 1957. Some mechanical tests on the lumbosacral spine with particular reference to intervertebral discs. *The Journal of Bone & Joint Surgery* 39, 135-1164.
- Cantournet, S., Boyce, M.C., Tsou, A.H., 2007. Micromechanics and macromechanics of carbon nanotube-enhanced elastomers. *Journal of the Mechanics and Physics of Solids* 55, 1321-1339.
- Cassidy, J.J., Hiltner, A., Baer, E., 1989. Hierarchical structure of the intervertebral disc. *Connective Tissue Research* 23, 75-88.
- Chevalier, Y., Charlebois, M., Pahra, D., Varga, P., Heini, P., Schneider, E., Zysset, P., 2008. A patient-specific finite element methodology to predict damage accumulation in vertebral bodies under axial compression, sagittal flexion and combined loads. *Medical & Biological Engineering & Computing* 11, 477-487.
- Costi, J.J., Stokes, I.A., Gardner-Morse, M., Laible, J.P., Scoffone, H.M., Iatridis, J.C., 2007. Direct measurement of intervertebral disc maximum shear strain in six degrees of freedom: motions that place disc tissue at risk of injury. *Journal of Biomechanics* 40, 2457-2466.
- del Palomar, A.P., Calvo, B., Doblare, M., 2008. An accurate finite element model of the cervical spine under quasi-static loading. *Journal of Biomechanics* 41, 523-531.
- Derrouiche, A., Zaouali, A., Zaïri, F., Ismail, J., Chaabane, M., Qu, Z., Zaïri, F., 2019a. Osmo-inelastic response of the intervertebral disc. *Proceedings of the Institution of Mechanical Engineers. Part H: Journal of Engineering in Medicine* 233, 332-341.
- Derrouiche, A., Zaïri, F., Zaïri, F., 2019b. A chemo-mechanical model for osmo-inelastic effects in the annulus fibrosus. *Biomechanics and Modeling in Mechanobiology* 18, 1773-1790.
- Derrouiche, A., Feki, F., Zaïri, F., Taktak, R., Moulart, M., Qu, Z., Ismail, J., Charfi, S., Haddar, N., Zaïri, F., 2020a. How pre-strain affects the chemo-torsional response of the intervertebral disc. *Clinical Biomechanics* 76, 105020.
- Derrouiche, A., Karoui, A., Zaïri, F., Ismail, J., Qu, Z., Chaabane, M., Zaïri, F., 2020b. The two Poisson's ratios in annulus fibrosus: relation with the osmo-inelastic features. *Mechanics of Soft Materials* 2, 1.
- de Souza Neto, E.A., Peric, D., Owen, D.R.J., 2008. *Computational Methods for Plasticity: Theory and Applications*, John Wiley and Sons Publication.
- Ebara, S., Iatridis, J.C., Setton, L.A., Foster, R.J., Mow, V.C., Weidenbaum, M., 1996. Tensile properties of nondegenerate human lumbar annulus fibrosus. *Spine* 21, 452-461.
- Ehlers, W., Karajan, N., Markert, B., 2009. An extended biphasic model for charged hydrated tissues with application to the intervertebral disc. *Biomechanics and Modeling in Mechanobiology* 8, 233-251.

- Emanuel, K.S., van der Veen, A.J., Rustenburg, C.M.E., Smit, T.H., Kingma, I., 2018. Osmosis and viscoelasticity both contribute to time-dependent behaviour of the intervertebral disc under compressive load: a caprine in vitro study. *Journal of Biomechanics* 70, 10-15.
- Feki, F., Taktak, R., Kandil, K., Derrouiche, A., Moulart, M., Haddar, N., Zaïri, F., Zaïri, F., 2020. How osmoviscoelastic coupling affects recovery of cyclically compressed intervertebral disc. *Spine* 45, 160553.
- Gent, A.N., 1996. A new constitutive relation for rubber. *Rubber Chemistry and Technology* 69, 59-61.
- Goel, V.K., Monroe, B.T., Gilbertson, L.G., Brinckmann, P., 1995. Interlaminar shear stresses and laminae separation in a disc. Finite element analysis of the L3-L4 motion segment subjected to axial compressive loads. *Spine* 20, 689-698.
- Grytz, R., Krishnan, K., Whitley, R., Libertiaux, V., Sigal, I.A., Girkin, C.A., Downs J.C., 2020. A mesh-free approach to incorporate complex anisotropic heterogeneous material properties into eye-specific finite element models. *Computer Methods in Applied Mechanics and Engineering* 358, 112654.
- Gurtin, M.E., Anand, L., 2005. The decomposition $F = F^c F^p$, material symmetry, and plastic irrotationality for solids that are isotropic-viscoplastic or amorphous. *International Journal of Plasticity* 21, 1686-1719.
- Heuer, F., Schmidt, H., Wilke, H.J., 2008. The relation between intervertebral disc bulging and annular fiber associated strains for simple and complex loading. *Journal of Biomechanics* 41, 1086-1094.
- Holzappel, G.A., Schulze-Bauer, C.A.J., Feigl, G., Regitnig, P., 2005. Single lamellar mechanics of the human lumbar annulus fibrosus. *Biomechanics and Modeling in Mechanobiology* 3, 125-140.
- Iatridis, J.C., Kumar, S., Foster, R.J., Weidenbaum, M., Mow, V.C., 1999. Shear mechanical properties of human lumbar annulus fibrosus. *Journal of Orthopaedic Research* 17, 732-737.
- Iatridis, J.C., ap Gwynn, I., 2004. Mechanisms for mechanical damage in the intervertebral disc annulus fibrosus. *Journal of Biomechanics* 37, 1165-1175.
- Iatridis, J.C., MacLean, J.J., O'Brien, M., Stokes, I.A., 2007. Measurements of proteoglycan and water content distribution in human lumbar intervertebral discs. *Spine* 32, 1493-1497.
- Jaramillo, H.E., Puttlitz, C.M., McGilvray, K., Garcia, J.J., 2016. Characterization of the L4-L5-S1 motion segment using the stepwise reduction method. *Journal of Biomechanics* 49, 1248-1254.
- Kandil, K., Zaïri, F., Derrouiche, A., Messenger, T., Zaïri, F., 2019. Interlamellar-induced time-dependent response of intervertebral disc annulus: a microstructure-based chemo-viscoelastic model. *Acta Biomaterialia* 100, 75-91.
- Kandil, K., Zaïri, F., Messenger, T., Zaïri, F., 2020a. Interlamellar matrix governs human annulus fibrosus multiaxial behavior. *Scientific Reports* 10, 19292.
- Kandil, K., Zaïri, F., Messenger, T., Zaïri, F., 2020b. A microstructure-based modeling approach to assess aging-sensitive mechanics of human intervertebral disc. *Computer Methods and Programs in Biomedicine*, 105890.
- Kim, K.H., Park, J.Y., Kuh, S.U., Chin, D.K., Kim, K.S., Cho, Y.E., 2013. Changes in spinal canal diameter and vertebral body height with age. *Yonsei Medical Journal* 54, 1498-1504.

- Koeller, W., Funke, F., Hartmann, F., 1984. Biomechanical behaviour of human intervertebral discs subjected to long lasting axial loading. *Biorheology* 21, 675-86.
- Lauzeral, N., Borzacchiello, D., Kugler, M., George, D., Rémond, Y., Hostettler, A., Chinesta, F., 2019. A model order reduction approach to create patient-specific mechanical models of human liver in computational medicine applications. *Computer Methods and Programs in Biomedicine* 170, 95-106.
- Markolf, K.L., 1972. Deformation of the thoracolumbar intervertebral joints in response to external load: a biomechanical study using autopsy material. *The Journal of Bone & Joint Surgery* 54, 511-533.
- Markolf, K.L., Morris, J.M., 1974. The structural components of the intervertebral disc. A study of their contributions to the ability of the disc to withstand compressive forces. *The Journal of Bone & Joint Surgery* 56, 675- 687.
- Masni, A., Tanaka, M., 2018. Biomechanical investigation on the influence of the regional material degeneration of an intervertebral disc in a lower lumbar spinal unit: a finite element study. *Computers in Biology and Medicine* 98, 26-38.
- Meakin, J.R., Hukins, D.W.L, 2000. Effect of removing the nucleus pulposus on the deformation of the annulus fibrosus during compression of the intervertebral. *Journal of Biomechanics* 33, 575-580.
- Meakin, J.R., Redpath, T.W., Hukins, D.W.L, 2001. The effect of partial removal of the nucleus pulposus from the intervertebral disc on the response of the human annulus fibrosus to compression. *Clinical Biomechanics* 16, 121-128.
- Mengoni, M., Luxmoore, B.J., Wijayathunga, V.N., Jones, A.C. Broom, N.D., Wilcox, R.K., 2015. Derivation of inter-lamellar behaviour of the intervertebral disc annulus. *Journal of the Mechanical Behavior of Biomedical Materials* 48, 164-172.
- Moramarco, V., Palomar, A.P., Pappalettere, C., Doblaré, M., 2010. An accurate validation of a computational model of human lumbosacral segment. *Journal of Biomechanics* 43, 334-342.
- Natarajan, R.N., Andersson, G.B., 1999. The influence of lumbar disc height and cross-sectional area on the mechanical response of the disc to physiologic loading. *Spine* 24, 1873-1881.
- O'Connell, G.D., Sen, S., Elliott, D.M., 2012. Human annulus fibrosus material properties from biaxial testing and constitutive modeling are altered with degeneration. *Biomechanics and Modeling in Mechanobiology* 11, 493-503.
- Ortolani, F., Raspanti, M., Franchi, M., Marchini, M., 1988. Localization of different alcian blue-proteoglycan particles in the intervertebral disc. *Basic and Applied Histochemistry* 32, 443-453.
- Panjabi, M.M., Oxland, T.R., Yamamoto, I., Crisco, J.J., 1994. Mechanical behavior of the human lumbar and lumbosacral spine as shown by three-dimensional load-displacement curves. *The Journal of Bone & Joint Surgery* 76, 413-424.
- Pearcy, M.J., Tibrewal, S.B., 1984. Axial rotation and lateral bending in the normal lumbar spine measured by three-dimensional radiography. *Spine* 9, 582-587.
- Rama, R.R., Skatulla, S., 2018. Towards real-time cardiac mechanics modelling with patient-specific heart anatomies. *Computer Methods in Applied Mechanics and Engineering* 328, 47-74.

- Rannou, F., Poiraudou, S., Corvol, M., Revel, M., 2000. Biochimie et biologie du disque intervertébral. *Revue du Rhumatisme* 67, 214-218.
- Razaghi, R., Biglari, H., Karimi, A., 2019. Risk of rupture of the cerebral aneurysm in relation to traumatic brain injury using a patient-specific fluid-structure interaction model. *Computer Methods and Programs in Biomedicine* 176, 9-16.
- Renner, S.M., Natarajan, R.N., Patwardhan, A.G., Havey, R.M., Voronov, L.I., Guo, B.Y., Andersson, G.B.J., An, H.S., 2007. Novel model to analyze the effect of a large compressive follower pre-load on range of motions in a lumbar spine. *Journal of Biomechanics* 40, 1326-1332.
- Ruberté, L.M., Natarajan, R.N., Andersson, G.B., 2009. Influence of single-level lumbar degenerative disc disease on the behavior of the adjacent segments - a finite element model study. *Journal of Biomechanics* 42, 341-348.
- Schmidt, H., Kettler, A., Rohlmann, A., Claes, L., Wilke, H.J., 2007a. The risk of disc prolapses with complex loading in different degrees of disc degeneration - a finite element analysis. *Clinical Biomechanics* 22, 988-998.
- Schmidt, H., Kettler, A., Heuer, F., Simon, U., Claes, L., Wilke, H.J., 2007b. Intradiscal pressure, shear strain, and fiber strain in the intervertebral disc under combined loading. *Spine* 32, 748-755.
- Schroeder, Y., Wilson W., Huyghe, J.M., Baaijens, F.P.T., 2006. Osmoviscoelastic finite element model of the intervertebral disc. *European Spine Journal* 15, 361-371.
- Shirazi-Adl, S.A., Shrivastava, S.C., Ahmed, A.M., 1984. Stress analysis of the lumbar disc-body unit in compression. A three dimensional nonlinear finite element study. *Spine* 9, 120-134.
- Spenciner, D., Greene, D., Paiva, J., Palumbo, M., Crisco, J., 2006. The multidirectional bending properties of the human lumbar intervertebral disc. *The Spine Journal* 6, 248-257.
- Subramani, A.V., Whitley, P.E., Garimella, H.T., Kraft, R.H., 2020. Fatigue damage prediction in the annulus of cervical spine intervertebral discs using finite element analysis. *Computer Methods in Biomechanics and Biomedical Engineering* 23, 773-784.
- Szilagyi, S.M., Szilagyi, L., Benyo, Z., 2011. A patient specific electro-mechanical model of the heart. *Computer Methods and Programs in Biomedicine* 101, 183-200.
- Tavakoli, J., Costi, J.J., 2018. New findings confirm the viscoelastic behaviour of the interlamellar matrix of the disc annulus fibrosus in radial and circumferential directions of loading. *Acta Biomaterialia* 71, 411-419.
- Urban, J.P., Maroudas, A., 1981. Swelling of the intervertebral disc in vitro. *Connective Tissue Research* 9, 1-10.
- Veres, S.P., Robertson, P.A., Broom, N.D., 2010. The influence of torsion on disc herniation when combined with flexion. *European Spine Journal* 19, 1468-1478.
- Violas, P., Estivalezes, E., Briot, J., Sales de Gauzy, J., Swider P., 2007. Objective quantification of intervertebral disc volume properties using MRI in idiopathic scoliosis surgery. *Magnetic Resonance Imaging* 25, 386-391.
- Wade, K.R., Robertson, P.A., Thambyah, A., Broom, N.D., 2014. How healthy discs herniate. *Spine* 39, 1018-1028.
- Wade, K.R., Schollum, M.L., Robertson, P.A., Thambyah, A., Broom, N.D., 2017. A more realistic disc herniation model incorporating compression, flexion and facet-constrained

- shear: a mechanical and microstructural analysis. Part I: Low rate loading. *European Spine Journal* 26, 2616-2628.
- Wang, S., Xia, Q., Passias, P., Wood, K., Li, G., 2009. Measurement of geometric deformation of lumbar intervertebral discs under in-vivo weightbearing condition. *Journal of Biomechanics* 42, 705-711.
- Wang, S., Park, W.M., Gadikota, H.R., Miao, J., Kim, Y.H., Wood, K.B., Li, G., 2013. A combined numerical and experimental technique for estimation of the forces and moments in the lumbar intervertebral disc. *Computer Methods in Biomechanics and Biomedical Engineering* 16, 1278-1286.
- Weis, J.A., Miga, M.I., Yankeelov, T.E., 2017. Three-dimensional image-based mechanical modeling for predicting the response of breast cancer to neoadjuvant therapy. *Computer Methods in Applied Mechanics and Engineering* 314, 494-512.

General conclusion and perspectives

The mechanical behavior of the intervertebral disc is very complex. In addition to the non-linear anisotropic highly heterogeneous conduct of the disc tissue, the living tissue interacts with the surrounding environment inducing a non-usual time-dependent volumetric response that affects the three-dimensional disc behavior; the time-dependent anisotropic transversal strain under mechanical loading leads to negative Poisson's ratio values in the radial plane of the disc and Poisson's ratio values exceeding 1 in the axial plane of the disc. The interlamellar zones separating the annulus layers have been found to play an essential role in this transversal behavior. Hence, accurate multi-axial modeling of the disc behavior requires their consideration.

Towards an accurate modeling of the intervertebral disc response a microstructure-based chemo-mechanical constitutive model was constructed using the recent discoveries about the disc mechanics and taking into account the different microstructural complexities and the regional dependency of the disc tissue.

By means of the fluid experimental based fluid kinetics and by considering the interlamellar zones as physical essential parts of the disc geometry, the three-dimensional anisotropic interaction with the physiological medium was successfully modeled allowing an accurate realistic strain response of the disc with realistic Poisson's ratio values in the different directions of the disc axis. The model was first constructed based on bovine experimental data and verified for local specimens extracted from two radial regions of the disc. It succeeded to reproduce the uniaxial stress-strain, transversal strains, and relaxation responses of the studied regions.

In order to apply the model for human, it was adapted by means of a novel strategy allowing the adjustment of some parameters of the model according to the difference in microstructure between bovine and human. The multi-axial capability of the model was then verified by reproducing, using the same set of parameters, the uniaxial, the biaxial and the shear responses of the four different circumferential and radial regions of the annulus allowing a complete treatment of the whole annulus. As well, the model permits tracking the age alterations induced by the long-term mechano-biological microstructural changes inside healthy intervertebral disc. Such ability of the model helped to give valuable explanations about non reasonable experimental observations about effect of age on the mechanical properties and the morphology of the disc.

Finally, the biggest objective of the thesis was attained by applying the locally validated model to the different regions of an MRI-based functional spine unit structure that considers the real unit geometry in order to go through the heart of the disc and observe the different lamellar-interlamellar-nucleus interactions under the different physiological movements while accounting for a correct volumetric strain of the disc. This represents a valuable tool helping for the detection of dangerous contact zones in the core of the disc highly susceptible to damage initiation and give important explanations about occurring biomechanical damage mechanisms and their relation to the microstructure and the structural construction of the intervertebral disc.

In the following steps of the project, the model should be extended by incorporating the biomechanical coupling between the disc nutrients (oxygen, glucose and lactate), the microstructure and therefore the disc mechanical response. It should consider, from one side, the distribution of the different nutrients induced by the mechanical loads, and from the other side the nutrients concentration effect on the microstructure components synthesis/deterioration which will affect by its turn the mechanical behavior of the disc. Such

tool would allow the continuous prediction of the long-term age-induced alterations of the biomechanical disc properties. It would permit also the study of the biological damage, recovery and self-healing mechanisms of the living tissue that are basically affected by the nutrient concentrations and reactions. Towards this objective, experimental studies are actually established to study the effect of rest on the viscoelastic recovery and healing capability of the disc after being loaded by the different physiological movements. During the actual thesis, it was noticed that experimental data about the multi-axial behavior of regional annulus specimens are very limited and misses a lot of information. A complete biaxial and shear testing sets will be established on different regions of the disc under different strain rates and osmotic conditions. The local strain fields will be captured using digital image correlation techniques in order to capture experimentally the lamellar-interlamellar interaction, in order to reveal all the missing data about the multi-axial mechanical role of interlamellar zones and improve the developed model that would be more in depth verified by the additional experimental tests.

Multi-physics and multi-scale modeling of laminated soft tissues: Application to the multi-axial response of human intervertebral disc

Abstract

The intervertebral disc is probably the most extraordinary tissue that the nature produces, mainly for its unusual time-dependent properties strongly influenced by the biochemical environment and the applied mechanical loading. Establishing accurate structure-property relationships for intervertebral disc annulus fibrosus tissue is a fundamental task for a reliable computer simulation of the human spine. The difficulty emanates from the multi-axiality and the anisotropy of the tissue response along with regional dependency of a complex hierarchic structure interacting with the biochemical environment. In addition, the annulus fibrosus exhibits an unusual time-dependent transversal behavior for which a complete constitutive representation is not yet developed. A physically-based chemo-viscoelastic constitutive model that takes into account an accurate disc annulus structure in relation with the biochemical environment is proposed. Numerical models of annulus specimens and lumbar functional spinal units (one disc and the adjacent vertebrae) are designed while taking into consideration the interlamellar matrix connecting the fibers-reinforced lamellae. At the specimen scale, the model capabilities are verified by experimental comparisons under various conditions in terms of osmolarity, strain-rate and multi-axiality while considering the regional dependency. Our results highlight the determinant role of the interlamellar matrix in the disc multi-axial response. The different scenarios applied to lumbar units show encouraging multi-axial predictive capabilities of our approach making it a promising tool for human spine behavior long-term prediction including age-dependency.

Keywords: Annulus fibrosus; Microstructure; Regional dependency; Osmo-induced transversal response; Time-dependent constitutive model; Finite element computations.

Modélisation multi-physique et multi-échelle des tissus mous stratifiés : Application à la réponse multi-axiale du disque intervertébral humain

Résumé

Le disque intervertébral est probablement le plus extraordinaire des tissus du vivant, principalement en raison de propriétés inhabituelles dépendantes du temps, fortement influencées par l'environnement biochimique et par la charge mécanique appliquée. L'établissement de relations structure-propriété précises pour le tissu de l'annulus fibrosus du disque intervertébral est fondamental afin d'obtenir une modélisation fiable de la colonne vertébrale humaine. La difficulté provient de la multi-axialité et de l'anisotropie de la réponse tissulaire ainsi que de la dépendance régionale d'une structure hiérarchique complexe interagissant avec l'environnement biochimique. De plus, l'annulus fibrosus présente un comportement transversal unique dépendant du temps pour lequel une représentation constitutive complète n'est pas encore développée. Un modèle constitutif chimio-viscoélastique à base physique prenant en compte l'architecture de l'annulus fibrosus et son environnement biochimique a ainsi été proposé. Des modèles numériques d'échantillons de l'annulus fibrosus et d'unités vertébrales fonctionnelles lombaires (disque et vertèbres adjacentes) ont été développés en tenant compte de la matrice interlamellaire reliant les lamelles renforcées de fibres. A l'échelle de l'échantillon, les capacités du modèle sont vérifiées par des comparaisons avec des observations expérimentales pour diverses conditions en termes d'osmolarité, de vitesse de déformation et de multi-axialité tout en considérant la dépendance régionale. Nos résultats démontrent le rôle déterminant de la matrice interlamellaire dans la réponse multi-axiale du disque. Les différents scénarios appliqués aux unités lombaires démontrent les capacités prédictives multi-axiales encourageantes de notre approche, ce qui en fait un outil prometteur pour la prédiction à long terme du comportement de la colonne vertébrale humaine, y compris la dépendance à l'âge.

Mots-clefs : Annulus fibrosus; Microstructure; Dépendance régionale; Réponse transversale induite par l'osmolarité; Modèle constitutif dépendant du temps; Simulations éléments finis.